

Structure-function studies of SLC15 peptide transporters

Anish Senan

Thesis submitted to Oxford Brookes University in partial fulfilment of requirements for the award of Doctor of Philosophy

August 2015

Dedication

I would like to dedicate this work to my parents, my wife, my sister and parents in-laws who have given me immense support and encouragement to work hard to achieve my goals. This work would not have been possible without your unconditional love and support.

I would also like to dedicate this work to my late uncle Balachandran K. aunt Ambika and my cousin Ambili kuttan, you will be always remembered.

Thank you

Acknowledgments

I owe my sincere gratitude to all those people who have made this thesis possible and because of whom my PhD research experience has been one that I will cherish forever.

Firstly, I am deeply grateful to God for providing me with the opportunity to pursue my PhD and for this I feel truly blessed.

I would like to express my gratitude to my mentor and advisor David Meredith for the continuous support and encouragement and that he gave me during the course of my PhD. He gave me the freedom to explore science on my own and guided me when I most needed it. Thank you, for your guidance, it helped me all the time during my research and for writing this thesis.

My sincere thanks also goes to Pat Bailey for helping me understand the chemistry and logic behind the functioning of the synthesised prodrugs and I am very thankful to him for helping me sort out the technical details of my work.

I am very thankful to my secondary-advisors, Simon Newstead and Isabel Bermudez-Diaz who have always been there to listen and give great advice. I am very grateful to Isabel for sharing her knowledge in molecular biology, for her constant support and encouragement.

I would like thank Michele Rawlings for making sure that I never ran out of consumables and kits for my experiments. I could not ask for a better colleague and a friend. Simon Giles thank you for your help with handling radioactivity and thanks to Richard Smith for help with my IT issues.

Jennina Taylor-Wells I appreciate and thank you for helping me find my way around the lab during the early days of my PhD, for sharing various tips and tricks with molecular biology techniques and for being a guiding friend.

I am also grateful to Munira Kadhim for gifting the Caco-2 cells and Ammar Al-Mayah for training me with tissue culture techniques.

I want to thank my colleagues Vidya Pawar Menon, Samantha Barry, Alessandra Rocchetti, Petra Kiviniemi, Frances Tolmie, Robbie Crickley, Axel Poulet and Alaaddine El-Chab for the amazing time we had engaging in thought-provoking

discussions, working together before deadlines and for all the fun we have had in the past four years.

Many friends have helped me stay sane during the last few years. Their support and care helped me go strong and focus on my PhD. Thanks to all my friends Simone Mazzaferro, Constanza Alcaïno Ayala, Federica Gasparri, Elena Mantione, Gabriele Mantione, Scott Bright, Britany Almond, Ayswarya Pavan, Pavan Kumar, Bhavya Rajgopal and Arpan Kumar, you guys made me feel at home.

I appreciate and am indebted to Oxford Brookes University for giving me the opportunity to pursue my PhD through the Nigel Groome studentship.

Finally and most importantly, none of this would have been possible without the love, patience and encouragement of my family. My immediate family to whom this thesis is dedicated to, have been a constant source of love, support and strength all these years. I would like to express my heart-felt gratitude to my Dad, Mom, Sister, Father-in-law, Mother-in-law and my wife Mili for being such an amazing friend and companion. I could not have done it without you.

Abstract

The proton coupled oligopeptide transporter (POT) family of proteins includes mammalian PepT1 (*SLC15A1*; high capacity, low affinity) and PepT2 (*SLC15A2*; low capacity, high affinity) transporters which are involved in the co-transport of protons and di- and tri- peptides and drugs similar in structure (peptidomimetics). PepT1, and to a lesser extent PepT2, have therefore gained attention due to their role in determining the absorption, retention and elimination of transported drugs. In this study three novel prodrug-carriers namely Amino-Isobutynyl-Alanyl-Serine (Aib), Cyclo-Leucyl-Serine (cLu) and Alanyl-[ψCS-NH]-Serine (Thio) were tested for PepT1 mediated transport in PepT1 expressing *Xenopus laevis* oocytes and differentiated Caco-2 cells grown on Transwell[®] inserts. The cLu- carrier was found to exhibit higher binding affinity towards PepT1 compared to Aib- and Thio- carriers and to transport the conjugated drugs both in the oocyte and Caco-2 assays. The Aib-and Thio- carriers exhibited similar affinities towards PepT1 and were also found to be transported. Therefore all three carriers were shown to have the potential to deliver a range of conjugated drugs/compounds with differing physicochemical properties through PepT1.

Homology models for PepT1/2 have been proposed due to the lack of crystal structure data available for mammalian peptide transporters, based on recent crystal structures of the bacterial POT family members. Although offering invaluable insights, all the bacterial transporters lack the mammalian large extracellular domain (ECD) between transmembrane (TMD) 9 and 10. Human PepT1 (hPepT1) and hPepT2 mutants with their ECD deleted (ECDΔ) or swapped (hPepT1-ECD2, hPepT2-ECD1) were tested for functional effects. The hPepT1-ECDΔ and hPepT1-ECD2 transporters were found not to express, showing a critical structural role for the ECD in hPepT1. In contrast, hPepT2-ECDΔ and hPepT2-ECD1 were found to function as the wild type hPepT2. In a collaborative project, Dr Simon Newstead and colleagues (Department of Biochemistry, Oxford University), crystallised the ECD of mouse PepT1 and rat PepT2. Despite the ECD having a thyroxine binding fold, no evidence of thyroxine hormone interaction with the ECD was found. However hPepT2-ECDΔ mediated transport of [³H]-D-Phe-L-Gln was significantly reduced compared to wild type at extracellular pH 6.5, the pH prevalent in the kidney where PepT2 is predominantly expressed, suggesting that the ECD could function like a pH sensor by allowing hPepT2 to perform at its maximum capacity.

Previous point mutation studies on PepT1 have identified several key conserved residues that play critical structure-functional roles. Mutation of the analogous residues in PepT2 indicated that the amino acid residues tested (Y42, Y94, Y188, R301, W313, and E622) played a similar role in PepT2, suggesting functional/structural as well as sequence homology.

Finally, rat peptide histidine transporter (ratPHT1, *SLC15A4*), has been reported to transport L-histidine in addition to di- and tri- peptides, and to be expressed on the neuronal lysosomal membrane. Surface expression studies of FLAG epitope tagged PHT1 protein confirmed that the protein localised to the plasma membrane of oocytes but no evidence for transport of [³H]-L-Histidine or any other amino acid (electrophysiology) was found. Therefore the exact function of the PHT1 transporter still remains unclear.

Together, these results presented here demonstrate novel findings into the structure-function relationship of SLC15 peptide transport proteins.

Abbreviations

AARE	Amino acid responsible element (Transcription factor binding site)
ABC	ATP binding cassette
Aib	Amino-Isobutynyl-Alanyl-Serine di-peptide (prodrug carrier)
AMPK	Adenosine monophosphate-activated protein kinase
AP-1	Activator protein 1 (Transcription factor)
BBB	Blood Brain Barrier
B ⁰ AT1	Neutral amino acid transporter
Caco-2	Colorectal adenocarcinoma cell line
cLu	Cyclo-Leucyl-Serine (prodrug carrier)
cpm	Counts per minute (scintillation counter units)
cRNA	complementary RNA
ECD	Extracellular domain
FBS	Foetal Bovine Serum
Gly-Gln	Glycyl-L-Glutamine
Gly-Glu	Glycyl-L-Glutamate
Gly-Leu	Glycyl-L-Leucine
Gly-Lys	Glycyl-L-Lysine
Gly-Sar	Glycl-Sarcosine (di-peptide)
[³ H]-D-Phe-L-Gln	Tritiated D-Phenylalanyl-L-Glutamine (di-peptide)
hPepT1	human PepT1
hPepT1-ECDΔ	hPepT1 with its ECD between TMD9 and TMD10 deleted
hPepT1-ECD2	hPepT1 with the ECD from hPepT2
hPepT2	human PepT2
hPepT2-ECDΔ	hPepT2 with its ECD deleted
hPepT2-ECD1	hPepT2 with ECD from hPepT1
K _i	Inhibition constant
K _m	Binding affinity
Lys-Lys	L-Lysyl-L-lysine (di peptide)
MFS	Multi facilitator superfamily
NF-κB	Nuclear factor kappa-light-chain-enhancer of activated B cells (Transcription factor)
NI	Non-injected
NOD1	Nucleotide-binding oligomerization domain-containing protein 1
NOD2	Nucleotide-binding oligomerization domain-containing protein 2
PepT	Peptide transporter
PepT1-RF	PepT1 regulatory factor
PHT	Peptide histidine transporter
POT	Proton-coupled oligopeptide transporter
rPepT1	Rabbit PepT1
SLC	Solute linked carrier
Thio-	Alanyl-[ψCS-NH]-Serine (prodrug carrier)
TMD	Transmembrane domain

V_{\max}

Maximum rate of a reaction when the enzyme (transporter) is saturated with the substrate

Table of contents

Acknowledgments.....	ii
Abstract	iv
Abbreviations	vi
List of figures	xiii
List of Tables.....	xvii
1 Introduction	1
1.1 Protein digestion.....	1
1.2 Membrane transport proteins.....	1
1.3 Types of transport proteins.....	3
1.3.1 Channel-type facilitated diffusion:.....	3
1.3.2 Carrier-type facilitated diffusion:.....	3
1.3.3 Primary active transport:	3
1.3.4 Secondary active transport:	3
1.3.5 Uniporters.....	3
1.3.6 Symporters	4
1.3.7 Antiporters	4
1.4 Major Facilitator Superfamily (MFS)	4
1.5 Proton-coupled oligopeptide transporters (POT)	4
1.6 Brief research into mammalian peptide transporters.....	5
1.7 <i>SLC15</i> peptide transporters	6
1.7.1 PepT1 (<i>SLC15A1</i>)	6
1.7.2 PepT2 (<i>SLC15A2</i>)	8
1.7.3 Peptide Histidine Transporter (PHT1)/ <i>SLC15A4</i>	8
1.7.4 Peptide Histidine Transporter (PHT2)/(<i>SLC15A3</i>)	10
1.8 Basolateral peptide transporters	11
1.9 Importance of peptide transporters.....	12
1.10 Regulation of peptide transporters.....	12
1.11 Factors affecting the kinetic properties of PepT1	15
1.12 Peptide transport mechanism	15
1.12.1 Alternating access mechanism of POT transporters	18
1.12.2 Structural requirements for PepT1 substrates	21
1.12.3 Substrate binding template for PepT1	22
1.12.4 Important amino acid residues contributing to PepT1 and PepT2.....	23
1.13 Genetic polymorphism in PepT1	24

1.14	Prodrugs	25
1.14.1	Classification of prodrugs	26
1.14.2	Applications of pro-drug strategy	26
1.14.3	Aims	29
2	Methods.....	30
2.1	Materials	30
2.1.1	Antibiotics	30
2.1.2	Bacterial cells for transformation.....	30
2.1.3	Chemicals.....	30
2.1.4	Clones.....	30
2.1.5	Caco-2 Cells	30
2.1.6	Restriction enzymes and Ligases	30
2.1.7	Vectors	31
2.2	Molecular biology techniques	31
2.2.1	Primer design:	31
2.2.2	PCR:	31
2.2.3	Purification of PCR products:	32
2.2.4	Gel electrophoresis.....	32
2.2.5	Purification of DNA obtained from Gel Electrophoresis.....	33
2.2.6	Plasmid Extraction and purification from <i>E. coli</i>	33
2.2.7	Restriction digest reactions	33
2.2.8	Purification of DNA using QIAquick PCR purification kit.....	34
2.2.9	Cloning.....	34
2.2.10	In vitro mRNA synthesis.....	37
2.2.11	Site directed mutagenesis	37
2.3	<i>Xenopus laevis</i> oocyte preparation, maintenance and cRNA injection.....	38
2.3.1	Collagenase treatment	39
2.3.2	cRNA injection.....	39
2.3.3	Transport experiments using oocytes.....	40
2.3.4	Determination of affinity of pro-drugs towards rPepT1	41
2.3.5	Efflux assay/Trans-stimulation protocol.....	42
2.3.6	Luminometric technique to establish surface expression of protein in oocytes	43
2.3.7	Electrophysiology	44
2.4	Caco-2 cell revival, storage and maintenance	45

2.4.1	Caco-2 cell culture maintenance	45
2.4.2	Routine sub-culturing of Caco-2 cells.....	46
2.4.3	Cryopreservation of Caco-2 cells.....	46
2.4.4	Revival of Caco-2 cells from Liquid nitrogen stocks	46
2.4.5	Transport assay using Caco-2 cells	47
2.4.6	HPLC analysis of Transwell assay.....	48
Results		50
3	Novel Prodrugs for PepT1 mediated transport.....	50
3.1.1	Introduction	50
3.1.2	Aims	55
3.1.3	Determination of K_i of novel prodrugs for rPepT1	56
3.1.4	Determination of K_i of native compounds (drugs only without a prodrug carrier) for rPepT1.....	72
3.1.5	Determination of PepT1 mediated transport of novel prodrugs and native drugs in rPepT1 cRNA injected oocytes using trans-activated efflux assay	73
3.1.6	Determination of hPepT1 mediated transport of novel prodrugs in differentiated Caco-2 cell monolayers grown on Transwell® plates.....	77
3.1.7	Discussion	88
4	Determining the function of the large extracellular domain between TMD9 and TMD10 in hPepT1 and hPepT2 transporters	96
4.1.1	Introduction:.....	96
4.1.2	Aims	101
4.1.3	Methods.....	102
4.1.4	Comparison of [3H]-D-Phe-L-Gln uptake between hPepT1 and hPepT2 ECD variant constructs	103
4.1.5	Comparison of [³ H]-D-Phe-L-Gln uptake between hPepT2 and hPepT2 ECD variant constructs	104
4.1.6	Comparison of [³ H]-D-Phe-L-Gln uptake between hPepT2 and hPepT2 ECD variant constructs	105
4.1.7	Luminometric estimation of surface expression of FLAG tagged PepT1 ECD variant constructs	106
4.1.8	Effect of ECD on affinity of hPepT2 and hPepT2 ECD variants their substrates.....	107
4.1.9	Effect of pH on uptake of [³ H]-D-Phe-L-Gln in hPepT2 and hPepT2-ECDΔ 110	
4.1.10	Effect of Thyroxin (T4) on transport of [³ H]-D-Phe-L-Gln in rPepT1 cRNA injected oocytes.....	112

4.1.11	Measurement of [³ H]-D-Phe-L-Gln uptake by rPepT1 cRNA injected oocytes in the presence of thyroxin (T4).....	113
4.1.12	Luminometric estimation of flagged rPepT1 expression after treatment with thyroxin (T4) in oocytes.....	114
4.1.13	Comparison of K _i of rPepT1 with di-peptide Gly-Gln in presence and absence of T4	115
4.1.14	Effect of tri-iodothyronine (T3) on uptake of [³ H]-D-Phe-L-Gln in rPepT1 cRNA injected oocytes.....	117
4.1.15	Effect of tri-iodothyronine (T3) on uptake of [³ H]-D-Phe-L-Gln in hPepT1 cRNA injected oocytes.....	118
4.1.16	Effect of tri-iodothyronine (T3) on uptake of [³ H]-D-Phe-L-Gln in hPepT2 and hPepT2-ECDA cRNA injected oocytes.....	119
4.1.17	Discussion	120
5	Transport characteristics of rat PHT1	125
5.1.1	Introduction.....	125
5.1.2	Aims	125
5.1.3	Methods.....	125
5.1.4	Determination of [³ H]-L-Histidine uptake in rat PHT1 injected oocytes.....	130
5.1.5	Comparison of [³ H]-L-Histidine uptake from day 4 to day 6 post rat PHT1 RNA injected oocytes and non-injected oocytes	131
5.1.6	Determination of effect of pH on rat PHT1 mediated uptake of Histidine	132
5.1.7	Luminometric estimation of surface expression of FLAG tagged rat PHT1	133
5.1.8	Electrophysiology experiment to determine amino acid transport in rat PHT1 injected oocytes	134
5.1.9	Uptake assay to determine the presence of endogenous histidine transporters in oocytes.....	136
5.1.10	Discussion	137
6	Effect of site directed mutations of conserved residues on hPepT2 transport characteristics.....	141
6.1.1	Introduction.....	141
6.1.2	Aims	142
6.1.3	Methods.....	142
6.1.4	Determination of the effect of site directed mutations on hPepT2 and hPepT1 mediated uptake of [³ H]-D-Phe-L-Gln	146
6.1.5	Determination of [³ H]-D-Phe- L-Gln uptake in hPepT2 FLAG epitope tagged cRNA injected oocytes	148

6.1.6	Luminometric estimation of surface expression of FLAG epitope tagged hPepT2 constructs	149
6.1.7	Comparison of K_i between hPepT2-WT and hPepT2-Y42A with dipeptide Glycine-L-Glutamine (Gly-Gln)	150
6.1.8	Discussion	151
7	General discussion and future work	160
8	Bibliography.....	164
9	Appendix I: Publication (in press)	173
10	Appendix II	174
10.1	Alignment of hPepT1 and hPepT2 ECD between TMD9 and TMD10	174
10.2	Alignment of hPepT1, hPepT2 and ratPHT1 sequences	175
10.3	Alignment of hPepT1 and hPepT2 conserved residues mutated in chapter 6 177	
10.4	PBF vector diagram	178
11	Appendix III: Presentations.....	180
12	Appendix IV: Permissions for copyright figures	181
13	Appendix IV: Publication	Error! Bookmark not defined.

List of figures

Figure 1.3.1-1 - Diagram showing various basic modes of transport of solutes/molecules into the cell.....	2
Figure 1.7.1-1 - Cartoon showing 12 TMD structure of PepT1.....	7
Figure 1.7.4-1- Cartoon showing the stoichiometry of H ⁺ coupled transport of neutral (Gly-Leu), acidic (Gly-Glu) and basic (Gly-Lys) peptides by PepT1 (Steel et al., 1997)	17
Figure 1.7.4-2 - Cartoon showing the PepT1 mediated transport of charged peptides (Irie <i>et al.</i> , 2005).....	17
Figure 1.12.1-1- Schematic representation showing the arrangement of Helices (H1-H14), with the proposed binding site (central cavity) of PepT _{so} , extracellular helix 1 (EH1) (Newstead <i>et al.</i> , 2011).	18
Figure 1.12.1-2 - Crystal structure of PepT _{so} representing the ligand bound (Central cavity) occluded confirmation state (Newstead <i>et al.</i> , 2011).....	19
Figure 1.12.1-3 - Alternating access mechanism of Peptide transporter showing the steps involved during proton coupled peptide transport (Solcan et al., 2012).....	20
Figure 1.12.3-1 - Substrate binding template for PepT1 showing the structural orientation of important atoms in the binding pocket of PepT1 transporter (Bailey et al., 2000)	22
Figure 1.12.4-1 - Diagrammatic representation of prodrug concept.....	25
Figure 2.3.2-1 Diagrammatic representation of cRNA injection in the vegetal pole of an oocyte	40
Figure 2.3.7-1 - Schematic representation of the two electrode voltage clamp technique.	44
Figure 3.1.1-1 - Structures of the novel carriers to test PepT1 mediated transport of drugs.....	51
Figure 3.1.1-2 - Prodrugs and their structures.....	54
Figure 3.1.3-1 - K _i of Aib-Baclofen.....	56
Figure 3.1.3-2 - K _i of Thio-Baclofen.	57
Figure 3.1.3-3 - K _i of cLu-Baclofen.	58
Figure 3.1.3-4 - K _i of Thio-Atenolol.	59
Figure 3.1.3-5 - K _i of Aib-Atenolol.....	60
Figure 3.1.3-6 - K _i of Aib-Relenza.	61

Figure 3.1.3-7 - Ki of Thio-Relenza.....	62
Figure 3.1.3-8 - Ki of Thio-Mycophenolate.....	63
Figure 3.1.3-9 - Ki of Aib-Mycophenolate.	64
Figure 3.1.3-10 - Ki of Thio-Sialic acid.....	65
Figure 3.1.3-11 - Ki of Aib-Gaba.....	66
Figure 3.1.3-12 - Ki of cLu-Gaba.	67
Figure 3.1.3-13 - Ki of cLu-Benzyl.	68
Figure 3.1.3-14 - Ki of cLu-Ibuprofen.	69
Figure 3.1.3-15 - Ki of Thio-Kinase inhibitor.....	70
Figure 3.1.5-1 - Diagrammatic representation of an efflux transport in the presence (right) and absence (left) of a prodrug.	74
Figure 3.1.5-2 - Histogram representing the results obtained from the efflux experiments performed on 2.5 mM concentration of native drugs.....	75
Figure 3.1.5-3 - Histogram representing the results obtained from the efflux experiments performed on prodrugs.	76
Figure 3.1.6-1 - Comparison of PepT1 mediated transport of positive control compound PheΨ[CS-NH]-Ala (FSA) in Caco-2 cell monolayers grown on Transwell® inserts with and without Gly-Gln.	78
Figure 3.1.6-2 - Comparison of PepT1 mediated transport of test compound cLu-Baclofen in Caco-2 cell monolayers grown on Transwell® inserts with and without Gly-Gln.....	79
Figure 3.1.6-3 - Comparison of PepT1 mediated transport of positive control compound PheΨ[CS-NH]-Ala (FSA) in Caco-2 cell monolayers grown on Transwell® inserts with and without Gly-Gln.	80
Figure 3.1.6-4 - Comparison of PepT1 mediated transport of test compound Aib-Baclofen in Caco-2 cell monolayers grown on Transwell® inserts with and without Gly-Gln.....	81
Figure 3.1.6-5 - Comparison of PepT1 mediated transport of test compound Thio-Atenolol in Caco-2 cell monolayers grown on Transwell® inserts with and without Gly-Gln.....	82
Figure 3.1.6-6 - Comparison of PepT1 mediated transport of test compound cLu-Ibuprofen in Caco-2 cell monolayers grown on Transwell® inserts with and without Gly-Gln.	83

Figure 3.1.6-7 - Comparison of PepT1 mediated transport of test compound Thio-Baclofen in Caco-2 cell monolayers grown on Transwell® inserts with and without Gly-Gln.....	84
Figure 3.1.6-8 - Comparison of PepT1 mediated transport of positive control compound FSA in Caco-2 cell monolayers grown on Transwell® inserts with and without Gly-Gln.	85
Figure 3.1.6-9 - Comparison of PepT1 mediated transport of positive control compound Aib-Atenolol in Caco-2 cell monolayers grown on Transwell® inserts with and without Gly-Gln.	86
Figure 4.1.1-1 - Structures PepT1 and PepT2 chimeras.	97
Figure 4.1.1-2 - Crystal structures of mouse PepT1-ECD (left) and rat PepT2 ECD (right).....	100
Figure 4.1.5-1 - Comparison of uptake between hPepT1 ECD variants.....	104
Figure 4.1.6-1 - Comparison of uptake between hPepT2 and its ECD variants. The histogram represents normalized uptake of [³ H]-D-Phe-L-Gln in cRNA injected oocytes.....	105
Figure 4.1.7-1 - Luminometric expression of hPepT1 ECD mutants.	106
Figure 4.1.8-1 - K _i of cefaclor in hPepT1.....	108
Figure 4.1.8-2 - K _i of cefaclor with hPepT2, hPepT2-ECD1 and hPepT2-ECDΔ.....	108
Figure 4.1.8-3 - K _i of Lys-Lys with hPepT1.	109
Figure 4.1.8-4 - K _i of hPepT2, hPepT2-ECD1 and hPepT2-ECDΔ with Lys-Lys.	109
Figure 4.1.9-1 - Effect of pH on transport of hPepT2 ECD. Uptake of hPepT2 wild type and hPepT2-ECDΔ using [³ H]-D-Phe-L-Gln.	111
Figure 4.1.10-1 - Effect of Thyroxin on the uptake of [³ H]-D-Phe-L-Gln in rPepT1. .	112
Figure 4.1.11-1 - Uptake of [³ H]-D-Phe-L-Gln in the presence of T4 in rPepT1 cRNA injected oocytes.....	113
Figure 4.1.12-1 - Luminometric estimation of rPepT1 expression after T4 treatment for one hour.....	114
Figure 4.1.13-1 - K _i estimation rPepT1 with Gly-Gln in the absence of T4	115
Figure 4.1.13-2 K _i estimation of rPepT1 with Gly-Gln in the presence of 1 μM T4 ...	116
Figure 4.1.14-1 - Uptake of [³ H]-D-Phe-L-Gln in the presence of T3 in rPepT1 cRNA injected oocytes.....	117
Figure 4.1.15-1 - Uptake of [³ H]-D-Phe-L-Gln in hPepT1 cRNA injected oocytes.....	118
Figure 4.1.16-1 - Effect of T3 on uptake of [³ H]-D-Phe-L-Gln in hPepT2 and hPepT2-ECDΔ cRNA injected oocytes.	119

Figure 5.1.3-1 - MEMSAT3 topology prediction of rat PHT1 protein.....	127
Figure 5.1.4-1 - Comparison of [³ H]-L-Histidine uptake between non injected and rat PHT1 RNA injected oocytes.....	130
Figure 5.1.5-1 – Comparison of [3H]-L-Histidine uptake between NI and rat PHT1 RNA injected oocytes from day 4 to day 6 post RNA injection.	131
Figure 5.1.6-1 - Comparison of uptake between non injected and rat PHT1 (rPHT1) RNA injected oocytes at pH 5.5 and pH 7.5.	132
Figure 5.1.7-1 - Luminometric expression of rat PHT1.....	133
Figure 5.1.8-1 Comparison of the change in maximum current measured between non injected control oocytes and rat PHT1 cNRA injected oocytes in a single electrophysiology experiment.	135
Figure 5.1.9-1 - Comparison of uptake in non injected and rat PHT1 RNA injected oocytes in the presence and absence of 2mM cold L-Histidine at pH 5.5.	137
Figure 6.1.3-1-MEMSAT3 topology prediction of hPepT2 protein.....	144
Figure 6.1.4-1 - Comparison of the effect of mutations on hPepT2 and hPepT1 constructs.	146
Figure 6.1.5-1 - Comparison of [3H]-D-Phe-L-Gln uptake between wild type hPepT2 and hPepT2 FLAG epitope tagged constructs.	148
Figure 6.1.6-1 - Luminometric expression of hPepT2 FLAG epitope tagged constructs.	149
Figure 6.1.7-1 - Ki of hPepT2-WT construct with Gly-Gln	150
Figure 6.1.7-2 - Ki of hPepT2-Y42A construct with Gly-Gln.....	151
Figure 6.1.8-1 - Comparison of the location of the predicted binding pocket in hPepT2 (using GK POT and PepTso) with the location of the amino acids mutated in the current study for hPepT2.	158

List of Tables

Table 2.2-1 - PCR reaction setup (50µl reaction)	32
Table 2.2-2 - PCR protocol for amplification of plasmid DNA using Pfu DNA polymerase using “Ramp” method.....	32
Table 2.2-3 - Restriction digest reaction setup.....	34
Table 2.2-4 - Components of dephosphorylation reaction.....	34
Table 2.2-5 - Components of a DNA ligation reaction.....	35
Table 2.2-6 - Constituents of cracking solution	36
Table 2.2-7 - PCR method of site directed mutagenesis.....	38
Table 2.3-1 - Recipe for Calcium free solution	38
Table 2.3-2 - Recipe for Barths Solutions.....	39
Table 2.3-3 - Recipe for Uptake solution.....	42
Table 2.4-1 - Components of complete media used for Caco-2 cell culture.....	46
Table 2.4-2 - Composition of Krebs Media	48
Table 2.4-3 - Conditions used for compound/prodrug detection in HPLC.....	49
Table 2.4-1 Summary of Ki values of prodrugs/carriers.....	71
Table 2.4-2 - Summary of Ki values of native compounds (drugs only).....	72
Table 2.4-3 - Conditions used for compound/prodrug detection in HPLC.....	77
Table 2.4-4 - Summary of rate of transport and Papp of the prodrugs as determined from Caco-2 Transwell assay.....	87
Table 2.4-5 - Summary of the absolute transport of compounds in the Caco-2 assay in the absence of Gly-Gln.....	88
Table 2.4-6 - Summary of Efflux data and Caco-2 data for prodrugs	92
Table 2.4-1 pGEM-T easy ligation reaction setup	129
Table 2.4-1 Sequences of the mutagenic primers	143
Table 2.4-2 List of primers used for introducing FLAG tag in hPepT2	145
Table 2.4-3 Summary of one sample t-test on hPepT2 and hPepT1 mutants with their respective wild type constructs	147
Table 2.4-4 Table showing the equivalent residues of the mutated hPepT2 residues in rPepT1 and hPepT1	154

1 Introduction

1.1 Protein digestion

Proteins are very important constituents of our daily diet as they are the main source of nitrogen and amino acids required for protein synthesis, energy production and to maintain cellular functions. These proteins are subjected to hydrolysis by proteases and peptidases secreted by the stomach and pancreas or by the enzymes bound to the brush border membrane of enterocytes, leading to generation of a variety of short and medium sized peptide chains and single amino acids. Earlier it was believed that proteins were digested to their constituent amino acids, which was later absorbed in the intestine. These experiments were carried out on intestinal mucosal lining and di-peptides which were not hydrolysis resistant (Newey and Smyth, 1959). Hence, the question as to whether the majority of hydrolysis of peptides took place in the lumen or after they are transported into the cells remained unclear. With the advent of molecular cloning techniques and bioinformatics approach coupled with heterologous gene expression systems it was understood that the breakdown products of proteins are absorbed as both amino acids and as smaller di- and tri- peptides (Gilbert *et al.*, 2008).

1.2 Membrane transport proteins

The cell or plasma membrane is a structure composed of proteins, lipids and carbohydrate moieties that acts as a physical barrier separating the inside of a cell and its organelles from the outside (Singer and Nicolson, 1972). The cell membrane is semi-permeable in nature, a feature attributed by its phospholipid bilayer structure having proteins embedded in the cell membrane which help facilitate the movement of water molecules via integral protein channels called aquaporin ((Huang *et al.*, 2003)Huang *et al.*, 2003), water soluble solutes, ions and other nutrients (non-lipid soluble) through the cell membrane. These transporter proteins transport solutes in and/or out of the cell to help absorb essential nutrients and eliminate metabolic waste which in turn help maintain homeostasis in the cell.

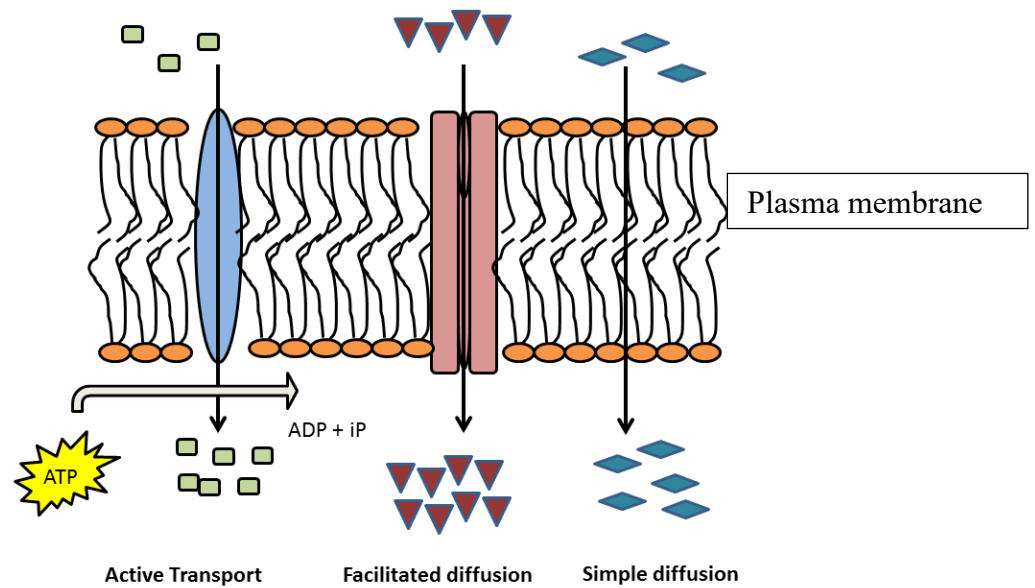


Figure 1.3.1-1 - Diagram showing various basic modes of transport of solutes/molecules into the cell

1.3 Types of transport proteins

1.3.1 Channel-type facilitated diffusion:

The transport of solute occurs through channels or pores present within the membrane, wherein solute molecules diffuse from a region of its higher concentration to a region of lower concentration.

1.3.2 Carrier-type facilitated diffusion:

In this type of transport, the transporter binds to the solute molecule, translocates along with the bound solute to the opposite side of the membrane, releases the solute, and then returns to its original position. Carrier mediated transport can further be classified into primary active transport and secondary active transport depending on the stage at which energy is utilised.

1.3.3 Primary active transport:

This is a process where the carrier transport directly requires energy. For example, the Na^+/K^+ exchanger, where in the transporter utilizes the energy released from the hydrolysis of ATP to transport three Na^+ ions in exchange for two K^+ ions.

1.3.4 Secondary active transport:

A process where there is no direct utilization of energy, but makes use of conditions such as an ion electrochemical gradient, created as a result of primary active transport. For example the $\text{Na}^+/\text{glucose}$ transporter, which couples the movement of glucose to movement of Na^+ from outside (higher concentration of Na^+) to the inside of the cell (lower concentration of Na^+) created by Na^+/K^+ exchanger (primary active transport) in the presence of a negative membrane potential.

Active transporters can be further classified as uniporters, symporters and antiporters.

1.3.5 Uniporters

These catalyse the transport of a single solute species and therefore are independent of movement of other solute molecules (e.g. GLUT1 transporter transports glucose into the cell by carrier-mediated facilitated diffusion).

1.3.6 Symporters

These catalyse the transport of two or more solute molecules in the same direction (e.g. PepT1, where in the transport of peptides into the cell is coupled to movement of H^+).

1.3.7 Antiporters

These catalyse the exchange of one or more type of solute molecules for another (e.g. Sodium hydrogen exchanger, which transports H^+ in the opposite direction to that of Na^+)

Genome-wide sequencing study coupled with biochemical and molecular genetic analysis has revealed the occurrence of a large number of primary and secondary transporter families. The ATP-binding cassette (ABC) superfamily and the major facilitator superfamily (MFS) seem to occur ubiquitously in all living organisms. These two superfamilies account for almost half of the transporters encoded in microbes and also in higher organisms (Pao *et al.*, 1998). For the purpose of the current study only the MFS family of peptide transporters will be considered.

1.4 Major Facilitator Superfamily (MFS)

Major facilitator superfamily of transporters are single polypeptide, secondary carrier proteins which have the ability to transport small solutes in the presence of chemiosmotic ion gradients (Pao *et al.*, 1998). The number of families within the MFS category was soon increased to 29 (Saier *et al.*, 1999), since its initial classification by Pao *et al.* 1998, when it only had 17 families, and now includes 74 families of solute linked carrier (SLC) proteins (Reddy *et al.*, 2012). The proton-coupled oligopeptide transporter (POT) family is one of the families within the MFS superfamily. The solute carrier protein family (SLC15) under study belongs to the POT family of transporters.

1.5 Proton-coupled oligopeptide transporters (POT)

POTs, also called peptide transporter (PTR) proteins, are a class of secondary active transporters which use an inwardly directed proton gradient for the transport of solutes into the cell. POT proteins are found to have a structure with putative 12 transmembrane domains (TMD) (Paulsen and Skurray, 1994; Steiner *et al.*, 1995). Proteins belonging to POT family have been found in bacteria, yeasts, plants and mammals (Meredith and Boyd, 2000). The size of the proteins in this family has been found to vary with the organism and their position in the evolutionary tree, thus the bacterial transporters have

smaller number of residues (between 463-500 amino acids) when compared to animals (707-786 amino acids)(Saier *et al.*, 1999)

1.6 Brief research into mammalian peptide transporters

By the beginning of the 20th century there had been a lot of debate as to what happens to protein once it was consumed. It was initially thought that proteins were digested to their constituent amino acids which would then be absorbed in the intestine (Newey and Smyth, 1959). This concept could not be challenged, as techniques for determining peptides in blood had not been established. It was assumed that the mechanism of peptide transport was similar to the transport of amino acids and sugars, wherein Na^+ -(amino acid/sugar)-carrier protein complex responds to the Na^+ gradient established by the Na^+ - K^+ -ATPase (Crane, 1962; Parrish and Kipnis, 1964; Riklis and Quastel, 1958). This sodium dependent transport of peptides was not observed with all di- and tri-peptides suggesting that the mechanism was not coupled to Na^+ transport. It was only in the early 1980's that more understanding was gained with respect to the fate of the ingested proteins and their absorption in the enterocytes using membrane vesicles (Ganapathy and Leibach, 1983). This study, using brush border membrane vesicles (BBMV) showed that the transport of peptides was coupled to the movement of protons down its electrochemical gradient and that it requires an inner negative membrane potential. The advent of molecular expression cloning technique confirmed this mechanism of peptide transport (Fei *et al.*, 1994) and also that the same peptide transporters were involved in the transport of pharmacological drugs (Boll *et al.*, 1994). This discovery has generated immense interest in understanding the structure and function of peptide transporters for their utilisation in drug delivery.

Several other transporters have also been identified in the intestine, kidney and liver that transport nutrients and drugs. The proton-coupled folate transporter (PCFT) is a high affinity transporter expressed in the intestine which is involved in the absorption of folic acid and anticancer drugs such as methotrexate (Qiu *et al.*, 2006). Proton-coupled amino acid transporter 1 (PAT1) is a low affinity, high capacity POT transporter expressed in the brush bordered membrane of the intestine involved in the absorption of neutral amino acids, the neurotransmitter GABA and drugs such as D-serine to treat schizophrenia (Anderson *et al.*, 2009; Boll *et al.*, 2002; Thwaites *et al.*, 1995). Organic anion transporter 1 and 3 (OAT1, OAT3) expressed in the kidney, liver, brain and eye are involved in the transport of estrone sulfate and organic anions such as probenecid (drug used to treat gout), bumetanide (drug to treat heart failure) (Kusuhara *et al.*,

1999). Besides the above mentioned transporters human apical sodium-dependent transporter (hSABT), glucose transporter 1 (GLUT1), monocarboxylate transporter 1 (MCT1) and sodium dependent vitamin C transporter (SVCT) have also been suggested as possible targets for prodrug strategy (Borthakur *et al.*, 2012; Kolhatkar *et al.*, 2012; Luo *et al.*, 2011; Matsushita *et al.*, 2012)

1.7 *SLC15* peptide transporters

Solute carrier (*SLC15*) peptide transporters are part of the proton coupled oligopeptide (POT) family of transporters which use proton motive force to transport solutes into the cell. This movement of solutes also requires that the cell maintains an inner negative membrane potential to bring about the movement of solutes (Daniel *et al.*, 2006). There are four protein isoforms that have been identified in this family of peptide transporters namely *SLC15A1* (PepT1), *SLC15A2* (PepT2), *SLC15A3* (PHT2) and *SLC15A4* (PHT1) (Fei *et al.*, 1994; Liu *et al.*, 1995; Sakata *et al.*, 2001; Yamashita *et al.*, 1997). This project is directed towards understanding the structural and functional aspects of PepT1, PepT2 and PHT1 plasma membrane proteins. PHT2 has been predicted to be localised on the lysosomal membrane (Sakata *et al.*, 2001) hence has not been included in the current study.

1.7.1 PepT1 (*SLC15A1*)

Rabbit PepT1 (rPepT1) was the first mammalian POT protein isolated and cloned by using expression cloning technique, in which rabbit small intestine cDNA library was screened by heterologous expression in *Xenopus laevis* oocytes and C-14 labelled dipeptide glycyl-sarcosine (Gly-Sar) used as a tracer to carry out transport assays (Fei *et al.*, 1994). Following the discovery of PepT1, homologues have been isolated from human (Liang *et al.*, 1995), rat (Saito *et al.*, 1995) and mouse (Fei *et al.*, 2000). The location of PepT1 in humans has been mapped to chromosome13 q33–34 (Liang *et al.*, 1995). PepT1 is predominantly expressed in the apical membrane of enterocytes of mammalian small intestine (duodenum, jejunum and to a lesser extent in ileum) specifically in the villi of the brush bordered epithelial cells (Ogihara *et al.*, 1996). PepT1 is also expressed in the kidney, with higher expression in the S1 segment of the proximal tubule and reduced expression towards S2 and no expression in the S3 segment of the proximal tubule (Shen *et al.*, 1999). The hPepT1 coding mRNA has also been detected in liver, placenta and skeletal muscle but their involvement in peptide absorption has not been established in these tissues (Liang *et al.*, 1995).

Transport activity can be defined by two parameters, affinity towards substrate (K_m) and maximum transport of the substrate at saturating concentrations ($V_{max}/Capacity$). PepT1 is a low affinity, high capacity peptide transporter which transports a wide array of di- and tri- peptides, including β -lactam antibiotics (Ganapathy *et al.*, 1995), angiotensin converting enzyme inhibitors (ACE) (Hu and Amidon, 1988; Zhu *et al.*, 2000) and various other peptide-mimetic drugs (Brodin *et al.*, 2002; Yan *et al.*, 2011). It is for this very reason PepT1 has been extensively studied over the past 21 years and still continues to be one of the most important transporters studied to improve drug permeability and improve oral absorption of drugs (Brandsch *et al.*, 2008; Foley *et al.*, 2009b). The human PepT1 open reading frame coding sequence is 2127 bp long, coding a protein of 708 amino acids. The encoded protein is approximately 79kDa in size and predicted to have 12 transmembrane domains (TMD), with a large extracellular loop between TMD9 and TMD10 bearing 7 N-linked glycosylation sites, and with the amino and carboxyl termini predicted to be on the cytoplasmic side (Liang *et al.*, 1995).

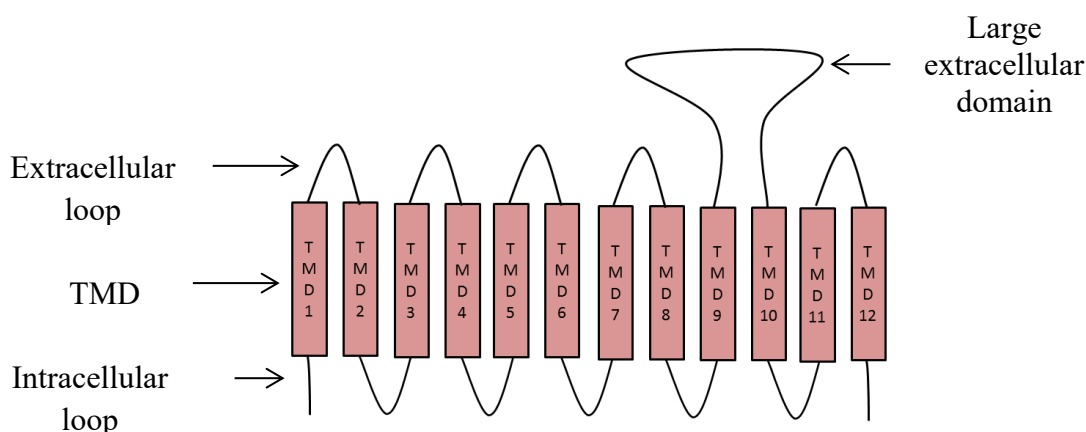


Figure 1.7.1-1 - Cartoon showing 12 TMD structure of PepT1

Epitope tagging and confocal imaging studies on PepT1 were used to partially confirm the 12 TMD structure of PepT1 (Covitz *et al.*, 1998). They established that the region between TMD 1 and 2, 3 and 4, 9 and 10 were extracellular and that region between 2 and 3 was cytoplasmic. They also confirmed that the C- terminal region of the protein was located in the cytoplasmic side. This 12 TMD structure is a common feature of POT transporters except for bacterial homologues, which are found to have 14 TMDs (Newstead *et al.*, 2011; Reddy *et al.*, 2012).

1.7.2 PepT2 (*SLC15A2*)

The next POT gene to be identified was PepT2, isolated by screening the human kidney cDNA library using a rabbit PepT1 cDNA probe (Liu *et al.*, 1995). PepT2 has also been isolated from rabbit (Boll *et al.*, 1996; Boll *et al.*, 1994), rat (Saito *et al.*, 1996) and mouse (Rubio-Aliaga *et al.*, 2000) kidney cDNA library. Human PepT2 (hPepT2) is expressed in the kidney, lung (Bahadduri *et al.*, 2005), mammary glands (Alcorn *et al.*, 2002), chodroid plexus (Shu *et al.*, 2002; Teuscher *et al.*, 2004) but not in the intestine. The hPepT2 gene has been mapped to be located on chromosome 3 q13-33.

PepT2 is a high affinity low capacity transporter involved in the absorption of amino nitrogen and certain drugs in the kidney; hence it also plays a very important role in nutrient re-absorption in addition to PepT1. PepT2 also requires a H^+ gradient to energise the absorption of di-peptides, tri-peptides and also β -lactam antibiotics into the cells (Liu *et al.*, 1995). This protein exhibits 50% amino acid identity and 70% sequence similarity to the human PepT1 transporter (Liu *et al.*, 1995). hPepT2 has an open reading frame of 2190 bp which codes a protein with 729 amino acids. PepT2 is also predicted to have 12 putative TMD with a large hydrophilic loop between TMD9 and TMD10, and five potential protein kinase C phosphorylation sites.

1.7.3 Peptide Histidine Transporter (PHT1)/ *SLC15A4*

PHT1 was isolated from rat brain using cDNA probes coding human PepT1 (Yamashita *et al.*, 1997). PHT1 has been reported to exhibit high affinity proton coupled co-transport of L-Histidine ($K_m = 17\mu M$). The transport of Histidine was inhibited by di-peptides and tri- peptides such as Histidine-Leucine, Methionine-Methionine, Glycine-Glycine, Glycine-Leucine, Glycine-Glycine-Glycine but not by other single amino acid such as glycine, glutamate, leucine, methionine, and aspartate. This shows that PHT1 is unique compared to PepT1 and PepT2 in that it has the added ability to transport single amino acid Histidine in addition to di and tri- peptides. Rat PHT1 protein is predicted to consist of 572 amino acid residues with 12 transmembrane domains with a predicted mass of 64.9 KDa. PHT1 shares a 50% sequence similarity with the plant (*Arabidopsis thaliana*) transporter NTR1 which is a high affinity oligopeptide transporter (Yamashita *et al.*, 1997). PHT1 shows lesser sequence similarity with the mammalian peptide transporters PepT1 (32%) and PepT2 (27%). Rat PHT1 mRNA has been detected with high concentration in rat brain (hippocampus, choroid plexus, cerebellum, and pontine nucleus) and eye and comparatively lower amounts in the lung, spleen and none in the

pancreas, kidney, intestine, liver, skeletal muscle or heart (Yamashita *et al.*, 1997). It has been predicted that PHT1 protein could play an active role in the uptake of neuromodulators (oligopeptides) and in the removal of degraded neuropeptides in the brain. Using bioinformatics approach several putative splice variants were detected for PHT1 in humans (hPHT1) which showed approximately 89% sequence identity to that of rat PHT1 (Botka *et al.*, 2000). Unlike rat PHT1, hPHT1 mRNA has been detected in skeletal muscle, kidney and intestine showing that the distribution of PHT1 protein could vary with species (Botka *et al.*, 2000). In a study performed to characterise the POT transporters present in the retina, it was found that PHT1 transcripts were present in the human and bovine retinal pigment cells and also in the retinal pigment epithelium cell line (ARPE-19) (Ocheltree *et al.*, 2003). Retinal pigment cells form a barrier which controls the diffusion of molecules between the retina and blood. ARPE-19 cell line did transport Glycyl-sarcosine (Gly-Sar, a hydrolysis resistant di-peptide) which is a POT substrate, but the transport rate was not enhanced by lower pH conditions. Also Gly-Sar transport was not inhibited by L-histidine which is a substrate for PHT1. It was found that the Gly-Sar transport seen in RPE cells was mediated by endocytotic pathway and not PHT1 mediated as previously proposed. This study suggested that PHT1 transporter might not be expressed on the plasma membrane of retinal pigment epithelia but on the lysosomal membranes to facilitate the removal of peptides resulting from the degradation of proteins within the lysosomes in RPE cells (Ocheltree *et al.*, 2003).

In another study the human PHT1 (hPHT1) cDNA was transiently transfected in COS-7 cells, which subsequently showed histidine, carnosine (di-peptide) and valacyclovir (drug) transport but not Gly-Sar (di-peptide) transport (Bhardwaj *et al.*, 2006). hPHT1 expressing cells showed higher transport rate of histidine and carnosine at pH 5 compared to pH 7.4 which is a characteristic feature of POT transporters. Western blot analysis showed the expression of hPHT1 in the stomach, duodenum, jejunum, ileum and colon. hPHT1 has been reported to have 86.5% sequence identity to rat PHT1. In the same study it was also observed that the COS-7 mock transfected cells (negative control) were reported to show a high background of histidine transport showing the presence of endogenous histidine transporters in COS-7 cell line.

The di-leucine motif (LZ, Z = A, V, I or L) usually found in the cytoplasmic end of proteins which directs proteins towards the lysosomal membrane was found but in N terminal sequence of hPHT1. However, the role of this di-leucine motif in hPHT1 was not addressed (Bhardwaj *et al.*, 2006). PHT1 and PepT2 mRNA was detected in rat

thyroid follicular cells using RT-PCR (Romano *et al.*, 2010). PepT2 was found to mediate peptide transport in the thyroid follicular cells by using fluorophore conjugated di-peptide derivative Ala-Lys-AMCA which is substrate of SLC15 peptide transporters. Although PHT1 mRNA was detected in the thyroid cells, there was no evidence of inhibition of Ala-Lys-AMCA by L-histidine, which has been reported to be a PHT1 substrate. This study concluded that PHT1 protein could be localised in the membranes of organelles such as lysosomes and early endosomes and not on the plasma membrane as previously reported (Ocheltree *et al.*, 2003; Sakata *et al.*, 2001; Yamashita *et al.*, 1997).

In a study conducted to determine the mechanism by which muramyl peptides (constituents of bacterial glycoproteins) are presented to the cytosolic NOD1 and NOD2 receptors to trigger an immune response, it was found that PHT1 mediated the transport of the processed NOD1 and NOD2 ligands from the endosome into the cytosol, triggering the release of NF- κ B which in turn stimulates an immune response (Lee *et al.*, 2009; Sen and Baltimore, 1986). This effect of NOD1 and NOD2 ligands in stimulating NF- κ B was substantially reduced in HEK293T cells (which endogenously express PHT1) when siRNA was used to knockdown PHT1 expression, confirming the participation of PHT1 in NOD1 and NOD2 ligand signalling (Lee *et al.*, 2009). The PHT1 transporter was localised to the endosome membrane as visualised from the immunofluorescence experiments (Lee *et al.*, 2009). PHT1 transporter has also been reported to be expressed on the mammalian dendritic cells which together with NOD1 and NOD2 receptor trigger the signals required to stimulate an immune response to bacterial peptides (Nakamura *et al.*, 2014). Furthermore, PHT1 has been implicated to play an active role in the manifestation of lupus (autoimmune disease) (Baccala *et al.*, 2013). It was found that lupus mice models with mutations in the PHT1 transporter showed reduced symptom of lupus, with a reduction in the amount of type 1 INF (interferons) which are characteristically upregulated in patients with lupus. These studies implicate PHT1 as playing an important role in the immune system.

1.7.4 Peptide Histidine Transporter (PHT2)/(SLC15A3)

PHT2 was first cloned from rat brain cDNA library (Sakata *et al.*, 2001). This has been reported to be similar in function to PHT1, in that it transports histidine, di-peptides but not single amino acid such as glycine. In 2000 Botka *et al.*, had identified a gene, the

mRNA of which was found to be highly expressed in lung, spleen, placenta and leukocytes (Botka *et al.*, 2000). It was only after the cloning of PHT2 from rat, that the gene identified by Botka *et al.*, was designated as hPHT2, i.e the orthologue of rat PHT2.

Rat PHT2 was found to have an open reading frame of 1748 bp coding a protein with 582 amino acids. The structure of the protein is predicted to have 12 putative transmembrane domains, a di-leucine based lysosome-sorting-motif at positions 19 and 20, glycosylation sites and four potential protein kinase C dependent phosphorylation sites. This protein is predicted to have a molecular mass of 64.6 kDa (Sakata *et al.*, 2001). Rat PHT2 only shows low identity to its mammalian counterparts, 22% identity to PepT1 and 24% identity to PepT2 (Saito *et al.*, 1996). The amino acid sequence of PHT2 was found to be 49% similar to PHT1 and also similar to CHL1 (nitrate transporter) and NTR1 (peptide transporter) from *Arabidopsis thaliana* (Sakata *et al.*, 2001). Interestingly PHT2 was found to have 81% sequence identity to that of mouse cyclic-AMP inducible 1 protein (Botka *et al.*, 2000) which is predicted to be a histidine transporter (Takahashi *et al.*, 2000). PHT2, like PHT1 has also been found to be expressed on lysosomes, endosomes and dendritic cells where it was found to be involved in the bacterial peptide mediated immune response through the NOD2 signalling pathway (Nakamura *et al.*, 2014).

1.8 Basolateral peptide transporters

Peptide transport studies performed on basolateral membrane vesicles derived from rabbit proximal intestine showed the presence of a distinct basolateral peptide transport system driven by proton gradient (Dyer *et al.*, 1990). Existence of a similar proton driven peptide transport system was described at the basolateral membrane of Caco-2 (human adenocarcinoma cell line) cell monolayer (Thwaites *et al.*, 1993). In contradiction to the above reports by Dyer *et al.*, and Thwaites *et al.*, another study carried out on the basolateral transporters in Caco-2 cells suggested that a single low affinity transporter system exists in the basolateral membrane which is not proton coupled but exhibited facilitative transport using [¹⁴C]-Gly-Sar uptake and inhibition studies using various β -lactam antibiotics (Terada *et al.*, 1999). The transporters expressed in the basolateral membrane facilitating the transport of PepT1 substrates still remain unknown.

1.9 Importance of peptide transporters

It had been estimated that PepT1 and PepT2 together are involved in the transport of 400 different di-peptides and 8000 different tri-peptides (Daniel and Kottra, 2004). More recently it has been reported that not all di- and tri-peptides that bind to PepT1 are transported, as some substrates only bind to PepT1 and do not induce the conformational changes in PepT1 required to initiate transport (Vig et al., 2006). Despite the fact that PepT1 and PepT2 cannot transport all di- and tri-peptides they are involved in the absorption of the majority of the pharmaceutical drugs (Brandsch et al., 2008; Ganapathy et al., 1995; Luckner and Brandsch, 2005). PepT1 is over expressed in human malignant ductal pancreatic cancerous cell lines such as AsPc-1 and Capan-2 and in the human fibrosarcoma cell line HT-1080 (Nakanishi et al., 2000). The interesting find is that PepT1 expression in normal pancreatic cells is very low and PepT1 expression is negligible in normal fibroblast cell line IMR-90. This difference in PepT1 expression has been used to deliver anticancer drug bestatin (which is a PepT1 substrate) specifically to tumour cells thereby enhancing drug targeting (Nakanishi et al., 2000) in both *in vitro* and *in vivo* models. This differential expression of peptide transporters could be used to improve drug targeting thereby reducing the side effects caused by systemic exposure of drugs.

1.10 Regulation of peptide transporters

The PepT1 mediated transport of substrates is driven by an inward directed proton gradient (Fei *et al.*, 1994). PepT1 has been predicted to have several putative phosphorylation sites which indicate that it could be regulated by phosphorylation. When Caco-2 cells prior to performing transport experiments were treated with compounds such as PMA, mezerin or PDBu (activators of protein kinase C) there was significantly reduced transport of PepT1 substrate Gly-Sar compared to the untreated Caco-2 cells (Brandsch *et al.*, 1994). This effect was suggested to be due to post translation modification such as phosphorylation of the PepT1 protein leading to reduction in PepT1 protein expression, as the K_m value for the substrate Gly-Sar did not change but with reduced V_{max} .

A study was performed to determine the effect of AMP-activated protein kinase (AMPK) on regulation of hPepT1 in differentiated Caco-2 monolayers using a compound called 5-aminoimidazole-4-carboxamine ribonucleoside (AICAR) (Pieri *et al.*, 2010; Takeda *et al.*, 2013). When the cells are stressed certain mechanisms of

maintaining cellular energy is activated such as the one performed by AMPK wherein the process of ATP synthesis is increased and energy dependent processes are reduced in order to maintain normal cell function (Hallows, 2005; Hardie, 2005). AICAR is suggested to be transported into the cells, which is phosphorylated to form AMP like substrate which in turn activates AMPK (Young *et al.*, 1996). It was found that AICAR treated Caco-2 cells exhibited reduced level of apical uptake of the dipeptide substrate [^3H]-D-Phe-L-Gln, an increase in the tight junctions in the Caco-2 cell monolayers and reduced levels of hPepT1 expressing microvilli like structures as visualised through electron microscope (Pieri *et al.*, 2010). This shows that AMPK regulates PepT1 mediated uptake of peptides which in turn is regulated by the metabolic state of the cells. Understanding these mechanisms of transporter regulation is important as this might negatively affect the delivery of prodrugs which use these transporters as a route of drug entry.

cDNA encoding a 208 amino acid long protein designated as PepT1-RF (regulatory factor) was isolated while performing a cDNA screen in Caco-2 cells, in which residues 18-195 are identical to residues 8-185 in hPEPT1, while residues 1-17 and 196-208 are unique to PepT1-RF (Saito *et al.*, 1995). This splice variant of PepT1 failed to demonstrate any uptake of PepT1 substrate (Gly-Sar) when expressed by itself but when co-expressed with hPepT1 cRNA in *X. laevis* oocytes it was found to function as a pH-sensing regulatory factor showing maximal transport at pH 6.0 compared to maximal transport at pH 5.5 for wild type hPepT1. In another study aimed at identifying the mechanism by which hPepT1-RF regulates PepT1 pH sensitivity, it was found that hPepT1-RF was not detected in either Caco-2 cells or from intestinal samples from healthy individuals, but another mRNA designated as hPepT1-RF1 was detected which was not translated due to deletions in this putative splice variant (Sondergaard *et al.*, 2012). The exact function of the splice variant hPepT1-RF1, if any, has not been established yet.

PepT1 transporter expression has been reported to be controlled by diet and nutritional conditions. When rats were starved, it was found that there was an increase in PepT1 protein expression evident from the increase in the mRNA levels in starved rats compared to control rats (Ihara *et al.*, 2000; Ogihara *et al.*, 1999). The up regulation of PepT1 in Caco-2 cell cultures were observed in presence of PepT1 substrates owing mostly to increased half-life of PepT1 mRNA and an increase in PepT1 mRNA synthesis (Walker *et al.*, 1998). PepT1 has also been suggested to be directed by diurnal

rhythm, which is related to the feeding habits and by the regulation carried out by albumin D site-binding protein (Pan *et al.*, 2002; Pan *et al.*, 2003; Saito *et al.*, 2008).

Characterisation of the rat PepT1 promoter showed that the AP-1 binding site (TGACTCAG) and AARE-like element binding region (CATGGTG) transcription factor binding sites were activated by PepT1 substrates (di-peptides), leading to the up regulation of PepT1 (Shiraga *et al.*, 1999). In Caco-2 cells a high GC rich site within the promoter region has been reported to bind Sp1 transcription factor to maintain basal PepT1 transcription regulation (Shimakura *et al.*, 2005). Another transcription factor Cdx2 was found to be expressed specifically in the intestinal cells which is proposed to regulate the intestine-specific expression of PepT1 by interacting via Sp1 transcription factor in humans (Shimakura *et al.*, 2006).

The effect of hormones on PepT1 activity has been performed by several groups. Insulin hormone was found to increase Vmax of substrate Glycyl-L-Glutamine (Gly-Gln) with no change in the affinity towards the substrate in PepT1 expressing Caco-2 cells 30 minutes after the exposure to the hormone. This effect was mainly attributed to the trafficking of preformed PepT1 proteins in a cytoplasmic storage pool to the plasma membrane (Thamotharan *et al.*, 1999). A similar effect was noticed when rat jejunum and Caco-2 cells expressing PepT1 when exposed to the hormone leptin, wherein the Vmax was found to increase and no change was noticed in the Michaelis-Menten rate constant (Km) of PepT1 substrates, namely Gly-Sar and the β -lactam antibiotic CFX (Buyse *et al.*, 2001).

Thyroid hormone 3,5,3'-Triiodothyronine (T3) reduced Gly-Sar uptake in Caco-2 cells pre-treated with T3 4 days prior to performing the transport experiments. This reduction in Gly-Sar uptake was attributed to the reduction in PepT1 mRNA levels or reduced PepT1 protein stability, but the exact mechanism of action of T3 was not established (Ashida *et al.*, 2002). Hyperthyroidism in rats has been shown to cause a reduction in PepT1 activity due to reduced level of PepT1 mRNA and protein expression (Ashida *et al.*, 2004).

The effect of epidermal growth factor (EGF) has been reported to be dependent on the duration of exposure and its concentration. When the basolateral membrane of Caco-2 cells were treated with EGF for longer than 5 days, it was found to reduce PepT1 expression (Nielsen *et al.*, 2001). This effect was however reversed when the Caco-2 cells were treated with EGF for less than an hour's duration, a dose dependent increase

in peptide uptake was noticed in the Caco-2 cells with increased V_{max} but no change in K_m (Nielsen *et al.*, 2003). The exact reason for this change in behaviour has not been established yet.

PepT1 expression has been found to be upregulated in case of inflammatory bowel diseases (IBD) such as Crohn's disease (CD) and Ulcerative colitis (UC) (Saleh and Elson, 2011). A small non-coding RNA called microRNA (miR-92b) was found to reduce PepT1 expression at the non-transcriptional and translational level during the differentiation of intestinal epithelial Caco-2-BBE cells by targeting the PepT1 RNA at the transcription stage (Dalmasso *et al.*, 2011). The same study also showed that bacterial peptide-induced pro-inflammatory response in the intestinal epithelial cells was suppressed by miR-92b by inhibiting PepT1 expression. Another microRNA, namely miR-193a-3p, has also been shown to regulate PepT1 expression in case of IBD by reducing the expression of PepT1 in colon leading to reduction in inflammatory response in the intestine (Dai *et al.*, 2015).

1.11 Factors affecting the kinetic properties of PepT1

The binding affinity (K_m) of peptide substrates is affected by their net charge, membrane potential (Mackenzie *et al.*, 1996a) and pH, thereby playing a role in determining the rate of absorption of peptides. It was found that decreasing external pH increased the transport rate of negatively charged peptides and to a smaller extent that of neutral peptides, while decreasing transport rate of positively charged peptides. On the contrary, increasing the external pH increased the transport rate of positively charged peptides and reduced that of negative and to a smaller extent neutral peptides (Jensen *et al.*, 2012). This effect on PepT1 transport has been linked to the peptide transport mechanism. The steps involved during peptide transport i.e. binding of the H^+ followed by substrate binding (peptide) to PepT1 transporter explains the way in which external factors alter the kinetic properties of peptide transport.

1.12 Peptide transport mechanism

Several peptide transport mechanisms have been suggested for the PepT1 transporter and some findings contradict the other. Using hPepT1 expressing *X. laevis* oocytes and computer simulations it was suggested that the first step in the activation of the peptide transport was the binding of the proton to PepT1 which has one negative charge in its empty state and that the transport of PepT1 substrate (Gly-Sar) was maximal at pH 6.0 (Mackenzie *et al.*, 1996b). Rabbit PepT1 was reported to transport negatively charged

β -Lactam antibiotic cefixime only in its neutral form with a co-transport of 1 proton and that the transport was independent of the transmembrane proton gradient (Wenzel *et al.*, 1996). Later it was revealed that the PepT1 transports neutral peptides with ratio of 1 H^+ : 1 substrate and is independent of the charge of the substrate but did require the transmembrane H^+ proton gradient as a driving force for PepT1 mediated transport (Mackenzie *et al.*, 1996a; Temple *et al.*, 1995).

At physiological pH 5.5 to 6.0 in the intestine, the proton-to-substrate stoichiometry was found to be 2:1 for acidic dipeptides, 1:1 for neutral dipeptides, 1:1 for basic dipeptides in rPepT1 expressing oocytes (Steel *et al.*, 1997). They also showed that the current induced due to peptide transport was independent of pH but their apparent affinity (K_{mapp}) was influenced by pH. A peptide transport model was proposed by Steel *et al.*, according to which PepT1 has a proton-binding site and a substrate-binding site with a histidine amino acid residue close to the substrate-binding site. For a neutral peptide, a proton binds to the proton binding site (the first step for all peptides transported), followed by the binding of the peptide to the substrate binding site, which is then transported into the cell, releasing the peptide and the proton (Figure 1.7.4-2). In the case of negatively charged (acidic) peptides, after the proton binds to the proton-binding site another proton binds to the negatively charged peptide, neutralizing the substrate net charge, which then binds to the substrate binding site before being transported. For positively charged (basic) peptides, the histidine residue adjacent to the substrate-binding site loses a proton (at higher pH) which then allows the peptide to bind to the peptide-binding site leading to the transport of the peptide. Hence at physiological condition in the intestine neutral and negatively charged peptides are preferentially transported due to favorable pH (acidic) conditions. These results confirmed what had been shown for neutral and negatively charged peptides in rat renal cortex BBMV experiments (Temple *et al.*, 1995). But the proton to peptide ratio as estimated by Temple *et al.*, was 0:1 which is different to 1:1 ratio as predicted by Steel *et al.*, and the exact reason for this disagreement is not known.

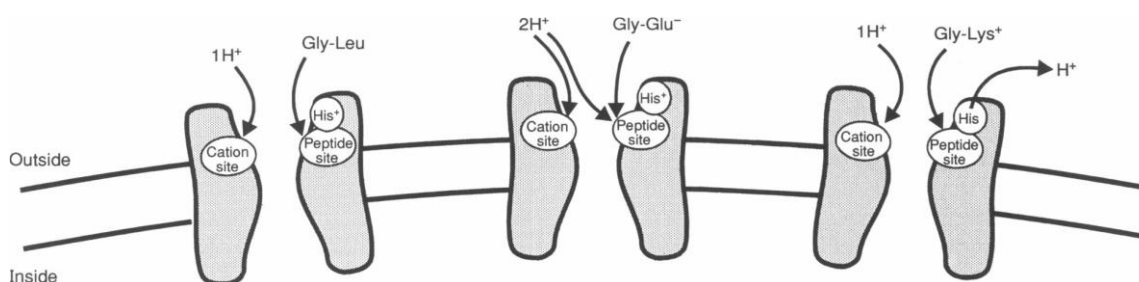


Figure 1.7.4-1- Cartoon showing the stoichiometry of H^+ coupled transport of neutral (Gly-Leu), acidic (Gly-Glu) and basic (Gly-Lys) peptides by PepT1 (Steel et al., 1997)

Another PepT1 mediated substrate transport model was proposed (Irie *et al.*, 2005) as shown in Figure 1.7.4-2. This model was proposed to accommodate the observation that neutral peptides showed decrease in K_m value with reduction in external pH from 7.0 to 5.5 but then the K_m value began to increase with further reduction in pH.

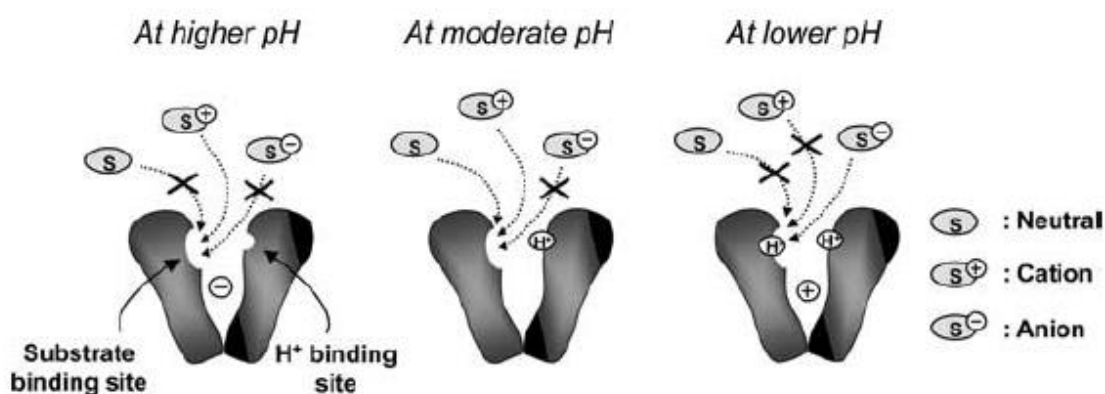


Figure 1.7.4-2 - Cartoon showing the PepT1 mediated transport of charged peptides (Irie *et al.*, 2005)

According to this model, the H^+ at the substrate binding site competitively inhibits the binding of neutral substrates at very low pH thereby reducing the uptake and increase in K_m value. But between pH 5.5 and 6.5 (moderate pH) the H^+ occupying the proton binding site is proposed to have an inductive effect positively effecting the binding of the substrate to the substrate binding site. This explains why PepT1 does not bind to the substrate as efficiently at very low pH. In the case of negatively charged substrates the H^+ at the substrate binding site enables the interaction of the negatively charged substrates and this process of substrate binding is enhanced at very low pH because of the inductive effect. For positively charged substrates the same mechanism proposed for neutral peptides is thought to exist.

1.12.1 Alternating access mechanism of POT transporters

The POT transporter PepTso from *Shewanella oneidensis*, a bacterial homologue functionally similar to PepT1 and PepT2, is the first of its kind to have been crystallized since the discovery of PepT1 in 1994 (Newstead *et al.*, 2011). PepTso was found to have 30% sequence identity to mammalian PepT1 and PepT2 and consists of 14 transmembrane (TMD) helices, with the N-terminal bundle composed of helices H1-H6, connected to the C-terminal bundle H7-H12 via two helices HA and HB (Figure 1.12.1-1).

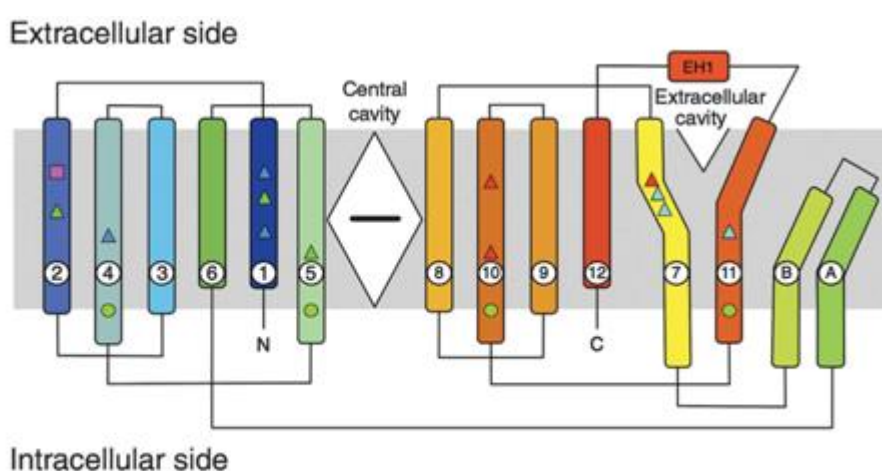


Figure 1.12.1-1- Schematic representation showing the arrangement of Helices (H1- H14), with the proposed binding site (central cavity) of PepT_{so}, extracellular helix 1 (EH1) (Newstead *et al.*, 2011).

Helices HA and HB are not only absent in mammalian peptide sequences but also in fungal and plant sequences, suggesting that they do not contribute towards the mechanism of peptide transport. PepTso crystal shows the presence of a central cavity (peptide binding site) formed by residues from helices H1, H2, H4, H5 from the N-terminal bundle and H7, H8, H10 and H11 from the C-terminal bundle. This crystal structure illustrates the intermediate stage in the mechanism of peptide transport between the outward facing (unbound) state and the inward facing (bound) state (Figure 1.12.1-2)

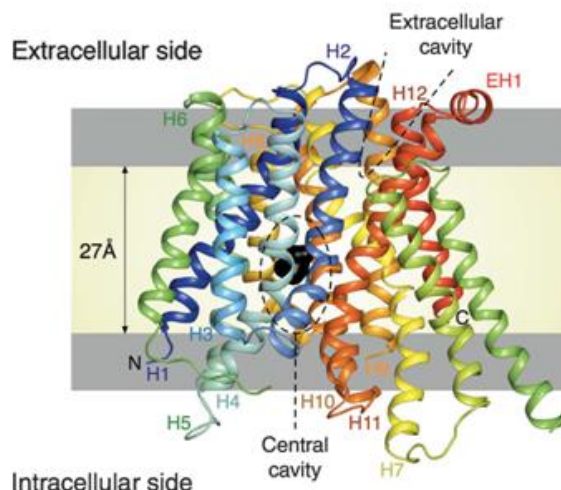


Figure 1.12.1-2 - Crystal structure of PepTso representing the ligand bound (Central cavity) occluded confirmation state (Newstead *et al.*, 2011)

Another POT protein, PepTst, has been crystallized from the bacterium *Streptococcus thermophiles*. PepTst is similar to PepTso and also has two bundles of six transmembrane helices connected by HA and HB helices (Solcan *et al.*, 2012). The mechanism involved in peptide transport has been termed as “alternating access mechanism” (Figure 1.12.1-3) according to which, in the outward facing confirmation (1st step), the extracellular side of the protein is open allowing the binding of proton followed by the binding of peptide. This results in the closure of the extracellular confirmation followed by the opening towards the intracellular space releasing the peptide and protons. In this mechanism the C-terminal half of the protein is proposed to undergo large movements facilitated by glycine residue which alternate the opening and closing of the transporters between the extracellular and cytoplasmic side.

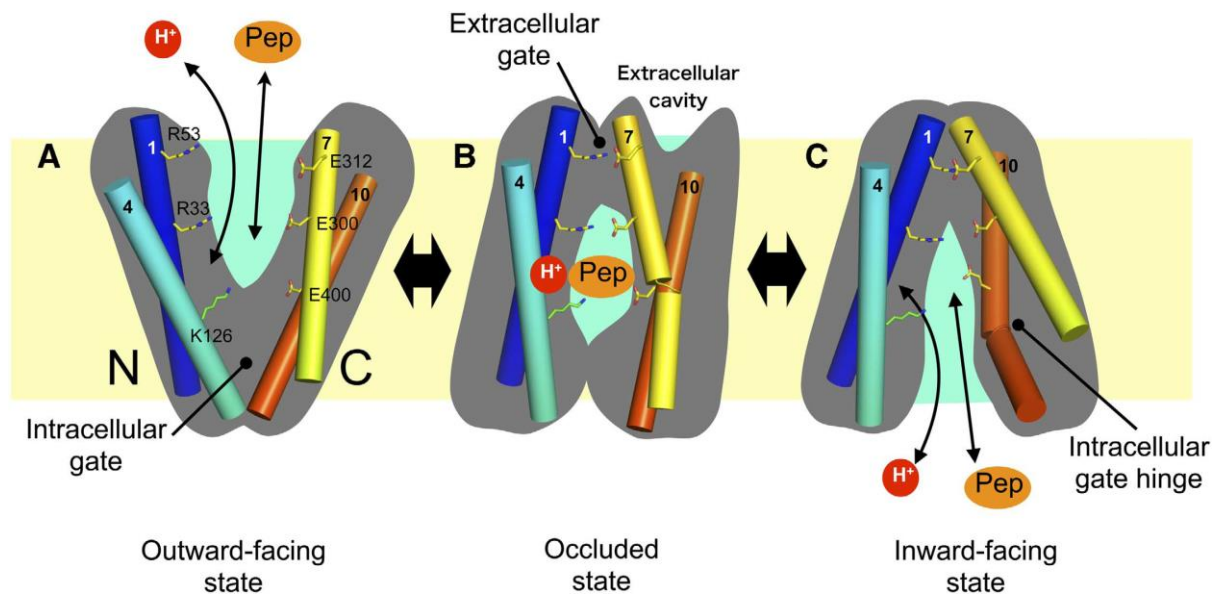


Figure 1.12.1-3 - Alternating access mechanism of Peptide transporter showing the steps involved during proton coupled peptide transport (Solcan et al., 2012)

Several other key features of the POT transporter were also revealed from the structure of PepTst. Two salt bridges between Arginine 53 (R53) and Glutamate 312 (E312) and R33 and E300 were found to affect the peptide transport mechanism (Lyons *et al.*, 2014). Mutating R53 and E312 and alanine reduced the transport by 50% and 70% respectively. But swapping the residues (E53 and R312) reduced the transport by 20% showing that this particular salt bridge only played a supportive role rather than an essential role in peptide transport. However mutating the amino acids in the second salt bridge completely abolished proton driven transport in the protein showing that these residues played a critical role in peptide transport and that E300 plays a crucial role in proton coupling. The ExxERFxyY motif in PepTst, which is a highly conserved motif in POT transporters, was shown to be essential for proton coupling as mutating these residues abolished proton driven transport of substrates. Another important amino acid was E400, which is equivalent to E595 in hPepT1, a highly conserved residue found to be necessary for the expression of a functional protein as mutating this residue to alanine completely abolished protein expression. In case of hPepT1 E595A mutation led to the reduction in transport of Gly-Sar by 95% in PepT1 (E595A) expressing HEK293 cells (Bolger *et al.*, 1998) and in rPepT1 no transport of peptides was detected when the equivalent glutamate residue (E594) was mutated to Aspartic acid (Meredith, 2003) in the *Xenopus leavis* oocyte model.

Since the crystallisation of bacterial POT protein PepTso (Newstead *et al.*, 2011) in the occluded state and PepTst (Solcan *et al.*, 2012) in the inward open state of the peptide

transport cycle respectively several other crystal structures of POT proteins have been obtained representing the substrate bound states of the transporter. PepTso2 from *Shewanella oneidensis* (Guettou *et al.*, 2013) in the inward open state with a bound substrate alafosfalin and GkPOT from *Geobacillus kaustophilus* (Doki *et al.*, 2013) bound to alafosfalin. From the crystal structure of GkPOT and molecular simulation studies, it was revealed that the salt bridge between R43 and E310 is broken by the protonation of E310 and the binding of the substrate to R43, at which point the transporter is in the occluded state with the bound substrate. The release of the proton from E310 and reformation of the salt bridge with R43 releases the substrate bringing the transporter back to the occluded state (Doki *et al.*, 2013). This process thereby brings about the transitioning from the inward open to the occluded state (without substrate). A crystal structure with the outward facing state will be required to complete the picture of the entire alternate access mechanism as the amino acid (in the transporter) and substrate interactions involved in this step during the peptide transport cycle is still unknown.

1.12.2 Structural requirements for PepT1 substrates

Based on experimental observations, several structural features have been suggested for a molecule to be a peptide transporter substrate. Studies on renal brush border membrane vesicles (BBMV) suggested that the presence of an L-amino acid rather than D-amino acid at amino - terminal of the peptide increased substrate affinity at low pH (Daniel *et al.*, 1992). A similar observation was made when affinity studies of L- and D-enantiomers of aminocephalosporins (β -lactam antibiotics) were carried out using rPepT1 cRNA injected oocytes and the Caco-2 cell model (Wenzel *et al.*, 1995). The presence of an α -amino group in a peptide substrate was also found to play an important role in peptide recognition and transport, this was due to the observation that changing the location of the amino group to a β position in the peptide substrate reduced its affinity to peptide transporters (Daniel *et al.*, 1992). In contrast to the above findings Daniel and Adibi showed that the presence of the amino group at the α - position was not necessary for a molecule to be a peptide transporter substrate (Daniel and Adibi, 1994).

It was originally proposed that a molecule should have a peptide bond for it to bind and to be transported by peptide transporters. This observation was disproved when 4-aminophenyl acetic acid (4-APAA), a peptide mimetic of di-peptide D-Phe-L-Ala which lacks a peptide bond, was found to be transported by PepT1 (Temple *et al.*,

1998). Another peptide mimic compound 4-aminomethylbenzoic acid was also shown to be a competitive non-transported inhibitor of PepT1 (Meredith *et al.*, 1998).

1.12.3 Substrate binding template for PepT1

Combining the binding and transport properties of various di- and tri- peptides, β -lactam antibiotics and peptidomimetic compounds, a binding template has been proposed which can be used to determine substrate specificity to PepT1 (Bailey *et al.*, 2000).

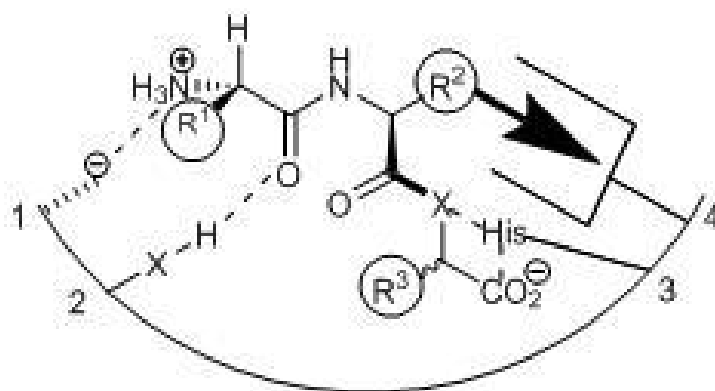


Figure 1.12.3-1 - Substrate binding template for PepT1 showing the structural orientation of important atoms in the binding pocket of PepT1 transporter (Bailey *et al.*, 2000)

Important features of the template are as below:

- A strong binding site (1) for the amino group (NH_3) at the N-terminal end of the substrate (1).
- L- stereochemical orientation for R^1 group increases affinity towards PepT1 compared to D- stereochemical orientation.
- A planar backbone extending from the C_α atom to the R^2 group of the second peptide.
- Hydrogen bond formation with the carboxylic group of the first peptide bond (2).
- Specific orientation of the R^2 , X and the carboxylic group of the second residue.
- Hydrophobic pocket which can accommodate large R groups but in a specific orientation shown by the arrow (4).
- Carboxylic binding site for the second residue (in case of di-peptide) or third residue (in case of tri peptide) with a histidine (3).

- h) The additional space for accommodating the side chain R³.
- i) Permission for the alkylation of the nitrogen of the peptide bond.

The template proposed explains why PepT1 substrates show different binding affinity to PepT1. Binding affinity of PepT1 substrates is determined by the interaction of the substrate with the transporter. If the above mentioned criteria are satisfied by the substrate then it will have high affinity. Not all substrates will interact with the transporter at all the points (as shown in Figure 1.12.3-1) in which case the interactions will tend to be of low affinity.

1.12.4 Important amino acid residues contributing to PepT1 and PepT2

Three histidine (His) residues at position 57 (TMD2), 121 (TMD4) and 260 (ECD between TMD6 and TMD7) are conserved in PepT1 across species. Furthermore analogous His residues at position 87, 142 and 278 in PepT2 (TMD and ECD location as hPepT1) are also conserved across species. Mutating residues at positions His-57 and His-87 to Glutamine (Q) or Asparagine (N) in PepT1 and PepT2 respectively, had detrimental effect on the transport function of the protein, showing that these residues are important for transporter function (Fei et al., 1997). This effect on PepT1 and PepT2 transport has been linked to the possibility that His-57 and His-87 are involved in proton coupling. The H121 and H260 mutants in hPepT1 and H278 mutant in hPepT2 maintained wild type transport and expression characteristics. However H142 in hPepT2 was found to show only 30% of transport compared to hPepT2 wild type even though the surface expression was the same as the wild type showing that H142 is important in maintaining its catalytic activity (Fei *et al.*, 1997). There is a high level of conservation of a positively charged amino acid in TM7 of PepT1 isoforms in mammals, arginine in rabbit, sheep, pig, and humans or lysine in mouse, rat and dog. Mutation of arginine (R) 282 to glutamate (E) in rabbit PepT1 causes uncoupling of the peptide transport to proton movement into the cell thereby reducing the ability of PepT1 to concentrate the substrate above its extracellular concentration (Meredith, 2004). This arginine residue is also conserved at a similar position in PepT2 of mouse, rat and rabbit and could play similar function as in PepT1. Mutation of Tyrosine 167 (Y167) in TMD5 of hPepT1 to alanine, phenylalanine, serine, or histidine completely abolished its transport function but did not affect the trafficking of the protein to the membrane. This showed that Y167 plays an important role in transport function of PepT1 (Yeung *et al.*, 1998). Mutating Tyrosine-12 (Y12), Arginine-282 (R282), Tryptophan-294 (W294) and

Glutamate-595 (E595) to alanine showed that Y12 and R282 had very modest effect of peptide transport whereas W294 and E595 reduced the transport by 80% and 95% compared to the wild type (Bolger *et al.*, 1998). In rPepT1, R282 to Glutamate was found not to be able to accumulate peptide substrate above equilibrium and that the positive residue at position 282 was required for the pH dependent transport of peptide. It was also suggested that R282 formed a salt bridge with aspartic acid (D) 341, which is broken during transport of peptide facilitating the conformational change in PepT1 during the transport cycle (Pieri *et al.*, 2008). A study carried out to determine the function of all the conserved tyrosine (Y) residues in rPepT1 showed that Y12, Y56, Y91, Y167 and Y345 reduced the transport function of PepT1 while Y64, Y287, Y587 did not affect PepT1 transport (Pieri *et al.*, 2009).

1.13 Genetic polymorphism in PepT1

PepT1 transporter is involved not only in the absorption of nitrogen in the form of peptides but also implicated in the transport of pharmaceutically important drugs such as ACE inhibitors, anti-virals and anti-cancer agents (Meredith, 2009). Mutations in the protein could possibly affect this ability of PepT1 to help in the absorption of nutrients and drugs equally. In a study aimed at analysing DNA polymorphism in 44 ethnically diverse individuals it was found that there were 9 single nucleotide polymorphisms (SNPs) which affected the sequence of the protein (non-synonymous polymorphism) in humans (Zhang *et al.*, 2004). Among these 9 SNPs only a proline 586 to leucine mutation (P586L) was found to affect the functioning of protein with reduced amount of transport, low protein expression and reduced expression on the plasma membrane as evident from Western blot analysis and immunocytochemistry tests respectively. There was no change in the affinity of the substrate in any of the 9 SNPs including the P586L showing that P586L could play a role in the expression, trafficking and insertion into the plasma membrane and not in substrate binding and transport. In a similar study where all the exons and introns in PepT1 was screened from 247 ethnically diverse individuals 9 nonsynonymous changes were observed (Anderle *et al.*, 2006). Among the 9 nonsynonymous the phenyl-alanine 28 to Tyrosine (F28Y) showed significant change in affinity without effecting the protein expression compared to the wild type. However, the occurrence of F28Y variant was found to be of very low frequency in the cohort studied. The mRNA splice variant hPepT1-RF was also quantified in this study but was again found not to have a significant impact on PepT1 protein expression. Taken

together it can be seen that there is no functional SNP reported which occurs at a high enough frequency to impact the bioavailability of PepT1 substrates.

1.14 Prodrugs

The original definition for prodrug refers to an agent that must undergo enzymatic conversion from a non-active state to its active state once it reaches the target site, triggering the required pharmacological response (Figure 1.12.4-1) (Albert, 1958; Testa, 2004). A drug is effective if it has low toxic effects and is able to reach the site of action at the appropriate pharmacological concentration to achieve the desired effect. This type of target/site specific delivery is achieved when the target site and the drug share compatible physiochemical properties (Stella and Himmelstein, 1980). An example is Valacyclovir, a prodrug version of acyclovir (antiviral drug), was found to have 4-fold higher bioavailability compared to acyclovir (Jacobson, 1993).

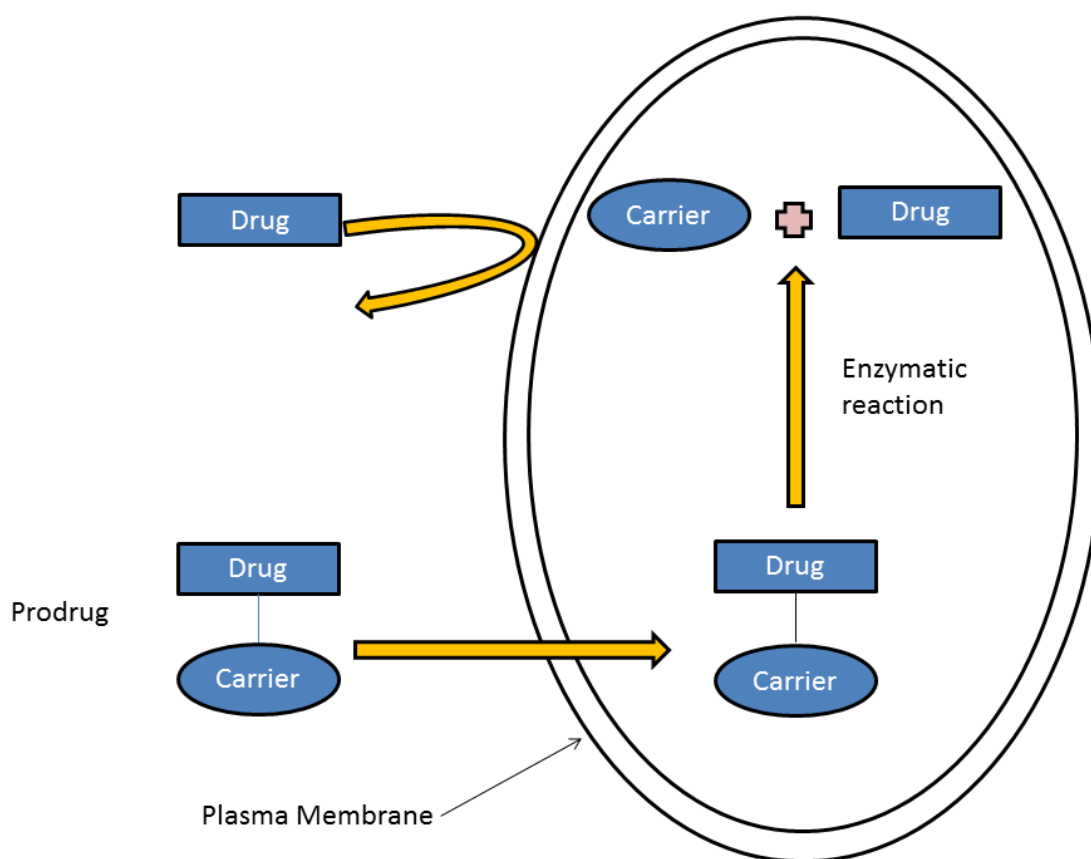


Figure 1.12.4-1 - Diagrammatic representation of prodrug concept

The prodrug approach has been used to optimize the absorption, distribution, metabolism and excretion (ADME) of drugs. In 2010 it had been estimated that 10% of

the medicines marketed globally were prodrugs and in 2008 alone, 33% of all the small molecule drugs sold were prodrugs (Rautio, 2010). The first prodrug designed was methenamine launched in 1899 which contained a formaldehyde based antibiotic, followed by aspirin (Testa, 2004). Later several drugs such as prontosil (antibiotic), isoniazid (anti-tuberculosis drug) were developed: the latter was only designated as a prodrug after 40 years of its initial use since the exact mechanism of action was not known (Huttunen *et al.*, 2011).

Several different strategies have been employed in designing a prodrug. Most common features in the prodrug design involve a carrier molecule directly linked to the active component (drug) which is released by enzymatic cleavage of the prodrug. Sometimes a linker/spacer is used to link the carrier to the drug molecule when direct linking of the drug to the carrier is not possible (Papot *et al.*, 2002).

1.14.1 Classification of prodrugs

Prodrugs have been categorised based on their chemical nature as follows (Testa, 2004):

Carrier-linked prodrugs: the active agent (the drug) is conjugated to a carrier (also known as a pro-moiety), and whose activation occurs by hydrolysis of esters, amides, imines or by an oxidation/reduction reaction. An example is Prontosil, an antibacterial compound in which the active ingredient is sulphanilamide (Foulis and Barr, 1937).

Bio-precursors: these do not contain a carrier but are activated by oxidation, reduction or hydrolysis. An example is clopidogrel (commercial name Plavix) that selectively inhibits platelet aggregation (Savi *et al.*, 2000).

Macromolecular prodrugs: In these prodrugs the active ingredient is linked to a large carrier molecule such as polyethylene glycol (Duncan, 1992).

Drug-antibody conjugates: In these types of prodrugs, the drug, usually a cytotoxic compound, is conjugated to an antibody raised against a specific protein (receptor) in a tumour to improve targeting of the drug (Dubowchik and Walker, 1999).

1.14.2 Applications of pro-drug strategy

The following section details some of the wide areas of application of prodrug strategy to solve problems faced by native drug with respect to solubility, lability of the drugs,

tissue specific delivery of drugs and as a way to improve bioavailability by prolonging the exposure of the drug systemically (Rautio *et al.*, 2008).

1.14.2.1 Improving the solubility of the drug

The solubility of a drug acts as a rate limiting factor in the drug discovery and design process (Horter and Dressman, 2001). These properties of the drug can be modified using the prodrug approach. One of the strategies used to overcome this issue is by using phosphate esters of drugs (prodrug) which release the drug molecule in the presence of endogenous phosphatases (alkaline phosphatase) predominantly found in the apical side of enterocytes (Stella and Nti-Addae, 2007). Here the phosphate group is cleaved from the prodrug releasing the active drug into the cells. An example of this is the HIV protease inhibitor drug Amprenavir which required the patients to take 8 capsules a day to achieve the therapeutic dose. The phosphate prodrug of Amprenavir (Fosamprenavir) was 10-fold more water soluble and required the patients to take only 2 capsules a day to achieve the equivalent dose (Wire *et al.*, 2006).

1.14.2.2 Targeting transporters to improve bioavailability

Amino acid esters and transporter-mediated peptide prodrugs, wherein the amino group is attached to the hydroxyl or carboxyl group of the drug are used to improve drug delivery. These drugs are targeted towards the transporter protein expressed in the intestinal epithelial cells to which the amino acids or peptides act as substrates. An example of this is Midodrine which is a glycine prodrug of desglymidodrine used in the treatment of dialysis hypotension. The prodrug is recognised and transported by PepT1 in the intestine increasing the oral bioavailability of the parent drug from 50% for the native drug desglymidodrine to 93% for the prodrug (Cruz, 2000).

1.14.2.3 Slow release of the drug

Once the drug reaches the systemic circulation it could be rapidly metabolised by the liver, thereby reducing the efficacy of the drugs. This problem of rapid metabolism can be eliminated by using the prodrug approach in which the functional group which is essential for the functioning of the drug but is also metabolically susceptible to modification is masked. An example of this is the prodrug version of β_2 -agonist terbutaline, namely bambuterol, used in the treatment of asthma. Terbutaline is rapidly metabolised in the liver reducing its systemic availability thereby reducing its efficacy. The prodrug bambuterol has a modification on its phenolic group which is slowly

converted to its active form by cholinesterase outside the lungs leading to prolonged therapeutic effect of the drug (Sitar, 1996).

1.14.2.4 To avoid undesirable effect of endogenous enzymes

The conversion of an inactive prodrug using enzymes is a common approach to improve the bioavailability of drugs. However the ubiquitous availability of endogenous enzymes involved in the conversion of the prodrug to its active drug reduces the ability to deliver the drug to a specific tissue where it is required (Denny, 2001). This has been overcome by using antibody-directed enzyme prodrug therapy in which non-ubiquitous or non-human enzyme required for activating the prodrug is separately administered conjugated to an antibody that binds to the specific cells/tissues at the site of action. This enzyme in turn activates the prodrug locally, thereby achieving targeted drug delivery. An example is the usage of prodrug Amygdalin. The enzyme β -glucosidase (extracted from sweet almonds) conjugated to tumour specific antibody is used which catalyses the conversion of amygdalin to glucose, benzaldehyde and hydrogen cyanide (toxin). Here the locally released hydrogen cyanide kills the tumour cells sparing the surrounding healthy cells (Deonarain and Epenetos, 1994). All the above examples of prodrug applications show the versatility of using the prodrug approach as a very effective technique in the tissue specific delivery of drugs and in reducing undesirable side effects.

1.14.3 Aims

- This research was aimed at providing novel insights into the POT family of transporters specifically PepT1, PepT2 and PHT1 with respect to their transport characteristics. PepT1 research was mainly focused on characterising novel prodrug carriers namely cLu-, Thio- and Aib- in utilizing PepT1 to deliver drugs using rPepT1 expressing *Xenopus laevis* oocytes and hPepT1 expressing Caco-2 cell culture models.
- The crystallisation of various bacterial POT proteins in the recent past has revealed several key features of the peptide transport mechanism. It was found that the mammalian POT transporters have a large extracellular domain between the TMD9 and TMD10 which is completely absent in the bacterial POT proteins. Hence experiments were set up to understand the functional significance of the large ECD in mammalian POT proteins using mutated hPepT1 and hPepT2 constructs in which the ECD's were either deleted or swapped between hPepT1 and hPepT2 in order to identify the function of the ECD.
- PepT1 protein has been studied to a very large extent due to its ability to transport a wide variety of di- peptides, tri- peptides and drugs using site directed mutations and various electrophysiology and transport experiments. Experiments were set up to determine if the previously identified functionally important residues in PepT1 mediated transport play a similar role in PepT2.
- The PHT1 protein has been predicted to be unique in its peptide transport characteristic in that it has been found to transport L-histidine amino acid in addition to di- and tri-peptides. The initial reports have claimed that PHT1 is a plasma membrane protein but later reports have suggested that it is localised to the lysosomal membrane. Experiments were set up to investigate the localisation of PHT1 and its ability to transport histidine.

2 Methods

2.1 Materials

2.1.1 Antibiotics

Ampicillin sodium salt (Sigma, UK)

Neomycin (Sigma, UK)

Penicillin/Streptomycin solution (Sigma, UK)

2.1.2 Bacterial cells for transformation

XL1-Blue subcloning grade competent cells: *Escherichia Coli* (Agilent Technologies, cat no: 200130)

2.1.3 Chemicals

All the Chemicals used were obtained from Sigma Aldrich (UK) unless stated otherwise

2.1.4 Clones

Rat *SLC15A4* (ratPHT1): Source Bioscience, UK; Accession no. BC087709

Rabbit *SLC15A1* (rPepT1): Source Bioscience, UK; Accession no. BC087709

Human *SLC15A1* (hPepT1), *SLC15A2* (hPepT2) Donated by Dr Simon Newstead, Oxford University.

2.1.5 Caco-2 Cells

Caco-2 cells: Gift from Professor Munira Kadhim, Department of Biological and Medical Sciences, Faculty of Health and Life Sciences, Oxford Brookes University, Oxford, UK.

2.1.6 Restriction enzymes and Ligases

All restriction enzymes were obtained from New England Biolabs (NEB) unless stated otherwise. Conditions for restriction digest were maintained as per manufacturer's instructions. Ligase enzymes were obtained from Promega UK unless otherwise stated.

2.1.7 Vectors

pXT7: *X. laevis* oocyte expression plasmid Antibiotic marker (Ampicillin); gift from Professor S.L Alper Harvard Medical School, Boston, MA, USA (Kurschat *et al.*, 2006)

pBF: *X. laevis* oocyte expression plasmid Antibiotic marker (Ampicillin); gift from Dr Simon Newstead, Oxford University

pGem-T easy: Antibiotic marker (Ampicillin); Promega UK, (cat no: A1360)

2.2 Molecular biology techniques

2.2.1 Primer design:

Primers were designed using Oligocalc (Kibbe, 2007) to either introduce mutations, the FLAG epitope tag or to sequence the target genes/vectors. Sequencing primers were designed to have a length of 18-22 bases with GC content greater than 40%, T_m of 60°C - 68°C and if possible with G or C nucleotides at the 3' and 5' ends of the primers. Mutagenic primers were between 25 – 60 bases in length with desired mutation in the middle of the primer with $T_m > 78^\circ\text{C}$. To sub clone a gene, new restriction sites present in the recipient vector were included in the primer at the 5' and 3' ends with 6 additional T bases for efficient recognition and cleavage by restriction enzymes. The restriction sites present in a gene or vector sequences were detected using NEBcutter (Vincze *et al.*, 2003). The primers were synthesised by Fisher Scientific (UK).

2.2.2 PCR:

A typical PCR reaction was setup as described in Table 2.2-1. The primers were diluted using nuclease free water (Ambion) as per manufacturer's instruction to a final concentration of 10 μM and stored at -20°C until required. The dNTPS (dATP, dTTP, dCTP, dGTP) stock was prepared and aliquots were stored at -20°C. Prior to setting up the PCR reaction, all the constituents except for the Pfu DNA polymerase (Promega) were thawed and placed on ice while assembling the reaction mixture.

Table 2.2-1 - PCR reaction setup (50µl reaction)

Reaction Contents	Volume (µL)
DNA template (100 ng/µl)	1
Forward primer (10 µM)	1
Reverse primer (10 µM)	1
dNTPS (10 mM each)	1
Pfu 10x reaction buffer	5
Pfu DNA polymerase	0.5
Nuclease free water	40.5

Table 2.2-2 - PCR protocol for amplification of plasmid DNA using Pfu DNA polymerase using “Ramp” method

Step	Temperature (°C)	Time (Minutes)	Number of cycles
1	95	1	1
2	94 63 72	0.5 1 (1min/Kb)	5
3	94 55 72	0.5 1 (1min/Kb)	5
4	94 45 72	0.5 1 (1min/Kb)	5
5	4	Hold	NA

The ramp method was used for carrying out all PCR reactions unless otherwise stated. This method uses three different annealing temperatures during the entire PCR reactions, thereby increasing the chances of amplifying the desired gene without the need for optimising PCR reactions for individual primer/template combination.

2.2.3 Purification of PCR products:

Since the RAMP method can produce multiple PCR products, the PCR products were subjected to gel electrophoresis in order to separate the various DNA products based on their size, after which the DNA band of the required length (bp) was isolated from the gel and purified (Section 2.2.4 and Section 2.2.5).

2.2.4 Gel electrophoresis

Gel electrophoresis was used to separate DNA fragments based on their size subsequent to PCR amplification or restriction enzyme double digest to extract the desired DNA fragment. In case of single restriction digest reaction gel electrophoresis was also

performed to check if the DNA had been linearized completely. 1% agarose gels were prepared using Type I-A, low EEO agarose, TRIS-Borate-EDTA (TBE) buffer (Invitrogen) along with ethidium bromide solution (10 mg/ml). The DNA was mixed with 6X blue/orange loading dye (Promega, UK) at a ratio of 6:1 prior to loading the gel. 8 µl of 1 Kb ladder (Promega, UK) was loaded into the first well in the gel followed by the DNA samples to be analysed. The gels were run at 80 V for 1 hour before visualising the gel on a UV transilluminator. Photographs of the gels were taken using an Uvitec camera with a hood (Cambridge, UK). When required, DNA bands (of the desired size) from the gels were excised using a sterile scalpel and stored in 1.5 ml centrifuge tubes. Care was taken not to expose the gels to UV light for extended periods, in order to avoid DNA damage.

2.2.5 Purification of DNA obtained from Gel Electrophoresis

The excised bands from the above step were purified using QIAquick gel extraction kit (Qiagen). DNA purification was performed as per manufacturer's instructions. The final elution of purified DNA was made using 30 µL of Nuclease free water (Qiagen) and stored at -20°C until required.

2.2.6 Plasmid Extraction and purification from *E. coli*

5ml of bacterial cultures grown overnight on a shaker incubator at 37°C were used for extraction of plasmids carrying the genes of interest. The Wizard Plus SV Miniprep DNA purification system (Promega, UK) was used for plasmid extraction and purification using manufacturer's instruction. Plasmid DNA was eluted into final volume of 30 µl of Nuclease free water (Ambion).

2.2.7 Restriction digest reactions

Restriction digest was used to prepare DNA for cloning genes of interest into plasmid vectors (pXT7, PBF) and also for linearizing DNA template for in-vitro mRNA synthesis. In case of double digest, where two restriction enzymes were used in a single reaction the compatibility of the enzyme buffers were checked using the online program "Double digest finder" from NEB. The enzyme compatibility check was carried out at the stage of designing primers in order to select only enzymes which were compatible. A 50 µl restriction digest reaction was set up as shown in Table 2.2-3. If a double digest was needed then 0.5 µl of the second enzyme was added and the final volume adjusted to 50 µl using Nuclease free water. Once the reaction mix was assembled, it was

digested at 37°C for 1 hour followed by purification using QIAquick PCR purification kit (Section 2.2.8)

Table 2.2-3 - Restriction digest reaction setup

Reaction constituents	Volume (μl)
DNA (1 μg)	1
10X reaction buffer	5
100X BSA (if suggested by manufacturer)	0.5
Restriction enzyme	0.5
Nuclease free water	to 50

2.2.8 Purification of DNA using QIAquick PCR purification kit

The DNA obtained from restriction digest reactions and PCR reactions (where gel electrophoretic separation was not required) was purified using QIAquick PCR purification kit (Qiagen). All the plasmid constructs used in this project were less than 10 Kb in size, which is maximum length of DNA that can be purified using the kit. QIAquick PCR purification procedure was carried out as per manufacturer's instructions. The final elution of purified DNA was made using 30 μl of Nuclease free water (Ambion) and stored at -20°C until required.

2.2.9 Cloning

2.2.9.1 De-phosphorylation of vectors using Antarctic phosphatase

To prevent re-ligation/self-ligation of restriction digested vector, the vector was treated with Antarctic phosphatase (NEB). Antarctic phosphatase removes the 5'-phosphate group from the DNA thereby preventing the ligase enzyme from re-ligating the vectors. A 50 μl de-phosphorylation reaction was setup as shown in Table 2.2-4. The assembled reaction was incubated for 30 minutes at 37°C followed by enzyme inactivation by incubating the reaction mix at 65°C for 5 minutes. This de-phosphorylated vector requires no further purification due to enzyme deactivation, and was directly used to assemble the ligation reaction.

Table 2.2-4 - Components of dephosphorylation reaction

Reaction constituents	Volume (μl)
Vector DNA	44
10X Antarctic phosphatase buffer	5
Antarctic phosphatase enzyme	1
Total	50

2.2.9.2 Ligation

Purified insert (target gene) and de-phosphorylated vector DNA were ligated using T4 DNA ligase (NEB). The insert to vector ratio of 2:1 and 3:1 was used for ligation reactions. The amount of insert required to set up a ligation reaction was calculate using the formula

$$\text{Insert (ng)} = N \times [\text{length of insert (bp)} / \text{length of vector (bp)}] \times \text{vector (ng)}$$

Where N is the insert to vector ratio

The ligation reaction was assembled according to the Table 2.2-5. In case of negative controls the insert DNA was replaced with DNase and RNase free water to assess vector re-ligation. The reactions were incubated overnight at 16°C and then transformed into bacteria as described in section 2.2.9.3.

Table 2.2-5 - Components of a DNA ligation reaction

Components	Volume (µl)
Vector DNA	X*
Insert DNA	Y*
T4 DNA ligase	1
T4 DNA ligase reaction buffer	1
Total volume	10

Note: * refers to the volume calculated according to the molar ratios and this varied for every reaction setup

2.2.9.3 Transformation of *E. coli* bacteria

XL1-Blue subcloning-grade competent *E. coli* cells (Invitrogen, USA) were routinely used to transform plasmid DNA (vectors carrying genes of interest). Approximately 5 ng to 50 ng of plasmid DNA was incubated with 50 µl of *E. coli* on ice for 20 minutes in thin walled 0.5 ml centrifuge tubes. This mixture was then given a heat shock at 42°C for 45 seconds followed by cooling the tubes immediately on ice for 2 minutes. This was then transferred into 15 ml tubes containing 900 µl of pre-warmed (37°C) SOC medium (Invitrogen) and placed in a shaker incubator at 37°C for 30 minutes. 200 µl of this mixture was plated onto LB agar media supplemented with 100 µg/ml ampicillin and incubated overnight at 37°C. The transformed colonies were analysed using cracking technique (Section 2.2.9.5) and positive colonies were grown overnight in 5ml of LB broth supplemented with 100 µg/ml ampicillin. These cultures were then used to

make permanent glycerol stocks (Section 2.2.9.4) and the remaining culture was subjected for plasmid DNA extraction and purification (Section 2.2.6). The purified DNA was stored at -20°C.

2.2.9.4 Preparation of bacterial glycerol stock

Overnight grown *E. coli* carrying plasmid DNA was used to prepare glycerol stocks. 140 µl of *E. coli* culture was mixed with 500 µl of 80% glycerol in dH₂O in 1.5ml sterile centrifuge tube. This stock was stored at -80°C freezer for long-term storage. When required, the bacterial cultures were revived by inoculating a small scoop of glycerol stock into LB agar supplement with 100 µg/ml ampicillin and grown overnight at 37°C in a shaker incubator.

2.2.9.5 Cracking method for analysing bacterial transformants

E. coli bacterial colonies obtained from transformation procedure (Section 2.2.9.3) were analysed using cracking technique (Personal communication, Dr Isabel Bermudez-Diaz, Oxford Brookes University, Oxford, UK). This technique enables a quick screening of large number of colonies and identification of positive transformants from gel electrophoresis of lysed bacteria before DNA extraction and sequencing. The cracking solution stock was prepared by dissolving the sucrose in dH₂O at 65°C followed by addition of the remaining constituents listed in the Table 2.2-6. The lysis buffer was prepared by combining 1:10 ratio of cracking solution and 6X loading dye (Promega). Approximately 12-16 colonies were screened from each plate. All the steps mentioned in this technique except gel electrophoresis were performed under a laminar airflow cabinet to avoid contamination of bacterial colonies.

Table 2.2-6 - Constituents of cracking solution

Constituents	Volume/Amount
Sucrose	25 g
10% SDS	2.5 ml
5M NaOH	5 ml
dH ₂ O	42.5 ml
Total volume	50 ml

Individual bacterial colonies were transferred into 1.5 ml sterile centrifuge tubes containing 15µl of nuclease free water and mixed by pipetting up and down. This pipette tip was then transferred into 1.5 ml sterile centrifuge containing 200 µl of sterile LB broth supplemented with 100 µg/ml ampicillin, which was stored at room

temperature until required. 7 µl of lysis buffer was added to the vials containing the colonies, mixed and immediately loaded into the 1% agarose gel for electrophoresis. After running gel for 40 minutes at 80V the DNA band patterns were compared with that of negative control (vector only). The DNA band patterns that looks different to that of the negative control were identified as potentially positive transformants and the corresponding 200 µl broth solutions from before were transferred into 5 ml LB broth with 100 µg/ml ampicillin supplement and grown overnight at 37°C. Glycerol stocks for these overnight grown colonies were made and the plasmid DNA was extracted using mini prep and sent for sequencing to confirm the presence of the insert DNA.

2.2.10 In vitro mRNA synthesis

5 µg of plasmid DNA was linearized overnight using restriction enzyme MluI (NEB) for gene constructs cloned in PBF vector and NdeI restriction enzyme (NEB) for genes cloned in pXT7 vector. The restriction enzymes were selected only if they did not have restriction digest site within the gene under study. The linearized DNA was purified using QIAquick PCR purification kit (Qiagen). The DNA was eluted into 30 µl of Nuclease free water. The concentration of the DNA was measured using Nanodrop (ND-1000, Thermo Scientific). If the concentration of DNA was less than 160 µg/µL then the DNA was concentrated by reducing the volume of water using a speed vac (DNA120, Thermo Fisher Scientific) The dried DNA pellet was then reconstituted in nuclease free water to obtain the concentration of 1 µg in 6 µL. The mRNA synthesis kit was mMessage mMachine SP6 (Ambion) for vectors with SP6 promoter and mMessage mMachine T7 for vectors with T7 promoters respectively. The mRNA was synthesised using the manufacturer's instructions. Purification of mRNA was performed using RNeasy Mini Kit (Qiagen) as per the manufacturer's instructions. The concentration of the RNA was checked using Nanodrop after which 2 µl aliquots of mRNA were placed in 0.5 ml RNAase free tubes and stored at -80°C until required.

2.2.11 Site directed mutagenesis

Site directed mutagenesis was used to perform single point mutations to study the effect the mutation had on the transport function of the proteins. The QuikChange site-directed mutagenesis kit (Stratagene, USA) was used to introduce single point mutations. The primers were designed as suggested in the kit wherein the desired mutation should be in the middle of the primer flanked by 10 to 15 bases on either side of the mutated sequence. The length of the mutagenic primers were between 25 and 45 bases having a

minimum of 40% GC content and with a melting temperature (T_m) at or above 78°C. The T_m for the primers were calculated using the formula

$$T_m = 81.5 + 0.42(\%GC) - 675/N - \% \text{ mismatch}$$

where % GC and % mismatch were whole numbers and N = number of bases in the primer. The PCR protocol used were set up per manufacturer's instructions (Table 2.2-7)

Table 2.2-7 - PCR method of site directed mutagenesis

Segment	Cycles	Temperature (°C)	Time (seconds)
1	1	95	30
2	18	95	30
		55	1
		68	2 minutes/kb of plasmid length

2.3 *Xenopus laevis* oocyte preparation, maintenance and cRNA injection

Xenopus laevis frogs were maintained at the animal house facility (Oxford University), which follows the guidelines of the 1986 Scientific Procedures Act of the United Kingdom. Frogs were anesthetized in 1:1 mixture of water and ice for 40 – 50 minutes following which they were decapitated by trained/licensed personnel at the animal house facility. A sterile scalpel was then used to make an incision on the posterior ventral side of the frog and the ovaries were isolated using forceps and transferred into a petri plate containing sterile calcium free solution (Table 2.3-1).

Table 2.3-1 - Recipe for Calcium free solution

Reagents	Final concentration (mM)
NaCl	80
CaCl	2
MgCl ₂	1
HEPES	5

The pH of the solution was adjusted to 7.6 using 10 mM NaOH solution before autoclaving the solution.

2.3.1 Collagenase treatment

The ovaries were separated into smaller segments of 5 to 10 mm using forceps and added into a 50 ml sterile centrifuge tube (Sarstedt, Germany) containing 10 ml of collagenase obtained from *Clostridium histolyticum* at a concentration of (1 mg/ml) in calcium free solution. This tube was placed on a tube roller at room temperature for 60 to 120 minutes in order to de-folliculate the oocytes. The de-folliculated oocytes were then washed with sterile Barths solution (Table 2.3-2) 3 to 4 times before transferring them into a petri plate with Barth's media supplemented with Penicillin/ Streptomycin (100 mg/ml) and Neomycin (50 mg/ml). The plates were incubated overnight at 18°C before injecting the cRNA of the proteins under study. After cRNA injections, the media was changed daily, simultaneously removing dead oocytes until the 3rd or 4th day, when the transport experiments were performed.

Table 2.3-2 - Recipe for Barths Solutions

Reagents	Final concentration (mM)
NaCl	88
KCl	1
MgSO ₄	0.82
CaNO ₃	0.33
NaHCO ₃	2.4
CaCl ₂	0.41
HEPES	15

The pH was adjusted to 7.6 using 10 mM NaOH before autoclaving the solution.

2.3.2 cRNA injection

Following collagenase treatment healthy looking oocytes with 1 mm diameter were selected for cRNA injection. Nanoject II injector (Drummond Scientific, c/o Alpha laboratories Ltd, Eastleigh UK) was used to inject oocytes under a Leica MZ6 light

microscope (Wetzlar, Germany). The disposable glass capillary needles made using PC-10 puller (Narishige, London UK) were filled with mineral oil before loading the needle with cRNA. Approximately 60 oocytes were injected with 25 ng of rPepT1/ratPHT1 cRNA or 15 ng of hPepT1/hPepT2 cRNA for each experimental condition respectively. The cRNA was injected into the vegetal pole of the oocytes to avoid damaging the nucleus (Figure 2.3.2-1). Non-injected oocytes were used as negative controls for the experiments as it was previously observed (in our lab) that no significant uptake was seen between water injected and non-injected oocytes. The injected and non-injected oocytes were transferred into sterile Barth's solution supplemented with 100 mg/ml penicillin/streptomycin and 50 mg/ml Neomycin antibiotics and incubated at 18°C for 72 to 96 hours before using the oocytes for performing experiments.

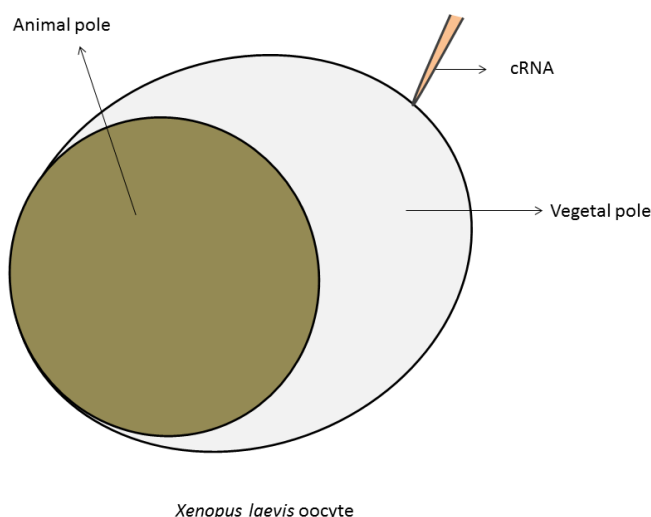


Figure 2.3.2-1 Diagrammatic representation of cRNA injection in the vegetal pole of an oocyte

2.3.3 Transport experiments using oocytes

Transport experiments were performed at room temperature using radioactive tracer [3H]-D-Phenylalanyl-L-Glutamine ([3H]-D-Phe-L-Gln, custom synthesised by Cambridge Research Biochemicals, UK) for PepT1 and PepT2 mediated transport in oocytes as it a hydrolysis resistant PepT substrate (Temple *et al.*, 1995). 5 to 10 oocytes were incubated with [3H]-D-Phe-L-Gln in uptake medium Table 2.3-3) for each experimental condition. The pH of the uptake medium used for all transport experiments was adjusted to pH5.5 (using 0.5M TRIS/MES buffer) except for

experiments where effect of pH was to be monitored, in which uptake solutions ranging in pH values from 5.5 to 7.5 were used.

2.3.4 Determination of affinity of pro-drugs towards rPepT1

rPepT1 cRNA injected and non-injected (control) oocytes were placed in uptake media (pH 5.5) for 10 minutes prior to carrying out uptake experiments. The oocytes were incubated in 100 μ l of uptake media containing 0.4 μ M [3 H]-D-Phe-L-Gln (17.4 Ci/mmol) and varying concentration of pro-drugs (5 to 10 oocytes for each prodrug concentration) for 60 minutes (Meredith *et al.*, 2000). The oocytes were then washed 5 times with 1 ml ice cold solution of 0.12 M NaCl. The washed oocytes were individually placed into a flexible 96 well microplate (Perkin Elmer, Cambridge UK). The oocytes were lysed using 20 μ l of 1% SDS on a plate shaker until the cells were completely lysed. 200 μ l of scintillation fluid (Optiphase supermix, Cambridge UK) was added into each well, and the plate sealed using plate sealer (Perkin Elmer) and placed on the plate shaker for 30 minutes. The plates were analysed using a Microbeta Trilux 1450 liquid scintillation and luminometry counter (Perkin Elmer). The amount of [3 H]-D-Phe-L-Gln in each well was calculated by counting the signal from each well for 1 minute expressed as counts per minute (cpm). The PepT1 mediated uptake (uptake in injected – uptake in non-injected oocytes) was expressed as mean cpm \pm standard deviation for each data point. K_i of pro-drugs were established by plotting the amount of radioactivity detected for each concentration of the pro-drug and the graph was plotted using Sigma plot (Software) utilizing the equation (Deves and Boyd, 1989)

$$f = (1/(1+(S/K_i))) \times V_o$$

Condition: fit f to y

Where the variables

f = calculated uptake fraction; y = (V/ V_o) fraction of uptake when V_o = 1

V_o = absolute transport of [3 H]-Phe-L-Gln in the absence of inhibitor

S = concentrations of the test compound (0, 0.125, 0.25, 0.5, 1, 5) mM

Table 2.3-3 - Recipe for Uptake solution

Reagents	Final Concentration (mM)
NaCl	95
KCl	2
CaCl ₂	1
MgCl ₂	0.1
Tris/Mes (pH 5.5 to 6.5) or Tris/HEPES (pH 7.0 to 7.5)	20

0.5M Tris/Mes, (pH 5.5 – 6.5) or Tris/Hepes (pH 7.0 to 7.5) prepared and mixed to obtain the required pH for uptake experiments

2.3.5 Efflux assay/Trans-stimulation protocol

The efflux experiments were setup as described (Temple *et al.*, 1998). *X. laevis* oocytes 3 days post rPepT1 cRNA injection were used for this experiment. The cRNA injected oocytes were injected with 27 nl of 1:5 diluted (with sterile distilled water) [³H]-Phe-L-Gln (17.4 Ci/mmol) and placed into uptake media at pH 5.5 to acclimatise to the uptake media. 100 µl of prodrug dissolved in uptake media (pH 5.5) was added to individual wells in a 96 well plate at a concentration of 5 times the K_i as determined in previous assays (Section 3.1.3). Five [³H]-D-Phe-L-Gln injected oocytes for each prodrug tested were incubated in a well of the prodrug solution in 96 well plates for 60 minutes. The oocytes were then sequentially washed 5 times with 1 ml of ice cold 0.12 M NaCl solution and scintillation counted as described (Section 2.3.4) to measure the amount of radioactivity retained in the oocytes at the end of the assay. The [³H]-D-Phe-L-Gln injected oocytes incubated with uptake media only was used as a negative control and [³H]-D-Phe-L-Gln injected oocytes incubated with 5 mM Gly-Gln served as a positive control for the efflux assay. Each experiment performed included the positive controls, negative controls and prodrugs with 5 oocytes for each of the condition. The efflux was normalised to negative controls and one sample t-test was used to determine

the significance of efflux observed for each of the prodrugs in a number of experiments (normally $n = 3$).

2.3.6 Luminometric technique to establish surface expression of protein in oocytes

The luminometry technique was used to check if the cRNA injected into oocytes was translated and protein successfully expressed onto the surface of the oocyte membrane. This technique was especially useful to check surface expression of proteins which failed to show significant uptake of radioactive tracer compared to non-injected oocytes. The FLAG epitope tag was introduced into the extracellular domain of the protein and the surface expression was detected using an anti- antibody conjugated to HRP, thus with addition of a substrate the light emitted could be detected quantitatively using a luminometer.

Barth's media and 1% BSA (w/v) in Barth's media were filtered using 0.2 μ m sterile filter and placed on ice. 20 oocytes for each flagged protein construct was used for carrying out luminometry. NI oocytes served as negative controls for the experiment. All the steps in this procedure was carried out on ice. Blocking was performed by incubating the oocytes in 1% BSA (w/v) in Barth's media for 1 hour. Following which the oocytes were incubated with HRP-conjugated anti-FLAG antibody for 30 minutes. The oocytes were sequentially washed 6 times in Barth's BSA solution with 15 minutes intervals. The oocytes were further washed 6 times in Barth's media with 5 minutes intervals. Each individual oocyte was transferred to a black frame white well 96 well plate (Perkin Elmer) containing 100 μ l Barth's media. 20uL of freshly prepared secondary antibody-substrate; Super Signal[®] Elisa Femto maximum sensitivity substrate (Thermo Scientific) was added to each well quickly, while simultaneously covering the wells with the substrate using an opaque cardboard. The plate was transferred into the luminometry counter (Perkin Elmer Trilux 1450) and light emitted was quantified with 5 sec long reads per well. The data was expressed as mean of the arbitrary light units \pm standard error. The significance of the surface expression was calculated using student's t-test p -value < 0.05 in comparison to non-injected oocyte controls.

2.3.7 Electrophysiology

Introduction

Two electrode voltage clamp is one of the most commonly used electrophysiology techniques to measure the amount of current passing across the plasma membrane of a cell (transporter proteins or ion channels). The measuring and recording process is illustrated in Figure 2.3.7-1. This technique measures the amount of current required to maintain a user specified holding voltage (voltage clamp) which is directly proportional to movement of ions across the membrane of the oocyte under study which in turn is directly proportional to the level of transporters expressed on the membrane of the oocyte and their rate of transport. Since the transport of peptide is suggested to be coupled to the transport of protons, If the peptides are transported by the transporter then this should be detected using electrophysiology. Hence electrophysiology can be used to indirectly measure peptide uptake by measuring the change in the current required to maintain the holding voltage in case of peptide transport.

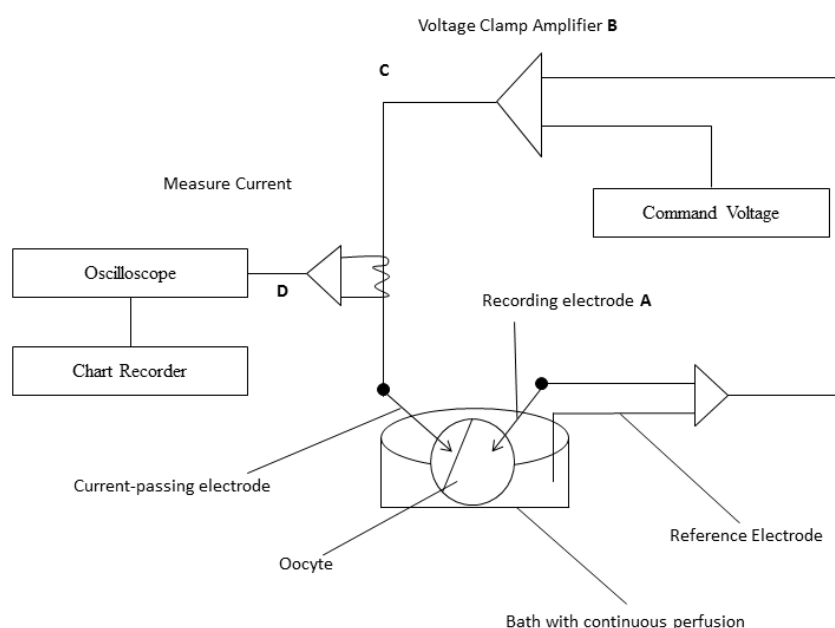


Figure 2.3.7-1 - Schematic representation of the two electrode voltage clamp technique.

With the two electrodes impaling the oocyte, the recording electrode connected to a unity gain amplifier monitors the membrane potential (A). The output voltage is

compared to the pre-set command voltage by the second amplifier (B). The difference in voltage between the two electrodes (C) is passed to the current passing electrode. The current is simultaneously monitored through a virtual amplifier (D)

Procedure

Oocytes were used to perform electrophysiology at room temperature three to four days post rat PHT1 RNA injections. An individual oocyte was placed in 50 μ l bath made from modified Petri dish on the stage of a low magnification inverted microscope (Nikon) using a Pasteur pipette with Sylgard (World Precision Instruments, UK). A gravity-driven perfusion system was used with Mg^{2+} free uptake media at pH 6.0 as the perfusion media and a flow rate of 5 ml/minute. A standard electrical pump (KNF, UK) was used to drive the output channel of the perfusion system. The entire arrangement was mounted to an anti-vibration table housed in a Faraday cage.

The electrodes were prepared from borosilicate glass capillaries (Clark Electromedical instruments: 150 TF GC) using a vertical two stage puller (Narishige PP-83) to obtain a tip diameter of 1 to 2 microns. The electrodes were then back filled with 3 M KCl and only the electrodes with a resistance of 0.5 M Ω to 1 M Ω were used to perform electrophysiology. The oocytes were clamped at a holding voltage of -60 mV and the response of the cell to substrates (amino acids) were monitored using an amplifier (Warner instruments, USA). Ionic current flowing through the membrane of the oocyte was continuously monitored on a paper chart recorder (Philips PM8254A). The amino acids used to test the response of transporters on the oocyte membrane were also dissolved in the perfusion media (test solution, pH adjusted to 6). The media was switched between the perfusion solution only and test solution to monitor the effect of amino acids on the holding current required to maintain the set holding voltage. Each pulse of test solution was applied for 30 seconds followed by a 3 minute wash step with the perfusion media and the maximum change in current during the 30 second pulse was recorded onto the chart sheet. Non-injected oocytes served as negative controls.

2.4 Caco-2 cell revival, storage and maintenance

2.4.1 Caco-2 cell culture maintenance

Caco-2 cells (gifted from Prof Munira Kadhim, Oxford Brookes University, Oxford) were routinely cultured in 75 cm² flasks in a CO₂ incubator with 5% CO₂ and 90% relative humidity at 37°C. The media was changed every two days. The cells were grown in complete media (Table 2.4-1) unless otherwise stated.

Table 2.4-1 - Components of complete media used for Caco-2 cell culture

Components	Volume (mL)
Dulbecco's Modified Eagle media with glucose and glutamine (Sigma, UK)	500
FBS (Life technologies)	50
Non-essential amino acids 100X (Sigma, UK)	5
Penicillin/streptomycin 100X	5

2.4.2 Routine sub-culturing of Caco-2 cells

Caco-2 cells were sub-cultured every 4 days or when they reached 85% confluence. Cells were not grown beyond passage number 70 to maintain uniform experimental conditions. The media was removed from the flask and washed with 5 mL sterile cell culture grade PBS. The cells were coated with 2ml of 0.05% trypsin-EDTA in PBS (Life Technologies, UK) following which the trypsin-EDTA mixture was removed and the flask was incubated at 37°C for 5 minutes. The cells were dislodged from the flask by gently knocking the flask against the palm and confirmed by visualising the cells on a Motic AE31 inverted light microscope. The residual trypsin was neutralised using 10 mL of complete media following which the cells were centrifuged at 1300 rpm (125 g) for 5 minutes. The supernatant was discarded and the cells were seeded at a density of 5×10^3 cells/cm². The complete media, PBS and Trypsin-EDTA were all pre-warmed to 37°C in a water bath before sub-culturing the cells.

2.4.3 Cryopreservation of Caco-2 cells

Caco-2 cell culture stocks were maintained for long term storage in liquid nitrogen. The cells were sub-cultured as mentioned in section 2.4.2. The cell pellet was re-suspended in 1 mL of complete media (10×10^6) with 10% DMSO which served as a cryoprotectant. The re-suspended cells were transferred immediately into cryogenic vial and stored in an isopropanol chamber overnight at -80°C after which they were transferred into liquid nitrogen for long term storage.

2.4.4 Revival of Caco-2 cells from Liquid nitrogen stocks

Individual cryogenic stocks of Caco-2 cells were removed from liquid nitrogen and thawed rapidly, by immersing the vials in a pre-warmed water bath at 37°C. The thawed stock was immediately transferred into a 50 mL tube and centrifuged at 1300 rpm for 5

minutes. The supernatant was discarded and the pellet was re-suspended in 5 mL of pre-warmed complete media and transferred into 25 cm² flask. The volume was made up to 10mL and incubated in a 37°C incubator for 24 hrs. The cells were trypsinised and transferred into a 75 cm² flask and sub-cultured thereafter as described in section 2.4.2.

2.4.5 Transport assay using Caco-2 cells

Principle:

PheΨ[CS-NH]-Ala (FSA) was used as positive control in every Caco-2 assay performed as, FSA is a PepT1 substrate which is known to be transported by PepT1 and can be detected by HPLC due to its UV absorbance at 210 nm. The di-peptide Gly-Gln is also a known PepT1 substrate which is transported by PepT1 with a K_i of 0.2 mM but has no absorbance at 210 nm. This property of Gly-Gln was used to determine PepT1 mediated transport in Caco-2 cells as using 20 mM Gly-Gln along with test compound should competitively inhibit the transport of test compounds that are transported by PepT1.

Method:

Caco-2 cells between passage numbers 60 to 65 were used for seeding the Corning Transwell inserts. Caco-2 cells were seeded in sterile tissue culture treated 6.5 mm diameter clear inserts (0.4 µm pore size) at a concentration of 5×10^4 cells/insert which were placed in sterile 24 well plates (supplied with the inserts). DMEM media supplemented with 4500 mg glucose/litre, 10% FCS, 1% non-essential amino acids (100x) and 1% Penicillin/streptomycin (10,000 units; Life technologies, USA), and added to the apical side of the inserts (200 µl) and in the basolateral side (600 µl) (wells of the 24 well plate) with the media replaced every 2nd day. The Caco-2 cell monolayers were grown for 21 days after they had reached 100% confluency (as observed under the microscope) and the transport experiments performed on the 22nd day. The media was replaced with fresh DMEM media 24 hrs before performing the transport experiments. On the day of the experiment the DMEM media was removed and the inserts were washed with pre-warmed Krebs media (pH 7.4) and placed into 24 well plates containing 600 µL of Krebs media (pH 7.4). To these inserts 200 µL of Krebs media (pH 5.5) was added and incubated for 30 minutes at 37°C before setting up the transport experiment to allow the Caco-2 cells to acclimatise. The compound and compound + Gly-Gln solutions were prepared using Krebs media (pH 5.5). The Krebs media in the inserts were replaced with 200 µL of Krebs media with the compound or compound +

Gly-Gln (3 inserts of each) and incubated at 37°C and 5% CO₂ incubator for a period of 30 minutes. At the end of 30 minutes, the inserts were carefully removed and discarded using sterile forceps following which the basolateral Krebs media in the 24 well plates were collected into labelled 1.5 ml centrifuge tube and stored at -20°C until performing the HPLC analysis.

Table 2.4-2 - Composition of Krebs Media

Compound	Concentration (mM)
NaCl	137
KCl	5.4
CaCl ₂	2.8
MgSO ₄	1
NaH ₂ PO ₄	0.3
KH ₂ PO ₄	0.3
Glucose	10
HEPES (for pH7.4) or Mes (for pH5.5)	10

2.4.6 HPLC analysis of Transwell assay

The prodrugs were analysed using a Jasco HPLC system with a reverse phase C-18 column 250 mm, 4 µ particle size (Max-RP, Phenomenex, UK). The wave length of the UV detector was set to 210 nm to detect peptide- and/or thio- bonds. The mobile phase flow rate was 1 ml/minute and HPLC grade solvents were used at all times unless otherwise specified. The column was equilibrated for 30 minutes with the mobile phase appropriate for the individual prodrug being analysed as shown below

Table 2.4-3). The equilibration of the column was followed by sample injection (100 µl) and running the mobile phase through the column for 10 minutes. This was followed by column wash with 100% methanol for 5 minutes followed by equilibration of the column with methanol in 21 mM KH₂PO₄ for 10 minutes before the next sample injections. The EZChrom Elite software was used to analyse the results obtained from the HPLC assay. The area under the curve (AUC) for each compound corresponding to 0.1 mM concentration and the AUC for each of the test compounds with and without Gly-Gln (obtained from Caco-2 assay) was determined using the EZChrom software.

The AUC were calculated as Mean \pm SD. The analysis of the apparent permeability was calculated using the formula

$$\left[\frac{V_A}{\text{Area} \times \text{Time}} \right] \times \frac{[\text{Drug}_A]}{[\text{Drug}_I]} \text{ (cm/sec) (Artursson and Karlsson, 1991)}$$

Where

V_A = volume in the acceptor well (0.6 cm³)

Area = area in the transwell filter (0.33 cm²)

Time = duration of experiment (1800 sec)

$[\text{Drug}_A]$ = concentration of drug in the acceptor well

$[\text{Drug}_I]$ = Initial concentration of drug (2 mM)

Table 2.4-3 - Conditions used for compound/prodrug detection in HPLC

Compounds/Prodrugs	Retention time the peak in HPLC (min)	Concentration of methanol : 21mM KH₂PO₄ (%)
FSA	5.1	30: 70
Thio-Atenolol	6.4	20: 80
Aib-Atenolol	6.1	10 : 90
Thio-Baclofen	5.6	20 : 80
Aib-Baclofen	8.8	30: 70
cLu-Baclofen	6.9	30: 70
cLu-Ibuprofen	7.9	30: 70
Thio-Mycophenolate	9.1	30: 70

Results

3 Novel Prodrugs for PepT1 mediated transport

3.1.1 Introduction

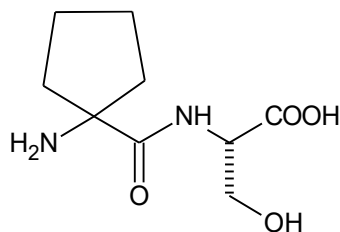
The PepT1 and PepT2 peptide/prodrug transporters are known to transport a wide variety of di peptides, tri peptides and drugs as previously mentioned. This transport is facilitated due to the drugs having a similar 3D shape to that of a di- or tri- peptides which, are substrates of the peptide transporters. The comparison of the common structural features of the substrates transported by PepT1 and PepT2 has led to the proposal of substrate template models by several groups (Bailey *et al.*, 2000; Biegel *et al.*, 2005).

The term “prodrug” refers to a chemical entity (drug with a linker) conjugated to a carrier molecule which is a substrate for the transporter or channel proteins expressed in the plasma membrane of cells. The carrier molecule in a prodrug interacts with the transport protein in the plasma membrane and is transported into the cell carrying along the conjugated drug with it. This prodrug conjugate then undergoes enzymatic cleavage either within the cell or on entering the blood by enzymes (for example proteases, esterases) releasing the drug to the site of action in its active state (Han and Amidon, 2000). This approach has been used in the delivery of several drugs which have undesirable side effects or for drugs that have low oral bioavailability. This approach helps in not only reducing undesirable effects of a drug but also delivery of a drug to its specific target site.

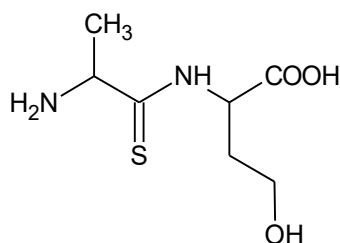
In the current study three novel carriers have been tested, to check the ability of the carrier to facilitate PepT1 mediated transport. These prodrugs have been designed and synthesised by Prof. Pat Bailey, Keele University based on the PepT1 substrate template model (Figure 1.12.3-1) (Bailey *et al.*, 2000).

All the drugs tested have been conjugated to carrier molecules namely.

- (i) Cyclo-Leucyl-Serine which will be referred henceforth to as “cLu”



- (ii) Alanyl-[ψCS-NH]-Serine di-peptide which will be referred henceforth to as “Thio”



- (iii) Amino-Isobutynyl-Alanyl-Serine di-peptide which will be referred henceforth to as “Aib”

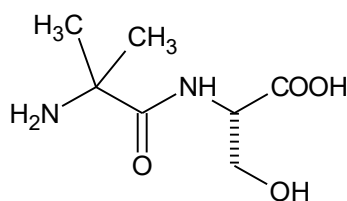


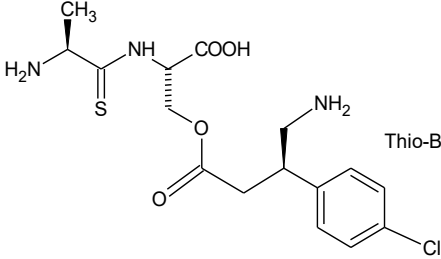
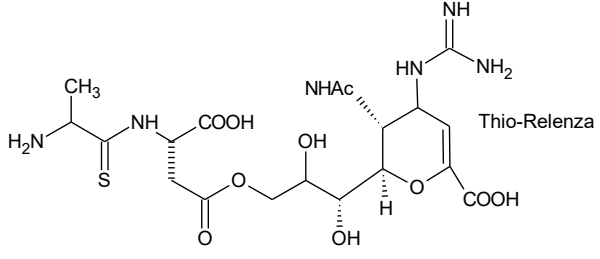
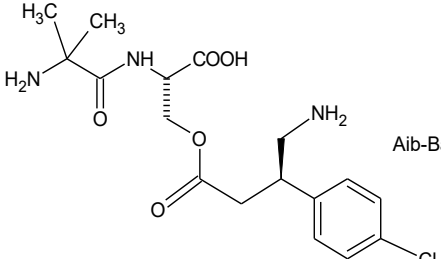
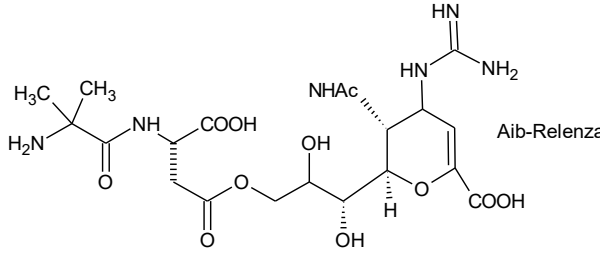
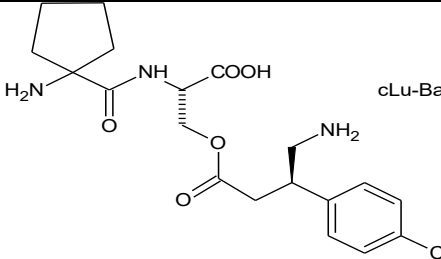
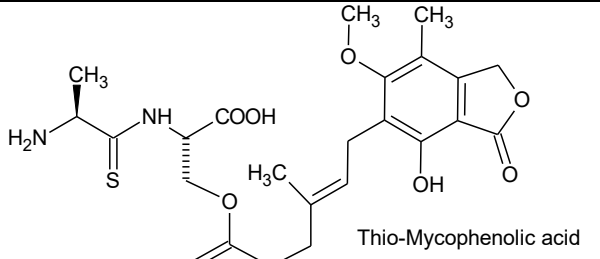
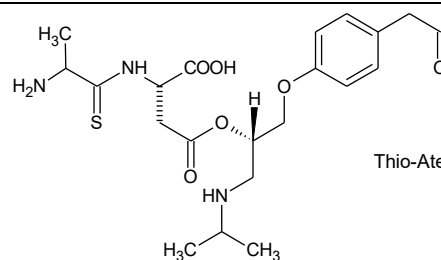
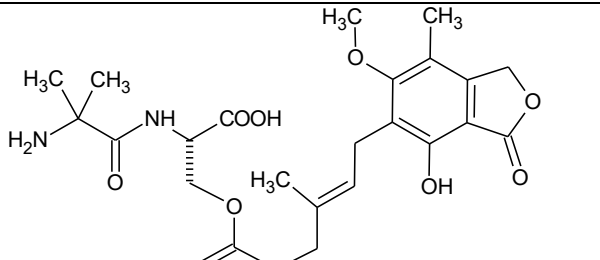
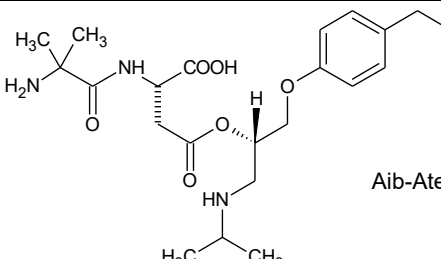
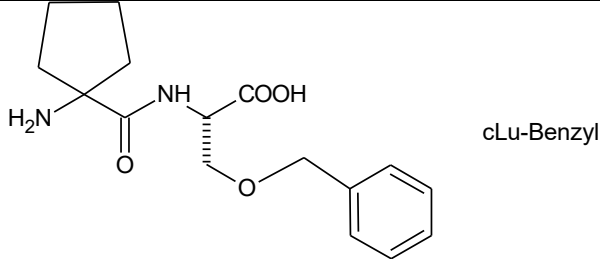
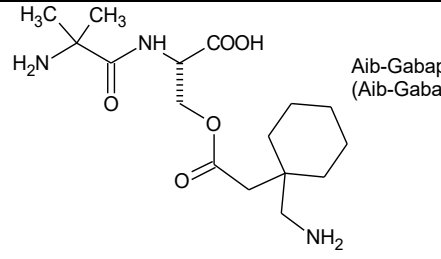
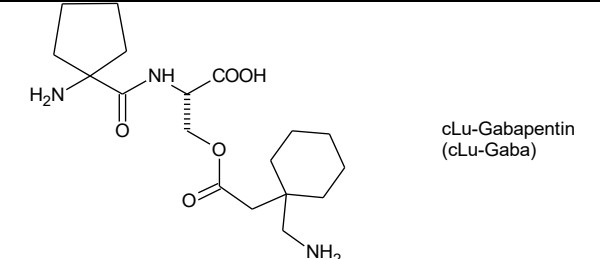
Figure 3.1.1-1 - Structures of the novel carriers to test PepT1 mediated transport of drugs

The novel carrier molecules were conjugated to drugs such as Baclofen (Gaba receptor agonist, muscle relaxant), Gabapentin (anti-epileptic drug), Relenza (anti-viral), Atenolol (beta blocker, antihypertensive agent), Mycophenolic acid

(immunosuppressive agent, antitumor agent), Ibuprofen (anti-inflammatory drug), Kinase Inhibitor (anti-cancer agent) and Sialic acid (Anekthananon *et al.*, 2013; Diamandis *et al.*, 2007; Mitsui *et al.*, 1981; Muzyk *et al.*, 2012; Petroff *et al.*, 1996) . The reasons for selecting these drugs to be conjugated to the carriers are as follows

- a) These compounds are structurally diverse with respect to their size and also the number/type of functional groups such as –OH groups and the presence of benzene rings.
- b) They have different biological effects (eg: anticancer, anti-inflammatory)
- c) They may or may not interact with PepT1 transporter (Ibuprofen is a non-competitive inhibitor of PepT1 (Omkvist *et al.*, 2010))

These drugs were conjugated to the carriers being tested to check if they were able to improve bioavailability of drugs. All the prodrug carriers were di- peptides of Alanine-Serine except for the Thio-kinase inhibitor which was an Alanine-Aspartate di-peptide carrier. The prodrug carriers were linked to the drugs using ester linkages except for cLu-Benzyl compound which was an ether linkage.

 <p>Thio-Baclofen</p>	 <p>Thio-Relenza</p>
 <p>Aib-Baclofen</p>	 <p>Aib-Relenza</p>
 <p>cLu-Baclofen</p>	 <p>Thio-Mycophenolic acid</p>
 <p>Thio-Atenolol</p>	 <p>Aib-Mycophenolic acid</p>
 <p>Aib-Atenolol</p>	 <p>cLu-Benzyl</p>
 <p>Aib-Gabapentin (Aib-Gaba)</p>	 <p>cLu-Gabapentin (cLu-Gaba)</p>

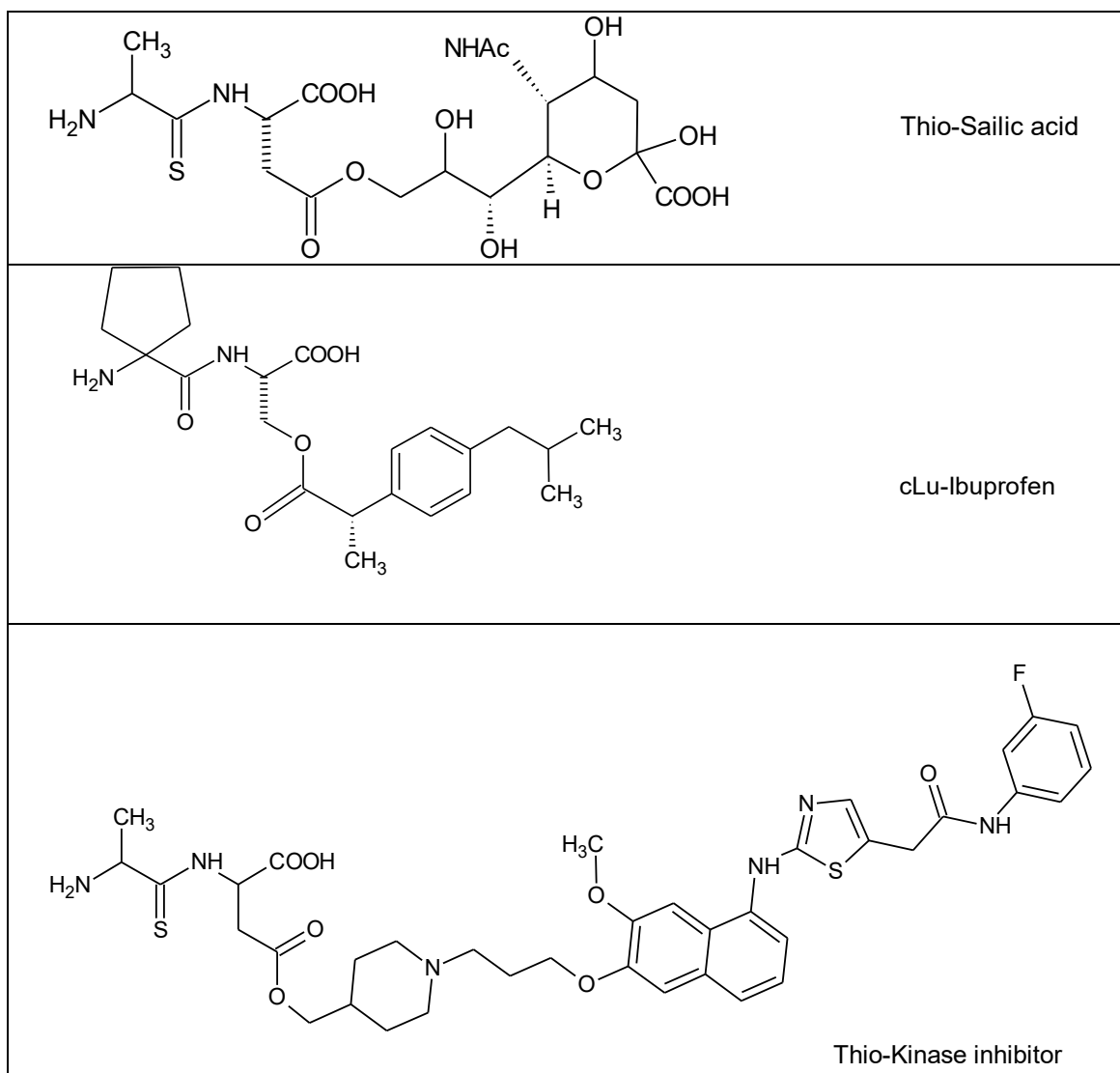


Figure 3.1.1-2 - Prodrugs and their structures

3.1.2 Aims

- Do the novel prodrugs bind to PepT1 transporter? If so, to determine their binding affinity (K_i) towards PepT1 using *X. laevis* oocytes model.
- To determine if these prodrugs are transported by PepT1 using efflux assays in *X. laevis* oocytes
- To study the transport of the prodrugs using Transwell[®] assay using Caco-2 cells and to determine if the prodrugs are transported from the apical to the basolateral membrane (replicating the conditions prevalent in the intestine which is the primary site of absorption of peptides and drugs)
- To determine which among the three carriers have a better binding and transport ability using PepT1 transporter.
- To determine if the structural features of the drug affects the ability of the carrier in transporting the drugs using PepT1.

3.1.3 Determination of K_i of novel prodrugs for rPepT1

rPepT1 (Rabbit PepT1) cRNA injected *X. laevis* oocytes 3 days post injection were used to determine the binding affinity (K_i) of the compounds. The K_i of compounds were determined as mentioned in section 2.3.4. In this method, the binding affinity of the test compound was estimated by inhibiting PepT1 mediated uptake of the radioactive tracer [^3H]-D-Phe-L-Gln at very low concentration of 0.4 μM compared to the inhibitor/test compound concentration; usually between 0.125 mM to 5 mM. Therefore the estimated K_m value will correspond very closely to the K_i value of the test compound.

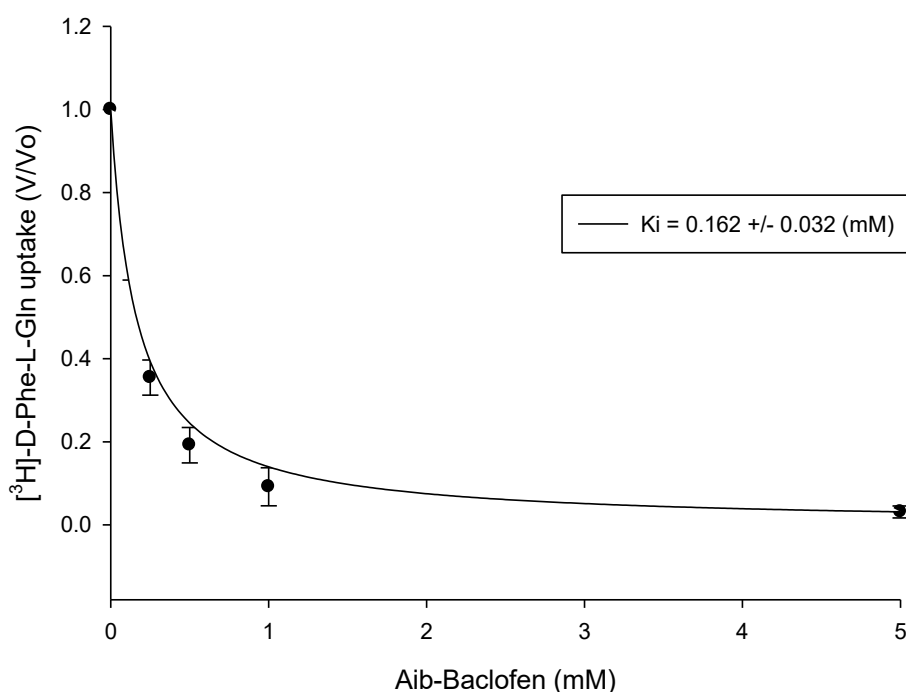


Figure 3.1.3-1 - K_i of Aib-Baclofen.

Uptake of [^3H]-D-Phe-L-Gln in rPepT1 cRNA injected oocytes in the absence of Aib-Baclofen was found to be 97 ± 12 fmoles/oocyte/hour. ($n = 3$)

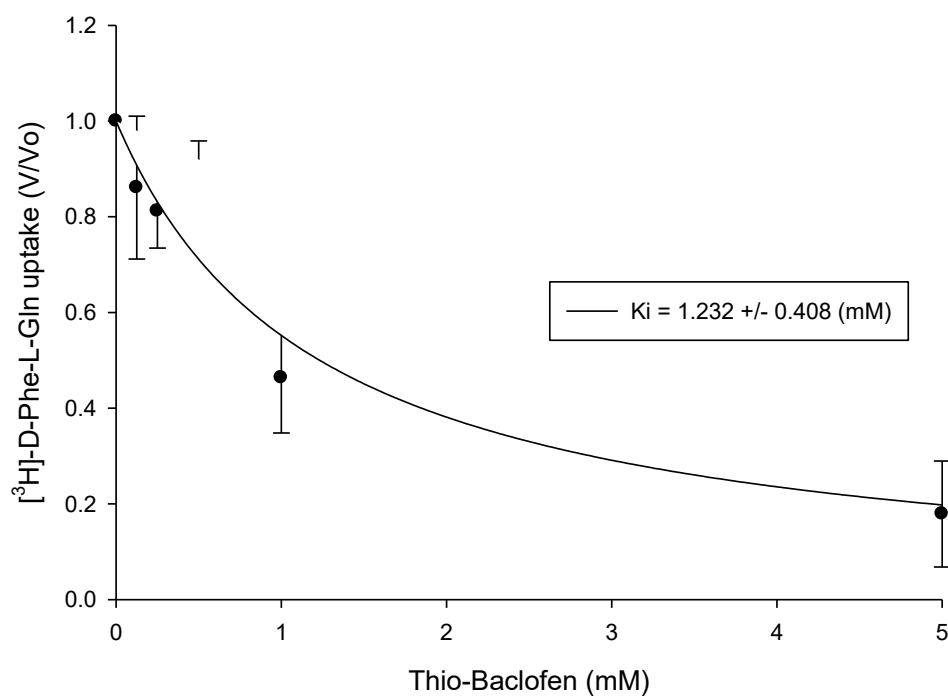


Figure 3.1.3-2 - K_i of Thio-Baclofen.

Uptake of [³H]-D-Phe-L-Gln in rPepT1 cRNA injected oocytes in the absence of Thio-Baclofen was found to be 41 ± 8 fmoles/oocyte/hour ($n = 3$)

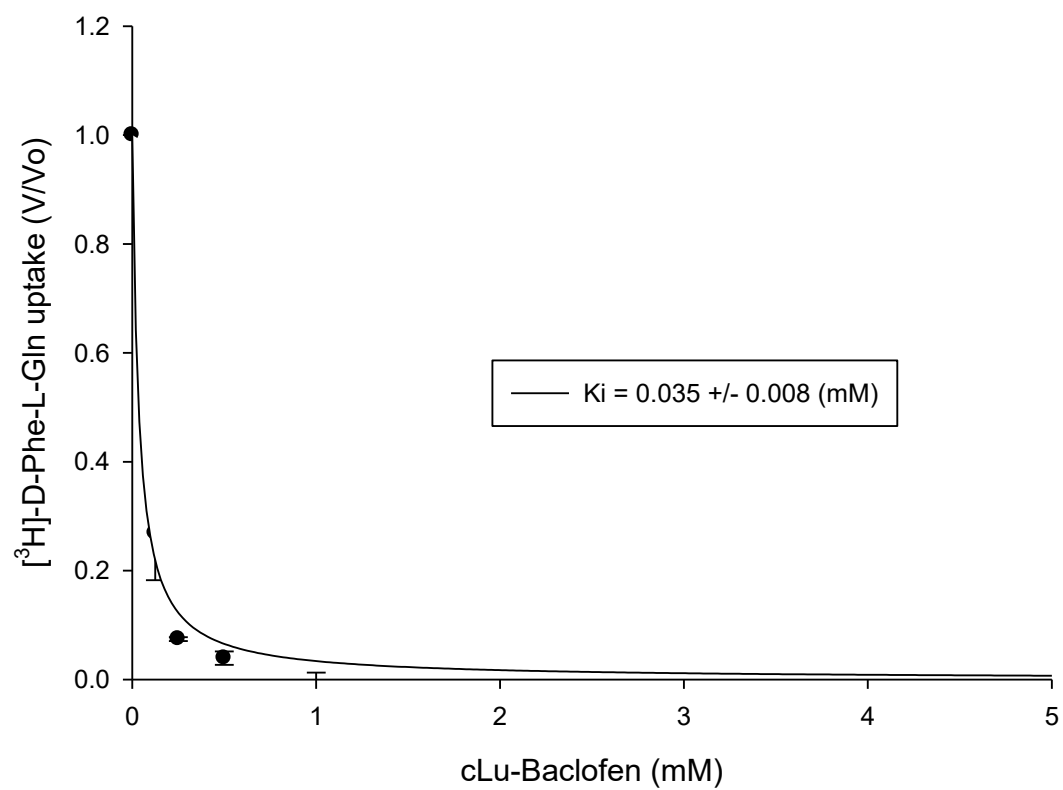


Figure 3.1.3-3 - K_i of cLu-Baclofen.

Uptake of $[^3\text{H}]\text{-D-Phe-L-Gln}$ in rPepT1 cRNA injected oocytes in the absence of cLu-Baclofen was found to be 65 ± 9 fmoles/oocyte/hour ($n = 2$)

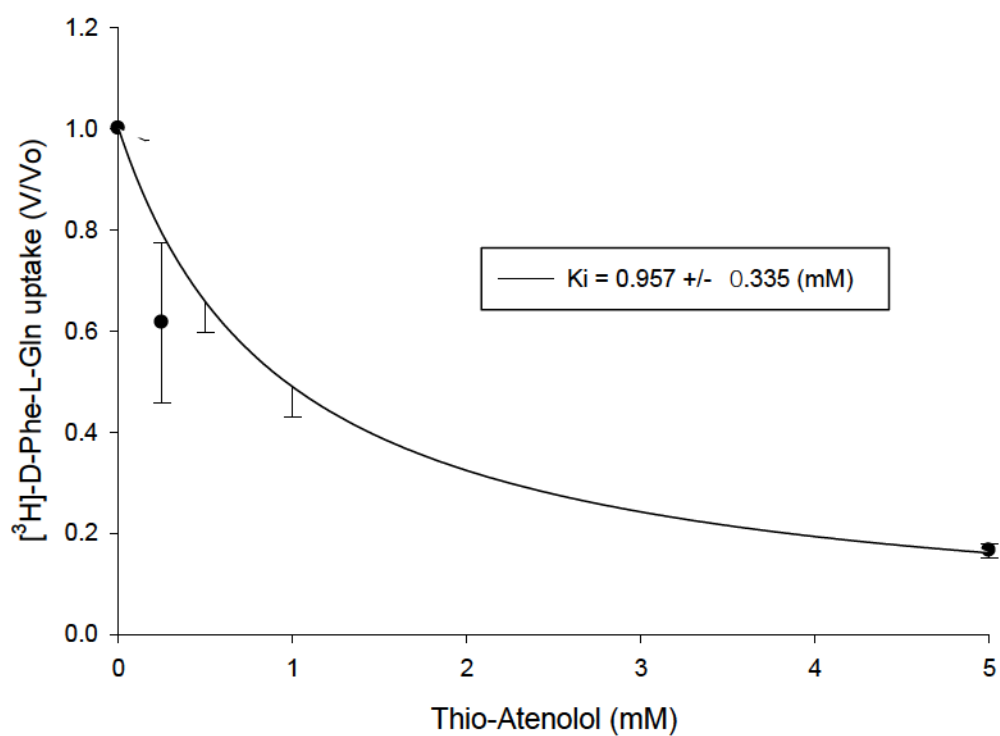


Figure 3.1.3-4 - K_i of Thio-Atenolol.

Uptake of [³H]-D-Phe-L-Gln in rPepT1 cRNA injected oocytes in the absence of Thio-Atenolol was found to be 43 ± 7 fmoles/oocyte/hour ($n = 4$)

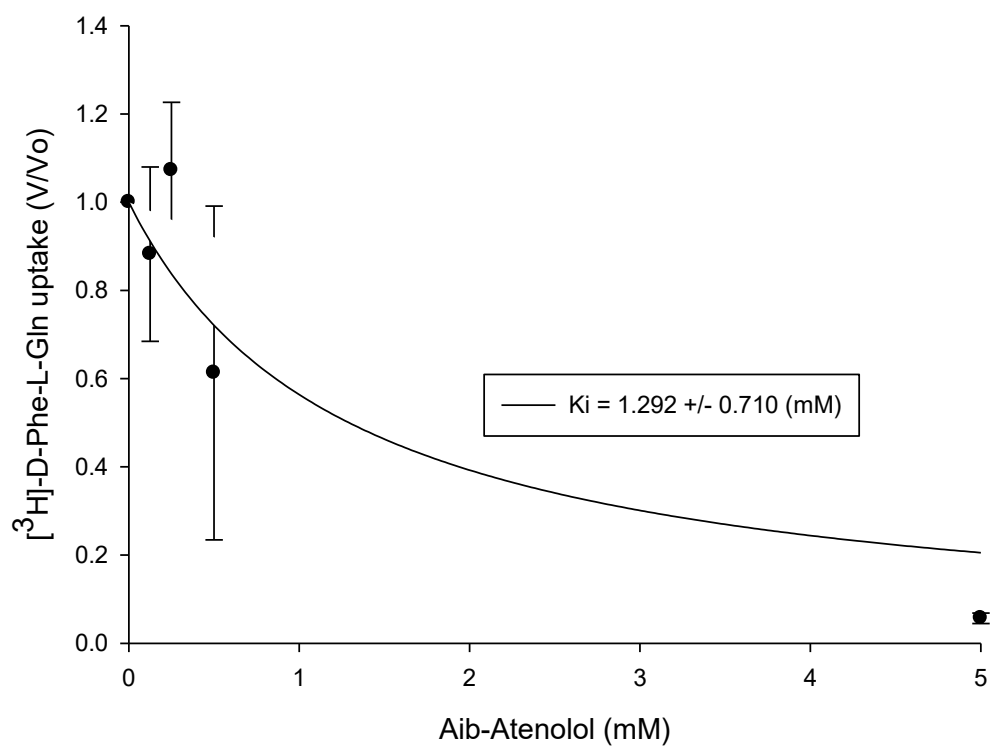


Figure 3.1.3-5 - K_i of Aib-Atenolol.

Uptake of [³H]-D-Phe-L-Gln in rPepT1 cRNA injected oocytes in the absence of Aib-Atenolol was found to be 39 ± 10 fmoles/oocyte/hour ($n = 3$)

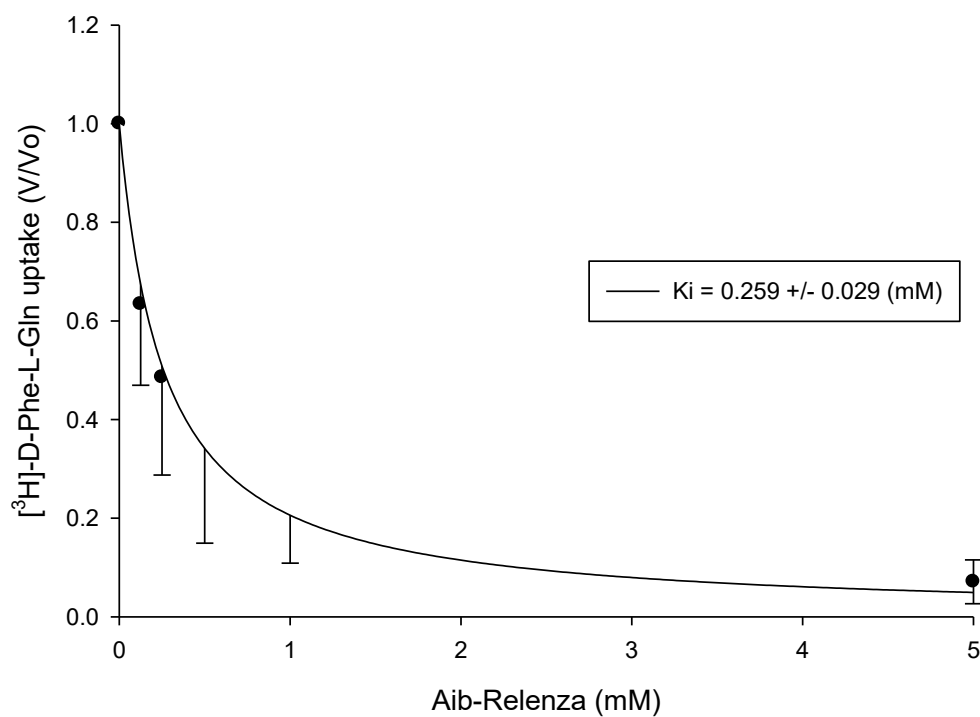


Figure 3.1.3-6 - K_i of Aib-Relenza.

Uptake of [³H]-D-Phe-L-Gln in rPepT1 cRNA injected oocytes in the absence of Aib-Relenza was found to be 57 ± 7 fmoles/oocyte/hour ($n = 3$)

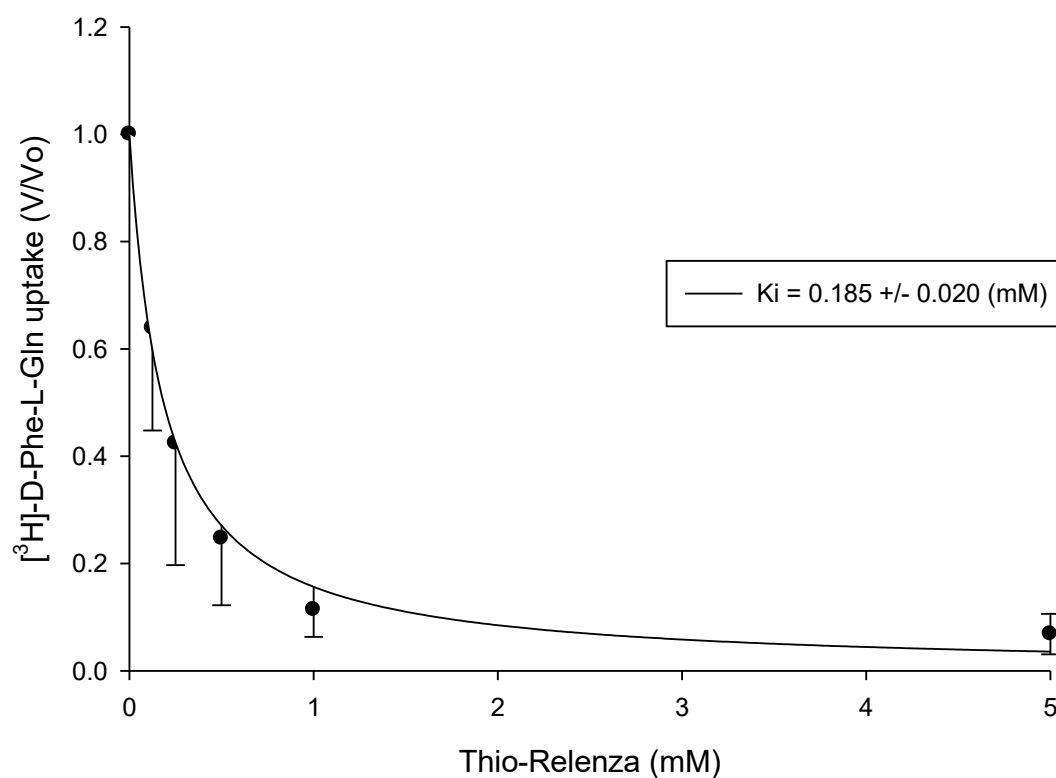


Figure 3.1.3-7 - K_i of Thio-Relenza.

Uptake of [³H]-D-Phe-L-Gln in rPepT1 cRNA injected oocytes in the absence of Thio-Relenza was found to be 131 ± 10 fmoles/oocyte/hour ($n = 3$)

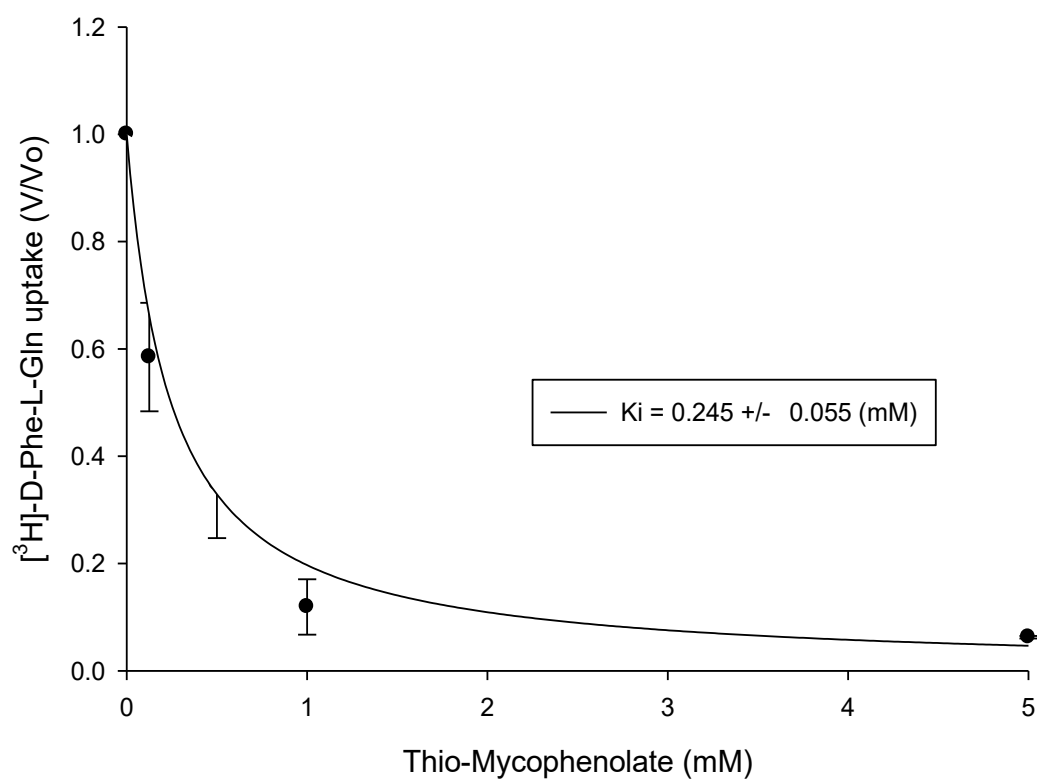


Figure 3.1.3-8 - K_i of Thio-Mycophenolate.

Uptake of [³H]-D-Phe-L-Gln in rPepT1 cRNA injected oocytes in the absence of Thio-Mycophenolate was found to be 81 ± 7 fmoles/oocyte/hour ($n = 2$)

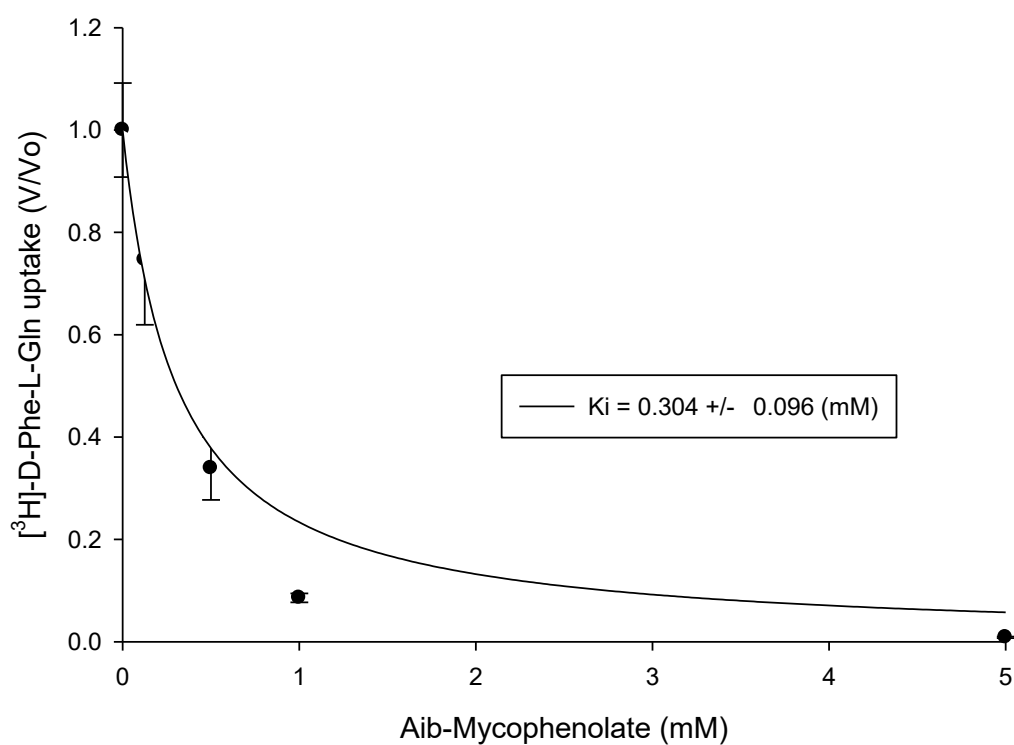


Figure 3.1.3-9 - K_i of Aib-Mycophenolate.

Uptake of [³H]-D-Phe-L-Gln in rPepT1 cRNA injected oocytes in the absence of Aib-Mycophenolate was found to be 81 ± 7 fmoles/oocyte/hour ($n = 2$)

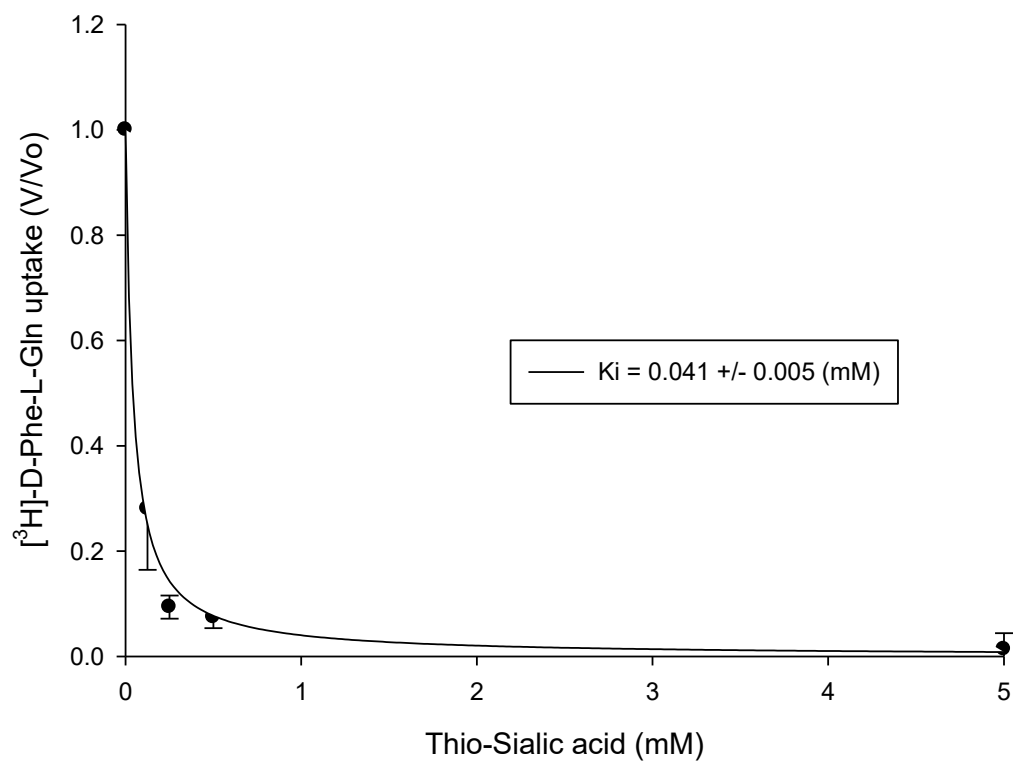


Figure 3.1.3-10 - K_i of Thio-Sialic acid.

Uptake of [³H]-D-Phe-L-Gln in rPepT1 cRNA injected oocytes in the absence of Thio-Sialic acid was found to be 131 ± 10 fmoles/oocyte/hour ($n = 2$)

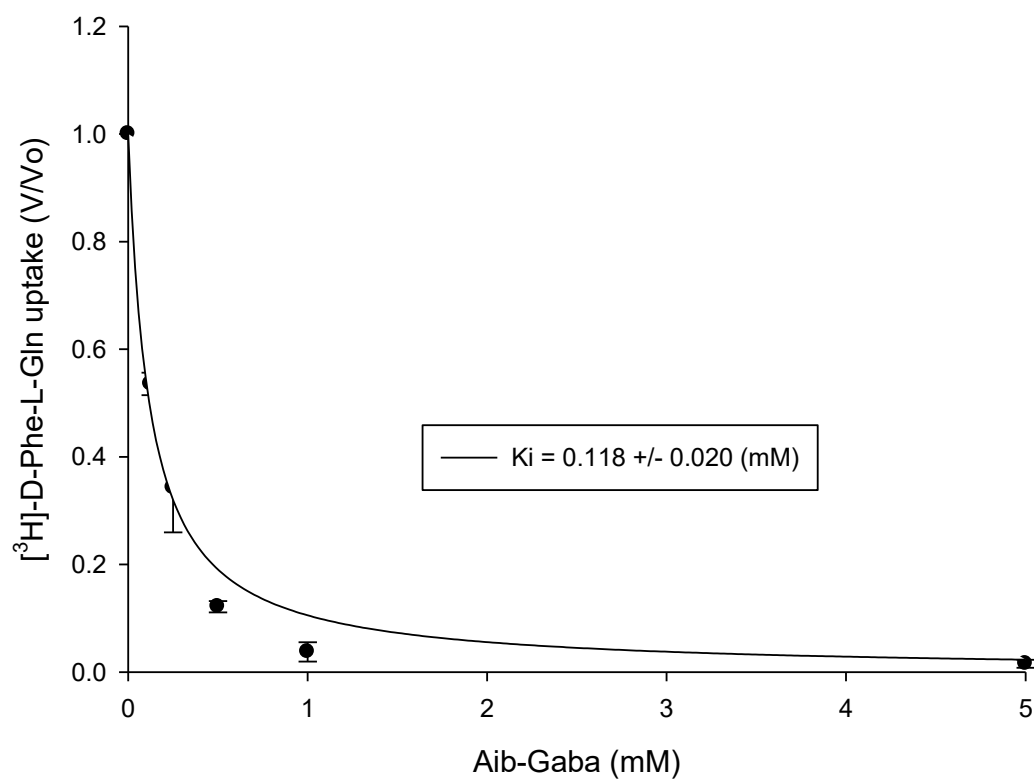


Figure 3.1.3-11 - K_i of Aib-Gaba.

Uptake of $[^3\text{H}]\text{-D-Phe-L-Gln}$ in rPepT1 cRNA injected oocytes in the absence of Aib-Gaba was found to be 152 ± 20 fmoles/oocyte/hour ($n = 2$)

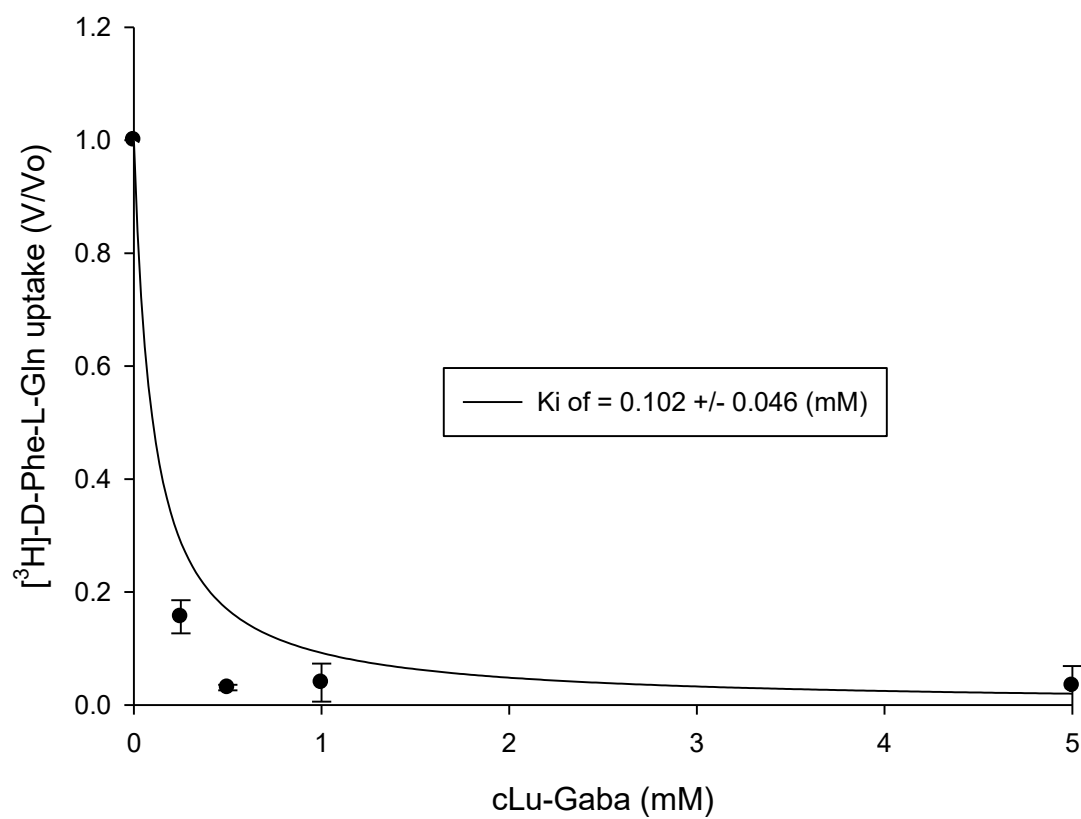


Figure 3.1.3-12 - K_i of cLu-Gaba.

Uptake of $[^3\text{H}]\text{-D-Phe-L-Gln}$ in rPepT1 cRNA injected oocytes in the absence of cLu-Gaba was found to be 112 ± 13 fmoles/oocyte/hour ($n = 2$)

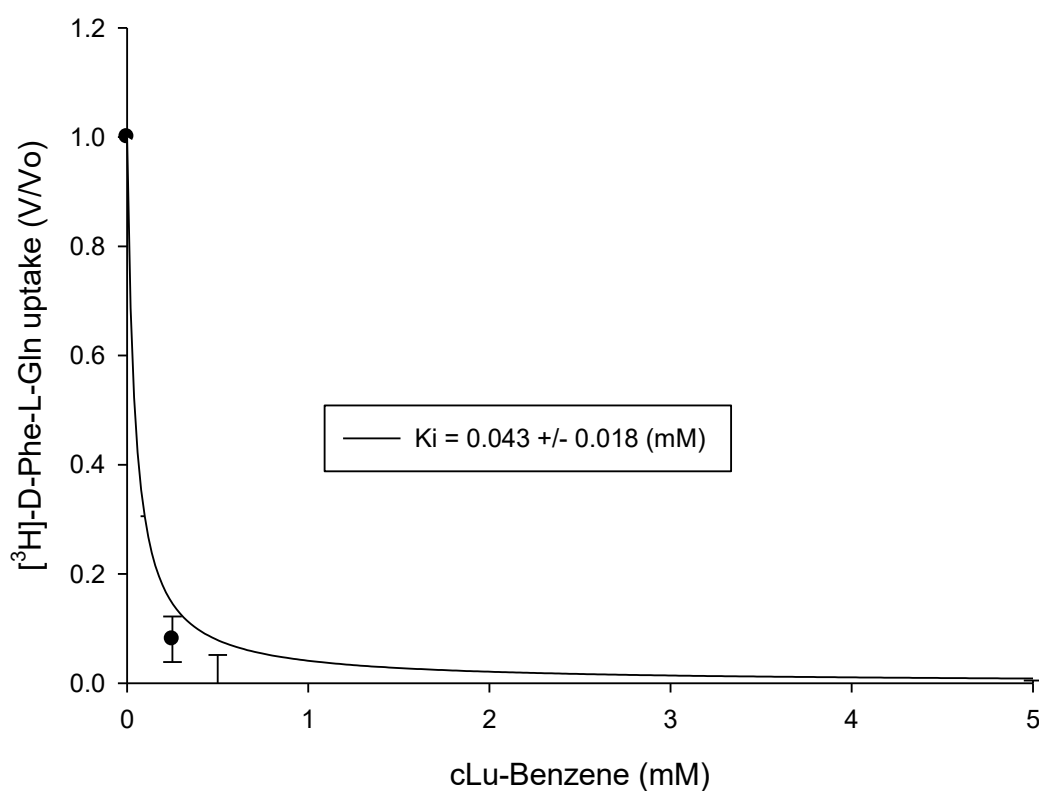


Figure 3.1.3-13 - K_i of cLu-Benzyl.

Uptake of [³H]-D-Phe-L-Gln in rPepT1 cRNA injected oocytes in the absence of cLu-Benzyl was found to be 94 ± 12 fmoles/oocyte/hour ($n = 2$)

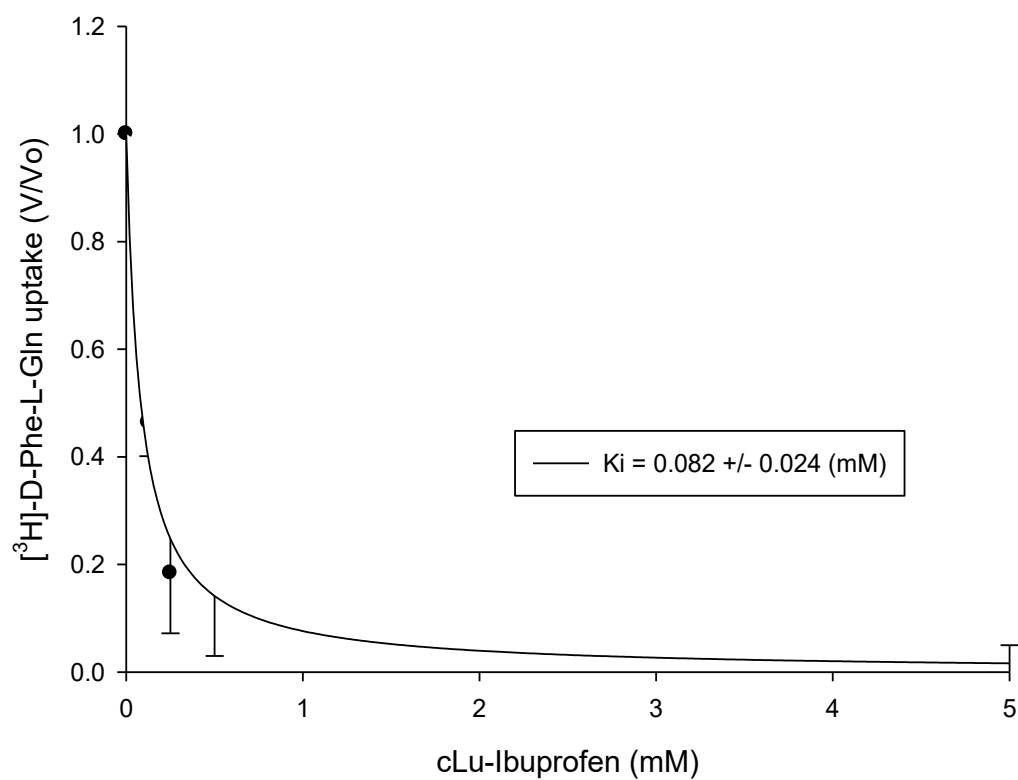


Figure 3.1.3-14 - K_i of cLu-Ibuprofen.

Uptake of $[^3\text{H}]\text{-D-Phe-L-Gln}$ in rPepT1 cRNA injected oocytes in the absence of cLu-Ibuprofen was found to be 106 ± 7 fmoles/oocyte/hour ($n = 2$)

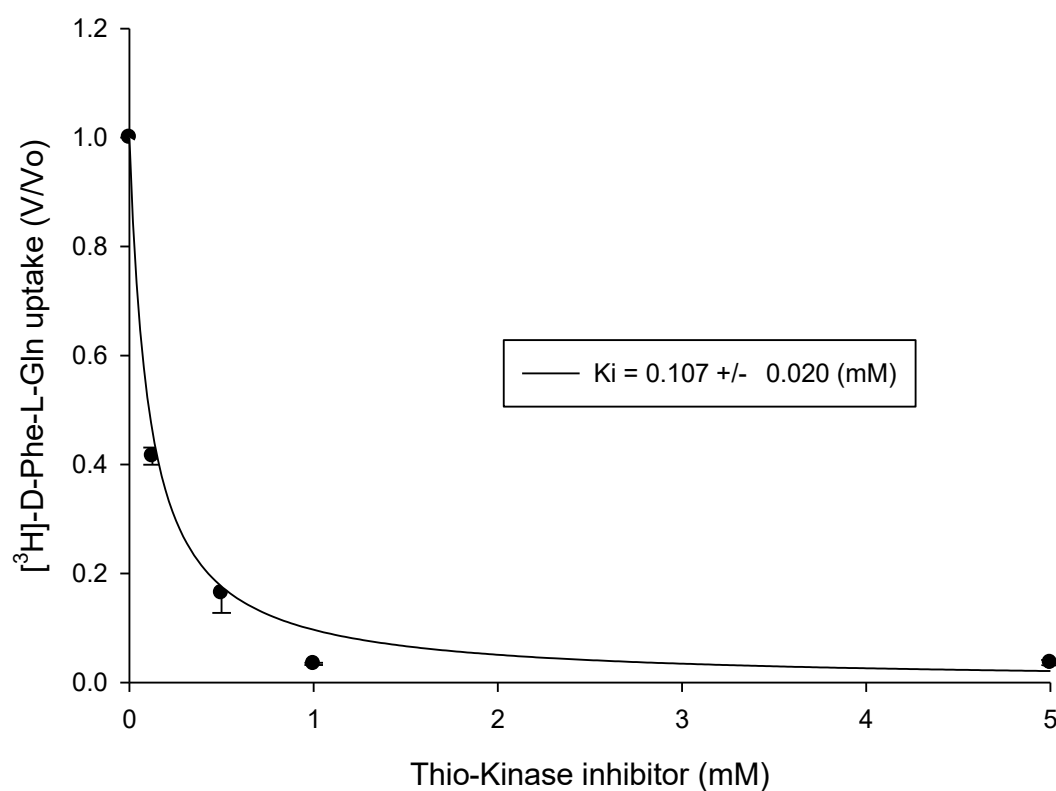


Figure 3.1.3-15 - K_i of Thio-Kinase inhibitor.

Uptake of $[^3\text{H}]\text{-D-Phe-L-Gln}$ in rPepT1 cRNA injected oocytes in the absence of Thio-Kinase inhibitor was found to be 134 ± 10 fmoles/oocyte/hour ($n = 2$)

Table 2.4-1 Summary of Ki values of prodrugs/carriers

Prodrugs/carriers	Ki (mM)
Aib-Baclofen	0.162 ± 0.032
Thio-Baclofen	1.232 ± 0.408
cLu-Baclofen	0.035 ± 0.008
Thio-Atenolol	0.957 ± 0.335
Aib-Atenolol	1.292 ± 0.710
Aib-Relenza	0.259 ± 0.029
Thio-Relenza	0.185 ± 0.020
Thio-Mycophenolate	0.245 ± 0.055
Aib-Mycophenolate	0.304 ± 0.096
Thio-sialic acid	0.041 ± 0.005
Aib-Gaba	0.188 ± 0.020
cLu-Gaba	0.102 ± 0.046
cLu-Benzyl	0.043 ± 0.018
cLu-Ibuprofen	0.082 ± 0.024
Thio-Kinase inhibitor	0.107 ± 0.020

The uptake experiments for estimating binding affinity of the prodrugs towards PepT1 only demonstrated if the prodrugs bind to the PepT1 transporter. From the above table it can be seen that all the compounds (prodrugs) tested bound to PepT1. The next step was to determine if the free drugs bound to PepT1 and if they were transported in their free form by PepT1. This would be followed with comparing the transport characteristics of the free drug with their respective prodrug versions to determine the efficacy of the prodrug carriers.

3.1.4 Determination of K_i of native compounds (drugs only without a prodrug carrier) for rPepT1

The binding affinity towards rPepT1 was determined for the free drugs namely, Baclofen, Ibuprofen, Mycophenolate, Atenolol, Relenza and Gabapentin as described previously (Section 2.3.4).

Table 2.4-2 - Summary of K_i values of native compounds (drugs only)

Native Drugs	K_i values (mM)
Baclofen	0.91 ± 0.93
Ibuprofen	0.15 ± 0.07
Mycophenolate	ND
Atenolol	0.8 ± 0.48
Relenza	ND
Gabapentin	ND
Kinase inhibitor	Not available

In the table above ND refers to the compounds which did not bind to rPepT1 in the K_i assay. These compounds did not inhibit the uptake of radiolabelled tracer [^3H]-D-Phe-L-Gln even at 5 mM concentration. The compounds Mycophenolate, Relenza and Gabapentin did not interact with the rPepT1 transporter whereas Baclofen, Ibuprofen and Atenolol did bind to the rPepT1 transporter. Sialic acid and Benzyl compounds were not active drugs, hence were not tested.

3.1.5 Determination of PepT1 mediated transport of novel prodrugs and native drugs in rPepT1 cRNA injected oocytes using trans-activated efflux assay

Efflux assays were set up to investigate if the novel prodrugs tested in the Ki assays (Section 3.1.3) were transported by PepT1 in rPepT1 cRNA injected oocytes.

3.1.5.1 Method

The main principle of efflux assay is that during carrier (PepT1) mediated uptake of peptides, the slowest step (rate limiting step) is the recycling of the empty carrier from the intracellular position to the extracellular position. When the rPepT1 expressing oocytes are injected with the [^3H]-Phe-L-Gln (PepT1 substrate) and incubated in uptake media (pH 5.5) with the prodrug (test compound), if the test compound is a PepT1 substrate then the PepT1 transporter is always bound to a substrate during the peptide transport cycle. It thereby eliminates the rate limiting step (recycling of the empty carrier) in the peptide transport cycle (Figure 3.1.5-1). If the substrate in the uptake media (extracellular location) is transported by PepT1, then the [^3H]-Phe-L-Gln within the oocyte will be transported out of the oocyte when the carrier returns to the extracellular side. Therefore the amount of [^3H]-Phe-L-Gln within the oocyte will reduce at a fast rate with the substrate, which allows the indirect measurement of PepT1 mediated transport of prodrugs in the oocytes expressing PepT1 transporter (Foley *et al.*, 2009a; Temple *et al.*, 1998). The efflux assays were performed as described in section 2.3.5.

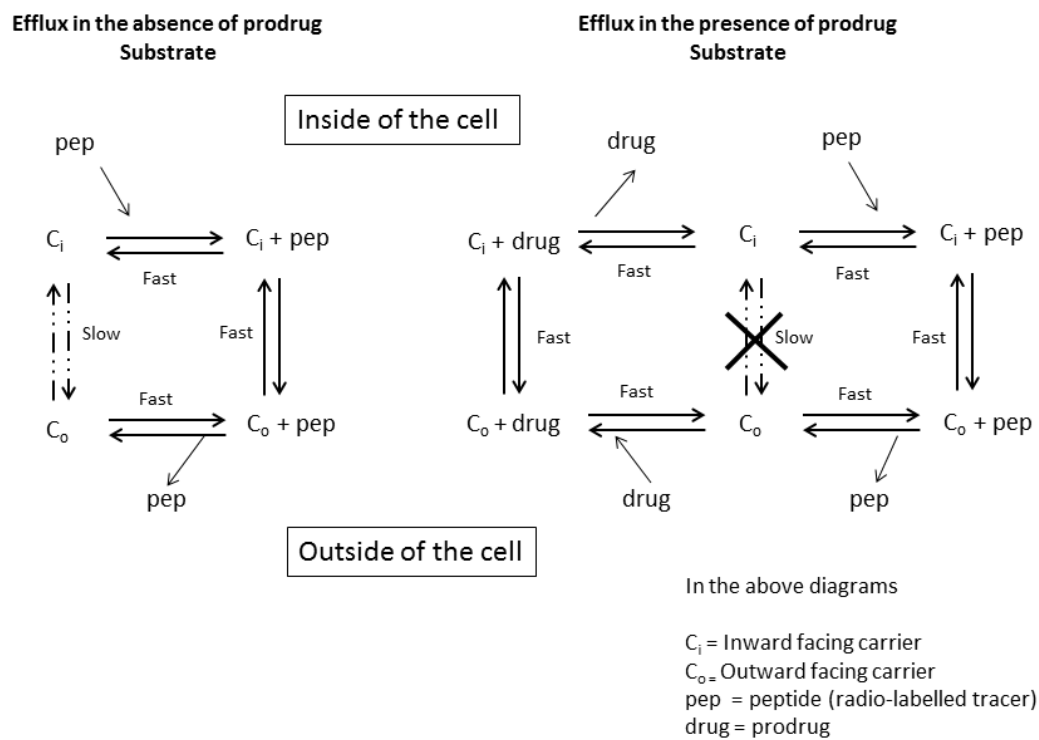


Figure 3.1.5-1 - Diagrammatic representation of an efflux transport in the presence (right) and absence (left) of a prodrug.

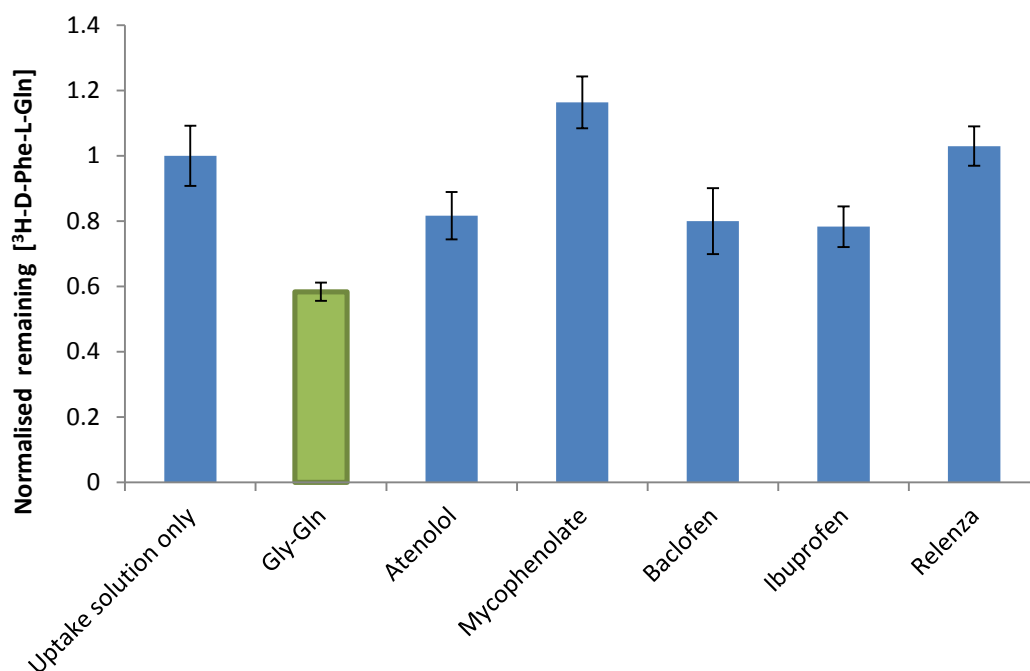


Figure 3.1.5-2 - Histogram representing the results obtained from the efflux experiments performed on 2.5 mM concentration of native drugs.

In the above histogram the bars coloured in green represents compounds that showed significant reduction in the amount of [^3H]-D-Phe-L-Gln detected compared to negative control oocytes with uptake solution only. (Significance was determined using one sample t-test, $p < 0.05$) ($n=2$).

From the above graph it can be seen that none of the native compounds showed rPepT1 mediated transport in the rPepT1 cRNA injected oocytes. The positive control 5mM Gly-Gln was the only compound that showed significant rPepT1 mediated transport showing that the efflux assays worked successfully. The next step was to determine if the drugs in their prodrug version were transported by PepT1.

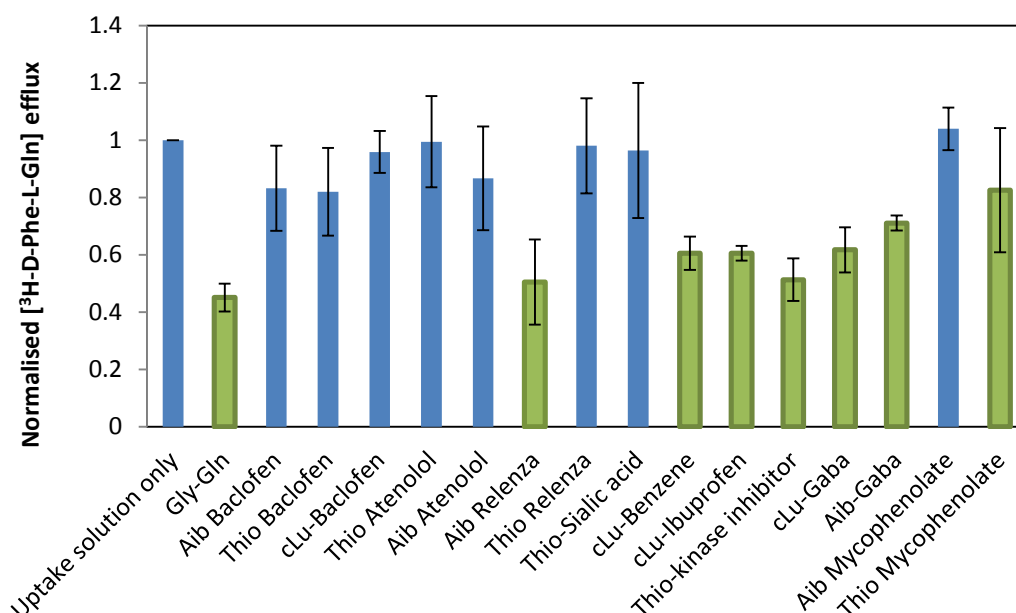


Figure 3.1.5-3 - Histogram representing the results obtained from the efflux experiments performed on prodrugs.

In the above graph the bars coloured in green represents compounds/prodrugs that showed significant reduction in the amount of [^3H]-D-Phe-L-Gln detected compared to negative control oocytes with uptake solution only. (Significance was determined using one sample t-test, $p < 0.05$) ($n=6$).

5 mM Gly-Gln was used a positive control for efflux experiments which showed significant transport evident from the reduction in the amount of [^3H]-Phe-L-Gln detected in the oocytes after 60 minutes. Among the prodrugs tested Aib-Relenza, cLu-Benzyl, cLu-Ibuprofen, Thio-Kinase inhibitor, cLu-Gaba, Aib-Gaba and Thio-mycophenolate showed significant efflux ($p < 0.05$) while the other compounds did not. To further verify PepT1 mediated transport of the compounds, trans-epithelial transport assays were setup using Caco-2 cells.

3.1.6 Determination of hPepT1 mediated transport of novel prodrugs in differentiated Caco-2 cell monolayers grown on Transwell® plates

The rPepT1 mediated transport of the novel compounds were analysed using efflux assays in rPepT1 cRNA injected oocytes. To further verify the PepT1 mediated transport of the novel compounds differentiated Caco-2 cells expressing hPepT1 transporter was used. This method of performing transport assays using differentiated Caco-2 monolayers in Transwell® inserts not only evaluates prodrug transport into the cell (from the apical side to the inside of the cell) but also the transport of prodrugs from inside the cells to the outside through the basolateral membrane. The Transwell assays were performed as mentioned in (Section 2.4.5)

Table 2.4-3 - Conditions used for compound/prodrug detection in HPLC

Compounds/Prodrugs	Retention time the peak in HPLC (min)	Concentration of methanol in 21mM KH_2PO_4 (%)
FSA	5.1	30
Thio-Atenolol	6.4	20
Aib-Atenolol	6.1	10
Thio-Baclofen	5.6	20
Aib-Baclofen	8.8	30
cLu-Baclofen	6.9	30
cLu-Ibuprofen	7.9	30
Thio-Mycophenolate	9.1	30

The above table lists the conditions used for detecting the prodrugs and FSA for analysing the transport of the compounds obtained from the Caco-2 assay. The rest of prodrugs could not be detected with the HPLC column (reverse phase) and the mobile phase (ranging from 10% to 95% Methanol supplemented with 21 mM KH_2PO_4) as the compounds eluted along with the solvent front during the HPLC run making it difficult to quantify the compounds. However, Caco-2 transport assays were performed on all the prodrugs available and the Krebs media (from the basolateral side of the Transwell) obtained from the Caco-2 assay were stored in -20°C freezer until a suitable HPLC column and a compatible mobile phase will be established for detecting these prodrugs.

3.1.6.1 Transport of FSA in differentiated Caco-2 cell (Experiment 1)

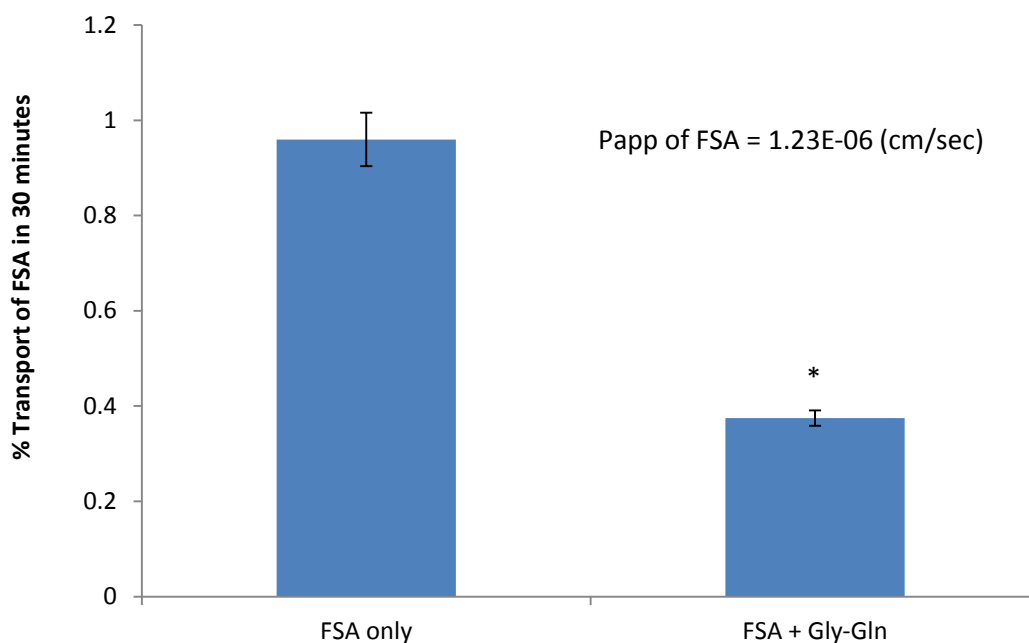


Figure 3.1.6-1 - Comparison of PepT1 mediated transport of positive control compound PheΨ[CS-NH]-Ala (FSA) in Caco-2 cell monolayers grown on Transwell® inserts with and without Gly-Gln.

Each bar in the histogram represents average transport of the test compound +/- standard deviation from 3 three separate inserts of Caco-2 cell monolayers. The rate of PepT1 mediated transport of FSA was found to be 2.9 nmoles/well/hr. (* = Unpaired t-test of transport of the test compound in the presence and absence of Gly-Gln, p-value < 0.05; n= 3)

3.1.6.2 Transport of cLu-Baclofen in differentiated Caco-2 cell (Experiment 1)

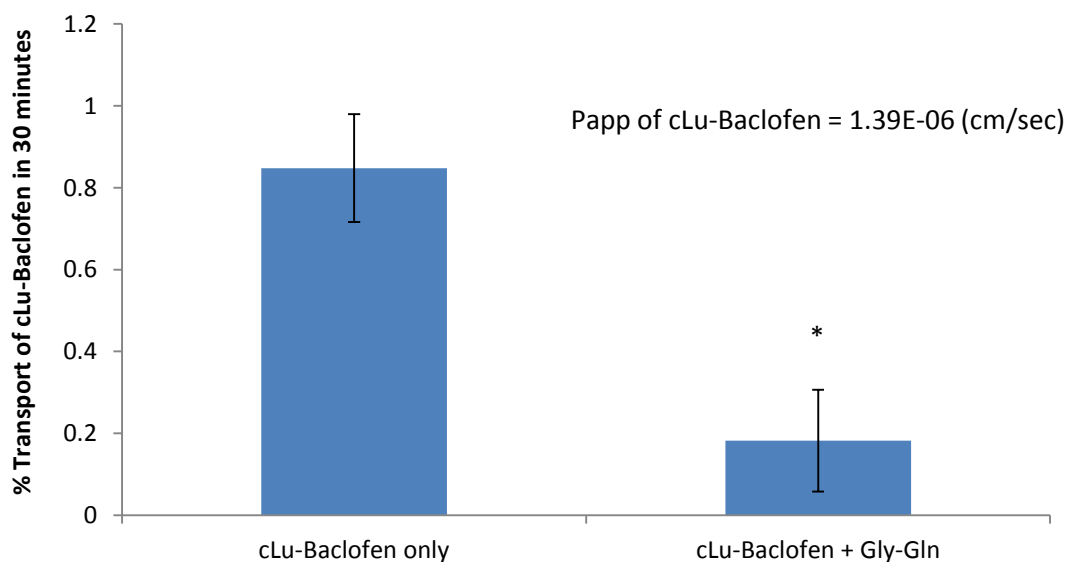


Figure 3.1.6-2 - Comparison of PepT1 mediated transport of test compound cLu-Baclofen in Caco-2 cell monolayers grown on Transwell® inserts with and without Gly-Gln.

Each bar in the histogram represents average transport of the test compound +/- standard deviation from 3 three separate inserts of Caco-2 cell monolayers. The rate of PepT1 mediated transport of cLu-Baclofen was found to be 3.31 nmoles/well/hr. (* = unpaired t-test of transport of the test compound in the presence and absence of Gly-Gln, p-value < 0.05; n= 3)

3.1.6.3 Transport of FSA in differentiated Caco-2 cell (Experiment 2)

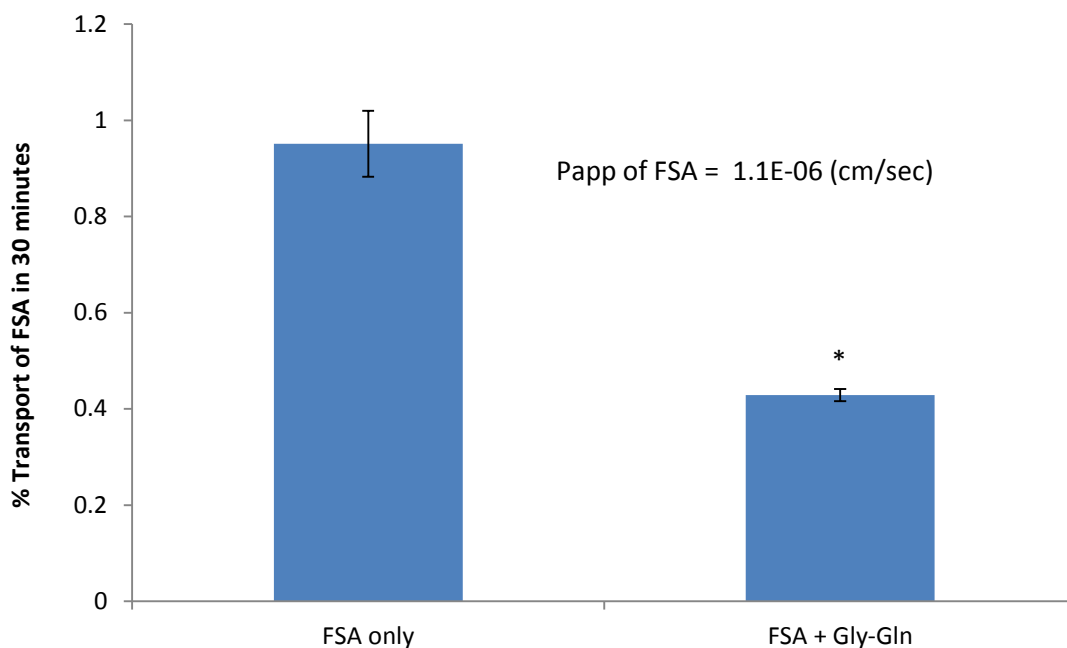


Figure 3.1.6-3 - Comparison of PepT1 mediated transport of positive control compound PheΨ[CS-NH]-Ala (FSA) in Caco-2 cell monolayers grown on Transwell® inserts with and without Gly-Gln.

Each bar in the histogram represents average transport of the test compound +/- standard deviation from 3 three separate inserts of Caco-2 cell monolayers. The rate of PepT1 mediated transport of FSA was found to be 2.6 nmoles/well/hr. (* = unpaired t-test of transport of the test compound in the presence and absence of Gly-Gln, p-value < 0.05; n= 3)

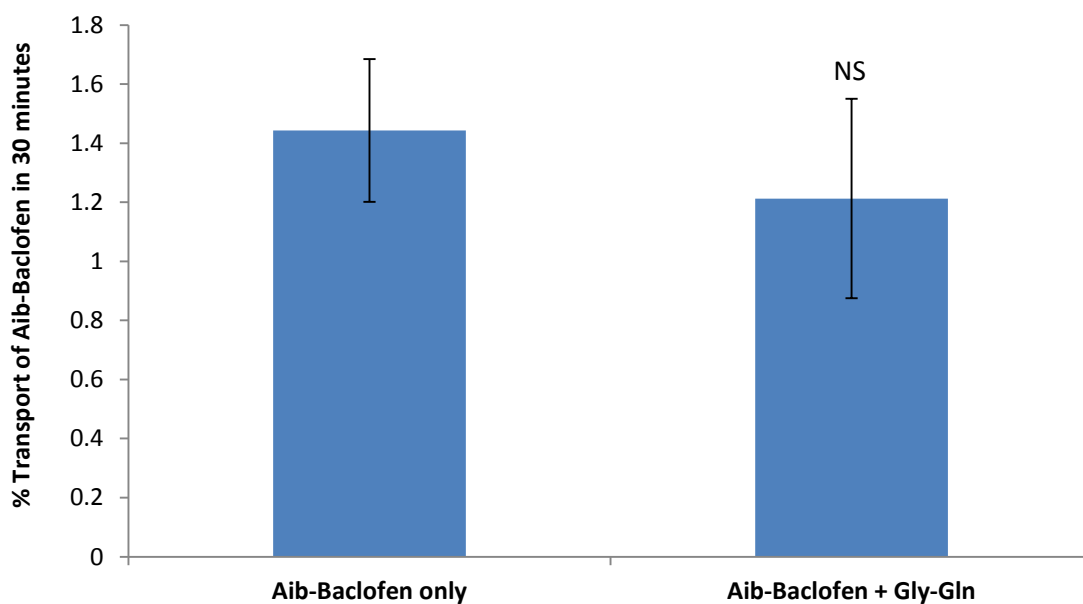
Transport of Aib-Baclofen in differentiated Caco-2 cell (Experiment 2)

Figure 3.1.6-4 - Comparison of PepT1 mediated transport of test compound Aib-Baclofen in Caco-2 cell monolayers grown on Transwell® inserts with and without Gly-Gln.

Each bar in the histogram represents average transport of the test compound +/- standard deviation from 3 three separate inserts of Caco-2 cell monolayers. (NS = non-significant, p-value > 0.05, unpaired t-test of transport of the test compound in the presence and absence of Gly-Gln; n= 3)

3.1.6.4 Transport of Thio-Atenolol in differentiated Caco-2 cell (Experiment 2)

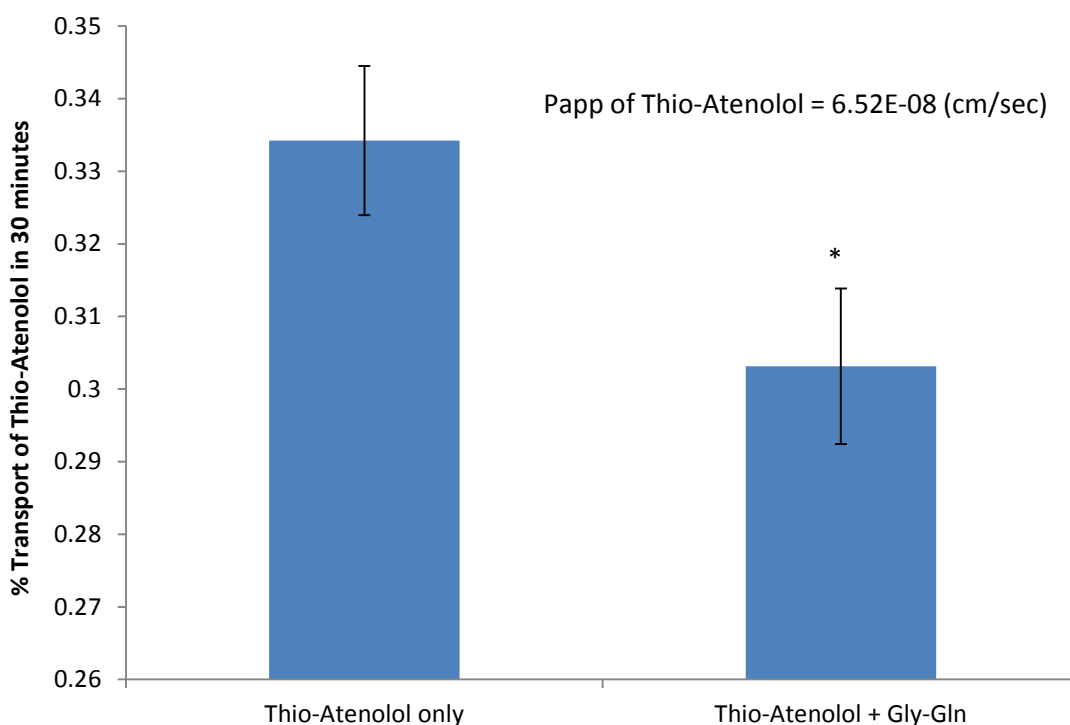


Figure 3.1.6-5 - Comparison of PepT1 mediated transport of test compound Thio-Atenolol in Caco-2 cell monolayers grown on Transwell® inserts with and without Gly-Gln.

Each bar in the histogram represents average transport of the test compound +/- standard deviation from 3 three separate inserts of Caco-2 cell monolayers. The rate of PepT1 mediated transport of Thio-Atenolol was found to be 0.15 nmoles/well/hr. (* = unpaired t-test of transport of the test compound in the presence and absence of Gly-Gln, p-value < 0.05; n= 3)

3.1.6.5 Transport of cLu-Ibuprofen in differentiated Caco-2 cell (Experiment 2)

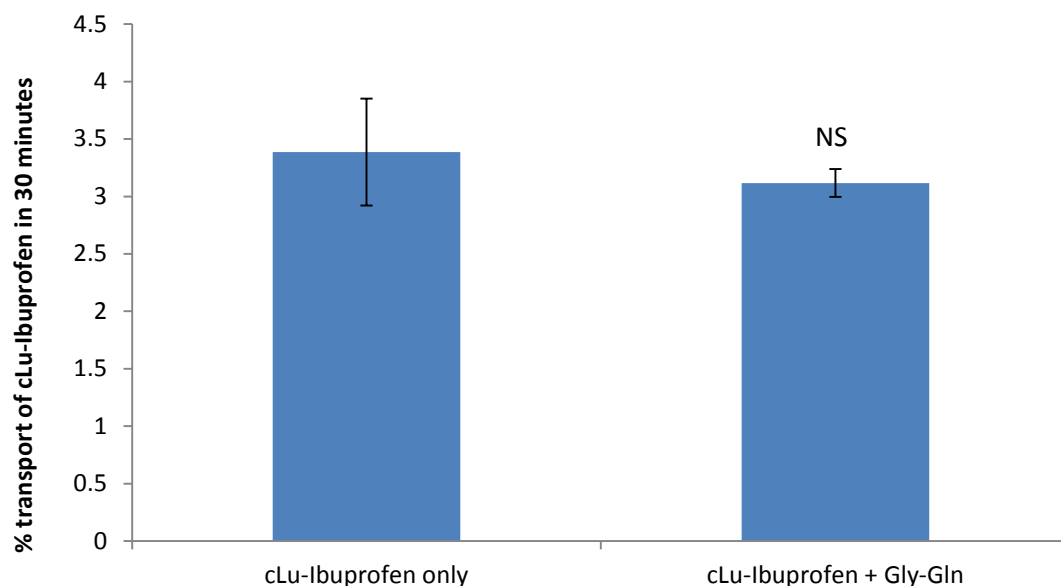


Figure 3.1.6-6 - Comparison of PepT1 mediated transport of test compound cLu-Ibuprofen in Caco-2 cell monolayers grown on Transwell® inserts with and without Gly-Gln.

Each bar in the histogram represents average transport of the test compound +/- standard deviation from 3 three separate inserts of Caco-2 cell monolayers. (NS = non-significant, p-value > 0.05, unpaired t-test of transport of the test compound in the presence and absence of Gly-Gln n= 3)

3.1.6.6 Transport of Thio-Baclofen in differentiated Caco-2 cell (Experiment 2)

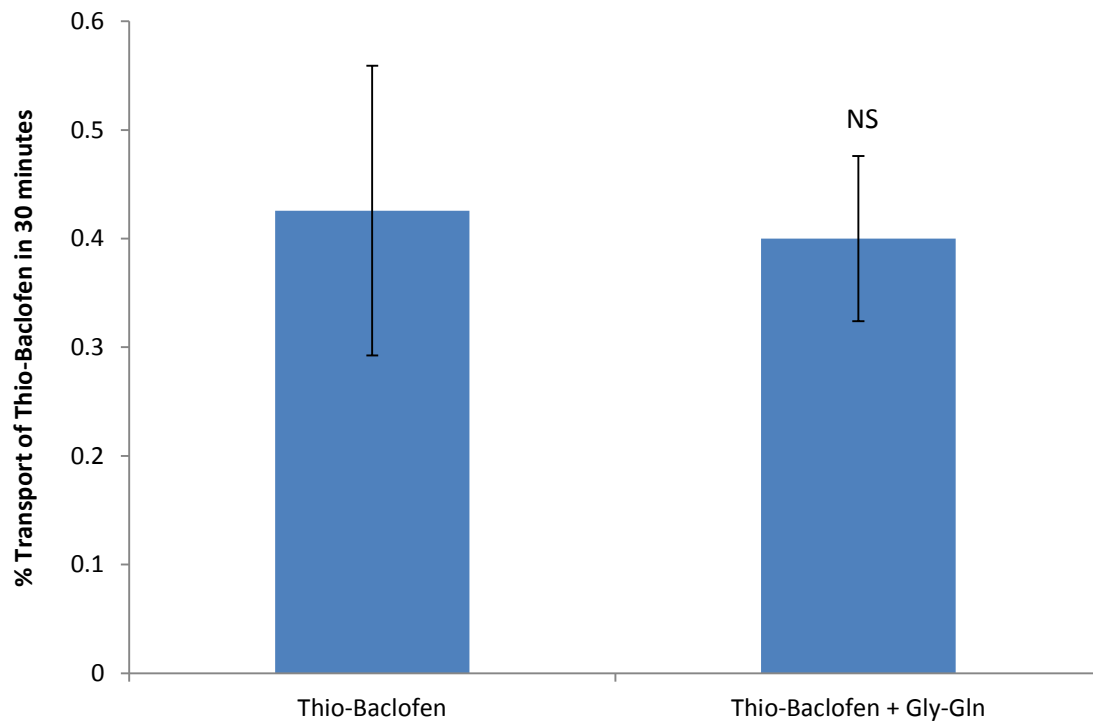


Figure 3.1.6-7 - Comparison of PepT1 mediated transport of test compound Thio-Baclofen in Caco-2 cell monolayers grown on Transwell® inserts with and without Gly-Gln.

Each bar in the histogram represents average transport of the test compound +/- standard deviation from 3 three separate inserts of Caco-2 cell monolayers. (NS = non-significant, p-value > 0.05, unpaired t-test of transport of the test compound in the presence and absence of Gly-Gln n= 3)

3.1.6.7 Transport of FSA in differentiated Caco-2 cell (Experiment 3)

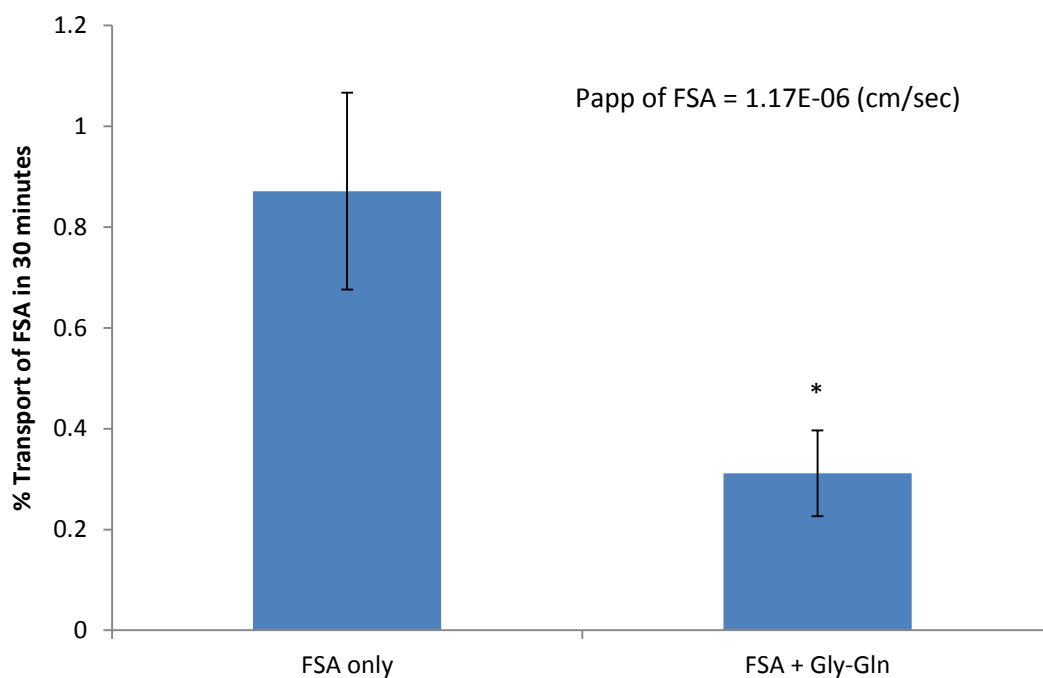


Figure 3.1.6-8 - Comparison of PepT1 mediated transport of positive control compound FSA in Caco-2 cell monolayers grown on Transwell® inserts with and without Gly-Gln.

Each bar in the histogram represents average transport of the test compound +/- standard deviation from 3 three separate inserts of Caco-2 cell monolayers. The rate of PepT1 mediated transport of FSA was found to be 2.79 nmoles/well/hr. (* = unpaired t-test of transport of the test compound in the presence and absence of Gly-Gln, p-value < 0.05; n= 3)

3.1.6.8 Transport of Aib-Atenolol in differentiated Caco-2 cell (Experiment 3)

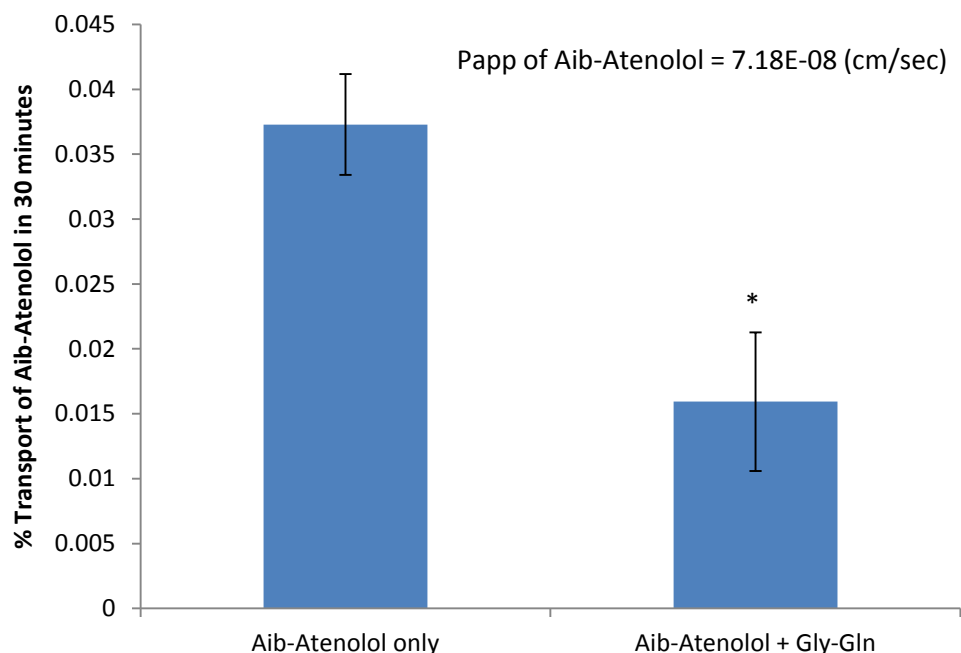


Figure 3.1.6-9 - Comparison of PepT1 mediated transport of positive control compound Aib-Atenolol in Caco-2 cell monolayers grown on Transwell® inserts with and without Gly-Gln.

Each bar in the histogram represents average transport of the test compound +/- standard deviation from 3 three separate inserts of Caco-2 cell monolayers. The rate of PepT1 mediated transport of Aib-Atenolol was found to be 0.18 nmoles/well/hr. (* = unpaired t-test of transport of the test compound in the presence and absence of Gly-Gln, p-value < 0.05; n= 3)

Table 2.4-4 - Summary of rate of transport and Papp of the prodrugs as determined from Caco-2 Transwell assay

Prodrug	Rate of PepT1 mediated transport of prodrugs in caco2 cells (nmoles/well/hr)	Papp (cm/sec)	Significance (PepT1 mediated Transport)
cLu-Baclofen	3.31	1.39×10^{-6}	Yes
Aib-Baclofen	N/A	N/A	No
Thio-Baclofen	N/A	N/A	No
cLu-Ibuprofen	N/A	N/A	No
Thio Atenolol	0.15	0.065×10^{-6}	Yes
Aib-Atenolol	0.18	0.071×10^{-6}	Yes
FSA (Average from 3 separate experiments)	2.76	1.16×10^{-6}	Yes

Note: In the above table N/A means not applicable. These compounds did not exhibit significant PepT1 mediated transport in Caco-2 assays.

Table 2.4-5 - Summary of the absolute transport of compounds in the Caco-2 assay in the absence of Gly-Gln

Prodrug	Total rate transport of prodrugs in caco2 cells (nmoles/well/hr)	Papp (cm/sec)
FSA	4.73	2×10^{-6}
Aib-Baclofen	2.10	0.88×10^{-6}
cLu-Ibuprofen	16.86	7.1×10^{-6}
Thio-Baclofen	9.21	3.9×10^{-6}

The above table shows the total rate of transport for the compounds in the absence of Gly-Gln which is a competitive inhibitor of PepT1 substrates.

3.1.7 Discussion

This study was performed to test if the novel peptide carriers, namely Aib-, cLu- and Thio-, enabled the conjugated drugs to be transported by the PepT1 transporter. The first step in this process was to determine the binding affinity of the prodrugs towards PepT1 by performing transport assays on rPepT1 cRNA injected oocytes. It was found that all the prodrugs tested did interact with rPepT1 with binding affinities ranging from a relatively high affinity of 0.041 ± 0.005 mM for Thio-Sialic acid to lower binding affinity of 1.292 ± 0.710 mM for Aib-Atenolol, as summarized in the Table 2.4-1. It must be noted that the binding affinities established for the prodrugs are similar to those obtained for natural di- and tri- peptides which have been previously reported to be PepT1 substrates with binding affinities such as Alanyl-Phenylalanine (0.07 mM), Glycyl-Arginine (1.82 mM) and Glycyl-Glycine-Glycine (1.07 mM) (Brandsch *et al.*, 2004; Vig *et al.*, 2006). The transport assay demonstrates that the prodrugs bind to PepT1 transporter but does not demonstrate if the prodrugs were transported into the cell as a substrate. To determine PepT1 mediated transport, trans-stimulation assays were setup in *X. laevis* oocytes as described in section 2.3.5. It was found that Aib-Relenza, Aib-Gabapentin, Thio-Kinase inhibitor, Thio-Mycophenolate, cLu-Benzyl, cLu-Ibuprofen and cLu-Gabapentin showed significant PepT1 mediated transport while the other prodrugs although bound to PepT1 they were not transported (Figure 3.1.5-3). The efflux assays demonstrates that 7 out of the 15 prodrugs tested were transported by PepT1 showing that all the carriers tested cLu-, Thio- and Aib were able to facilitate the PepT1 mediated transport.

To further verify PepT1 mediated transport of the novel prodrugs all the 15 prodrugs were subjected to transport assays (direction of transport = apical to basolateral) using differentiated Caco-2 cells which express hPepT1 transporter when grown on Transwell® inserts (Hidalgo *et al.*, 1989). This model of differentiated Caco-2 cells mimics the conditions prevalent in the intestine (site of absorption of nutrients and drugs) wherein the drugs/nutrients only reach the blood circulation from the intestinal lumen after passing through the apical and basolateral membranes as well as being exposed to membrane bound and cytoplasmic enzymes. The Caco-2 experiments were performed with FSA as a positive control and only experiments in which the FSA transport was significantly inhibited by 20 mM Gly-Gln (a competitive inhibitor of PepT1 transport) were used for measuring PepT1 mediated transport of prodrugs as this indicated an intact monolayer of differentiated Caco-2 cells. Similarly, 20 mM Gly-Gln was also used as a PepT1 inhibitor to delineate PepT1 mediated transport of prodrugs in Caco-2 cell assays such that a high concentration of Gly-Gln would completely saturate the PepT1 transporter, thus enabling the determination of PepT1 mediated transport of the prodrugs.

The performing of Caco-2 assay on each individual prodrug was limited by the amount of prodrug available and the ability to resolve the prodrugs using HPLC, as some of the prodrugs could not be resolved. In the Caco-2 assay it was found that cLu-Baclofen (Figure 3.1.6-2), Thio-Atenolol (Figure 3.1.6-5) and Aib-Atenolol (Figure 3.1.6-9) were transported significantly by PepT1 with apparent rate of PepT1 mediated transport (P_{app}) of 1.39×10^{-6} (cm/sec), 0.065×10^{-6} (cm/sec), and 0.071×10^{-6} (cm/sec) respectively. Compared to the known PepT1 substrate FSA (P_{app} in this study = 1.16 cm/sec) the P_{app} of cLu-Baclofen was 1.19 fold faster than FSA while the P_{app} of Thio-Atenolol and Aib-Atenolol was slower than FSA by 17 and 16 fold respectively. From a previous study set up to determine the drug transport characteristics of Thio- dipeptides it was found that prodrugs with P_{app} values ranging from 0.34×10^{-6} (cm/sec) to 2.6×10^{-6} (cm/sec) had K_i values of 0.79 ± 0.44 mM and 0.03 ± 0.005 mM respectively, showing that higher affinity prodrugs demonstrated better P_{app} values for PepT1 in Caco-2 assays (Foley *et al.*, 2009b). The lower P_{app} values for Thio- and Aib-forms of Atenolol could be due to the lower affinity of these prodrugs towards PepT1 when compared to cLu-Baclofen. The transport demonstrated by Caco-2 cells have been previously shown to underestimate PepT1 mediated transport of drugs (Balimane *et al.*,

2007). Therefore future *in vivo* experiments in rat models could be used to further test the oral bioavailability of the Aib- and Thio- carriers to deliver drugs.

The binding affinity of native Atenolol and Baclofen compounds (Table 2.4-2) was estimated to be similar (0.8 to 1.0 mM) but these drugs in their native forms were not found to be transported by PepT1 in the oocyte efflux assay (Figure 3.1.5-2). This shows that by linking the compounds Atenolol and Baclofen to carriers, the compounds could now be transported via the PepT1 showing that the carriers Aib-, Clu- and Thio- are effective carrier moieties. It can be seen that this is in contradiction with the results obtained from the efflux assays (Figure 3.1.5-3) in which cLu-Baclofen, Thio-Atenolol and Aib-Atenolol failed to show PepT1 mediated transport. This observation of PepT1 substrates giving a false negative in efflux assays in *X. laevis* but positive results in Caco-2 cells has been previously reported (Foley *et al.*, 2009b) where it was suggested that the recycling of the empty carrier (Figure 3.1.5-1) is no more the rate limiting step for the transport of certain compounds in the efflux assays.

The prodrugs Aib-Baclofen (Figure 3.1.6-4), cLu-Ibuprofen (Figure 3.1.6-6) and Thio-Baclofen (Figure 3.1.6-7) were detected in the basolateral isolates obtained from the Caco-2 assay. However it can be seen that there was no significant inhibition of these three prodrugs in the presence of the PepT1 inhibitor Gly-Gln. The prodrug cLu-Ibuprofen which showed positive PepT1 mediated transport in the efflux assay was not transported by PepT1 in the Caco-2 assay. When the absolute rate of transport in Caco-2 cells for cLu-Ibuprofen was calculated i.e. the rate of transport of cLu-Ibuprofen in the absence of Gly-Gln it was found that the rate of transport of cLu-Ibuprofen was 4 times higher than the absolute rate of transport of FSA (Table 2.4-5). A similar observation had been made in an earlier study in which a prodrug was found to show positive efflux results in the *X. laevis* oocyte assay but did not show significant transport of the prodrug in Caco-2 assay (Foley *et al.*, 2009b). It was suggested that since the rate of transport of the prodrug in Caco-2 cells was 2.8 fold greater than FSA it meant that other routes of absorption which did not exist in the simpler oocyte system were masking the PepT1 mediated component of transport. The transport observed (not mediated by PepT1) in case of Aib-Baclofen and Thio-Baclofen could be due to the non-transporter mediated diffusion/leakage of prodrugs through the Caco-2 monolayers or other transporters expressed by Caco-2 cells such as MRP, MDR, OATP OCT1 and MCT1

The PepT1 mediated transport of the cLu-Ibuprofen not being detected in the Caco-2 assay despite a positive oocyte efflux could be due to the presence of multi drug resistance proteins (MRP) on the apical membrane of Caco-2 cells (Gutmann *et al.*, 1999) which might have overlapping substrate specificity with PepT1. Therefore these MRP's could have actively expelled the drug back across the apical membrane of Caco-2 cells and no PepT1 mediated transport of the prodrug was seen. Another potential factor affecting the detection of the prodrugs in the Caco-2 assays are the transporters expressed in the basolateral membrane which might not mediate the transport of the prodrug through the basolateral side, thereby preventing the detection of the prodrugs in the basolateral isolates obtained from the Caco-2 assay. It was found that most of the prodrugs when tested for stability (pH and extracellular enzyme activity; Caco-2 cell homogenate) were found to be extremely stable with no degradation observed in the assays which lasted for up to 3 hours (unpublished work by project students). Therefore the instability of the prodrugs as a reason for negative results in Caco-2 assay can most likely be ruled out. The prodrug concentration within the Caco-2 cells, for prodrugs not transported by basolateral membrane cannot be estimated due to the compound being diluted by the cell content. However if prodrugs were radiolabeled, then this could provide an alternate way of detecting the remaining prodrug in the cells.

The Thio-Mycophenolate prodrug which showed positive efflux was also subjected to Caco-2 assay where it was found not to show significant transport of the pro-drug (data not shown). During the initial runs used to establish the concentration of the mobile phase and the elution time for Thio-Mycophenolate in the HPLC assay, it was found that the area representing 1mM concentration in the graph (highest concentration of the compound used for obtaining trace of the compounds) was significantly lower when compared to the area obtained for 1mM concentration for the other prodrugs tested. This showed that Thio-Mycophenolate had a relatively low UV absorption co-efficient and so the lowest amount detectable may be higher than the concentration of Thio-Mycophenolate in the basolateral compartment.

The HPLC analysis of the remaining prodrugs (Aib-Relenza, Thio-Relenza, Aib-Gaba, cLu-Gaba, cLu-Benzyl compound, Thio-Kinase inhibitor and Aib-Mycophenolate) could not be performed as they could not be separated efficiently using the HPLC column available. The analysis of the basolateral fraction obtained from the Caco-2 assay on these compounds using a suitable HPLC column would further strengthen and

verify the results obtained from the efflux assay studies performed using *X. laevis* oocytes.

Table 2.4-6 - Summary of Efflux data and Caco-2 data for prodrugs

Compound	Ki (mM)			
	Native compound	Aib-version	cLu-version	Thio-version
Baclofen	0.910 +/- 0.930 ◆	0.190 ± 0.51 ◆ ●	0.035 ± 0.008 ◆ ● (Papp = 1.39 x 10 ⁻⁶ cm/sec)	1.232 ± 0.408 ◆ ●
Atenolol	0.8 +/- 0.048 ◆	1.292 ± 0.710 ◆ ● (Papp = 0.071 x 10 ⁻⁶ cm/sec)	X	0.957 ± 0.335 ◆ ● Papp = (0.065 x 10 ⁻⁶ cm/sec)
Relenza	does not bind to ◆ PepT1	0.259 ± 0.029 ◆ (ND)	X	0.185 ± 0.020 ◆ (ND)
Mycophenolate	does not bind to ◆ PepT1	0.304 ± 0.096 ◆ (ND)	X	0.245 ± 0.055 ◆ (ND)
Sialic acid	Compound not available	X	X	0.041 ± 0.005 ◆ (ND)
Gaba	Does not bind to ◆ PepT1	0.188 ± 0.020 ◆ (ND)	0.102 ± 0.046 ◆ (ND)	1.01 ± 0.330 ◆ ●
Benzyl	Compound not available	0.13 ◆ ●	0.043 ± 0.018 ◆ (ND)	0.25 ± 0.40 * ◆ ●
Ibuprofen	0.15 ± 0.07 ◆	0.07 ± 0.01 ◆ ●	0.082 ± 0.024 ◆ ●	0.04 * ◆ ●
Kinase inhibitor	Compound not available	X	X	0.107 ± 0.020 ◆ (ND)

In the Above table;

X = Compound not synthesised

ND = Compounds could not be detected using HPLC

● = Positive in Caco-2 assay

● = Negative in Caco-2 assay

◆ = Positive efflux

◆ = Negative efflux

The above Table 2.4-6 includes data from unpublished work at Oxford Brookes University; Thio-Gaba (David Meredith), Aib-Ibuprofen (Jay Rajamanickam), Aib-Benzyl (Myrtani Pieri). * = (Foley *et al.*, 2009b).

From the Table 2.4-6, it can be seen that the cLu- carrier consistently demonstrated higher affinity towards PepT1 followed by Aib- and Thio- carriers, both of which had comparable affinity profiles towards PepT1. Previously, computational studies of comparative molecular field analysis (CoMFA) and comparative molecular similarity indices analysis (CoMSIA), were performed on 79 di-peptides, 32 tri-peptides, 25 β -lactam antibiotics (PepT1 substrates) in order to establish a 3D quantitative structure-activity relationship (QSAR) model for predicting affinities of compounds towards PepT1 (Biegel *et al.*, 2005; Gebauer *et al.*, 2003). According to these studies it was found that the addition of a bulky side chain (R1 group) to the N terminus amino acid in a di-peptide increases the affinity of the substrate towards the PepT1 transporter. This prediction is in agreement with the finding that the cLu- carrier with the bulky cyclic R1 group at the amino terminal consistently showed higher binding affinities compared to Aib- and Thio carriers. This model also predicted the presence of a hydrophobic pocket for accommodating the R2 group at the C terminal in a dipeptide, which was in turn predicted to increase the affinity of the substrate with added bulky side chains. If this is the case then the affinity of the benzyl versions of the carriers should have demonstrated lower binding affinities compared to the carriers conjugated to the larger sized drugs such as kinase inhibitor, Atenolol and Relenza. From the results obtained in this study it can be seen that although the Thio-Kinase inhibitor demonstrated a slightly higher affinity towards PepT1 compared to the Thio-Benzyl compound (in agreement with the QSAR prediction), the Aib- and Thio- versions of Atenolol and Relenza show lower binding affinities compared to their respective benzyl forms. These results could be possibly explained by establishing the various structural conformers of the prodrugs and comparing the orientation of the C terminal R2 groups within the predicted binding site in the QSAR model developed by Gebauer *et al.*, 2003. This comparison could demonstrate if the R2 group in the low energy conformer of the prodrug occupies an area within the 3D QSAR model which has been predicted to have a negative effect on the binding of the prodrug, thereby reducing the affinity towards PepT1. In a previous study carried out to determine the effect of the size of the R1 group at the amino terminal of a di-peptide on binding affinity and transport by PepT1, the R group was replaced by 3 carbon to 6 carbon containing cyclic ring structure (unpublished work by David Meredith, Oxford Brookes University and Wilson Gayle, Keele University). It was found that the affinity of the di-peptide increased from 0.79 ± 0.41 mM to 0.17 ± 0.05 mM for the 3 carbon containing R1 group and 6 carbon containing R1 group respectively. However, efflux was significant for all the di- peptides except for the di-

peptide with 6 carbon containing R group. This further supports the prediction that increasing the bulk of the N terminal R1 group of di-peptides increases the affinity of PepT1 substrates.

The prodrug carriers Aib-, Thio- and cLu- were designed using the substrate binding template (Section 1.12.3). One of the important features for a substrate to bind efficiently to PepT1 is that the R1 group attached to the C α carbon of the first amino acid should be in the L- orientation (preferred) to a D- orientation. The Thio- carrier was designed to make the carrier resistant to hydrolysis by enzymes. In the Aib- carrier the H and R1 of the C α atom were both replaced by a methyl (CH₃) groups. In this case, the Aib conjugated prodrug on entering the substrate binding site would have a CH₃ group in both L and D orientation, which was predicted to have a much lower binding affinity towards PepT1. However, from the data obtained so far it can be seen that the affinity of the Aib- prodrugs was not affected dramatically as predicted, but in fact promoted binding and transport by PepT1 with similar binding affinity and transport to the Thio-prodrugs. The cLu- carrier was predicted to show reduced affinity towards PepT1 due to the increase in size of the R group at the NH₃- terminal and due to the inability of this cyclic group to re-orient itself on entering the substrate binding site. However, the converse was found: that cLu- carrier had much higher affinity towards PepT1 compared to the Aib- and Thio- carriers. The reason for this could be that the cLu-carrier as discussed earlier could be due to its increased bulk at the amino terminal which promoted better binding to PepT1 by forming more interactions with amino acid residues in the substrate binding site which were not accessible to the Aib- and Thio-carriers. The drugs conjugated to the carriers were highly diverse with respect to their size and also their hydrophobicity. Parent compounds arranged in decreasing order of hydrophobicity (Kinase inhibitor > Mycophenolate > Baclofen > Ibuprofen > Atenolol > Gaba > Gabapentin > Relenza > Sialic acid). From the current data obtained it can be said that the hydrophobicity of the native drugs did not affect the binding and transport of the prodrugs, showing that the carriers tested were efficient at delivering a diverse range of drugs utilizing PepT1 transporter.

From the above results it can be shown that carriers namely Clu-, Aib- and Thio- do have the ability to deliver drugs through PepT1 transporter. This conclusion can be drawn from the observation that the native drugs that bound to the PepT1 (Baclofen, Ibuprofen, Atenolol) and the drugs that did not interact with PepT1 (Mycophenolate, Relenza, Gabapentine) were all shown to be transported by one of the three carriers

tested. This shows that PepT1 is still a very important protein to be utilized for targeted delivery of drugs and for improving their bioavailability and the current drug carriers tested are all promising candidates to hijack the PepT1 transporters for drug deliver

4 Determining the function of the large extracellular domain between TMD9 and TMD10 in hPepT1 and hPepT2 transporters

4.1.1 Introduction:

The mammalian proton-coupled peptide transporter family (SLC15) are membrane proteins involved in the absorption of di- peptide and tri-peptides thereby acting as the major route of absorption of dietary nitrogen. These transporters utilize the inward directed proton gradient as the driving force to transport their substrates. PepT1 is expressed in both the intestine and kidney, while PepT2 is expressed predominantly in the kidney. The peptide transporters are also found to be involved in the absorption of peptide-like drugs such as angiotensin-converting enzyme inhibitors, aminoccephalosporins, anti-viral and anti-cancer drugs. It is this feature of the peptide transporters, of transporting peptide like drugs which has gained them considerable importance in the pharmaceutical industry facilitating targeted drug delivery.

PepT1 is widely considered as a low affinity, high capacity transporter whereas PepT2 as a high affinity, low capacity transporter. The hPepT1 and hPepT2 transporters share 50% amino acid identity and 70% amino acid similarity (Liu *et al.*, 1995). While the conserved areas lie in the putative TMD, most of the differences in the sequence appear in the loops connecting the TMD, particularly the large extracellular loop between the TMD9 and TMD10 with only 28% sequence identity (Appendix 10.1)

Several studies have been performed using PepT1 and PepT2 chimeras to establish the domains responsible for PepT1 and PepT2 specific characteristics. The chimera (Figure 4.1.1-1 a) containing the N terminal (1 to 401 amino acids, shaded black) from rPepT2 and the C terminal (402 to 707 amino acids, not shaded) from rPepT1 showed kinetic properties, such as substrate specificity, affinity and pH dependence of activation to be similar to that of PepT2. This suggested that the N terminal half is the region which contributes towards the specific transport characteristics of PepT2 (Doring *et al.*, 1996).

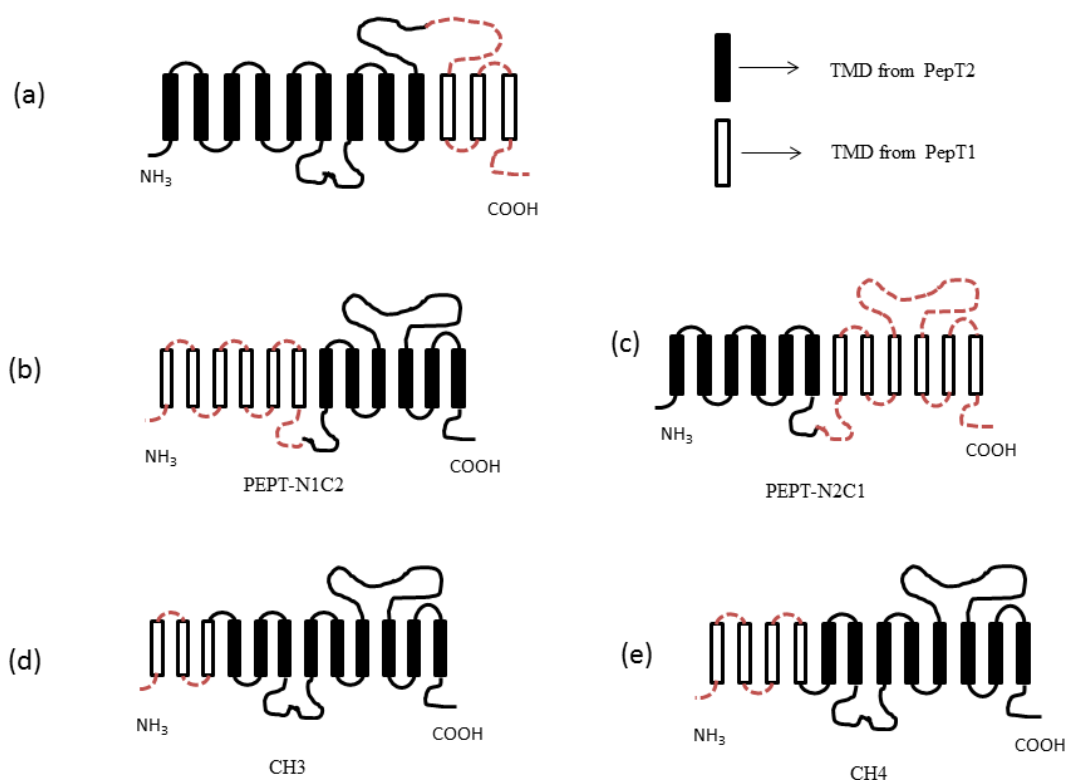


Figure 4.1.1-1 - Structures PepT1 and PepT2 chimeras.

Using the chimera with N terminal half (TMD1 to TMD6) of ratPepT1 with C terminal half (TMD7 to TMD12) from rat PepT2 designated as PEPT-N1C2 (Figure 4.1.1-1b) and vice versa PEPT-N2C1 (Figure 4.1.1-1c), it was found that the substrate affinity and pH dependency of PepT1 was controlled by the N terminal half. However, for PepT2 both the N terminal and C terminal halves were involved in substrate binding, and that C terminal alone played an active role in determining the affinity of PepT2 to its substrates (Terada *et al.*, 2000).

In a further study, when a chimera (designated as CH3, Figure 4.1.1-1d) containing the N- terminal from rPepT1 up to the 3rd TMD was fused with the C- termini of rPepT2 (4th TMD to 12th TMD), it was found that the chimera demonstrated the affinity features of PepT1 but the pH dependency of that of PepT2 (Doring *et al.*, 2002). In the same experiment, with another chimera (designated as CH4, Figure 4.1.1-1e) with 1st 4 TMD of PepT1 and the remaining TMD from PepT2 showed extreme pH dependency, wherein the chimera required very high external pH to reach half maximal transport. This study concluded that substrate affinity is controlled by N terminal domain within

the first three TMD and the pH dependency of PepT1 and PepT2 transporters are controlled by the interaction of the region between TMD3 and TMD4 with other protein domains.

The above studies did not completely narrow down on the exact region responsible for PepT1- and PepT2-like characteristics but suggested regions which could play an active role. Several features such as amino acids involved in substrate binding and proton binding have been published but none of the mammalian PepT transporters have been crystallised yet to confirm these findings. In the absence of crystal structures for these transporters computer based 3-D models have been proposed and these models were found to fit the data relating to the mutation studies performed on PepT transporters (Bolger *et al.*, 1998; Lee *et al.*, 1999; Yeung *et al.*, 1998). In 2003 crystallisation of 12 TMD containing, proton coupled lactose permease (LacY) (Abramson *et al.*, 2003) and glycerol-3-phosphate/inorganic phosphate anti-porter (GlpT) (Huang *et al.*, 2003) belonging to the MFS super family provided new insights into the structural similarity of the proteins in this super family. Since PepT1 belongs to the MFS superfamily of proteins, a homology model of PepT1 was proposed using a truncated rPepT1 protein sequence with the large extracellular loop between TMD9 and TMD10 removed from the wild type rPepT1. This was done to align the PepT1 sequence with LacY protein crystal, which lacks the large ECD present in PepT1 (Meredith and Price, 2006).

More recently a bacterial POT protein designated as PepTso, from the bacterium *Shewanella Oneidensis* was crystallised revealing the possible 3D structure of the mammalian PepT1 and PepT2 counterparts (Newstead *et al.*, 2011). PepTso shares 30% sequence identity with mammalian PepT1 and PepT2 transporters. The PepTso protein also shows conservation of all the previously identified amino acid residues found to play a critical role in the PepT1 and PepT2 proteins, including Histidine 61 (Histidine 57 in hPepT1) which when mutated, completely abolishes the transport mediated by PepT1 transporters (Uchiyama *et al.*, 2003). This protein was crystallised in the ligand bound occluded state, providing deeper insights about the peptide binding site and the mechanism of peptide transport. Since PepTso, several more crystals of bacterial proteins belonging to this family of proteins were made available such as PepTst from *Streptococcus thermophiles* (Solcan *et al.*, 2012) and GK POT from *Geobacillus kaustophilus* (Doki *et al.*, 2013) and PepTso₂ from *Shewanella Oneidensis* (Guettou *et al.*, 2013). Unlike the mammalian PepT1 and PepT2 transporters, all the crystallized bacterial POT proteins have 14 TMD i.e. two bundles of six transmembrane domains

connected by HA and HB helices. These bacterial proteins lack the large extracellular loop between TMD9 and TMD10 present in mammalian PepT1 and PepT2 transporters.

Dr Simon Newstead and colleagues at the Department of Biochemistry, University of Oxford crystallized only the extracellular domain (ECD) between TMD9 and TMD10 from the mouse PepT1 and rat PepT2 proteins respectively (in press). These crystal structures, for the first time showed that the ECD had a complex 3D structure made of beta sheets which form two lobes. The elucidation of this complex 3D structure presented the possibility of understanding the function of ECD, if any. The mouse PepT1 ECD and rat PepT2 ECD were crystallized which showed the presence of two immunoglobulin-like folds connected in tandem. The crystals structures obtained for mouse PepT1 and rat PepT2 (Figure 4.1.1-2) had a final resolution of 2.1 and 2.0 Angstroms (Å) respectively.



Figure 4.1.1-2 - Crystal structures of mouse PepT1-ECD (left) and rat PepT2 ECD (right).

PDB structures provided by Johnny Beale (Department of Biochemistry, Oxford University). Images rendered/coloured using PyMOL. (The PyMOL Molecular Graphics System, Version 1.7.4 Schrödinger, LLC).

PepT1 and PepT2 ECD's were determined to be monomers at physiological conditions. The ECD structures consisted of two compact β -sandwich immunoglobulin-like folds each made of four-stranded β -sheets. It was found that although the sequence identity between the two ECDs was less than 30%, their tertiary structures adopted the same overall structure which when superimposed had a root mean square deviation (r.m.s.d) of 1.83 Å. Using the bacterial crystal structures of PepTst and PepTso and the mammalian ECDs, homology models for the full-length mammalian transporters were constructed. Using small angle X-ray scattering (SAX) and analytical ultracentrifugation, it was observed that increasing the pH from 5.5 to 8.0 resulted in the weakening of the interface between the lobes in PepT2, such that the ECD became more elongated (unpublished, Dr Newstead). This observation was in contrast to PepT1, where the lobes in the ECD remained closely associated, in a more compact state. Molecular dynamics simulation suggested that the ECD would adopt a vertical orientation on top of the transporter. This would suggest the ECD's from the PepT1 and PepT2 could bind to an external regulatory component present in the lumen of the intestine. Interestingly it was found that the 3D structure of the ECD resembles the thyroxine hormone binding domain. This coupled to the fact that there was a very low sequence identity between PepT1 and PepT2 ECDs, presented the opportunity to pose the following questions:

4.1.2 Aims

- Does the ECD play a critical role in maintaining the structure and function of PepT1 and PepT2 proteins?
- Does the ECD contribute towards the differences in the kinetic properties of PepT1 and PepT2 proteins?
- Does the hormone thyroxine, bind to the ECD and does it have a regulatory function in PepT1 and PepT2 proteins?

4.1.3 Methods

4.1.3.1 FLAG epitope insertion in hPepT1 constructs

Flag Tag epitope DYKDDDDK was inserted in hPepT1 at 108 amino acid position using the following primers

- **hPT1PBFF-1 (5' end of hPepT1 in PBF vector)**

TTTGGCAGGGATCCGCCGCC

GGATCC (BamHI restriction site)

- **hPT1PBFR-2 (reverse primer sequence, 3' end of hPepT1 in PBF vector)**

AGCTGCAGATCTTCACTTGTCATC

(AGATCT = BglII restriction site)

- **hP1FLAGF-1 (FLAG forward primer)**

GTAAGCTCCATTAATGACCTCACAGACT**TACAAGGATGATGATGATA**
AG CACAACCATGATGGCACCCC CGACAGC

- **hP1FLAGR-1 (FLAG reverse primer)**

GCTGTCGGGGGTGCCATCATGGTTGTG**CTTATCATCATCATCCTTGT**
A GTCTGTGAGGTCATTAATGGAGCTTAC

In the above primers, hP1FLAGF-1 and hP1FLAGR-1 are the primer sequences containing the FLAG epitope (bold, underlined). Using hPepT1 wild type as template, two PCR reactions were set up simultaneously. The first with hPT1PBFF-1 (forward primer) + hP1FLAGR-1 (FLAG reverse primer) and the second reaction with hP1FLAGF-1 (FLAG forward primer) + hPT1PBFR-2 (hPepT1 reverse primer). The resulting PCR products were gel purified and 50ng of this purified PCR product was mixed together and a new PCR reaction was set up using hPT1PBFF-1 (forward primer) + hPT1PBFR-2 (hPepT1 reverse primer). The resulting PCR product was digested with BamHI and BglII and cloned into PBF vector digested with the same restriction enzymes.

4.1.4 Comparison of [³H]-D-Phe-L-Gln uptake between hPepT1 and hPepT2 ECD variant constructs

To establish the function of the ECD in PepT transporters, hPepT1 and hPepT2 ECD mutants were constructed. All the hPepT1 and hPepT2 constructs used in the experiments were gifted to us by Dr Simon Newstead (Oxford University). The hPepT constructs were cloned into PBF vector, between the 5'-BamHI and 3'-BglII restriction sites, under the control of SP6 promoter. A Kozak sequence GCCGCC was inserted between the restriction site and start codon on the hPepT constructs to improve translation of mRNA synthesized. The hPepT1 and hPepT2 ECD constructs used are as follows;

hPepT1-ECDΔ = hPepT1 with the ECD removed

hPepT1-ECD2 = hPepT1 with the ECD from hPepT2

hPepT2-ECDΔ = hPepT2 with the ECD removed

hPepT2-ECD1 = hPepT2 with the ECD from hPepT1

Transport experiments were performed with hPepT1 and hPepT2 ECD variants using [³H]-D-Phe-L-Gln. All the transport experiments were performed with wild type hPepT constructs serving as positive controls and NI oocytes as negative controls.

4.1.5 Comparison of [^3H]-D-Phe-L-Gln uptake between hPepT2 and hPepT2 ECD variant constructs

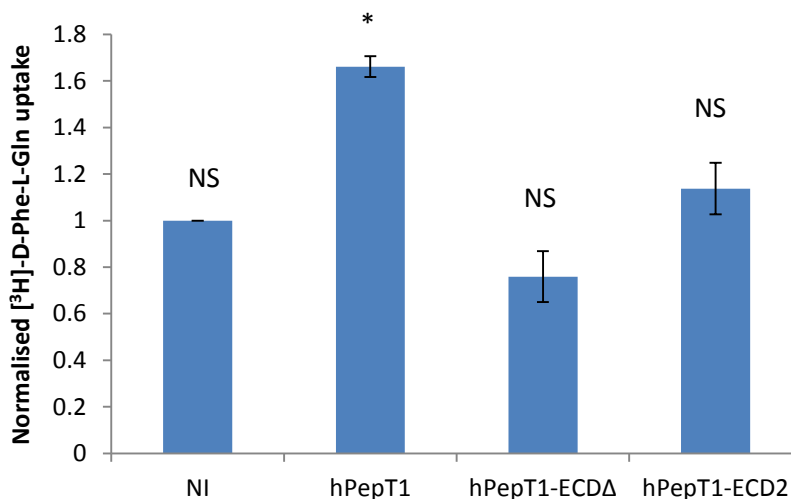


Figure 4.1.5-1 - Comparison of uptake between hPepT1 ECD variants.

The histogram represents normalized uptake of [^3H]-D-Phe-L-Gln in cRNA injected oocytes. Each bar is the mean \pm Standard error of 3 experiments with 5 oocytes replicates. NI uptake was found to be 32.43 ± 4.32 fmoles/oocyte/hour. (* = unpaired t-test with NI, p-value < 0.05)

From the uptake experiments with hPepT1 and its ECD variants (Figure 4.1.5-1) it was seen that both hPepT1 ECD variants, hPepT1-ECD Δ and hPepT1-ECD2 did not show significant transport of [^3H]-D-Phe-L-Gln when compared to the wild type. The wild type flagged hPepT1 construct was found to show lower transport rate compared to rPepT1 flagged construct. This could be mostly due to lower amount of flagged hPepT1 protein as the K_i of this construct was found to be similar to that of wild type hPepT1 without flag when Gly-Gln was used as a substrate (approx 0.2mM, data not shown)

4.1.6 Comparison of [³H]-D-Phe-L-Gln uptake between hPepT2 and hPepT2 ECD variant constructs

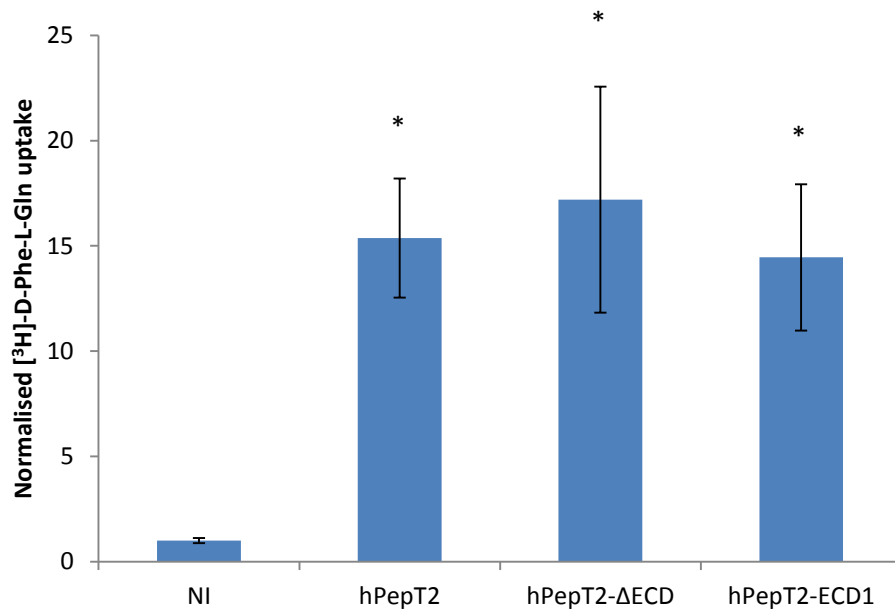


Figure 4.1.6-1 - Comparison of uptake between hPepT2 and its ECD variants. The histogram represents normalized uptake of [³H]-D-Phe-L-Gln in cRNA injected oocytes.

Each bar is the mean ± Standard error of 3 experiments with 5 oocytes replicates. NI uptake was found to be 5.42 ± 0.63 fmoles/oocyte/hour. (* = unpaired t-test with NI, p-value < 0.05)

In comparison to PepT1 ECD variants, both hPepT2-ECDΔ and hPepT2-ECD1 variants transported [³H]-D-Phe-L-Gln (Figure 4.1.6-1) which showed uptake similar to that of the wild type hPepT2.

Since the hPepT1 ECD variants failed to transport, their surface expression in oocytes were checked. The FLAG epitope tag (DYKDDDDK) was introduced at the 108 amino acid position, as this position has previously been shown to result in a functional hPepT1 transporter after the insertion of an EE epitope tag (Covitz *et al.*, 1998). The surface expression of the FLAG tagged hPepT1 ECD constructs were checked using the luminometry technique (Section 2.3.6)

4.1.7 Luminometric estimation of surface expression of FLAG tagged PepT1 ECD variant constructs

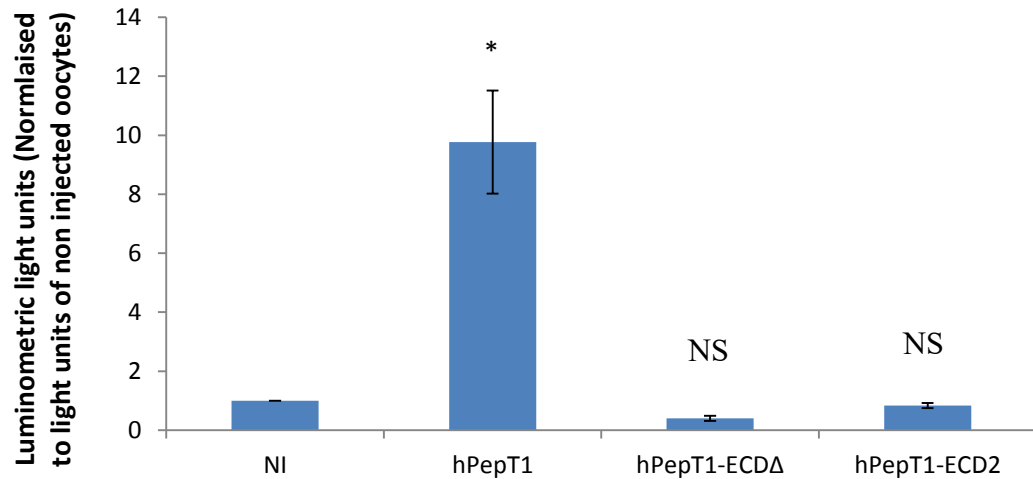


Figure 4.1.7-1 - Luminometric expression of hPepT1 ECD mutants.

Each bar represents the mean \pm standard error of 3 experiments with 12 oocyte replicates. NI luminescence was found to be 3155 ± 488 luminometric light units. (* = unpaired t-test with NI, p-value < 0.05 ; NS = Not significant)

The FLAG tagged wild type hPepT1 served as a successful positive control with significant surface expression which was 9 times higher than the NI negative control Figure 4.1.7-1. However, the hPepT1 ECD variants did not show significant surface expression. Western blot analysis showed that the hPepT1 ECD variants were not synthesised (Johnny Beale, Oxford University, unpublished data).

To check if the ECD played a crucial role in determining the affinity of hPepT2 towards its substrates, experiments were performed to determine the inhibition constant (K_i) of hPepT2 and hPepT1 which is an indicator of affinity of the transporter to its substrates.

4.1.8 Effect of ECD on affinity of hPepT2 and hPepT2 ECD variants their substrates.

In order to check if the ECD in hPepT2 plays an active role in determining the affinity of hPepT2 towards its substrates, the K_i (inhibition constant against [^3H]-D-Phe-L-Gln) were established for hPepT2 and its ECD variants. The K_i was also determined for hPepT1 wild type to check if the hPepT2-ECD1 construct would have the affinity characteristics of hPepT1. The antibiotic Cefaclor and di-peptide L-Lysyl-L-Lysine (Lys-Lys) were the two substrates chosen to establish the affinity of hPepT1, hPepT2 and its ECD variants. Cefaclor and Lys-Lys were chosen as they have been previously reported to have a different affinity towards PepT1 and PepT2 (Bretschneider *et al.*, 1999; Luckner and Brandsch, 2005; Theis *et al.*, 2002). If the ECD made a significant contribution to the affinity of PepT1 and PepT2 then this would result in the swapping of affinity between hPepT2 and hPepT1 constructs. Since hPepT1-ECD Δ and hPepT1-ECD2 do not transport or express, these constructs were not included in the tests.

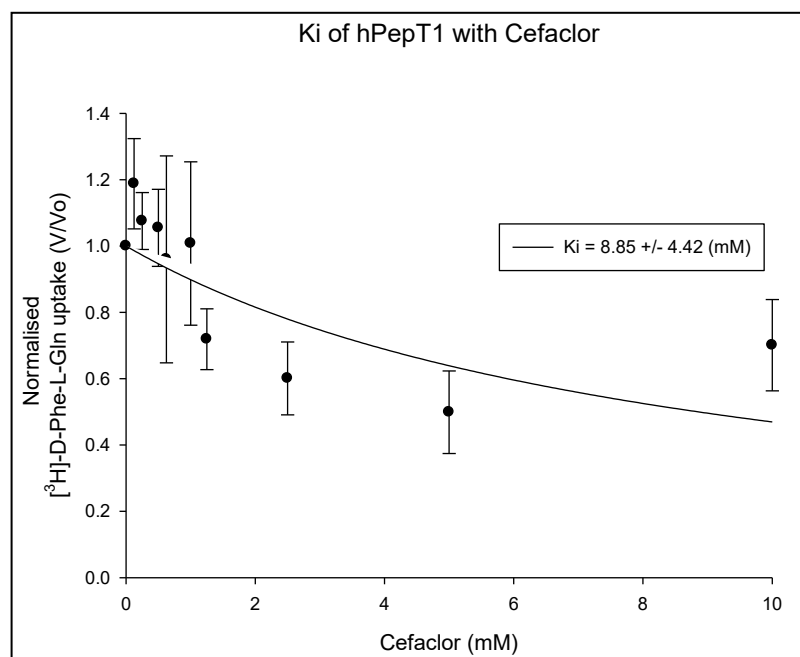


Figure 4.1.8-1 - K_i of cefaclor in hPepT1.

Data was normalised to hPepT1 wild type uptake in the absence of cefaclor. Normalised hPepT1 uptake with 0mM concentration of cefaclor was found to be 46.86 ± 8.95 fmol/oocyte/hour ($n = 5$)

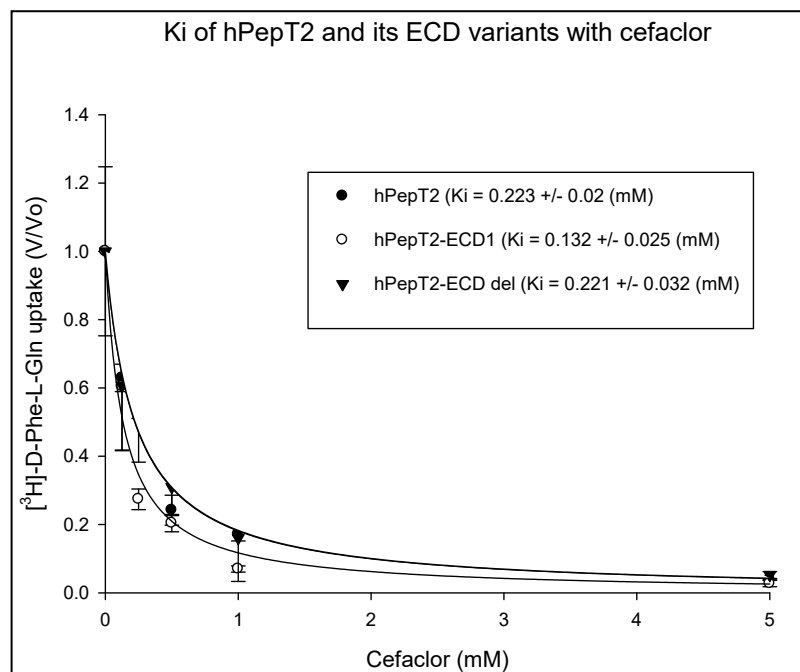


Figure 4.1.8-2 - K_i of cefaclor with hPepT2, hPepT2-ECD1 and hPepT2-ECDΔ

Data was normalised to hPepT2 wild type uptake in the absence of cefaclor. Normalised hPepT2 wild type uptake with 0mM concentration of Cefaclor was found to be 83 ± 15 fmol/oocyte/hour, 109 ± 34 fmol/oocyte/hour, 78 ± 18 for hPepT2, hPepT2-ECDΔ and hPepT2-ECD1 respectively. ($n = 2$)

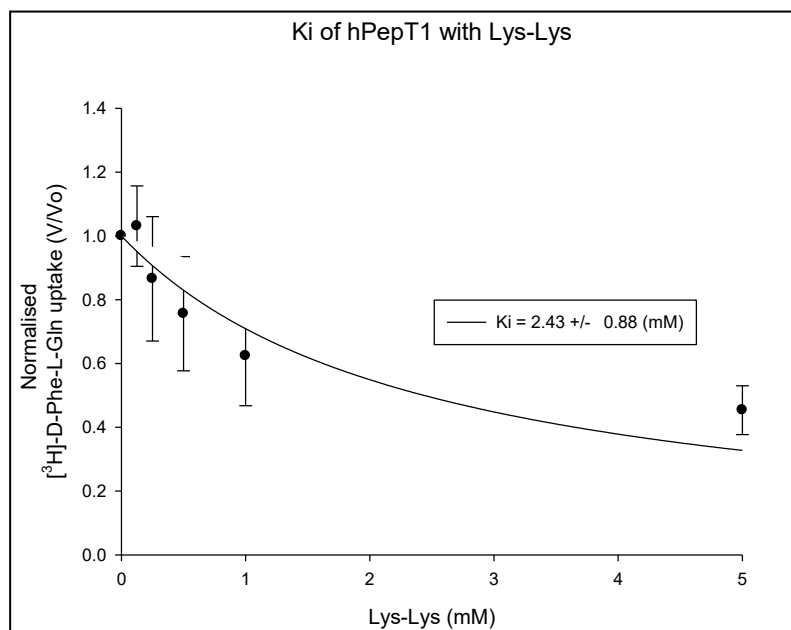


Figure 4.1.8-3 - Ki of Lys-Lys with hPepT1.

Data was normalised to hPepT1 wild type uptake in the absence of Lys-Lys. Normalised hPepT1 uptake with 0mM concentration of Lys-Lys was found to be 46.86 ± 8.95 fmol/oocyte/hour ($n = 3$)

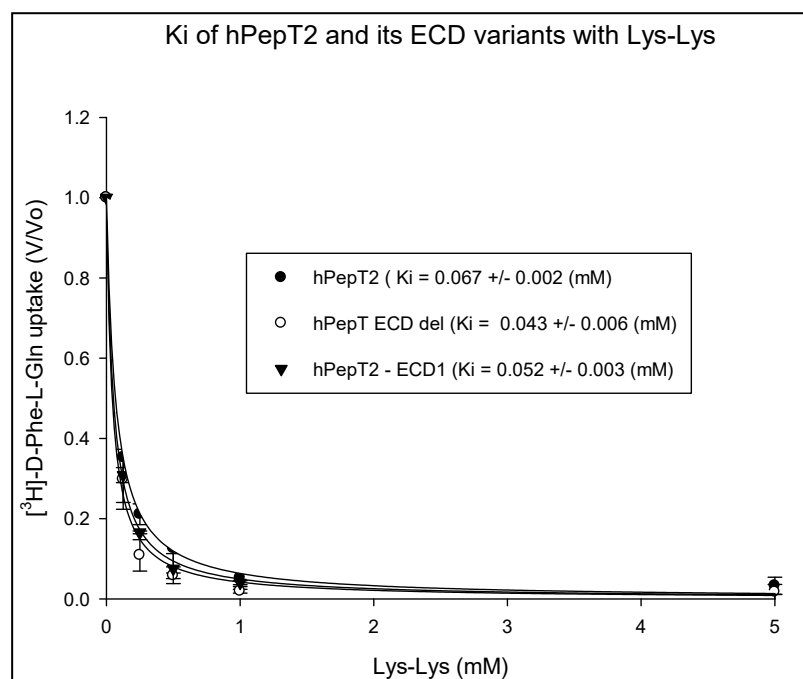


Figure 4.1.8-4 - Ki of hPepT2, hPepT2-ECD1 and hPepT2-ECDΔ with Lys-Lys.

Data was normalised to hPepT2 wild type uptake in the absence of Lys-Lys. Normalised hPepT2 wild type uptake with 0mM concentration of Lys-Lys was found to be 83 ± 15 fmol/oocyte/hour, 109 ± 34 fmol/oocyte/hour, 78 ± 18 for hPepT2, hPepT2-ECDΔ and hPepT2-ECD1 respectively. ($n = 2$)

The K_i of hPepT1 with Cefaclor and Lys-Lys was found to be 8.85 ± 4.42 mM (Figure 4.1.8-1) and 2.43 ± 0.88 mM respectively (Figure 4.1.8-3). Compared to hPepT1, hPepT2 and its ECD variants showed higher affinity ranging from 0.223 mM for cefaclor and 0.043 mM for Lys-Lys. The affinities of hPepT2 ECD variants were found to be similar to that of the wild type hPepT2 with both the substrates Cefaclor and Lys-Lys.

Since the ECD in hPepT2 did not seem to play a significant role in determining the affinity of hPepT2 towards its substrates, experiments were performed to check if the ECD could affect the pH sensitivity of hPepT2. The effect of pH on PepT2 ECD was selected as a parameter to investigate, as it was observed that increasing the pH from 5.5 to 8.0 resulted in the weakening of the interface between the lobes in PepT2 ECD, such that the ECD become more elongated (Newstead and group, unpublished). This was in contrast to PepT1, where the lobes remained closely associated, in a more compact state as suggested from SAXS and AUC data.

4.1.9 Effect of pH on uptake of [3 H]-D-Phe-L-Gln in hPepT2 and hPepT2-ECDA

In order to check if the ECD deletion in hPepT2 affects its transport optimum, hPepT2 wild type and hPepT2-ECDA cRNA injected oocytes were used. Uptake assay was performed using [3 H]-D-Phe-L-Gln for one hour with pH value of uptake media ranging from 5.5 to 7.5.

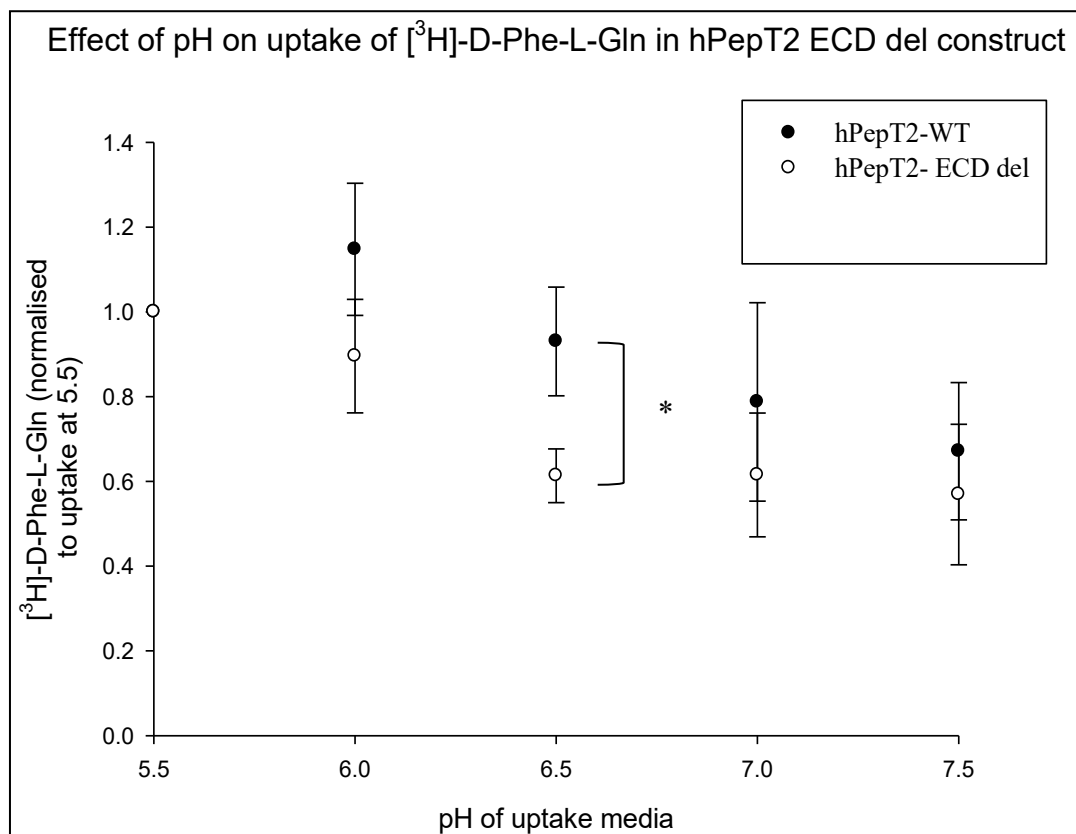


Figure 4.1.9-1 - Effect of pH on transport of hPepT2 ECD. Uptake of hPepT2 wild type and hPepT2-ECD Δ using [3 H]-D-Phe-L-Gln.

The pH of the uptake media ranging from 5.5 to 7.5 from 5 independent experiments with 5 oocyte replicates. Data was normalized to uptake of hPepT2 wild type and hPepT2-ECD Δ at pH 5.5 for the respective constructs. Normalized hPepT2 wild type uptake was 107 ± 16 fmol/oocyte/hour and that of hPepT2-ECD Δ was 114 ± 15 fmol/oocyte/hour. (* = unpaired t-test between uptake at pH 5.5 and pH 7.5, p-value < 0.05)

As seen from the Figure 4.1.9-1, hPepT2-ECD Δ showed a tendency towards reduced transport compared to wild type at all pH values tested, with a statistically significant reduction at pH 6.5 (p value < 0.05)

4.1.10 Effect of Thyroxin (T4) on transport of [3 H]-D-Phe-L-Gln in rPepT1 cRNA injected oocytes

Since the crystal structure of the ECD showed protein folds similar to that of Transthyretin like protein (TLP) domain, uptake assays were performed using thyroxin hormone to check if thyroxin had an effect on transport of [3 H]-D-Phe-L-Gln in rPepT1.

Method:

The oocytes were incubated in Barth's media containing 1 μ M to 100 μ M concentrations of T4 at room temperature, before carrying out the uptake assays.

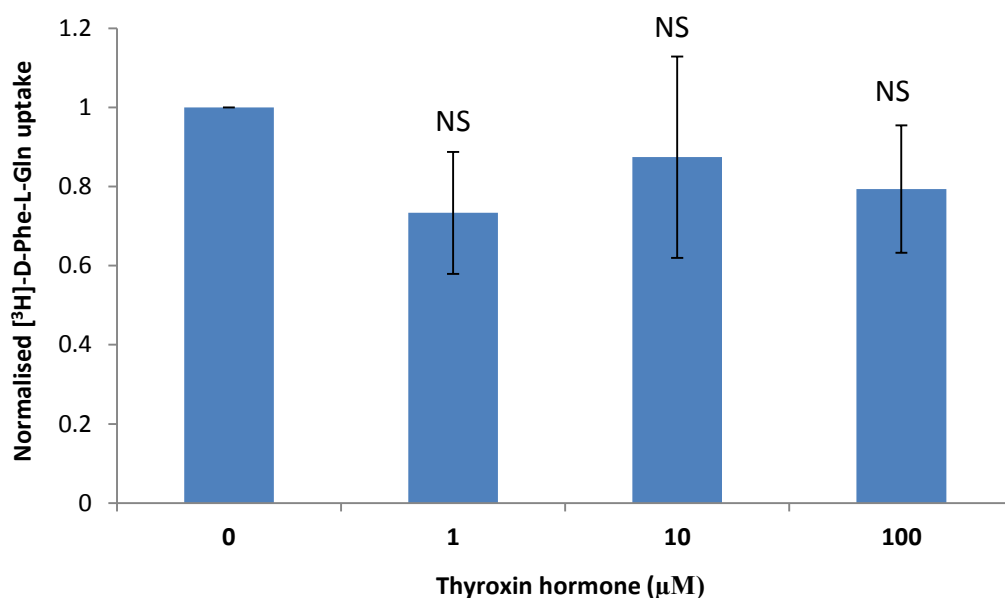


Figure 4.1.10-1 - Effect of Thyroxin on the uptake of [3 H]-D-Phe-L-Gln in rPepT1.

Each bar is the mean \pm standard error of 3 experiments with 5 oocyte replicates with background uptake removed as obtained from NI oocytes. Wild type rPepT1 uptake was found to be 157 ± 14 fmoles/oocyte/hour. (NS = Not significant)

From the above graph (Figure 4.1.10-1) it can be seen that thyroxin hormone treatment on rPepT1 cRNA injected oocytes for one hour had no significant effect on the uptake of [3 H]-D-Phe-L-Gln.

4.1.11 Measurement of [^3H]-D-Phe-L-Gln uptake by rPepT1 cRNA injected oocytes in the presence of thyroxine (T4)

Since treating the oocytes with thyroxine prior to uptake assay did not show a significant effect on the transport of [^3H]-D-Phe-L-Gln, uptake experiments were set up in the presence of T4 to check if this showed any effect on rPepT1 mediated uptake.

Method

The uptake experiments were performed as before (2.3.4) but this time the 100 μL uptake media was prepared to include 10 μM T4 along with [^3H]-D-Phe-L-Gln.

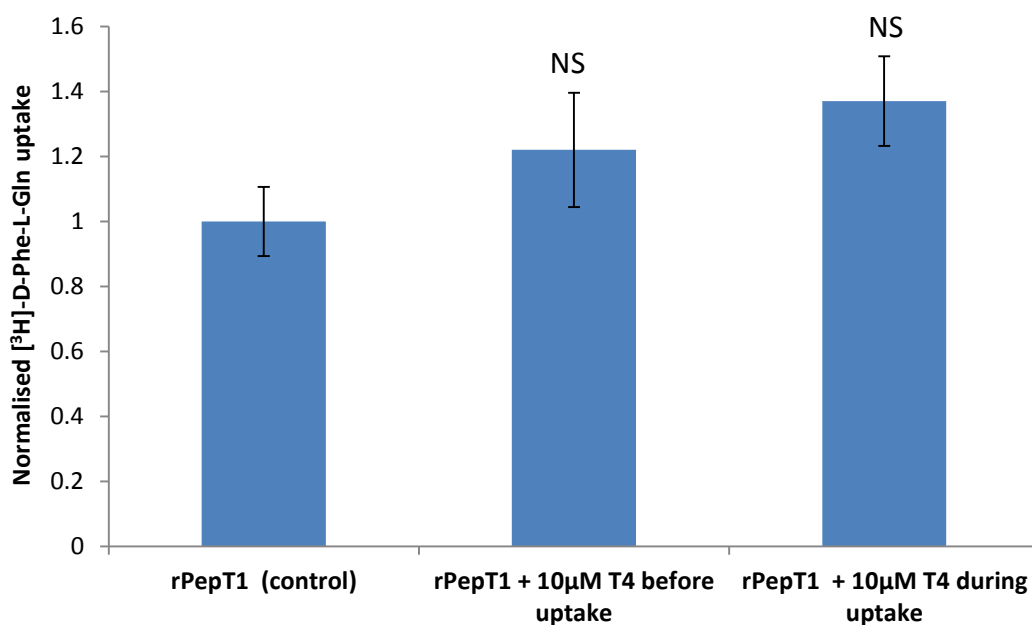


Figure 4.1.11-1 - Uptake of [^3H]-D-Phe-L-Gln in the presence of T4 in rPepT1 cRNA injected oocytes.

Each bar is the mean \pm standard error of one experiment with 5 oocyte replicates with the NI background removed. Wild type rPepT1 uptake was found to be 91 \pm 9 fmoles/oocyte/hour. (NS = Not-significant)

From the above graph (Figure 4.1.11-1) it can be seen that when compared to the wild type there was no difference in the amount of rPepT1 mediated uptake when the assay was performed in the presence of T4.

4.1.12 Luminometric estimation of flagged rPepT1 expression after treatment with thyroxin (T4) in oocytes

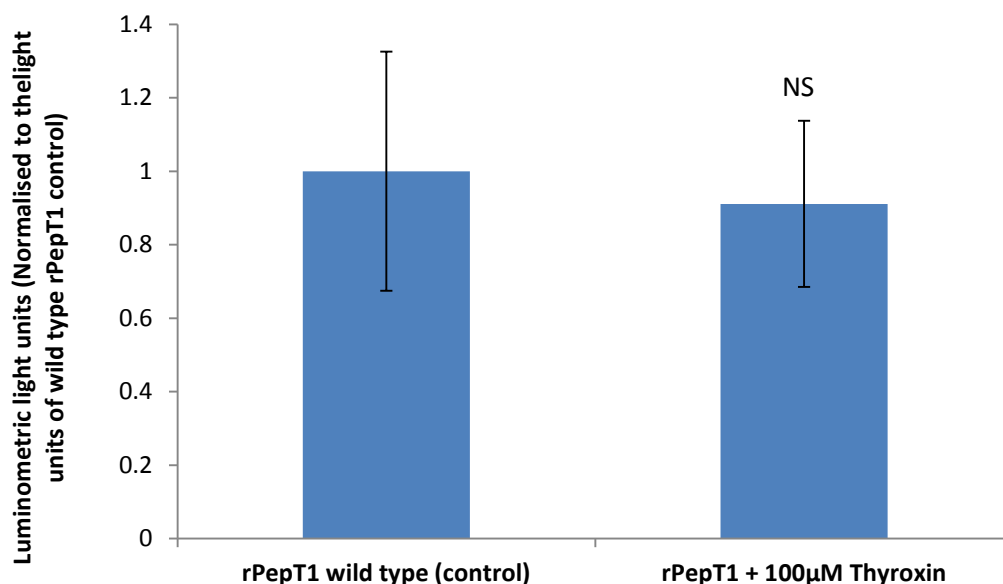


Figure 4.1.12-1 - Luminometric estimation of rPepT1 expression after T4 treatment for one hour.

Each bar is the mean \pm standard error of one experiment with 12 oocyte replicates. Data was normalised to the luminescence detected in rPepT1 wild type which was found to be 5846 ± 1900 luminometric light units. (NS = not significant)

From the above graph (Figure 4.1.12-1) it can be seen that there was no significant difference in the amount of rPepT1 expression between the thyroxin treated and untreated oocytes.

4.1.13 Comparison of K_i of rPepT1 with di-peptide Gly-Gln in presence and absence of T4

The [^3H]-D-Phe-L-Gln uptake experiments with thyroxine treated rPepT1 expressing oocytes showed slight variations in uptake compared to untreated rPepT1 expressing oocytes. To check if this was because of competition for the binding site between the substrate [^3H]-D-Phe-L-Gln and thyroxine, K_i of rPepT1 towards Gly-Gln was determined with and without thyroxine in the uptake media

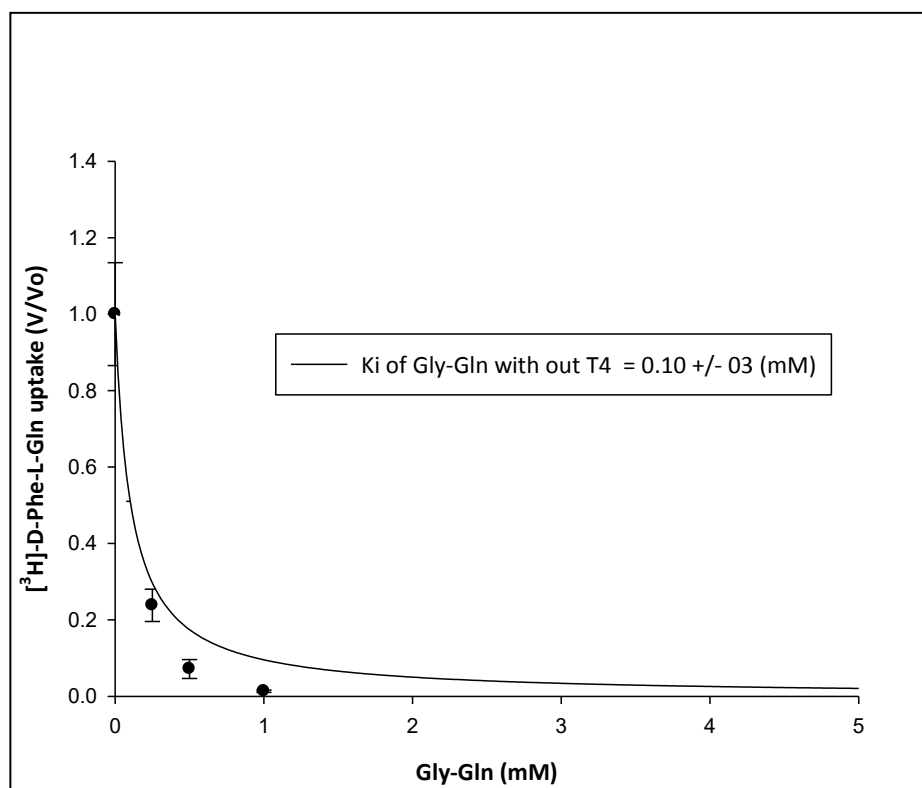


Figure 4.1.13-1 - K_i estimation rPepT1 with Gly-Gln in the absence of T4

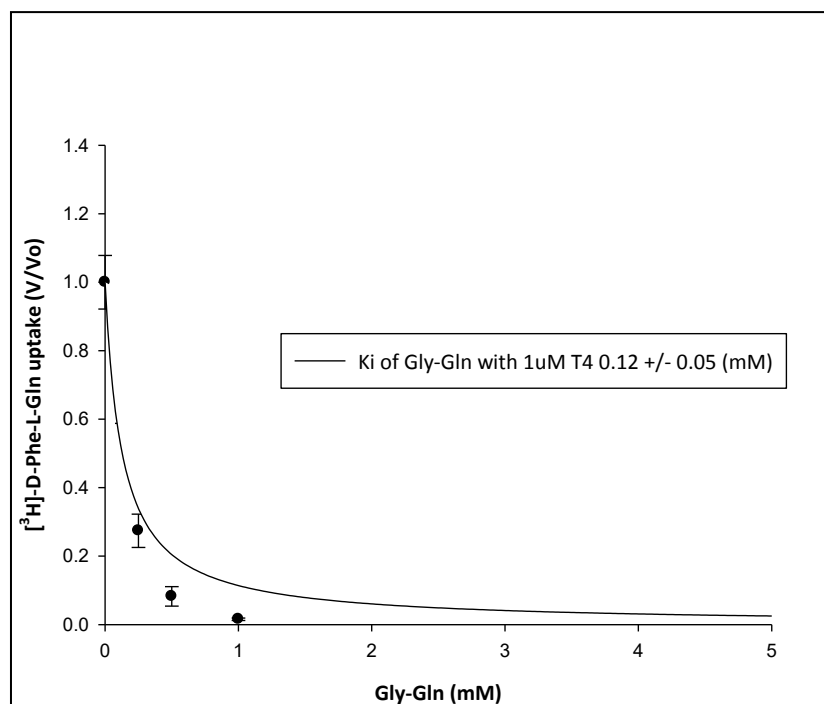


Figure 4.1.13-2 Ki estimation of rPepT1 with Gly-Gln in the presence of 1 μ M T4

The K_i of rPepT1 with Gly-Gln was found to be 0.10 ± 0.03 (mM) in the absence of T4 and in the presence of T4 the K_i of Gly-Gln was found to be 0.12 ± 0.05 (mM). Since tri-iodothyronine (T3) is the active form of thyroxine, T3 was used to check if this might show any effect on the uptake of radioactive tracer [³H]-D-Phe-L-Gln which was not shown by the inactive form of thyroxine (T4).

4.1.14 Effect of tri-iodothyronine (T3) on uptake of [^3H]-D-Phe-L-Gln in rPepT1 cRNA injected oocytes

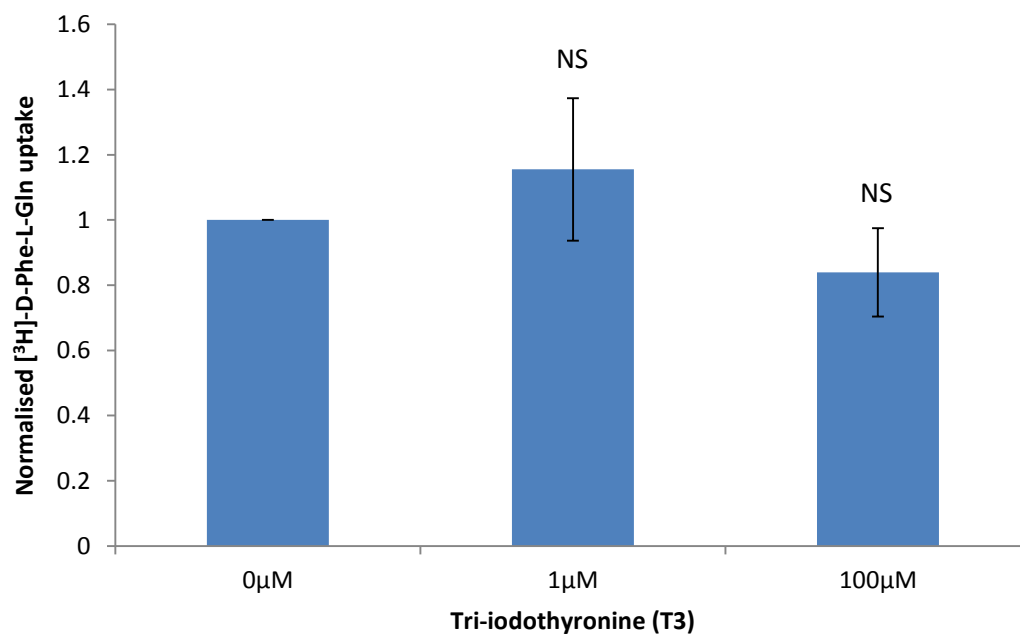


Figure 4.1.14-1 - Uptake of [^3H]-D-Phe-L-Gln in the presence of T3 in rPepT1 cRNA injected oocytes.

Each bar is the mean \pm standard error of two experiments with 5 oocyte replicates with the NI background removed. Wild type rPepT1 uptake was found to be 106.044 ± 9.653 fmoles/oocyte/hour. (NS = Not significant)

4.1.15 Effect of tri-iodothyronine (T3) on uptake of [3 H]-D-Phe-L-Gln in hPepT1 cRNA injected oocytes

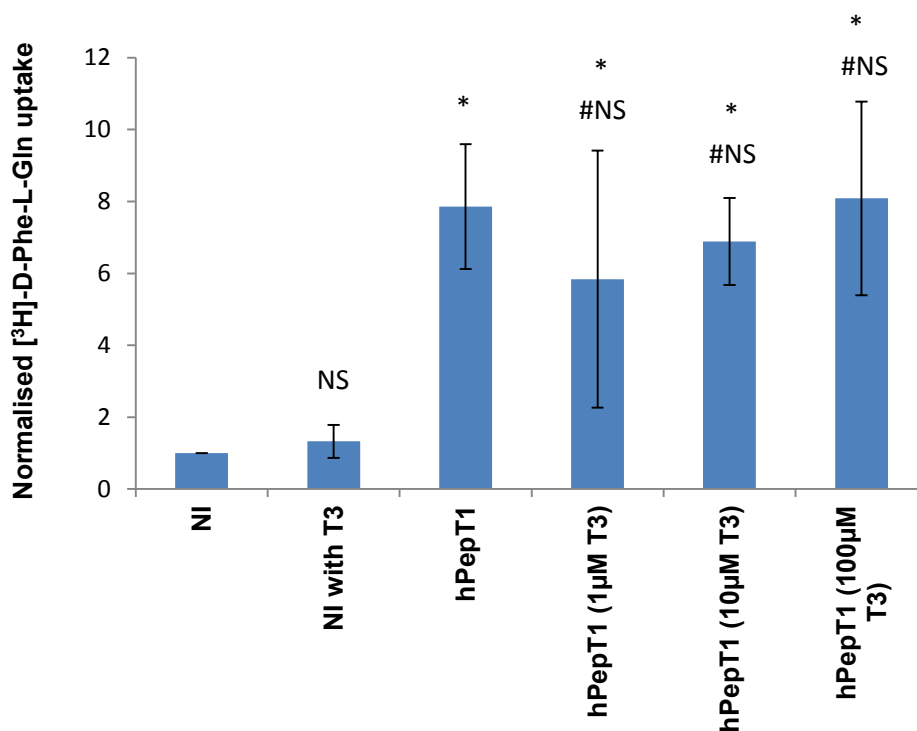


Figure 4.1.15-1 - Uptake of [3 H]-D-Phe-L-Gln in hPepT1 cRNA injected oocytes.

Each bar is the mean \pm standard error of 3 experiments with 5 oocyte replicates. The data was normalised to uptake in NI oocytes (negative control). The uptake in NI controls was found to be 16.784 ± 6.56 fmol/oocyte/hour. (*unpaired t-test with NI oocyte, p-value < 0.05; “#” = unpaired t-test with hPepT1, NS = Not significant, p-value>0.05)

From the above graph (Figure 4.1.15-1) it can be seen that there was no difference in the uptake of [3 H]-D-Phe-L-Gln between the T3 treated and untreated hPepT1 cRNA injected oocytes.

4.1.16 Effect of tri-iodothyronine (T3) on uptake of [3 H]-D-Phe-L-Gln in hPepT2 and hPepT2-ECDA cRNA injected oocytes

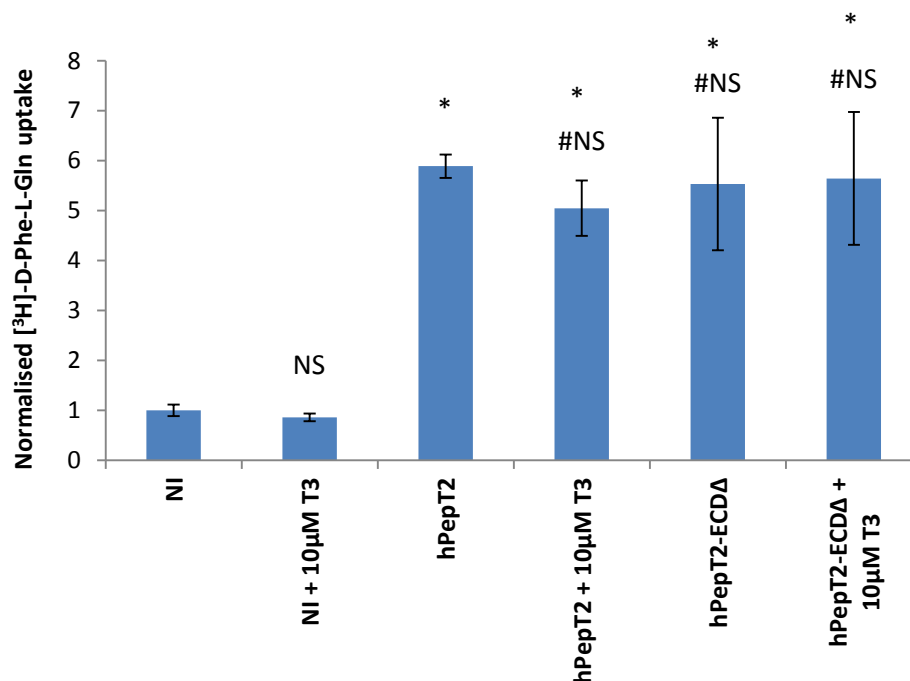


Figure 4.1.16-1 - Effect of T3 on uptake of [3 H]-D-Phe-L-Gln in hPepT2 and hPepT2-ECDA cRNA injected oocytes.

Each bar is the mean \pm standard error of 6 oocyte replicates. The data was normalised to uptake in NI oocytes (negative control). The uptake in NI controls was found to be 44 ± 5 fmol/oocyte/hour. (“#”= unpaired t-test with hPepT2 wild type, NS = Not significant, p-value > 0.05 . * = unpaired t-test with NI oocyte, p-value < 0.05). NI oocytes showed no difference in uptake with and without 10 μ M T3.

From the above graph (Figure 4.1.15-1) it can be seen that there is no significant difference in the amount of uptake between T3 treated and untreated hPepT2 and hPepT2-ECDA constructs.

4.1.17 Discussion

The large extracellular domain (ECD) between TMD9 and TMD10 is a feature that is found only in the mammalian POT transporters and not in the bacterial POT transporters. In order to elucidate the function of the ECD, hPepT1 and hPepT2 mutant constructs were made where the ECD had either been deleted (hPepT1-ECDA, hPepT2-ECDA) or the ECDs were swapped between hPepT1 and hPepT2 (hPepT1-ECD2, hPepT2-ECD1). The main hypothesis tested by creating these mutants was that the ECD contributed towards the functional attribute found in the wild type PepTs and that swapping the ECDs between hPepT1 and hPepT2 would lead to the swapping of that functional attribute. The first test was carried out to check if the ECD plays a structurally important role in hPepT1 and hPepT2 proteins. This was done by performing uptake assays with [³H]-D-Phe-L-Gln in cRNA injected oocytes. From (Figure 4.1.5-1 and Figure 4.1.6-1) it can be seen that removal or swapping of ECD in hPepT1 abolished the transport of the radioactive substrate. This is evident from the observation that the transport demonstrated by hPepT1-ECDA and hPepT1-ECD2 is similar to that of the non-injected oocytes (negative control). Whereas, the hPepT2-ECDA and hPepT2-ECD1 showed uptake similar to that of the wild type hPepT2, showing that the ECD in hPepT2 did not affect the transport characteristics of hPepT2. The reduced transport demonstrated by hPepT1-ECDA and hPepT1-ECD2 could be as a result of the protein not being expressed on the surface of the membrane. The reduced transport could also be due to the protein being expressed on the surface of the membrane but unable to transport the substrate. To check the surface expression of hPepT1 ECD mutants, a FLAG epitope tag was introduced between the TMD2 and TMD3. This location was selected to insert the FLAG as it has been previously shown to yield a functional transporter which can be detected using anti FLAG antibodies (Panitsas *et al.*, 2006). Luminometric estimation of wild type hPepT1 with the FLAG showed significant uptake compared to NI oocytes and was detected using luminometry technique (Figure 4.1.7-1). The PepT1 ECD mutant to check surface expression showed that the alterations made to the ECD resulted in total loss of surface expression of the hPepT1-ECDA and hPepT1-ECD2 proteins (Figure 4.1.7-1). Hence it can be concluded that the hPepT1 protein only expresses and transports with its own ECD and there was no measurable function with the ECD from hPepT2. On the contrary hPepT2 seems to work without its own ECD and also works with the ECD from hPepT1. This is the first difference in function observed between the ECD in hPepT1 and hPepT2.

In order to check if the ECD influences the kinetic properties of hPepT2 the inhibition constants (K_i) for hPepT2 ECD mutants were established using a drug (Cefaclor) and di-peptide (Lysyl-Lysine, Lys-Lys). The K_i of hPepT1 was also established in order to check if the affinity of hPepT2 would be swapped to that of hPepT1 in case of hPepT2-ECD1 construct. Cefaclor and Lys-Lys were chosen as substrates as they had previously been shown to have different affinities towards PepT1 and PepT2 (Luckner and Brandsch, 2005; Theis *et al.*, 2002) which would allow the comparison of K_i characteristics between hPepT1 and hPepT2. The K_i of hPepT1 was found to be 8.85 ± 4.42 mM and 2.43 ± 0.88 mM for Cefaclor and Lys-Lys respectively (Figure 4.1.8-1 and Figure 4.1.8-3). The K_i for hPepT2 was found to be 0.22 mM and 0.06 mM for Cefaclor and Lys-Lys. It can be seen from the above K_i values that the hPepT2 has much higher affinity towards Cefaclor and Lys-Lys when compared to hPepT1. The K_i values for hPepT2-ECD Δ and hPepT2-ECD1 remained similar to that of hPepT2 wild type for Cefaclor and Lys-Lys (approx. 0.2 mM and 0.05 mM respectively). If the ECD influenced the affinity of hPepT2 towards its substrates then we would have expected to see significant differences in the K_i values observed between the hPepT2 wild type and hPepT2 ECD variants; no such results were obtained with the hPepT2 ECD variants. This result is in accordance with an earlier observation made on a rPepT1 and rPepT2 chimera CHIPep, which had amino acids 1-401 from rPepT2 (TMD1 to TMD9) and amino acids 402-707 including the large extracellular loop (TM10 to TMD12) from rPepT1. This study concluded that the N terminal half is the region which contributes towards the K_i characteristics of CHIPep, thereby retaining PepT2 like affinity characteristics (Doring *et al.*, 1996). If the CHIPep had shown K_i values similar to that of rPepT1 then this would have been a result of the interaction of the substrate with the C terminal region of CHIPep which included the ECD. The chimera named CH2 (made of amino acid 1 to 401 of rabbit PepT1 and 402 to 707 from rabbit PepT2) showed no measurable uptake of the di-peptide substrate $^3\text{[H]-D-Phe-Ala}$ but was found to be expressed on the plasma membrane using GFP-tagged CH2 construct when expressed in the oocyte expression system (Doring *et al.*, 2002). Compared to this data, hPepT1-ECD2 and hPepT1-ECD Δ constructs like CH2 did not show transport of the di-peptide $^3\text{[H]-D-Phe-L-Gln}$ but unlike CH2 the hPepT1-ECD2 and hPepT1-ECD Δ were not expressed on the plasma membrane. This could either be a species specific difference or it could be an effect caused as a reduction in the length of PepT1 used in the construction of the chimeras; with the hPepT1 ECD variants having 1 to 392 amino acids as opposed to 1 to 401 amino acids in the CH2 construct. Since neither the

deletion nor swapping of the ECD in hPepT2 had an effect on the K_i of hPepT2 it can be concluded that the ECD does not play a critical role in determining the affinity of hPepT2 towards its substrates. These results complement the information obtained from the crystal structures of bacterial POT proteins which show that the peptide binding site in POT proteins are formed by the interaction between TMD 1, 2, 4, 5 from the N-terminal domain with TMD 7, 8, 10 and 11 from the C-terminal domains (Doki *et al.*, 2013; Newstead, 2011; Solcan *et al.*, 2012).

From the crystal structure of the ECD of mouse PepT1 (mPepT1) and rat PepT2 it was found that (Beale *et al.*, 2014, in press) the ECDs had the Transthyretin-like protein (TLP) domain suggesting an interaction of PepT1 and PepT2 ECDs with the hormone Thyroxine (T4). Thyroxine hormone enters the cell and binds to the thyroid hormone receptor in the nucleus. This complex is thought to interact with the regulatory elements of the target genes, thereby either increasing or decreasing the expression on the target gene (Yen and Chin, 1994). Earlier studies have found that pre-treatment of caco-2 cells with T3 for 4 days prior to carrying out transport experiments with [14 C]-Glycylsarcosine (PepT1 substrate) showed a dose dependent reduction in the V_{max} but no effect on the K_m for [14 C]-Glycylsarcosine (Ashida *et al.*, 2002). This demonstrated that thyroxine had a genomic effect on the regulation of PepT1 in Caco-2 by inhibition of PepT1 transcription and /or reduced stability of PepT1 mRNA. The direct interaction of thyroxine hormone on PepT1 and/or PepT2 had never been performed so far. Hence experiments were performed to check the effect of T4 and T3 on the transport characteristics of rPepT1, hPepT1 and hPepT2.

Treatment of rPepT1 cRNA injected oocytes with T4 for one hour prior to performing uptake assays using [3 H]-D-Phe-L-Gln did not show any significant difference between T4 treated and untreated oocytes (Figure 4.1.10-1). Luminometric estimation of FLAG tagged rPepT1 did not show a significant difference in the amount of rPepT1 protein expression between T4 treated and untreated oocytes (Figure 4.1.12-1). This shows that T4 treatment does not alter the number of rPepT1 transporters. A similar result was obtained when the rPepT1 cRNA injected oocytes were incubated with T4 simultaneously with the [3 H]-D-Phe-L-Gln while performing the uptake assays (Figure 4.1.11-1). This experiment was done to check if T4 modified rPepT1 mediated transport in the presence of a substrate ([3 H]-D-Phe-L-Gln). It was again seen that the addition of T4 did not make a significant difference to the amount of rPepT1 mediated uptake.

To check if T4 influences the binding of the substrate to rPepT1 the K_i values of rPepT1 was determined using known PepT1 substrate Glycyl-Glutamine (Gly-Gln) in the presence and absence of T4. The K_i of rPepT1 for Gly-Gln was 0.12 ± 0.05 (mM) and 0.10 ± 0.03 (mM) with and without T4 respectively (Figure 4.1.13-1 and Figure 4.1.13-2). Here it can be seen that T4 did not elucidate a drastic effect on the K_i of rPepT1 towards Gly-Gln, showing that T4 did not compete with Gly-Gln at the substrate binding site. Since T3 is an active form of T4, the effect of T3 on uptake of [3 H]-D-Phe-L-Gln in rPepT1 cRNA injected oocytes was performed. Again it was observed that there was no significant difference between T3 treated and untreated rPepT1 (Figure 4.1.14-1). Similar results were obtained for hPepT1 (Figure 4.1.15-1) and hPepT2 (Figure 4.1.16-1) where the addition of T3 did not make a difference to the transport of [3 H]-D-Phe-L-Gln. No further repetitions of T4 and luminometry were performed on hPepT1 and hPepT2 as it is most likely to be similar to the results obtained from rPepT1.

Since the ECD in hPepT2 did not play significant roles in either maintaining the structure of the protein or in determining the affinity of hPepT2 towards its substrates, and since there was no regulatory effect of T3 or T4 on hPepT2, the effect of pH on the uptake characteristics on hPepT2 ECD was studied. The effect of pH on PepT2 ECD was selected as a parameter to investigate as it was observed that increasing the pH from 5.5 to 8.0 resulted in the weakening of the interface between the lobes in PepT2, such that the ECD become more elongated (Beale *et al.*, 2015). This was in contrast to PepT1, where the lobes remained closely associated, in a more compact state as suggested from SAXS and AUC data. The pH range of the uptake media used to perform the transport experiments varied from 5.5 to 7.5. It was observed that hPepT2-ECD Δ construct showed reduced transport compared to wild type hPepT2 at all pH tested, showing significant reduction at pH 6.5 (Figure 4.1.9-1). It has previously been identified that the pH in the lumen of proximal kidney tubules, the region where PepT2 is expressed was approximately 6.6 (Yoshitomi and Fromter, 1984). Since there is a significant difference between the hPepT2 wild type and hPepT2-ECD Δ at pH 6.5, it could be possible that the ECD in hPepT2 functions like a pH sensor, allowing hPepT2 to perform transport at the maximum rate in vivo. From the results presented here it can be concluded that the ECD plays different roles in hPepT1 and hPepT2. The ECD in hPepT1 plays a critical role in maintaining the structure of hPepT1 where as ECD in hPepT2 possibly plays a pH sensing role, which helps hPepT2 protein to transport its

substrates at the physiological pH prevalent in the lumen of kidney tubules where PepT2 is expressed predominantly.

The crystallisation of the PepT1 and PepT2 ECD by Dr Newstead and group initially hypothesised that complex structure of the ECD's might interact with thyroxine hormone due to observation of TLP domain. As reported in the current study this hypothesis was found to be negative as no such interaction with PepT1 or PepT2 by thyroxine hormone was observed. The second hypothesis was that the ECD might interact with the intestinal proteases which create di- and tri- peptides, which are substrates of PepT1 and PepT2. Subsequently it has been found that trypsin binds to the ECD via electrostatic interactions facilitated by Aspartate 550 (D550) and Glutamate 573 (E573) in the PepT1-ECD and D576 and E599 in PepT2-ECD respectively (Beale et al., in press). Microscale thermophoresis binding analysis assay showed that mutating the D550, E573 and PepT1-ECD, D576 and E599 in PepT2-ECD to Alanine abolished interaction with trypsin hormone showing that these residues help bind trypsin to PepT1 and PepT2 transporters. This kind of interaction would facilitate increased cleavage of peptides to di- and tri- peptides by trypsin thereby improving the efficiency of uptake of these peptides by PepT1 and PepT2 transporters. Taken together, these studies present novel findings in the functioning of the ECDs in PepT1 and PepT2 transporters

5 Transport characteristics of rat PHT1

5.1.1 Introduction

The earliest of the SLC15 class of peptide transporters belonging to the POT family isolated namely *SLC15A1* and *SLC15A2* were found to transport di- and tri- peptides only or drugs which had structural similarity to di- and tri- peptides. PHT1 from rat brain was reported to be the first mammalian peptide transporter from SLC15 class of peptide transporters which had the added ability to transport single amino acid (L-Histidine) in addition to di- and tri- peptides (Yamashita *et al.*, 1997). Histidine transport by rat PHT1 was found to exhibit a proton-coupled, high affinity transport system. hPHT1 was isolated and expressed transiently in COS-7 cells which also demonstrated proton coupled transport of histidine, in addition to that of several di and tri- peptides (Bhardwaj *et al.*, 2006). These two reports indicate that PHT1 is expressed on the plasma membrane, inferred from the observation that histidine was transported in PHT1 injected oocytes and PHT1 transfected COS-7 cells. However, studies performed since these initial reports suggest that PHT1 could be involved in transport of histidine but in the lysosomal and endosomal membrane (Ocheltree *et al.*, 2003; Romano *et al.*, 2010), and not on the plasma membrane as previously suggested.

Since there are discrepancies regarding the localisation of the PHT1 protein, experiments were performed to verify the localization and peptide transport characteristics of PHT1.

5.1.2 Aims

- To determine if the PHT1 transporter is expressed on the plasma membrane.
- To establish if PHT1 transports histidine amino acid as previously suggested.

5.1.3 Methods

5.1.3.1 PHT1 clone selection

PHT1 clone from rat (rat PHT1) was selected to determine the localisation and transport characteristics of PHT1 with the intention of verifying the find in human PHT1 (hPHT1) once PHT1 was successfully expressed and histidine transport was confirmed. The PHT1 clone coding the complete coding sequence was purchased from Source

Bioscience (UK) with the IMAGE number 7315369. The rat PHT1 clone purchased was indicated to be inserted between 5' EcoRV and 3' NotI restriction sites in p-Express1 vector under the control of 5' SP6 promoter with ampicillin as a selectable marker. The presence of rat PHT1 sequence was verified by sequencing using the SP6 primer.

5.1.3.2 Prediction of secondary structure of Rat PHT1 using MEMSAT3

The membrane topology has to be available in order to determine the amino acid position at which the FLAG epitope tag can be inserted in order to determine surface expression of the protein. The online software MEMSAT3 (Jones, 2007) was used to predict the topology of rat PHT1. This particular program was used as it had been previously used to successfully predict the secondary structure of PepT1 to introduce FLAG epitope tag (Foley *et al.*, 2010; Panitsas *et al.*, 2006)

Sequence analysis results for job: pht1

ID: 884fabf6-71d5-11e2-83ec-00163e110593

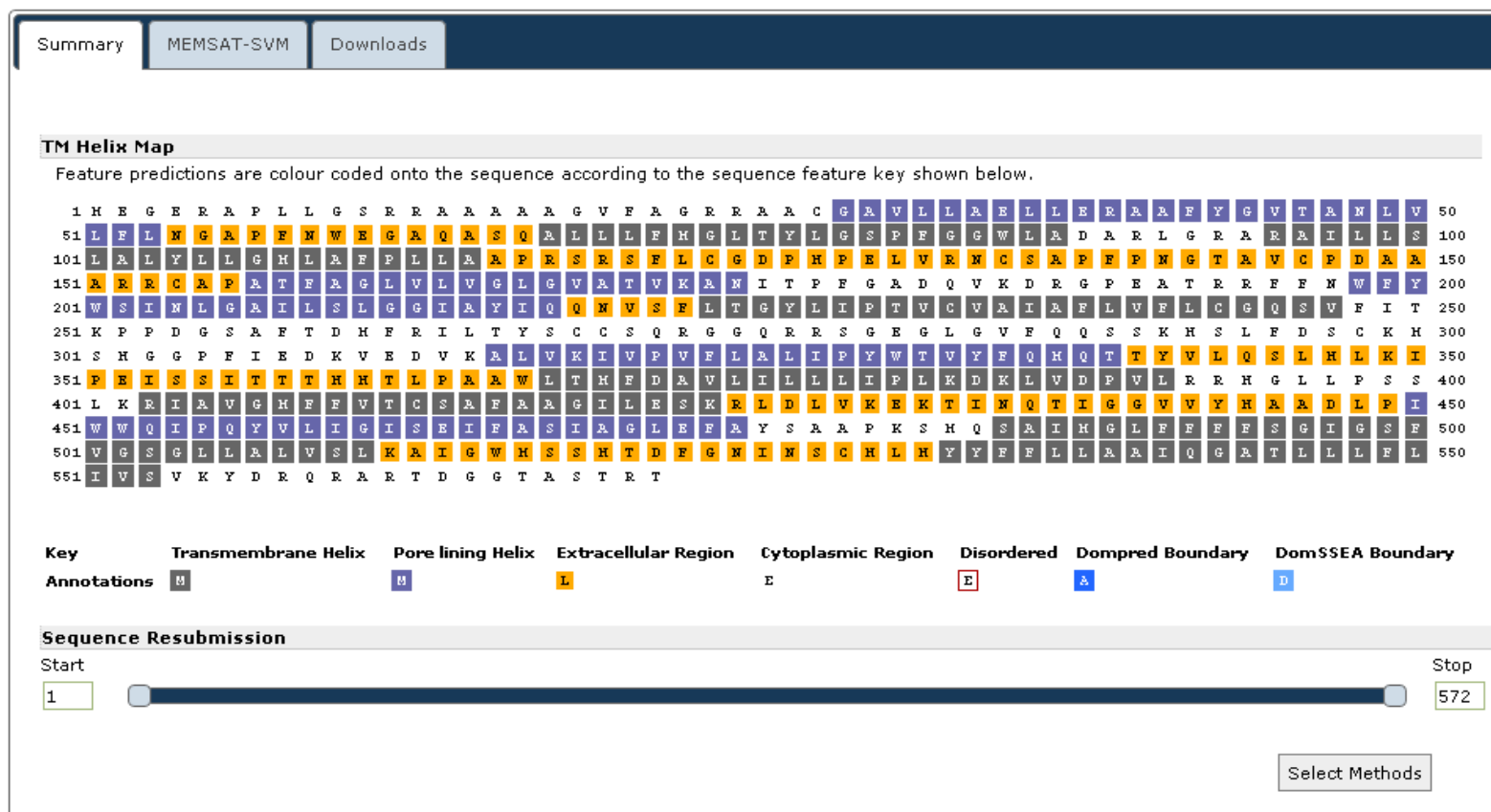


Figure 5.1.3-1 - MEMSAT3 topology prediction of rat PHT1 protein

5.1.3.3 Introduction of FLAG tag epitope

From the MEMSAT3 software, it was predicted that the 1st extracellular domain extended from the residue 54 to 67 and the 2nd extracellular domain stretched between the residues 116 to 156. The 2nd extracellular domain was chosen as a site for FLAG insertion since it was longer compared to the 1st extracellular domain. Overlapping PCR was used to introduce the FLAG at the position 125 amino acid onwards. The FLAG tagged rat PHT1 sequence was sub cloned into PBF vector. FLAG tagged rat PHT1 was introduced between 5' HpaI (GTTAAC) and 3' XhoI (CTCGAG) restriction sites of PBF vector under the control of SP6 promoter.

List of primers used

FLAG Forward primer

Name: r1FLAGF-1

GGGGATCCGCACCCGGAGCTGGTGGGATTACAAGGATGATGATGATAAGC
GCAAC TGCTCGGCTCCCTTCCCT

FLAG Reverse primer

Name: r1FLAGR-1

AGGGAAGGGAGCCGAGCAGTTGCGCTTATCATCATCATCCTTGTAATCCA
CCAGCTCCGGGTGCGGATCCCC

Forward Primer for sub cloning into PBF vector

Name: RP1PBF-1

TTTTTTGTTAACGCCGCCACCATGGAGGGCGAGCGGGCGCCGCTGTTAGGTT
CG

Reverse Primer for sub cloning into PBF vector

Name: RP1PBR-1

CTCGAGTCAGGTCCTCGTGCTGGCTGTCCCCCATCTGTCC

In the above primers, r1FLAGF-1 and r1FLAGR-1 are the primer sequences containing the FLAG epitope (**Bold, underlined**). Using rat PHT1 wild type as template, two PCR reactions were set up simultaneously. The PCR program used was as setup as per Table 2.2-7. The first with RP1PBF-1 (PHT1 forward primer) + r1FLAGR-1 (FLAG reverse primer) and the second reaction with r1FLAGF-1 (FLAG forward primer) + RP1PBR-1 (PHT1 reverse primer). The resulting PCR product was gel purified (Section 2.2.4 and 2.2.5) and 50ng of this purified PCR product was mixed together which served as a template for the new PCR reaction using RP1PBF-1 (forward primer) + RP1PBR-1 (PHT1 reverse primer). This PCR product was gel purified. The resulting product was used directly (without purification) to sub clone FLAG tagged rat PHT1 into pGEM-T easy vector as per the manufacturer's instructions (Promega, UK)

Table 2.4-1 pGEM-T easy ligation reaction setup

Reaction components	(μ L)
2X Rapid ligation buffer	5
pGEM-T easy vector (50ng)	1
PCR product	*x
T4 DNA ligase	1
Nuclease-free water	Total volume of 10 μ l

*x = amount of PCR product varies with respect to insert:vector ratio used. Two different insert:vector ratios were used namely 3:1 and 1:3 while keeping the vector concentration the same between the reactions. A negative control was setup in which the insert volume was replaced with nuclease free water.

The above reaction mix was incubated at 25°C for 2 hours followed by transformation into XL1-Blue subcloning grade competent cells and grown overnight on LB agar plates supplemented with ampicillin (50 μ g/ml). The positive colonies were selected using cracking technique (Section 2.2.9.5) and sent for sequencing using T7 and SP6 primers. The plasmids containing FLAG tagged rat PHT1 sequence was sub cloned into PBF vector using HpaI and XhoI restriction enzymes (Section 2.2.7). RNA was synthesised using SP6 mMessage Machine kit (2.2.10) to perform transport and luminometry experiments. Once rat PHT1 was cloned into PBF vector the presence of the complete

sequence was verified and confirmed by sequencing using SP6 and r1FLAGF-1 primers.

5.1.4 Determination of [^3H]-L-Histidine uptake in rat PHT1 injected oocytes

To determine the histidine transport by rat PHT1, 15 ng rat PHT1 RNA was injected into *Xenopus laevis* oocytes and incubated at 18°C for 3 days before performing transport experiments using [^3H]-L-Histidine (Section 2.3.3), the pH of the uptake media was adjusted to 5.5 (Yamashita et al., 1997). All uptake experiments were performed for a period of 1hr before the oocytes were lysed and the radioactivity counted using a scintillation counter. The bars in the graphs below represent the mean \pm standard error of “n” number of experiments with 5 oocyte preparations for each data point/ experimental condition.

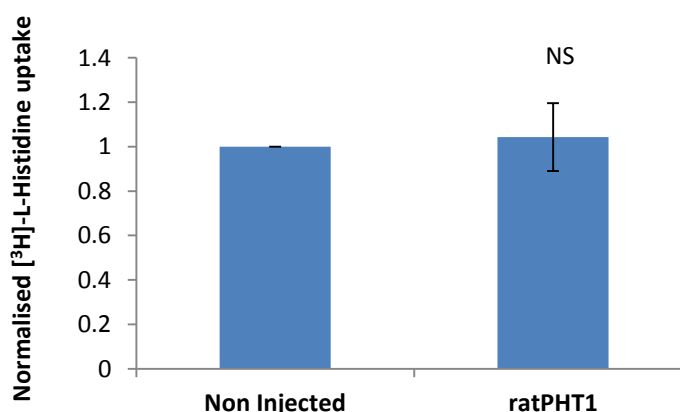


Figure 5.1.4-1 - Comparison of [^3H]-L-Histidine uptake between non injected and rat PHT1 RNA injected oocytes.

The graph represents normalized uptake of [^3H]-L-Histidine in cRNA injected oocytes. NI uptake was found to be 55.16 ± 7.52 fmoles/oocyte/hour. (NS = non-significant; n= 5)

From the above graph it can be seen that rat PHT1 injected oocytes did not show significant uptake of histidine compared to the NI negative control oocytes.

5.1.5 Comparison of [^3H]-L-Histidine uptake from day 4 to day 6 post rat PHT1 RNA injected oocytes and non-injected oocytes

The uptake of histidine in rat PHT1 injected oocytes were found to be similar to that seen in NI oocytes. This could have been due a low rate of rat PHT1 surface expression. In order to determine if the uptake of histidine by rat PHT1 transporter would be enhanced with longer incubation period at 18°C between injection and performing the uptake assays, the histidine uptake was performed from the 4th to the 6th day post RNA injection.

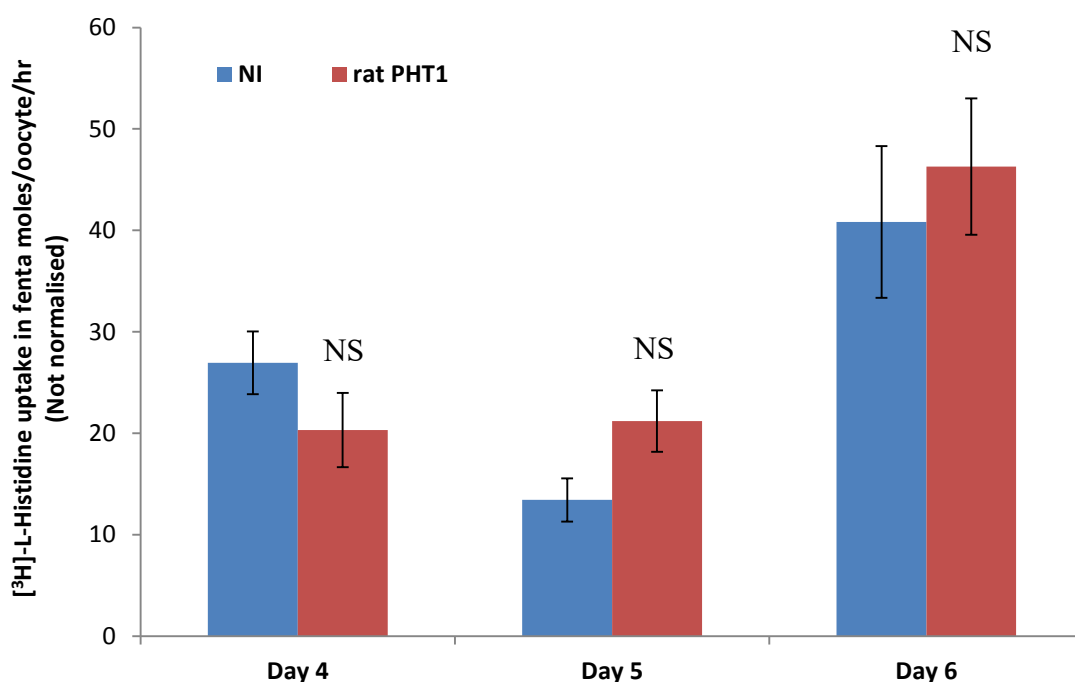


Figure 5.1.5-1 – Comparison of [^3H]-L-Histidine uptake between NI and rat PHT1 RNA injected oocytes from day 4 to day 6 post RNA injection.

Since this experiment was performed to compare total uptake in NI and rat PHT1 injected oocytes, the data has not been normalised. (Unpaired t-test of Rat PHT1 injected oocytes with NI on the same day; NS = non significant, p-value >0.05; n= 2)

From the above graph (Figure 5.1.5-1) it can be seen that there was no significant increase of Rat PHT1 mediated transport of L-Histidine compared to non-injected controls even after increasing the incubation period from 4 to 6 days post cRNA injection.

5.1.6 Determination of effect of pH on rat PHT1 mediated uptake of Histidine

To check if the pH of the uptake solution affected the histidine uptake in rat PHT1 RNA injected oocytes the uptake of [^3H]-L-Histidine was compared between NI oocytes and rat PHT1 injected oocytes at pH 5.5 and pH 7.5.

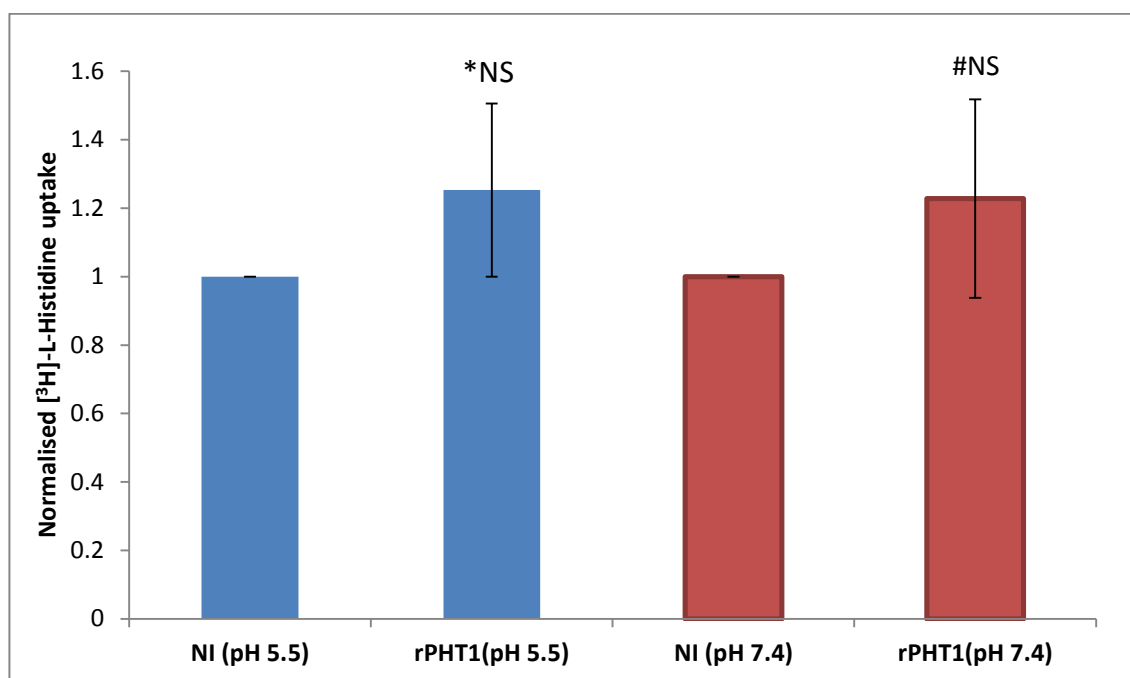


Figure 5.1.6-1 - Comparison of uptake between non injected and rat PHT1 (rPHT1) RNA injected oocytes at pH 5.5 and pH 7.5.

The graph represents normalized uptake of [^3H]-L-Histidine in cRNA injected oocytes. NI uptake was found to be 14 ± 2 fmoles/oocyte/hour at pH 5.5 and 17 ± 1 fmoles/oocyte/hour at pH 7.5. (*NS = unpaired t-test between NI and rat PHT1 RNA injected oocytes at pH 5.5 and #NS = unpaired t-test between NI and rat PHT1 RNA injected oocytes at pH 7.5, p-value > 0.05; NS = non significant; n=2).

As observed in the previous experiment (Figure 5.1.4-1) there was no significant transport of histidine between NI and rat PHT1 RNA injected oocytes. This experiment showed that there was no effect of external pH on Histidine transport in rat PHT1 RNA injected oocytes, as there was no significant difference between NI oocytes and RNA injected oocytes at pH 5.5 and pH 7.5. The apparent lack of histidine transport observed so far could be due to the PHT1 protein was not expressed in the cRNA injected

oocytes. The surface expression of the Rat PHT1 protein could be verified using luminometry of FLAG tagged rat PHT1 protein.

5.1.7 Luminometric estimation of surface expression of FLAG tagged rat PHT1

To determine the surface expression of rat PHT1 in oocytes 15ng of FLAG epitope tagged rat PHT1 RNA was injected into the oocytes and incubated at 18°C for 3 days. 15 ng of FLAG-tagged rabbit PepT1 (rPepT1) was used as a positive control for luminometric detection of FLAG tagged protein. Luminometry was performed as described in section 2.3.6.

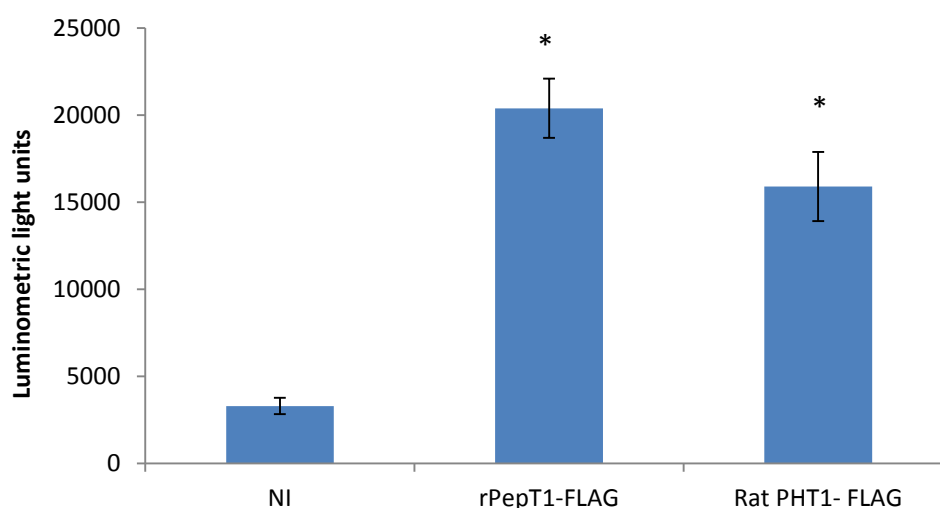


Figure 5.1.7-1 - Luminometric expression of rat PHT1.

Each bar represents the mean \pm standard error of 2 experiments with 12 oocyte replicates. NI luminescence was found to be 3291 ± 470 luminometric light units. (* = unpaired t-test with NI, p-value < 0.05)

The luminometry experiment showed that there was approximately 6 fold increase in the amount of light detected in rat PHT1 RNA injected oocytes compared to the non-injected (NI) negative control. This was similar to the positive control rPepT1-flagged

(8 fold increase) indicating that the rat PHT1 protein is expressed and is located on the surface of the membrane of RNA injected oocytes.

5.1.8 Electrophysiology experiment to determine amino acid transport in rat PHT1 injected oocytes

Since the radio labelled uptake of [^3H]-L-Histidine did not show transport of histidine, electrophysiology technique was used to detect if rat PHT1 transports any of the single amino acids including histidine. Electrophysiology was performed as described earlier (Section 2.3.7) with single amino acids. If any of the amino acid being tested is transported then there would be a difference in the amount of current required to maintain the holding potential of -60mV, provided the transport process is electrogenic. Once, a particular group of amino acid solution shows significant transport compared to non-injected controls, then electrophysiology would be performed on each individual amino acids in that positively tested group in order to identify which specific amino acid was transported by rat PHT1 transporter. The amino acids were grouped into categories based on their charge and properties of their side chains. The groups used were as follows

Positive amino acids: Arginine, Histidine, Lysine

Negative amino acids: Aspartic acid, glutamic acid

Polar uncharged side chains: Serine, Threonine, Asparagine, Glutamine

Amino acids with hydrophobic side chains: Group A (Alanine, Isoleucine, Leucine, Methionine) Group B (Phenylalanine, Tryptophan, Tyrosine, Valine)

Special amino acids: Cysteine, Glycine, Proline

The above amino acids were dissolved at concentration of 2mM in electrophysiology buffer (pH 6.0), which has the same constituents as the uptake media used for radio-labelled uptake (Table 2.3-3) but without MgCl_2 which was previously found to introduce fluctuations in the baseline obtained from performing electrophysiology experiments in our lab. Once the amino acids were dissolved in the electrophysiology buffer, the pH was re adjusted using 0.5M Tris or 0.5M Mes.

Method:

The non-injected oocytes (control) and rat PHT1 RNA injected (15ng) oocytes were incubated in Barth's media supplemented with Penicillin/Streptomycin/Neomycin at 18°C for 3 to 4 days before performing electrophysiology. The oocytes were clamped at a holding potential of (-) 60mV. A 30 second pulse of each of the groups of amino acids was given with 3 minute intervals between each pulse. The variation in current measured during each pulse was recorded in nanoamps (nA) onto a chart recorder and the corresponding maximum values of current in nA was noted.

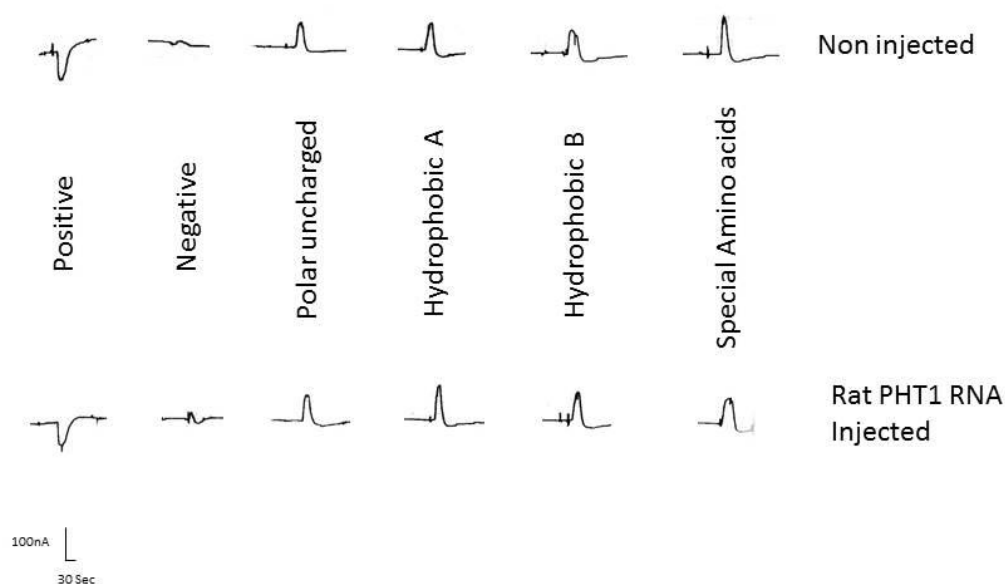


Figure 5.1.8-1 Comparison of the change in maximum current measured between non injected control oocytes and rat PHT1 cNRA injected oocytes in a single electrophysiology experiment.

At the end of the experiment the graph sheets with the electrophysiology reads were scanned and individual peaks for each of pulse (amino acid groups) were isolated using the software Photoshop (Adobe) to make a comparison between the amounts of current measured between the non-injected oocytes and the rat PHT1 RNA injected oocytes

It can be seen from the Figure 5.1.8-1 that there is no difference in the response to amino acid pulse between non-injected and rat PHT1 RNA injected oocytes. The

change in current recorded (peaks in the figure above) was approximately 100nA for both non-injected and rat PHT1 RNA injected oocytes whenever there was prominent peak seen on the electrophysiology trace. This shows that rat PHT1 does not transport any of the single amino acids tested in an electrogenic process.

5.1.9 Uptake assay to determine the presence of endogenous histidine transporters in oocytes

From the electrophysiology experiment performed in section 5.1.8 it was observed that the non-injected oocytes and the rat PHT1 cRNA injected oocytes showed change in current when a 30 sec pulse of the positive amino acid solution was applied (Figure 5.1.8-1). This change in current could have resulted due to the presence of endogenous histidine transporters or due to diffusion of the amino acids into the oocytes while performing electrophysiology. In order to determine if this change in current was due to endogenous histidine transporters an uptake assay was performed in both non injected and rat PHT1 cRNA injected oocytes in both the presence and absence (control) of 2 mM cold L-histidine. If the oocytes have endogenous histidine transporters then a drop in the amount [^3H]-L-histidine taken up by the oocytes would be observed in the presence of 2 mM cold histidine due to competition indication the presence of endogenous histidine transporters.

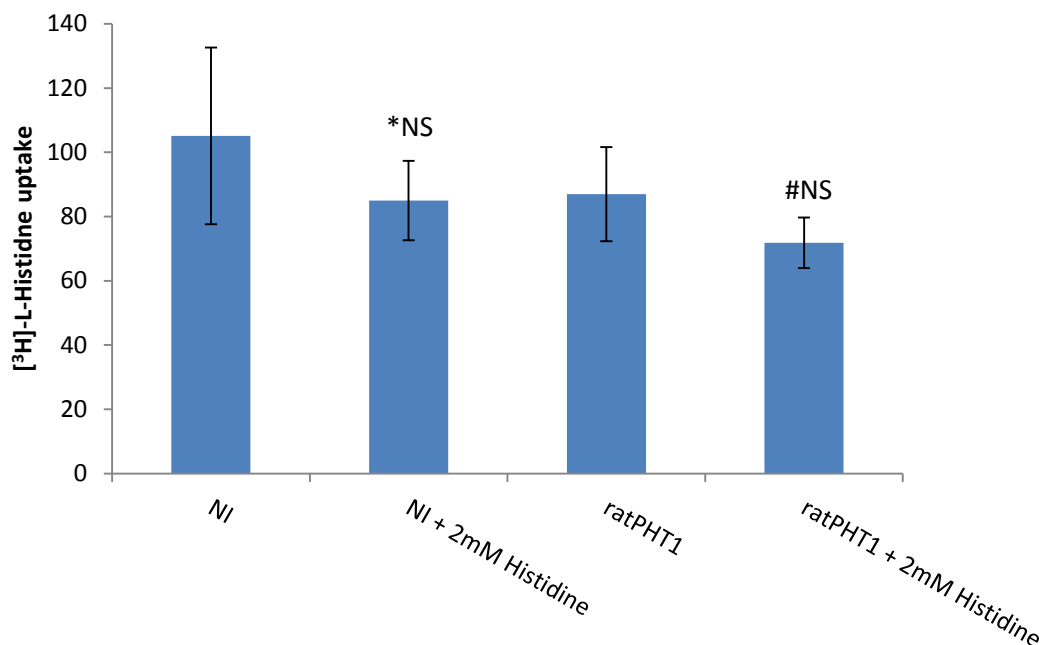


Figure 5.1.9-1 - Comparison of uptake in non injected and rat PHT1 RNA injected oocytes in the presence and absence of 2mM cold L-Histidine at pH 5.5.

NI uptake was found to be 5 fmoles/oocyte/hour and in rat PHT1 RNA injected was 4 fmoles/oocyte/hour. (*NS = unpaired t-test between NI oocytes with and without 2mM cold L-Histidine; #NS = unpaired t-test between rat PHT1 RNA injected oocytes with and without 2 mM cold L-Histidine, p-value < 0.05; NS = non significant; n=1).

Form the above experiment it was observed that there was no significant reduction in the amount of [³H]-L-histidine detected in the non-injected oocytes in the presence of 2 mM cold L-Histidine. This shows that histidine detected in non-injected oocytes is probably due to diffusion of histidine into the oocytes and not transporter mediated.

5.1.10 Discussion

To determine if PHT1 protein transports histidine, rat PHT1 cRNA cloned into PBF vector was injected into *X. laevis* oocytes which were incubated for 3 days at 18°C before performing uptake assays with [³H]-L-histidine. The rat PHT1 injected oocytes did not show significant uptake of [³H]-L-histidine when compared to non-injected oocytes (Figure 5.1.4-1.). This could have been either due to the rat PHT1 protein itself was not synthesised by the oocytes or that rat PHT1 transporter was not being expressed on the surface of rat PHT1 injected oocytes to show histidine transport.

The 3 day incubation period for rat PHT1 was selected as this was the standard incubation time post cRNA injection for rabbit PepT1, hPepT1 and hPepT2 in all the experiments performed in the lab. Also, this was the same duration used in the initial rat PHT1 experiments which was reported to have shown 5 fold histidine transport compared to non-injected oocytes, but this data was not shown in the original paper (Yamashita *et al.*, 1997). In order to determine if a longer incubation period would allow increased transport of [^3H]-L-histidine in rat PHT1 injected oocytes, uptake experiments with [^3H]-L-histidine was performed from the 4th to the 6th day post cRNA injection. This experiment showed that the rat PHT1 injected oocytes showed an increase in histidine uptake on day 6 but the same amount of histidine uptake was seen in non-injected oocytes as well. This showed that the histidine uptake demonstrated by the oocytes was caused due to the endogenous amino acid transporters or due to histidine diffusion into the oocytes and that rat PHT1 cRNA injection did not significantly increase histidine transport. This experiment demonstrated that rat PHT1 does not transport histidine even with an extended incubation period after RNA injection.

Since PHT1 is described to be a POT transporter the pH of the uptake media was adjusted to 5.5 to drive proton coupled transport of histidine into the oocytes. Uptake experiments were performed at pH 5.5 and pH 7.4 to check if increasing the external pH had an effect on histidine uptake in rat PHT1 injected oocytes. This experiment demonstrated that increasing the pH of the uptake media from 5.5 to 7.4 did not affect the histidine uptake in rat PHT1 injected oocytes (Figure 5.1.6-1). From these experiments it was seen that non-injected oocytes showed transport of histidine at pH 5.5 and pH 7.4 which could have been due to endogenous transporters or due to diffusion of histidine into the non-injected oocytes. To determine the endogenous transporter mediated transport of histidine cis inhibition of [^3H]-L-histidine experiment was performed with cold L-histidine (Section 5.1.9). It was found that addition of cold histidine did not have a significant effect on the amount of [^3H]-L-histidine detected in the non-injected oocytes. This therefore shows that the movement of [^3H]-L-histidine non-oocytes is due to diffusion of histidine through the plasma membrane and not via endogenous transporter.

Luminometry technique was used to determine if rat PHT1 is expressed on the surface of the rat PHT1 cRNA injected oocytes. A FLAG epitope tag (DYKDDDDK) was introduced into the 2nd extracellular domain (residues 116 to 156) as predicted by the

membrane topology program MEMSAT3 (Figure 5.1.3-1). The luminometric estimation of FLAG tagged rat PHT1 showed 6 times more luminescence signal compared to the non-injected oocytes (negative control) showing that the rPHT1 protein was expressed on membrane of cRNA injected oocytes (Figure 5.1.7-1). The FLAG epitope tagged rabbit PepT1 (rPepT1-FLAG) cRNA injected oocytes served as a positive control in this assay which showed 8 times more luminescence signal compared to the non-injected oocytes showing that the luminometry assay had worked successfully.

The luminometric estimation of rat PHT1 expression clearly demonstrates that rat PHT1 protein is expressed on the surface of the oocytes showing that it is a plasma membrane bound protein with access to the extracellular space but does not transport histidine. Since histidine transport by rat PHT1 protein was not detected, the two electrode voltage clamp electrophysiology technique was used to check if rat PHT1 protein transports any other single amino acid. To perform this experiment amino acids were grouped into different categories namely positive, negative, polar uncharged, hydrophobic and special amino acids which were dissolved in uptake media (pH 6.0) without MgCl_2 as described in section 5.1.8. The results obtained from electrophysiology (Figure 5.1.8-1) showed that there was a negative current of approximately -100nA detected for every 30 sec pulse of positive amino acid solution, showing that the transport of these positive amino acids induced an inward negative current. This was the case for both rat PHT1 injected and non-injected oocytes. All the other amino acid groups tested gave a positive current of approximately +100nA for both non injected and rat PHT1 injected oocytes with the exception of negative amino acid group which did not show any significant read of current.

These above experiments show that rat PHT1, as previously described (Yamashita *et al.*, 1997) was detected on the plasma membrane but unlike in previous observations, PHT1 did not induce transport of histidine in rat PHT1 cRNA injected oocytes. The concentration of rat PHT1 cRNA synthesised using the SP6 mMessage Machine was between 300 and 350 ng/ μl and a 50 nl micro injection into the oocytes could only introduce a maximum concentration of 17.5 ng of RNA into the oocytes. This concentration (15 – 17 ng/oocyte) of the rat PHT1 RNA injected was less compared to the original experiment which used 25 ng of RNA. It could be possible that the RNA concentration used in the current study was not high enough to show a significant higher uptake of histidine compared to non-injected oocytes. Higher than 50 nl

injections were not made in this study as this was found to reduce the viability of the injected oocytes. Yamashita *et al.*, reported that background histidine uptake in non-injected oocytes was 5 fold lesser (1160 fmoles/oocyte/hr) than the histidine uptake observed in rat PHT1 expressing cells (5800 fmoles/oocyte/hr) allowing them to study the rat PHT1 transporter in detail. In the current study the histidine uptake in non-injected and rat PHT1 cRNA injected oocytes was found to be similar (55 fmoles/oocyte/hr) which is only about 2 fold less than the histidine uptake detected in NI oocytes in the previous study when the difference in the concentration of [^3H]-L-Histidine is taken into account (0.1 μM here versus 1 μM in study by Yamashita *et al.*). A 30% reduction in the amount of rat PHT1 RNA injected seems unlikely to have been the reason for histidine transport not being detected as even a 3 fold increase should have been visible since the background histidine uptake had very low variation between experimental replicates. Moreover there was a significant amount of surface expression of FLAG tagged rat PHT1 (6 fold higher than NI controls) detected in the luminometry experiments (Section 5.1.7). The electrophysiology experiments (Section 5.1.8.) also showed that rat PHT1 injected oocytes did not show a significant transport of L-histidine compared to non-injected oocytes. This experiment also showed that rat PHT1 was not able to transport any of the single amino acids tested as previously reported. However, if PHT1 is a histidine transporter only expressed in the lysosome, it is possible that the over expression of PHT1 in *X. laevis* oocytes might have led to the trafficking of PHT1 protein to the plasma membrane. A proton coupled small neutral amino acid transporter LYAAT1 isolated from rat brain which is expressed in the lysosomal membrane was also found to be expressed in the plasma membrane of transfected COS-7 cells and in cRNA injected *X. laevis* oocytes (Sagne *et al.*, 2001; Wreden *et al.*, 2003). This is an example of a lysosomal transporter protein expressed on the cell membrane due to over expression of the protein in the expression system. This could also be the reason why PHT1 was detected in the plasma membrane but does not explain why unlike Yamashita *et al.*, we were unable to detect histidine transport as the histidine transport rates were reported to be at 5800 fmoles/oocyte/hour which is approximately 10 fold higher than the amount of histidine transport detected in the current study (considering the difference in [^3H]-L-Histidine used as explained earlier). So the possibility of PHT1 being a lysosomal protein cannot be completely excluded. From the current study it can be said that the PHT1 protein requires further investigation in order to determine the exact function of the protein and its localisation in the cells.

6 Effect of site directed mutations of conserved residues on hPepT2 transport characteristics.

6.1.1 Introduction

In the absence of a crystal structure of the mammalian peptide transporters several homology models have been proposed for the structure of PepT1 transporter (Bolger *et al.*, 1998; Meredith and Price, 2006). Site-directed mutagenesis studies have been performed in order to determine the functionally important amino acids involved in substrate binding and proton coupling as predicted from the homology modelling. The aromatic residues such as Tyrosine (Y), Tryptophan (W) and Phenylalanine (F) residues in membrane proteins have been known to play a role stabilizing positive charges within the electric field of the membrane through cation- π interactions (Dougherty, 1996). The mutation of Y12A and R282A in transfected HEK293T cells resulted in the expression of hPepT1 transporter with slightly reduced peptide transport of Gly-Sar compared to wild type hPepT1. In the same study W294A, E595A and Y167A mutants resulted in the expression of hPepT1 transporter which reduced the transport of Gly-Sar by 80% and 95% and 100% respectively (Bolger *et al.*, 1998). Mutating R282 to Glutamate (E) was found to transport peptides like the wild type rPepT1 by decoupling the movement of peptides with protons and losing the inability to accumulate substrate above equilibrium (Meredith, 2004). It was also proposed that R282 could form a charged pair with Aspartate 341 (D341) as double mutant R282D-D341R had similar transport characteristics as the wild type rPepT1. (Pieri *et al.*, 2008). The W294F mutation resulted in the expression of rPepT1 protein but lacked the ability to transport di-peptide and this mutation was used to establish that rPepT1 functioned as a tetramer (Panitsas *et al.*, 2006). In a study performed with the *Xenopus laevis* oocytes model system and [3 H]-D-Phe-L-Gln as PepT1 tracer to determine the key tyrosine residues involved in the functioning of rabbit PepT1 (rPepT1) the tyrosine residues at positions 12, 56, 64, 91, 167, 287, 345, 587 and 648 were mutated to phenylalanine (Pieri *et al.*, 2009). It was found that tyrosine (Y) to Phenylalanine (F) substitution did not affect the trafficking of rPepT1 mutant proteins to the oocyte membrane nor the proton coupling of peptide transport. The rPepT1 mutants Y64F, Y287F, Y587F and Y645F transported as the wild type rPepT1. The Y12F, Y91F and Y345F showed

significantly reduced transport whereas Y56F and Y167F showed 90% reduction in transport compared to the wild type rPepT1. It was also observed that none of the tyrosine mutants altered the pH dependence of the rPepT1.

6.1.2 Aims

The current experiment was set up to investigate if a selected few conserved residues found to alter the rPepT1 and hPepT1 mediated transport had a similar effect on PepT2 mediated transport. The hPepT2 residues selected for mutations were Y42, Y94, Y188, R301, W313, E622 corresponding to amino acids at locations Y12, Y64, Y167, R282, W294, and E595 in rPepT1 respectively (Appendix 10.3). These mutants were also FLAG tagged to check if mutating the selected residues affected the hPepT2 protein expression. An additional hPepT1-Y64F mutant equivalent to hPepT2-Y94F was constructed in order to compare the effect of substituting phenylalanine residue instead of a tyrosine as this substitution was not done in the earlier studies.

6.1.3 Methods

6.1.3.1 Site-directed mutagenesis in hPepT1 and hPepT2 constructs

The hPepT2 and hPepT1 mutants were synthesised using QuickChange site-directed mutagenesis kit as described in section 2.2.11. The primer design and mutation protocol was followed as per the manufactures instructions. The wild type hPepT1 and hPepT2 constructs (cloned into PBF vector with the C terminal FLAG tag) used for these experiments were a gift from Professor Simon Newstead (Oxford University).

Table 2.4-1 Sequences of the mutagenic primers

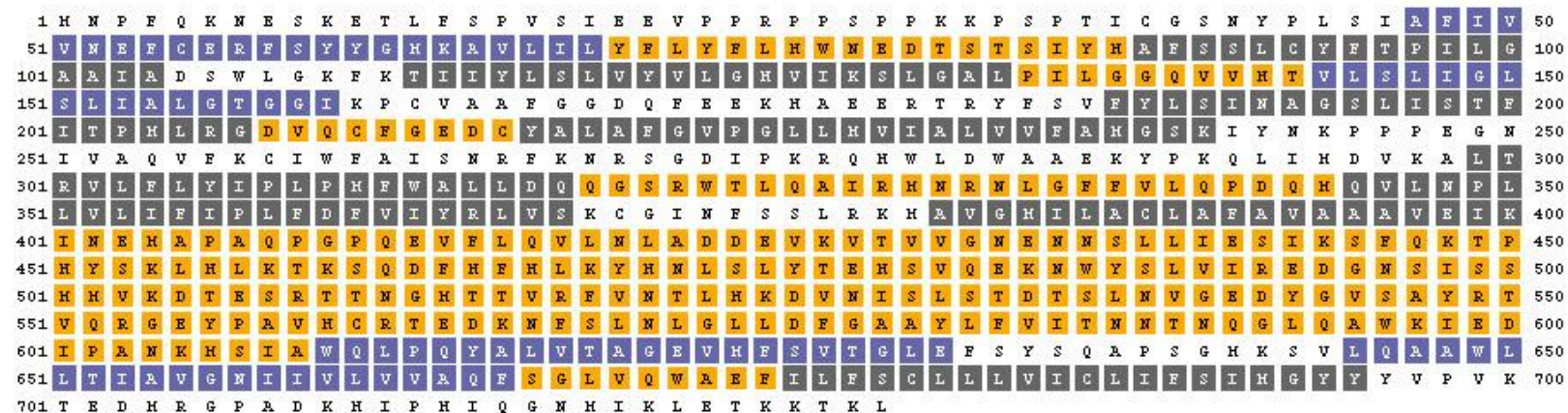
Forward primer	Sequence
hPepT2-Y42A	GACAATCTGTGGCTCCAAC G CTCCACTGAG
hPepT2-Y94A	GCCTTCAGCAGCCTCTGT G CTTTTACTCCC
hPepT2-Y188A	TAGATACTTCTCAGTCTTC G CCCTGTCCAT
hPepT2-R301A	TGGATGTAAAGGCACTGAC C GCGGTACTAT
hPepT2-W313A	TCCCATTGCCCATGTT C GCGGCTCTTTTGG
hPepT2-E622A	CTGGTTACAGCTGGGG C GGTCATGTTCTCT
hPepT2-Y42F	CAATCTGTGGCTCCA A CTTTCCACTGAGCATTGCCTTC
hPepT2-Y94F	CCTTCAGCAGCCTCTGTT T TTTTTACTCCCATCCTG GG
hPepT1-Y64F	GTTTGTGGCTCTGTGCT T CCTGACGCCAATTCTCG

Note: The mutated residues in the primers in the above table are highlighted in bold. The reverse primers used for the PCR step in the synthesis of the mutants were the reverse complements of their respective forward primers.

6.1.3.2 Prediction of secondary structure of hPepT2 using MEMSAT3

TM Helix Map

Feature predictions are colour coded onto the sequence according to the sequence feature key shown below.



Key	Transmembrane Helix	Pore lining Helix	Extracellular Region	Cytoplasmic Region	Disordered	Dompred Boundary	DomSSEA Boundary
Annotations	M	M	L	E	E	A	D

Figure 6.1.3-1-MEMSAT3 topology prediction of hPepT2 protein

According to the MEMSAT3 topology prediction (Figure 6.1.3-1) the 1st ECD was predicted to be between the amino acids 70 to 87, 2nd ECD between amino acid 134 -143 , 3rd ECD between amino acids 208 - 216 and the 4th ECD between amino acids 319 – 344.

Table 2.4-2 List of primers used for introducing FLAG tag in hPepT2

Primers	Sequence
hPepT2PBF-1	TTTGGCAGGGATCCGCCGCCA
hPepT2PBR-1	TTTTTTAGATCTTCACTTGTCATCGTCGTCCTTATAGTC
hPT2FLAGF-1	GATCAAGTCCTTGGGTGCCTTACCAATACTGG ACTACAAG GATGATGATGATAAGGGAGGACAAGTGGTACACACGTCC TATCAT
hPT2FLAGR-1	ATGATAGGACTGTGTGTACCACTTGTCTCCCTTATCATC ATCATCCTTGTAAGTCCAGTATTGGTAAGGCACCCAAGGA CTTGATC
hPT2FLAGF-2	GCTCTTTTGGATCAGCAGGGTTCACGATGGG GATTACAAGG ATGATGATGATAAGACTTTGCAAGCCATCAGGATGAATA GGAATT
hPT2FLAGR-2	AAATTCCTATTCATCCTGATGGCTTGCAAAGTCTTATCAT CATCATCCTTGTAATCCCATCGTGAACCCTGCTGATCCAA AAGAGC
hPT2FLAGF-3	CCTGTATTTCTGCCTGCACTGGAATGAAG ATTACAAGGATGAT GATGATAAG ACCTCCACATCTATATACCATGCCTTC
hPT2FLAGR-3	GAAGGCATGGTATATAGATGTGGAGGTCTTATCATCATC ATCCTTGTAATCTTCATTCCAGTGCAGGAAATACAGG

Note: In the above table, GGATCC = BamHI restriction site and AGATCT = BgIII restriction site.

MEMSAT3 was used to predict the topology of hPepT2. The primers were designed for introducing the FLAG epitope tag in the hPepT2 constructs using MEMSAT3 prediction. In the above primers hPT2FLAGF-1 and hPT2FLAGR-1 were the primer sequences used for FLAG epitope (Bold) tagging the 2nd ECD. hPT2FLAGF-2 and hPT2FLAGR-2 were used for the 4th ECD and hPT2FLAGF-3 and hPT2FLAGR-3 were the FLAG primers used for the 1st ECD.

The cRNA of the mutated hPepT2 and hPepT1 constructs including the FLAG epitope tagged hPepT2 constructs were synthesised as described in section 2.2.10 using SP6 mMessage Machine kit (Ambion). 10 ng of each of the cRNA was injected into *X. laevis* oocytes and uptake experiments and luminometry experiments were performed 3 days after cRNA injection as described in section 2.3.3.

6.1.4 Determination of the effect of site directed mutations on hPepT2 and hPepT1 mediated uptake of [³H]-D-Phe-L-Gln

3 days post cRNA injection uptake experiments were performed using [³H]-D-Phe-L-Gln as a radio labelled tracer. The uptake experiments were performed as described in section 2.3.3 using uptake media at pH 5.5 and when the effect of pH on a particular mutation was to be determined the pH was adjusted to 7.4 and the results were compared.

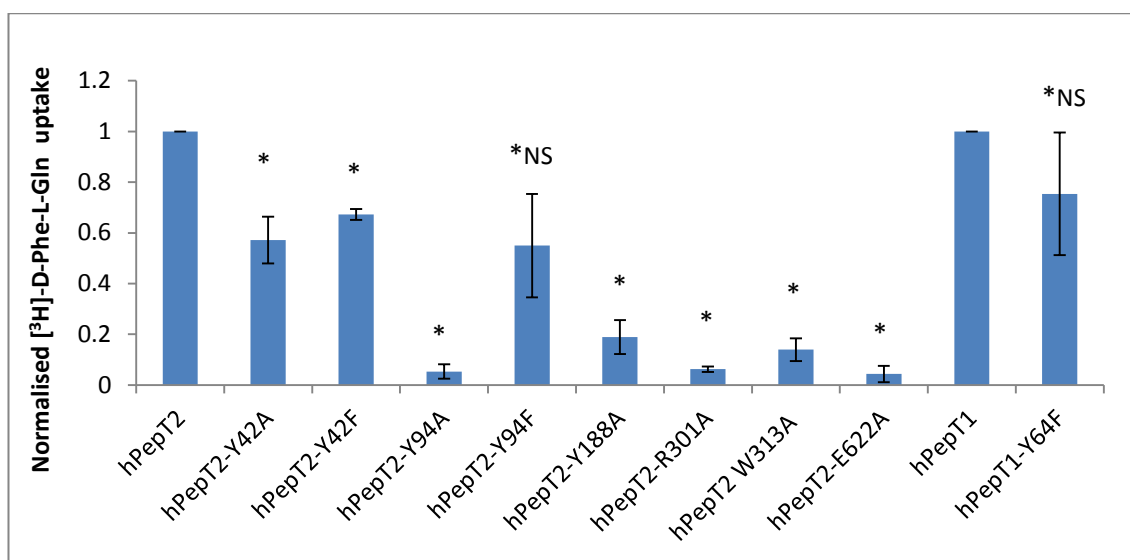


Figure 6.1.4-1 - Comparison of the effect of mutations on hPepT2 and hPepT1 constructs.

The histogram represents normalized uptake of [³H]-D-Phe-L-Gln in cRNA injected oocytes after removing the back ground uptake detected in the NI oocytes. The normalization was performed using uptake seen in wild type hPepT1 for hPepT1 mutations and wild type hPepT2 for hPepT2 mutations. The hPepT2 WT uptake was found to be 85 ± 2 fmoles/oocyte/hour at pH 5.5. The hPepT1 WT uptake was found to be 101 ± 22 fmoles/oocyte/hour at pH 5.5.

(* = one sample t-test between hPepT2 wild type and hPepT2 mutant RNA injected oocytes p-value < 0.05; and # = one sample t-test between hPepT1 wild type and hPepT1 mutant RNA injected oocytes, p-value < 0.05; NS = non-significant; n=3).

From the Figure 6.1.4-1 it can be seen that there was a reduction in the amount of transport of the radioactive tracer [^3H]-D-Phe- L-Gln in all the hPepT2 mutant constructs except Y94F, as compared to the wild type hPepT2. This could have resulted due to impaired transport function of the hPepT2 mutants or due to the reduction in protein expression.

Table 2.4-3 Summary of one sample t-test on hPepT2 and hPepT1 mutants with their respective wild type constructs

cRNA injected	one sample t test (* = $P < 0.05$, NS = not significant versus non-injected oocytes)	% reduction in transport (N/A = not applicable)
hPepT2-Y42A	*	30
hPepT2-Y42F	*	30
hPepT2-Y94A	*	99
hPepT2-Y94F	NS	N/A
hPepT2-Y188A	*	80
hPepT2-R301A	*	99
hPepT2 W313A	*	85
hPepT2-E622A	*	99

6.1.5 Determination of [3 H]-D-Phe- L-Gln uptake in hPepT2 FLAG epitope tagged cRNA injected oocytes

In order to determine hPepT2 protein expression FLAG epitope tag was introduced into the hPepT2-WT construct. The MEMSAT3 topology prediction used earlier with hPepT1 and ratPHT1 protein was used to predict the extracellular domain in hPepT2. Based on MEMSAT3 topology prediction (Figure 6.1.3-1) FLAG epitope tag was introduced into the 1st (hPepT2-1st ECD FLAG), 2nd (hPepT2-2nd ECD FLAG) and the 4th ECD (hPepT2- 4th ECD FLAG) constructs. These constructs were subjected to transport and luminometry assays to determine their transport and protein expression characteristics.

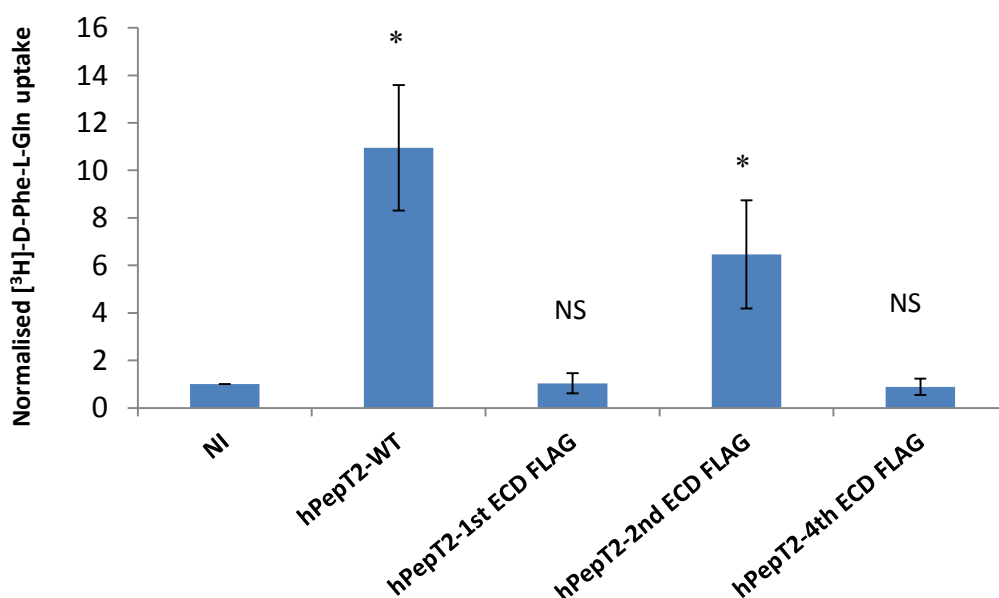


Figure 6.1.5-1 - Comparison of [3 H]-D-Phe-L-Gln uptake between wild type hPepT2 and hPepT2 FLAG epitope tagged constructs.

The histogram represents normalized uptake of [3 H]-D-Phe- L-Gln in cRNA injected oocytes. NI uptake was found to be 9.34 ± 0.9 fmoles/oocyte/hour. (*p-value < 0.05, = unpaired t-test with NI, NS = Not significant; n = 3)

hPepT2-2nd ECD flagged construct showed significant amount transport of [3 H]-D-Phe- L-Gln compared to the NI oocytes while the hPepT2-1st ECD FLAG and 4th ECD FLAG tagged constructs did not show significant transport.

6.1.6 Luminometric estimation of surface expression of FLAG epitope tagged hPepT2 constructs

A luminometry experiment was set up to determine if any of the FLAG tagged hPepT2 constructs could be detected using luminometry as described in section 2.3.6. FLAG tagged rPepT1 was used as a positive control for this experiment.

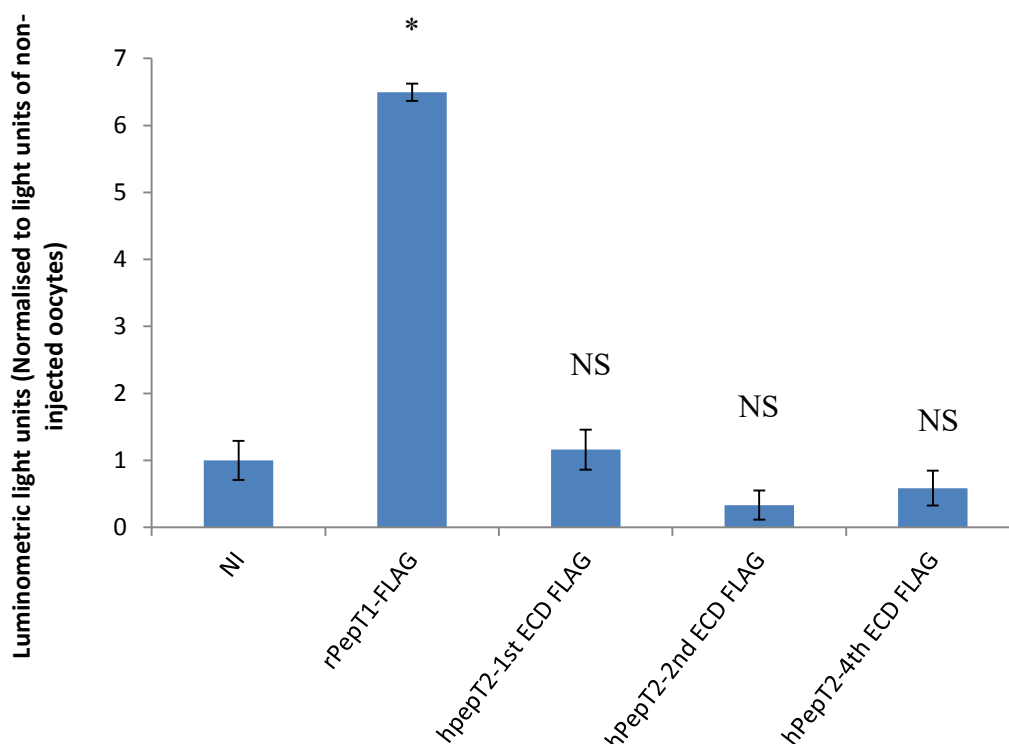


Figure 6.1.6-1 - Luminometric expression of hPepT2 FLAG epitope tagged constructs.

Each bar represents the mean \pm standard error of 3 experiments with 12 oocyte replicates. NI luminescence was found to be 5067 ± 1028 luminometric light units. (* = unpaired t-test with NI, p-value < 0.05 ; NS = Not significant)

From the above figure it can be seen that none of FLAG epitope tagged hPepT2 construct could be detected using luminometry. The positive control rPepT1 FLAG construct was however shown to have 5 times more luminometric signal compared to the NI oocytes showing that the assay worked effectively.

6.1.7 Comparison of K_i between hPepT2-WT and hPepT2-Y42A with dipeptide Glycine-L-Glutamine (Gly-Gln)

The K_i for hPepT2-WT and hPepT2-Y42A was set up to investigate if the reduction in the amount of transport seen in the mutant construct (hPepT2-Y42A, Figure 6.1.4-1) was due to change in the affinity of the transporter towards its substrates. If a change in affinity was detected between the hPepT2-WT and hPepT2-Y42A then this would suggest that the Y42 is part of the substrate binding site. It was found that the affinity of the hPepT2-Y42A construct towards Gly-Gln remained unchanged when compared to the hPepT2-WT (Figure 6.1.7-1 and Figure 6.1.7-2).

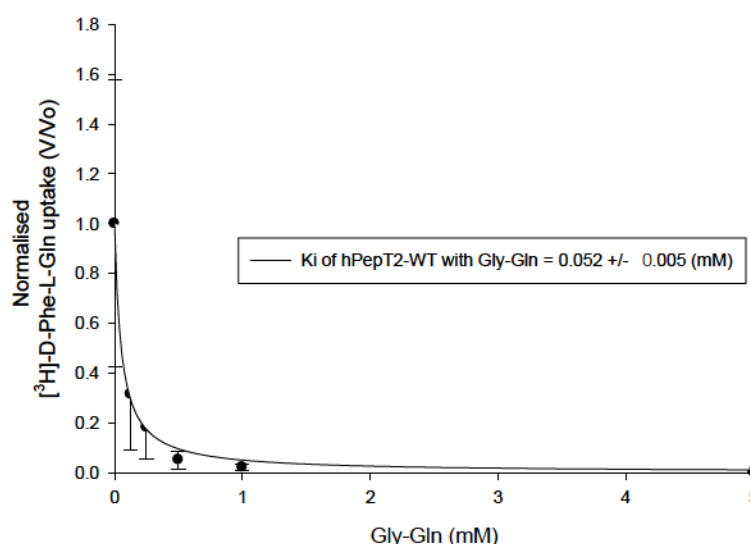


Figure 6.1.7-1 - K_i of hPepT2-WT construct with Gly-Gln

(n = 1)

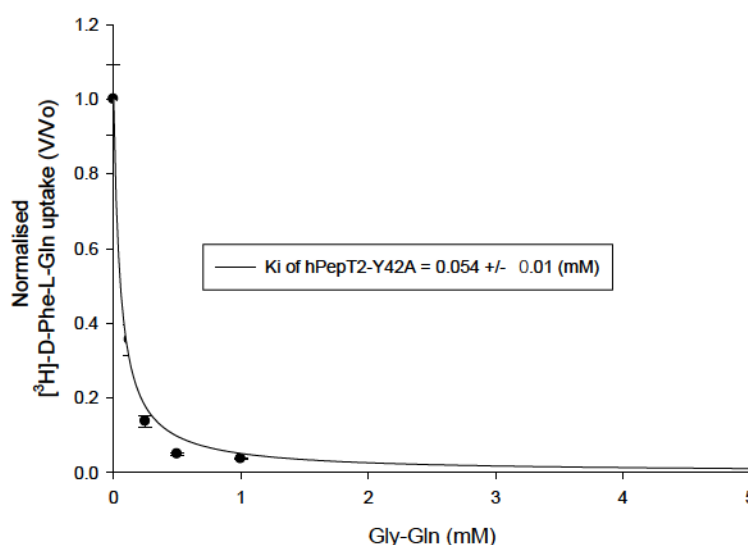


Figure 6.1.7-2 - K_i of hPepT2-Y42A construct with Gly-Gln
(n=1)

6.1.8 Discussion

Several investigations have been carried out on the effect of mutating conserved tyrosine (Y), arginine (R), tryptophan (W) and glutamate (E) residues in hPepT1 and rPepT1 (Bolger *et al.*, 1998; Kulkarni *et al.*, 2007; Meredith, 2004; Pieri *et al.*, 2009) but none of these mutations have been performed on PepT2. This experiment was set up to confirm if mutations on conserved residues in PepT2 would result in similar changes in the transport characteristics of hPepT2 as seen in hPepT1 and rPepT1 mutated transporter constructs.

It can be seen from Figure 6.1.4-1 that there was a reduction in the amount of transport in most of the mutated hPepT2 constructs. This reduction in the amount of transport observed in hPepT2 mutants could have been due to a decrease in the amount of hPepT2 protein (surface expression) in the cRNA injected *X. laevis* oocytes. In order to quantify the protein expression levels of the hPepT2 mutants, FLAG epitope tag was introduced in the 1st, 2nd and 4th ECD as predicted by MEMSAT topology prediction software (Figure 6.1.3-1). The 1st and 4th ECD were selected as they were predicted to be made of long stretches of amino acids offering flexibility to the site of FLAG insertion, while 2nd ECD was selected as insertion of FLAG in the 2nd ECD in hPepT1 and rPepT1 yielded a functional transporter (Covitz *et al.*, 1998; Panitsas *et al.*, 2006).

The uptake experiments with the FLAG epitope tagged constructs (Figure 6.1.5-1) showed that hPepT2 transporter with a FLAG in the 2nd ECD had significant transport of [³H]-D-Phe-L-Gln compared to non-injected oocytes but corresponded to only 50% transport seen in wild type hPepT2, whereas the hPepT2 constructs with FLAG in the 1st and 4th ECD did not transport the substrate at all. It was observed that the FLAG epitope tag in the 1st, 2nd and the 4th ECD could not be detected using luminometry (Figure 6.1.6-1). In the case of hPepT2 with FLAG epitope insertion in the 2nd ECD, the inaccessibility of the FLAG region by the antibody could have been the reason for not being detected in the luminometry experiments. For the hPepT2 constructs with FLAG epitope insertions in the 1st and 4th ECD, since they did not transport in addition to not being detected in the luminometry assay, showed that the introduction of the FLAG could have also interfered with the protein folding and might have caused the protein not to be expressed on the surface of the cell. FLAG epitope tagged rPepT1 (positive control) was detected in the luminometry assay which gave 5 times more signal compared to the non-injected control oocytes confirming that the luminometry technique worked successfully. Since none of the FLAG tagged hPepT2 constructs could be detected using luminometry, the quantification of protein expression levels of hPepT2 mutant constructs was not possible.

The mutation of tyrosine (Y) residue 42 to alanine (A) and phenylalanine (F) corresponding to tyrosine residue 12 (Y12) in PepT1 (Figure 6.1.4-1) resulted in a significant reduction of transport of [³H]-D-Phe-L-Gln compared to wild type hPepT2 (hPepT2-WT). A summary of the mutated residues and their equivalent residues in rPepT1 and hPepT1 is given in Table 2.4-4. The Y12A mutation in rPepT1 and hPepT1 showed a similar reduction in transport of substrate (Bolger *et al.*, 1998; Pieri *et al.*, 2009). This was found to be due to the reduction in protein expression (confirmed using luminometry assay on FLAG epitope tagged rPepT1) rather than a reduction in affinity of the transporter, as the K_m was found to be unchanged between rPepT1-Y12A and rPepT1 wild type transporter. The hPepT2-Y42F mutation also showed a similar significant reduction in transport compared to the wild type hPepT2 and the affinity of hPepT2-WT towards Gly-Gln was the same as that of hPepT2-Y42F ($K_i = 0.05\text{mM}$ as shown in Figure 6.1.7-1 and Figure 6.1.7-2 respectively). This suggests that Y42 in hPepT2 does not participate in substrate binding but is required for maintaining optimum protein expression levels.

The hPepT2-Y94A mutation (corresponding to Y64 in PepT1) almost completely abolished transport. This decrease in transport was regained when a more conservative mutation of hPepT2-Y94F was introduced instead of Y94A. It must be noted that Y94F mutation had larger error compared to the rest of the mutations, so this experiment could be repeated in the future if a more absolute value is required. Since hPepT1-Y64F mutation had not been performed in previous studies, this mutation was also tested to study the effect of Y64F mutation on the transport of substrate in hPepT1. Similar results were obtained to that seen in hPepT2-Y94F in which the substitution of Y64 with phenylalanine residue did not affect transport of [3H]-D-Phe- L-Gln significantly. The Y64F mutation in rPepT1 also showed that there was no effect in the transport compared to wild type rPepT1. This shows that the aromatic group in the tyrosine residue is important in maintaining wild type transport characteristics in PepT2 as introduction of phenylalanine residue at position 94 in hPepT2 does not show a change in transport but an alanine residue at this position abolished transport almost completely. In the crystal structure of bacterial POT protein PepTst, Y68 (corresponding to Y94 in hPepT2) was located in the peptide binding site (Solcan *et al.*, 2012). This tyrosine residue was found to determine substrate specificity and not proton coupling as Y68F mutants in PepTst protein were shown to have decreased affinity towards the di-peptide Glu-Glu compared to wild type, whilst maintaining the same level of transport as the wild type. In the same experiment Y68A similar to Y94A in hPepT2 was found to be inactive in the proton driven transport experiment which is similar to the results obtained for Y94A mutant in hPepT2.

Table 2.4-4 Table showing the equivalent residues of the mutated hPepT2 residues in rPepT1 and hPepT1

rPepT1	hPepT1	Effect of mutation in PepT1 compared to PepT1-WT and predictions of location based on crystal structures from bacterial homologues where available	hPepT2 mutants	Effect of mutation in hPepT2
Y12	Y12	Reduced rate of transport due reduction in the level of protein expression (Bolger <i>et al.</i> , 1998; Pieri <i>et al.</i> , 2009)	Y42A, Y42F	Reduced transport
Y64	Y64	No change in transport (Pieri <i>et al.</i> , 2008)	Y94F	No change in transport
Y64	Y64	Transport reduced by >90%. Aromatic ring in Y is required for maintaining wild type transport	Y94A	>90% reduction in transport
Y167	Y167	Reduction in transport >90%. Predicted to be involved in substrate transport cycle from PepT _{st} crystal structure (Newstead <i>et al.</i> , 2011)	Y188A	>80% reduction in transport
R282	R282	Reduction in transport (Pieri <i>et al.</i> , 2008)	R301A	>90% reduction in transport
W294	W294	Abolition of transport. Predicted to be in the substrate binding site in PepT _{so} crystal structure (Newstead, 2011)	W313A	>90% reduction in transport
E594	E595	Abolition of transport. Involved in salt bridge formation during substrate transport in GkPOT crystal structure (Doki <i>et al.</i> , 2013) Binds amino terminus of substrate (Bailey <i>et al.</i> , 2000; Newstead, 2011; Solcan <i>et al.</i> , 2012)	E622A	Abolition of transport

The mutations Y188A, W313A and E622A in hPepT2, corresponding to Y167, W294 and E595 in hPepT1, showed transport levels only marginally above the NI oocytes but less than 20% transport of that observed in wild type hPepT2. This is similar to the results obtained in rPepT1 and hPepT1 where mutations in the corresponding residues resulted in the expression of a functional transporter in which the transport of substrate [3 H]-D-Phe-L-Gln (rPepT1) and Gly-Sar (hPepT1) was almost completely abolished (Bolger *et al.*, 1998; Pieri *et al.*, 2009; Yeung *et al.*, 1998). Mutation of the highly conserved PTR2_2 motif (FYxxINxG) in the *PTR2* gene was reported to alter either the substrate affinity, substrate transport: and/or protein expression in *Saccharomyces cerevisiae* (Hauser *et al.*, 2005). In this model the Y248 residue (part of the PTR2_2 motif, corresponding to Y167 in PepT1) failed to express in *S. cerevisiae* in the case of the Y248A mutant, whereas Y167A (PepT1) mutant protein expressed but failed to transport substrate. The corresponding mutation Y188A in hPepT2 showed greater than 80% reduction in transport compared to wild type hPepT2. In the crystal structure of the bacterial transporter PepTso Y154 (equivalent to the residue Y167 in PepT1) was located in the central peptide binding cavity and was suggested to play a role in regulating the exit of peptides into the cell during peptide transport (Newstead *et al.*, 2011). Additionally W312 and E419 residues in the PepTso crystal structure (corresponding to W313 and E622 in hPepT2) were also found to be located in the predicted substrate binding site. This may explain why the mutation of the residues Y188A, W313A and E622A in hPepT2 had a detrimental effect on peptide transport. In the more recently crystallised bacterial POT protein (GkPOT) from *Geobacillus kaustophilus* in complex with the substrate alafosfalin the amino acid residue E310 (equivalent to E622 in hPepT2) was found to play key role in the formation of a salt bridge with the conserved R43 (equivalent to K64 in hPepT2) in the transition from the inward facing open state of the transporter to an occluded conformation in the peptide transport cycle (Doki *et al.*, 2013). This could explain why the E622A mutant did not transport substrates as the transport cycle would have been interrupted due to the lack of an acidic amino acid at position 622 (hPepT2) to form the salt bridge affecting the transport of substrates.

The hPepT2-R301A construct (corresponding to R282 in PepT1) was found to show very low transport compared to hPepT2-WT showing that R301 residue plays a crucial role hPepT2 mediated transport of substrates. The reduction in transport by rPepT1-R282A was not as detrimental as that seen in hPepT2-R301A which allowed further

analysis for example; the rPepT1-R282A construct was found to have lost the ability to increase the transport rates when the external pH was reduced from 7.5 to 5.5 compared to the wild type rPepT1. In case of hPepT2-R301A construct this effect could not be determined since the transport rate was very low such that any effect introduced on transport by the change in external pH would not be detected. This difference in amount of transport in hPepT2-R301A compared to rPepT1-R282A could be either due to reduced protein expression or change in binding affinity. The experiment to determine binding affinity for hPepT2-R301A could not be performed, again due to very low levels of transport in this construct. Also, since luminometry had failed on hPepT2 FLAG epitope tagged constructs the level of protein expression could not be established for the hPepT2 mutants. The R282A mutant in both rPepT1 and hPepT1 were found to have the same binding affinity as PepT1-WT but had a lower V_{max} compared to PepT1-WT but this study did not monitor protein expression (Bolger *et al.*, 1998; Pieri *et al.*, 2008). The exact reason for such low levels of transport in hPepT2-R301A construct might be understood once the exact location of R301 in the crystal structure of PepT2 is determined.

This is the first time a systematic site directed mutagenesis study has been performed on conserved residues in hPepT2 protein. Introduction of mutations in the tyrosine, glutamate and tryptophan residues showed largely similar transporter behaviour as previously observed in rPepT1 and hPepT1. The main difference was the R301A mutation which showed significantly reduced transport (almost to the level of the non-injected) which was not the case with equivalent mutations in rPepT1 and hPepT1. The interpretation of the hPepT2 mutation findings was hampered by not being able to measure the protein expression levels by luminometry. Hence a suitable location in the extracellular domain of hPepT2 which maintains wild type hPepT2 transport and which can also be detected using luminometry technique would have to be established to determine the reason for difference in substrate transport in hPepT2 mutants. Additionally monoclonal antibodies raised against extracellular PepT2 domains could be used if available. However given that the equivalent mutations in PepT1 and PepT2 did give largely similar results strongly suggests that the overall architecture and mechanism of action of the various members of the SLC15 family of transporters will be similar.

The knowledge gained regarding the structure of the peptide transporters has come a long way since the initial isolation and functional characterisation of rPepT1 (Fei *et al.*,

1994). Site-directed mutation studies helped narrow down the important amino acids involved in peptide binding and transport, allowing the first substrate template model which predicted the important features required for a substrate to efficiently bind to by PepT1 (Bailey *et al.*, 2000). The full length hPepT1 homology model based on the crystal structure of bacterial transporter lactose permease (LacY) was generated and docking studies were performed using 50 known substrates of hPepT1 (Pedretti *et al.*, 2008). This model explained that PepT1 substrates could tolerate modifications in the amino and carboxyl termini due to the stabilizing interactions of residues at amino and carboxyl termini of the substrate with the predicted binding pocket and due to several interactions of residues with the peptide backbone of the substrate. The key residues involved in peptide recognition were predicted to be located in TMD1, 8 and 10. The crystal structures of PepTso and GkPOT agree with this prediction (Doki *et al.*, 2013; Newstead, 2014).

The homology model of hPepT2 based on the bacterial POT (provided by Firdaus Samsudin and Dr Philip Fowler, Department of Biochemistry, Oxford University) was used to locate and compare the residues previously suggested to form the binding pocket with the locations of the residues mutated in the current study (Figure 6.1.8-1). Figure 6.1.8-1C shows that the residues Y94, Y188, W313 and E622 all point towards the predicted binding pocket as previously shown in the crystal structure of GkPOT bound to alafosfalin (Figure 6.1.8-1A, G310, Y40, R43 from GkPOT and Y29, R25, N151 from PepTso2, equivalent residues highlighted in the hPepT2 homology model within circle) (Doki *et al.*, 2013; Guettou *et al.*, 2013) which suggests a direct interaction of these residues with the substrate during peptide transport.

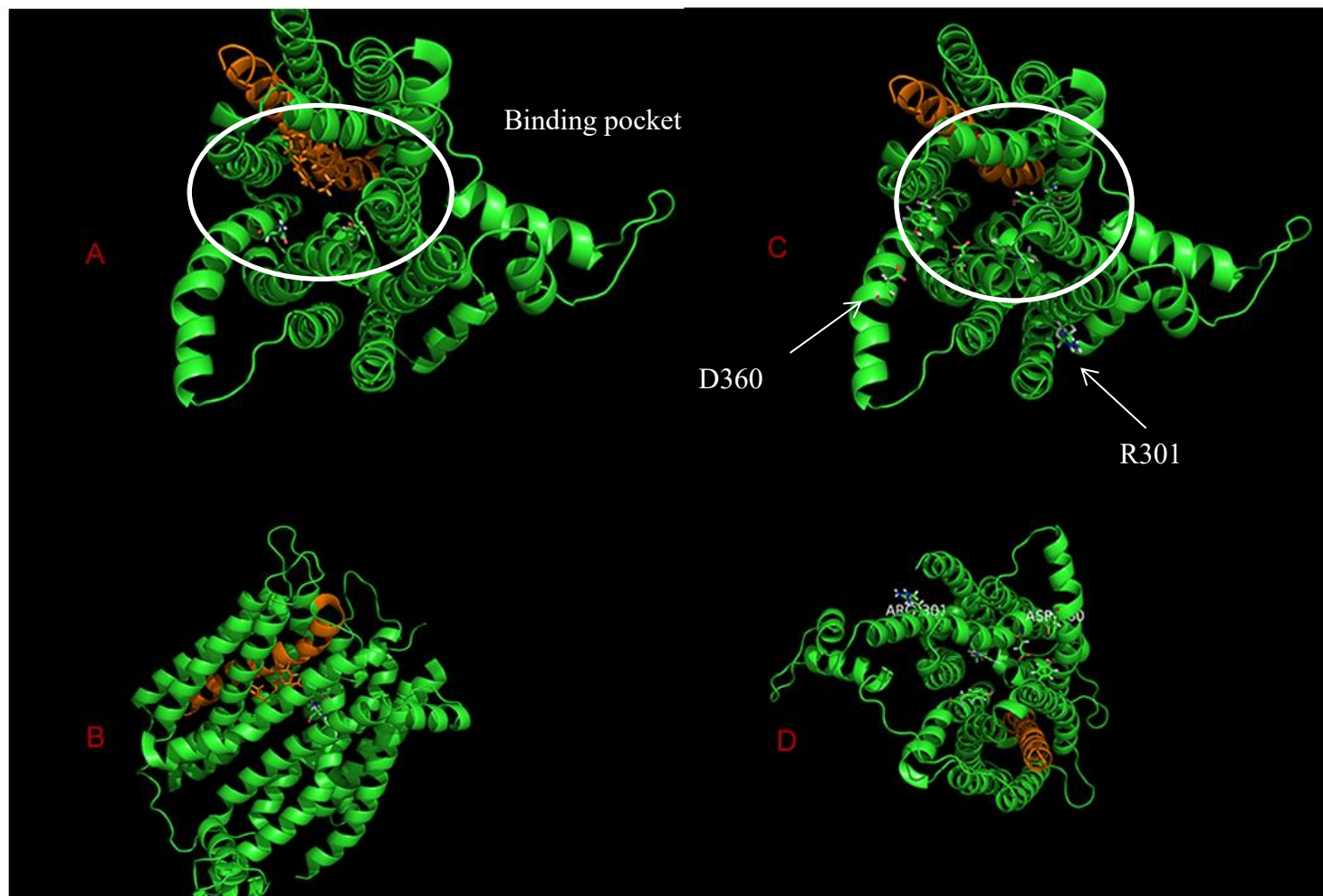


Figure 6.1.8-1 - Comparison of the location of the predicted binding pocket in hPepT2 (using GKPOT and PepTso) with the location of the amino acids mutated in the current study for hPepT2.

In all the figures the 1st predicted TMD is coloured in orange. A and B represent hPepT2 structures showing the predicted binding pocket, C and D show the location of the mutations in the current study, except for Y42 which was not included in the homology model (but would be located at the beginning of TMD1).

The residues which were predicted to form a charge pair during the peptide transport cycle (Pieri *et al.*, 2008) namely R301 (R282 in PepT1) and D360 (D341 in hPepT1) are located at opposite edges as seen in Figure 6.1.8-1C. This large separation of the two residues in the current homology model would not allow the formation of an intramolecular salt bridge. However, a previous study had predicted PepT1 to be a homo tetramer (Panitsas *et al.*, 2006). Therefore another possible explanation of the charge pair interaction between the arginine and aspartate could be that PepT2 also exists as a tetramer and that the charge pair is formed between adjacent R and D residues from separate hPepT proteins in the homo multimeric assembly. In support of this, PepTso2 was shown to have a tetrameric assembly in the negative stain EM imaging which supports the possibility of POTs to exist in monomeric or oligomeric forms (Guettou *et al.*, 2013).

The interactions observed in the crystal structures between the substrate and transporter only gives a snap shot of the interactions made at the time of crystallisation and does not reveal the movements made by the protein during the transport process. The current protein model predictions are also based on the bacterial POTs which might not be the most accurate model to explain the results obtained from previous point mutation analysis on mammalian PepT1 and PepT2 proteins. The crystallisation of the mammalian PepT1 and/or PepT2 would further provide a better understanding of the ligand binding and transport in SLC15 peptide transporters and validate the accuracy of the homology models.

7 General discussion and future work

In the current study a number of complementary approaches have been taken to investigate the structure-function relationship of SLC15 peptide transporters. The screening of novel prodrug carriers namely Aib-, cLu- and Thio- which were designed using the previously established PepT1 substrate template (Bailey *et al.*, 2000) gave novel insights into the structure of PepT1 substrates. The cLu- carrier was found to be very effective in binding to PepT1 transporter with high affinity and was found to be transported by PepT1. The Aib- and Thio- carriers were also found to be efficient PepT1 substrates in binding and transporting prodrugs but with lesser binding affinity characteristics compared to cLu- carrier. These novel carriers were able to transport a range of substrates with different size and hydrophobicity which make them excellent carriers for delivering drugs and other pharmaceuticals to improve their oral bioavailability. This shows that there is still potential in designing novel carriers that specifically target PepT1 with its ability to transport a diverse range of substrates.

PepT1 is a low affinity high capacity transporter whereas PepT2 is a high affinity low capacity transporter. None of the studies so far including site directed mutagenesis or chimeras with N terminal and C terminal swaps between PepT1 and PepT2 have been able to determine the exact reason for this difference in characteristics. In the hPepT1 and hPepT2 ECD swap/deleted experiments it was found that hPepT1 ECD plays a structural role in that the hPepT1 failed to express in the absence of its own ECD. However in hPepT2 the ECD plays a role of a pH sensor and is able to function without its own ECD. It was also found to function with the ECD from hPepT1 while maintaining hPepT2 wild type characteristics. These observations show that ECD in hPepT1 and hPepT2 does not determine binding affinities of the transporter. With the recently crystallised structure of the ECDs from mouse PepT1 and rat PepT2 it has also been demonstrated that the ECD binds to trypsin (protease) which is predicted to help in increasing the concentration of di- and tri- peptides locally in the intestine and kidney to improve absorption of peptides.

For the first time site directed mutagenesis was performed on conserved hPepT2 residues to determine if these residues although conserved played different roles in hPepT2 compared to PepT1. From the uptake experiments it was found that the conserved tyrosine, glutamate, arginine and tryptophan residues tested played similar

roles in PepT1 and PepT2. The PHT1 transporter was previously suggested to be a plasma membrane protein involved in the transport of histidine in the brain (Bhardwaj *et al.*, 2006; Yamashita *et al.*, 1997). In our hands PHT1 was found to be localised to the plasma membrane but it did not transport histidine in both transport assays and electrophysiology experiments. The exact reason for this discrepancy is not known. However, it has also been suggested that PHT1 could be a lysosomal transporter involved in the efflux of histidine amino acids resulting from protein digestion in the lysosomes (Ocheltree *et al.*, 2003).

Future work would involve synthesising the cLu- conjugated versions of Atenolol, Relenza, Mycophenolate, Sialic acid and Kinase inhibitor and determining their respective binding affinity characteristics in order to establish if cLu- carrier continues to demonstrate PepT1 mediated transport. Establishing a suitable HPLC column and mobile phase for detecting the compounds which could not be analysed (ND in Table 2.4-6) in the current study would allow to further obtain data with respect to the ability of Aib-, Thio- and cLu- carriers to hijack PepT1 transporter for delivering drugs. Alternatively, mass spectroscopy (MS) or Liquid Chromatography - MS (LC-MS) techniques could also be explored to detect the prodrugs. Once the crystal structure of mammalian peptide transporters namely PepT1 and PepT2 depicting the various stages of peptide transport i.e. outward facing, occluded and inward facing is determined, this would allow to locate the specific amino acid residues involved in peptide transport. This would further allow docking studies to be performed using PepT1 substrates and validate the substrate binding template proposed and possibly obtain a better understanding of how PepT1 and PepT2 interact with their substrates. Experiments can also be performed to determine substrate selectivity between rPepT1 and hPepT1. The recently published paper which has provided further explanation on the poly-specific nature of POT transporters based on PepTst bacterial crystal and modelling studies has suggested the di- and tri- peptides are transported by different binding mechanisms which is thought to have evolved with time to accommodate a wider variety of substrates/nutrients (Parker *et al.*, 2014). However, whether the same modes of transport are involved in mammalian POTs is yet to be established.

The ECD's in PepT1 and PepT2 have been proposed to bind to trypsin (Beale *et al.*, 2015 in press). Similar interaction of an amino peptidase N enzyme (APN), carboxypeptidase ACE2, with neutral amino acid transporter (B⁰AT1) which transports single amino acids namely glutamine, alanine, phenylalanine and leucine in the

intestinal brush border membrane has been reported (Fairweather *et al.*, 2012). It was found that the co-expression of APN and B⁰AT1 in *X. laevis* increased the apparent affinity of B⁰AT1 mediated transport of leucine compared to B⁰AT1 expressing oocytes. This was found to be due to increase in the availability of leucine amino acid by APN. A similar study could also be performed with by co-expressing proteases (for example: trypsin, chymotrypsin) with either PepT1 or PepT2 in *X. laevis* oocytes and comparing the kinetics with PepT1 and PepT2 expressing oocytes to test if the ECD in PepT1 and PepT2 could have more than one interacting protein partner besides trypsin. The reason why PepT2 was able to demonstrate transport in the absence of this large ECD and PepT1 did not transport needs to be further looked into. It could be possible that the chimeras constructed in PepT1-ECD Δ and PepT1-ECD2 constructs had important amino acid residues removed from the predicted transmembrane domain which led to the improper folding of PepT1 mutant constructs. Further studies could be carried out using varying lengths of amino acids between the predicted TMD9 and ECD junction between TMD9 and TMD10 to determine if reintroduction of the missing amino acids at this junction can restore PepT1 expression and transport.

Since the surface expression of hPepT2 using FLAG tag in the predicted 1st, 2nd and 4th ECD's did not yield a positive result, using the homology model to predict a suitable location for the insertion of the ECD would enable to quantify protein expression in case of hPepT2 mutants.

Finally, rat PHT1 was found not to transport histidine or any of the other single amino acids in our experiments; further investigation needs to be performed using electrophysiology and different di- and tri- peptide combinations to determine the transported substrates of PHT1 transporter. This would enable the design of prodrug carriers specifically targeting PHT1 transporters which could be used to deliver drugs which require to pass through the blood brain barrier (BBB) in order to reach the site of action (Tashima, 2015). Another possible substrate to be tested is the bacterial cell associated muramyl di- and tri- peptides which have been found to be transported by PHT1 in endosomal and lysosomal membranes to facilitate an immune response during bacterial infections (Lee *et al.*, 2009; Nakamura *et al.*, 2014).

In conclusion, the results presented in this thesis build on the current knowledge of the mammalian POT transporters with respect to their diverse structure-function relationships. These and future studies will hopefully pave the way for their better

utilization for targeted drug delivery and to improve bioavailability of difficult to deliver/absorb pharmaceutical compounds.

8 Bibliography

- Abramson, J. *et al.* (2003). Structure and mechanism of the lactose permease of *Escherichia coli*. *Science* 301 (5633), pp.610-615.
- Albert, A. (1958). Chemical aspects of selective toxicity. *Nature* 182 (4633), pp.421-422.
- Alcorn, J. *et al.* (2002). Transporter gene expression in lactating and nonlactating human mammary epithelial cells using real-time reverse transcription-polymerase chain reaction. *J Pharmacol Exp Ther* 303 (2), pp.487-496.
- Anderle, P. *et al.* (2006). Genetic variants of the human dipeptide transporter PEPT1. *J Pharmacol Exp Ther* 316 (2), pp.636-646.
- Anderson, C. M. *et al.* (2009). Taurine uptake across the human intestinal brush-border membrane is via two transporters: H⁺-coupled PAT1 (SLC36A1) and Na⁺- and Cl⁻-dependent TauT (SLC6A6). *J Physiol* 587 (Pt 4), pp.731-744.
- Anekthananon, T. *et al.* (2013). Oseltamivir and inhaled zanamivir as influenza prophylaxis in Thai health workers: a randomized, double-blind, placebo-controlled safety trial over 16 weeks. *J Antimicrob Chemother* 68 (3), pp.697-707.
- Artursson, P. and Karlsson, J. (1991). Correlation between oral drug absorption in humans and apparent drug permeability coefficients in human intestinal epithelial (Caco-2) cells. *Biochem Biophys Res Commun* 175 (3), pp.880-885.
- Ashida, K. *et al.* (2002). Thyroid hormone regulates the activity and expression of the peptide transporter PEPT1 in Caco-2 cells. *Am J Physiol Gastrointest Liver Physiol* 282 (4), pp.G617-623.
- Ashida, K. *et al.* (2004). Decreased activity and expression of intestinal oligopeptide transporter PEPT1 in rats with hyperthyroidism in vivo. *Pharm Res* 21 (6), pp.969-975.
- Baccala, R. *et al.* (2013). Essential requirement for IRF8 and SLC15A4 implicates plasmacytoid dendritic cells in the pathogenesis of lupus. *Proc Natl Acad Sci U S A* 110 (8), pp.2940-2945.
- Bahadduri, P. M. *et al.* (2005). Functional characterization of the peptide transporter PEPT2 in primary cultures of human upper airway epithelium. *Am J Respir Cell Mol Biol* 32 (4), pp.319-325.
- Bailey, P. D. *et al.* (2000). How to Make Drugs Orally Active: A Substrate Template for Peptide Transporter PepT1. *Angew Chem Int Ed Engl* 39 (3), pp.505-508.
- Balimane, P. V. *et al.* (2007). Peptide transporter substrate identification during permeability screening in drug discovery: comparison of transfected MDCK-hPepT1 cells to Caco-2 cells. *Arch Pharm Res* 30 (4), pp.507-518.
- Beale, J. H. *et al.* (2015). Crystal Structures of the Extracellular Domain from PepT1 and PepT2 Provide Novel Insights into Mammalian Peptide Transport. *Structure* 23 (10), pp.1889-1899.
- Bhardwaj, R. K. *et al.* (2006). The functional evaluation of human peptide/histidine transporter 1 (hPHT1) in transiently transfected COS-7 cells. *Eur J Pharm Sci* 27 (5), pp.533-542.
- Biegel, A. *et al.* (2005). Three-dimensional quantitative structure-activity relationship analyses of beta-lactam antibiotics and tripeptides as substrates of the mammalian H⁺/peptide cotransporter PEPT1. *J Med Chem* 48 (13), pp.4410-4419.
- Bolger, M. B. *et al.* (1998). Structure, function, and molecular modeling approaches to the study of the intestinal dipeptide transporter PepT1. *J Pharm Sci* 87 (11), pp.1286-1291.
- Boll, M. *et al.* (2002). Functional characterization of two novel mammalian electrogenic proton-dependent amino acid cotransporters. *J Biol Chem* 277 (25), pp.22966-22973.
- Boll, M. *et al.* (1996). Expression cloning and functional characterization of the kidney cortex high-affinity proton-coupled peptide transporter. *Proc Natl Acad Sci U S A* 93 (1), pp.284-289.

- Boll, M. *et al.* (1994). Expression cloning of a cDNA from rabbit small intestine related to proton-coupled transport of peptides, beta-lactam antibiotics and ACE-inhibitors. *Pflugers Arch* 429 (1), pp.146-149.
- Borthakur, A. *et al.* (2012). A novel nutrient sensing mechanism underlies substrate-induced regulation of monocarboxylate transporter-1. *Am J Physiol Gastrointest Liver Physiol* 303 (10), pp.G1126-1133.
- Botka, C. W. *et al.* (2000). Human proton/oligopeptide transporter (POT) genes: identification of putative human genes using bioinformatics. *AAPS PharmSci* 2 (2), p.E16.
- Brandsch, M., Knutter, I. and Bosse-Doenecke, E. (2008). Pharmaceutical and pharmacological importance of peptide transporters. *J Pharm Pharmacol* 60 (5), pp.543-585.
- Brandsch, M., Knutter, I. and Leibach, F. H. (2004). The intestinal H⁺/peptide symporter PEPT1: structure-affinity relationships. *Eur J Pharm Sci* 21 (1), pp.53-60.
- Brandsch, M. *et al.* (1994). Expression and protein kinase C-dependent regulation of peptide/H⁺ co-transport system in the Caco-2 human colon carcinoma cell line. *Biochem J* 299 (Pt 1), pp.253-260.
- Bretschneider, B., Brandsch, M. and Neubert, R. (1999). Intestinal transport of beta-lactam antibiotics: analysis of the affinity at the H⁺/peptide symporter (PEPT1), the uptake into Caco-2 cell monolayers and the transepithelial flux. *Pharm Res* 16 (1), pp.55-61.
- Brodin, B. *et al.* (2002). Transport of peptidomimetic drugs by the intestinal Di/tri-peptide transporter, PepT1. *Pharmacol Toxicol* 90 (6), pp.285-296.
- Buyse, M. *et al.* (2001). PepT1-mediated epithelial transport of dipeptides and cephalixin is enhanced by luminal leptin in the small intestine. *J Clin Invest* 108 (10), pp.1483-1494.
- Covitz, K. M., Amidon, G. L. and Sadee, W. (1998). Membrane topology of the human dipeptide transporter, hPEPT1, determined by epitope insertions. *Biochemistry* 37 (43), pp.15214-15221.
- Crane, R. K. (1962). Hypothesis for mechanism of intestinal active transport of sugars. *Fed Proc* 21, pp.891-895.
- Cruz, D. N. (2000). Midodrine: a selective alpha-adrenergic agonist for orthostatic hypotension and dialysis hypotension. *Expert Opin Pharmacother* 1 (4), pp.835-840.
- Dai, X. *et al.* (2015). MicroRNA-193a-3p Reduces Intestinal Inflammation in Response to Microbiota via Down-regulation of Colonic PepT1. *J Biol Chem*.
- Dalmasso, G. *et al.* (2011). MicroRNA-92b regulates expression of the oligopeptide transporter PepT1 in intestinal epithelial cells. *Am J Physiol Gastrointest Liver Physiol* 300 (1), pp.G52-59.
- Daniel, H. and Adibi, S. A. (1994). Functional separation of dipeptide transport and hydrolysis in kidney brush border membrane vesicles. *FASEB J* 8 (10), pp.753-759.
- Daniel, H. and Kottra, G. (2004). The proton oligopeptide cotransporter family SLC15 in physiology and pharmacology. *Pflugers Arch* 447 (5), pp.610-618.
- Daniel, H., Morse, E. L. and Adibi, S. A. (1992). Determinants of substrate affinity for the oligopeptide/H⁺ symporter in the renal brush border membrane. *J Biol Chem* 267 (14), pp.9565-9573.
- Daniel, H. *et al.* (2006). From bacteria to man: archaic proton-dependent peptide transporters at work. *Physiology (Bethesda)* 21, pp.93-102.
- Denny, W. A. (2001). Prodrug strategies in cancer therapy. *Eur J Med Chem* 36 (7-8), pp.577-595.
- Deonarain, M. P. and Epenetos, A. A. (1994). Targeting enzymes for cancer therapy: old enzymes in new roles. *Br J Cancer* 70 (5), pp.786-794.
- Deves, R. and Boyd, C. A. (1989). The determination of kinetic parameters for carrier-mediated transport of non-labelled substrate analogues: a general method applied to the study of divalent anion transport in placental membrane vesicles. *Proc R Soc Lond B Biol Sci* 237 (1286), pp.85-97.
- Diamandis, P. *et al.* (2007). Chemical genetics reveals a complex functional ground state of neural stem cells. *Nat Chem Biol* 3 (5), pp.268-273.

- Doki, S. *et al.* (2013). Structural basis for dynamic mechanism of proton-coupled symport by the peptide transporter POT. *Proc Natl Acad Sci U S A* 110 (28), pp.11343-11348.
- Doring, F. *et al.* (1996). Functional analysis of a chimeric mammalian peptide transporter derived from the intestinal and renal isoforms. *J Physiol* 497 (Pt 3), pp.773-779.
- Doring, F. *et al.* (2002). Importance of a small N-terminal region in mammalian peptide transporters for substrate affinity and function. *J Membr Biol* 186 (2), pp.55-62.
- Dougherty, D. A. (1996). Cation- π interactions in chemistry and biology: a new view of benzene, Phe, Tyr, and Trp. *Science* 271 (5246), pp.163-168.
- Dubowchik, G. M. and Walker, M. A. (1999). Receptor-mediated and enzyme-dependent targeting of cytotoxic anticancer drugs. *Pharmacol Ther* 83 (2), pp.67-123.
- Duncan, R. (1992). Drug-polymer conjugates: potential for improved chemotherapy. *Anticancer Drugs* 3 (3), pp.175-210.
- Dyer, J. *et al.* (1990). Glycyl-L-proline transport in rabbit enterocyte basolateral-membrane vesicles. *Biochem J* 269 (3), pp.565-571.
- Fairweather, S. J. *et al.* (2012). Intestinal peptidases form functional complexes with the neutral amino acid transporter B(0)AT1. *Biochem J* 446 (1), pp.135-148.
- Fei, Y. J. *et al.* (1994). Expression cloning of a mammalian proton-coupled oligopeptide transporter. *Nature* 368 (6471), pp.563-566.
- Fei, Y. J. *et al.* (1997). Identification of the histidyl residue obligatory for the catalytic activity of the human H⁺/peptide cotransporters PEPT1 and PEPT2. *Biochemistry* 36 (2), pp.452-460.
- Fei, Y. J. *et al.* (2000). cDNA structure, genomic organization, and promoter analysis of the mouse intestinal peptide transporter PEPT1. *Biochim Biophys Acta* 1492 (1), pp.145-154.
- Foley, D. *et al.* (2009a). Targeting ketone drugs towards transport by the intestinal peptide transporter, PepT1. *Org Biomol Chem* 7 (6), pp.1064-1067.
- Foley, D. *et al.* (2009b). The in vitro transport of model thiodipeptide prodrugs designed to target the intestinal oligopeptide transporter, PepT1. *Org Biomol Chem* 7 (18), pp.3652-3656.
- Foley, D. W. *et al.* (2010). Bioavailability through PepT1: the role of computer modelling in intelligent drug design. *Curr Comput Aided Drug Des* 6 (1), pp.68-78.
- Foulis, M. A. and Barr, J. B. (1937). Prontosil Album in Puerperal Sepsis. *Br Med J* 1 (3973), pp.445-446.
- Ganapathy, M. E. *et al.* (1995). Differential recognition of beta -lactam antibiotics by intestinal and renal peptide transporters, PEPT 1 and PEPT 2. *J Biol Chem* 270 (43), pp.25672-25677.
- Ganapathy, V. and Leibach, F. H. (1983). Role of pH gradient and membrane potential in dipeptide transport in intestinal and renal brush-border membrane vesicles from the rabbit. Studies with L-carnosine and glycyl-L-proline. *J Biol Chem* 258 (23), pp.14189-14192.
- Gasteiger, E. *et al.* (2003). ExPASy: The proteomics server for in-depth protein knowledge and analysis. *Nucleic Acids Res* 31 (13), pp.3784-3788.
- Gebauer, S. *et al.* (2003). Three-dimensional quantitative structure-activity relationship analyses of peptide substrates of the mammalian H⁺/peptide cotransporter PEPT1. *J Med Chem* 46 (26), pp.5725-5734.
- Gilbert, E. R., Wong, E. A. and Webb, K. E., Jr. (2008). Board-invited review: Peptide absorption and utilization: Implications for animal nutrition and health. *J Anim Sci* 86 (9), pp.2135-2155.
- Guettou, F. *et al.* (2013). Structural insights into substrate recognition in proton-dependent oligopeptide transporters. *EMBO Rep*.
- Gutmann, H. *et al.* (1999). Evidence for different ABC-transporters in Caco-2 cells modulating drug uptake. *Pharm Res* 16 (3), pp.402-407.

- Hallows, K. R. (2005). Emerging role of AMP-activated protein kinase in coupling membrane transport to cellular metabolism. *Curr Opin Nephrol Hypertens* 14 (5), pp.464-471.
- Han, H. K. and Amidon, G. L. (2000). Targeted prodrug design to optimize drug delivery. *AAPS PharmSci* 2 (1), p.E6.
- Hardie, D. G. (2005). New roles for the LKB1-->AMPK pathway. *Curr Opin Cell Biol* 17 (2), pp.167-173.
- Hauser, M. *et al.* (2005). Substrate preference is altered by mutations in the fifth transmembrane domain of Ptr2p, the di/tri-peptide transporter of *Saccharomyces cerevisiae*. *Mol Membr Biol* 22 (3), pp.215-227.
- Hidalgo, I. J., Raub, T. J. and Borchardt, R. T. (1989). Characterization of the human colon carcinoma cell line (Caco-2) as a model system for intestinal epithelial permeability. *Gastroenterology* 96 (3), pp.736-749.
- Horter, D. and Dressman, J. B. (2001). Influence of physicochemical properties on dissolution of drugs in the gastrointestinal tract. *Adv Drug Deliv Rev* 46 (1-3), pp.75-87.
- Hu, M. and Amidon, G. L. (1988). Passive and carrier-mediated intestinal absorption components of captopril. *J Pharm Sci* 77 (12), pp.1007-1011.
- Huang, Y. *et al.* (2003). Structure and mechanism of the glycerol-3-phosphate transporter from *Escherichia coli*. *Science* 301 (5633), pp.616-620.
- Huttunen, K. M., Raunio, H. and Rautio, J. (2011). Prodrugs--from serendipity to rational design. *Pharmacol Rev* 63 (3), pp.750-771.
- Ihara, T. *et al.* (2000). Regulation of PepT1 peptide transporter expression in the rat small intestine under malnourished conditions. *Digestion* 61 (1), pp.59-67.
- Irie, M. *et al.* (2005). Computational modelling of H⁺-coupled peptide transport via human PEPT1. *J Physiol* 565 (Pt 2), pp.429-439.
- Jacobson, M. A. (1993). Valaciclovir (BW256U87): the L-valyl ester of acyclovir. *J Med Virol Suppl* 1, pp.150-153.
- Jensen, J. M. *et al.* (2012). Probing the Putative Active Site of YjdL: An Unusual Proton-Coupled Oligopeptide Transporter from *E. coli*. *PLoS One* 7 (10), p.e47780.
- Jones, D. T. (2007). Improving the accuracy of transmembrane protein topology prediction using evolutionary information. *Bioinformatics* 23 (5), pp.538-544.
- Kibbe, W. A. (2007). OligoCalc: an online oligonucleotide properties calculator. *Nucleic Acids Res* 35 (Web Server issue), pp.W43-46.
- Kolhatkar, V. *et al.* (2012). Identification of novel nonsteroidal compounds as substrates or inhibitors of hASBT. *J Pharm Sci* 101 (1), pp.116-126.
- Kulkarni, A. A. *et al.* (2007). A charge pair interaction between Arg282 in transmembrane segment 7 and Asp341 in transmembrane segment 8 of hPepT1. *Pharm Res* 24 (1), pp.66-72.
- Kurschat, C. E. *et al.* (2006). Alkaline-shifted pHo sensitivity of AE2c1-mediated anion exchange reveals novel regulatory determinants in the AE2 N-terminal cytoplasmic domain. *J Biol Chem* 281 (4), pp.1885-1896.
- Kusuhara, H. *et al.* (1999). Molecular cloning and characterization of a new multispecific organic anion transporter from rat brain. *J Biol Chem* 274 (19), pp.13675-13680.
- Lee, J. *et al.* (2009). pH-dependent internalization of muramyl peptides from early endosomes enables Nod1 and Nod2 signaling. *J Biol Chem* 284 (35), pp.23818-23829.
- Lee, V. H. *et al.* (1999). Biopharmaceutics of transmucosal peptide and protein drug administration: role of transport mechanisms with a focus on the involvement of PepT1. *J Control Release* 62 (1-2), pp.129-140.
- Liang, R. *et al.* (1995). Human intestinal H⁺/peptide cotransporter. Cloning, functional expression, and chromosomal localization. *J Biol Chem* 270 (12), pp.6456-6463.
- Liu, W. *et al.* (1995). Molecular cloning of PEPT 2, a new member of the H⁺/peptide cotransporter family, from human kidney. *Biochim Biophys Acta* 1235 (2), pp.461-466.

- Luckner, P. and Brandsch, M. (2005). Interaction of 31 beta-lactam antibiotics with the H⁺/peptide symporter PEPT2: analysis of affinity constants and comparison with PEPT1. *Eur J Pharm Biopharm* 59 (1), pp.17-24.
- Luo, S. *et al.* (2011). Targeting SVCT for enhanced drug absorption: synthesis and in vitro evaluation of a novel vitamin C conjugated prodrug of saquinavir. *Int J Pharm* 414 (1-2), pp.77-85.
- Lyons, J. A. *et al.* (2014). Structural basis for polyspecificity in the POT family of proton-coupled oligopeptide transporters. *EMBO Rep* 15 (8), pp.886-893.
- Mackenzie, B. *et al.* (1996a). The human intestinal H⁺/oligopeptide cotransporter hPEPT1 transports differently-charged dipeptides with identical electrogenic properties. *Biochim Biophys Acta* 1284 (2), pp.125-128.
- Mackenzie, B. *et al.* (1996b). Mechanisms of the human intestinal H⁺-coupled oligopeptide transporter hPEPT1. *J Biol Chem* 271 (10), pp.5430-5437.
- Matsushita, K. *et al.* (2012). Glycolysis inhibitors as a potential therapeutic option to treat aggressive neuroblastoma expressing GLUT1. *J Pediatr Surg* 47 (7), pp.1323-1330.
- Meredith, D. (2004). Site-directed mutation of arginine 282 to glutamate uncouples the movement of peptides and protons by the rabbit proton-peptide cotransporter PepT1. *J Biol Chem* 279 (16), pp.15795-15798.
- Meredith, D. (2009). Review. The mammalian proton-coupled peptide cotransporter PepT1: sitting on the transporter-channel fence? *Philos Trans R Soc Lond B Biol Sci* 364 (1514), pp.203-207.
- Meredith, D. and Boyd, C. A. (2000). Structure and function of eukaryotic peptide transporters. *Cell Mol Life Sci* 57 (5), pp.754-778.
- Meredith, D. *et al.* (1998). 4-aminomethylbenzoic acid is a non-translocated competitive inhibitor of the epithelial peptide transporter PepT1. *J Physiol* 512 (Pt 3), pp.629-634.
- Meredith, D. and Price, R. A. (2006). Molecular modeling of PepT1--towards a structure. *J Membr Biol* 213 (2), pp.79-88.
- Meredith, D. *et al.* (2000). Modified amino acids and peptides as substrates for the intestinal peptide transporter PepT1. *Eur J Biochem* 267 (12), pp.3723-3728.
- Mitsui, H. *et al.* (1981). Antitumor activity of a new compound, ethyl O-[N-(p-carboxyphenyl)-carbamoyl]-mycophenolate, against various experimental tumors upon oral administration. *Gan* 72 (1), pp.66-71.
- Muzyk, A. J., Rivelli, S. K. and Gagliardi, J. P. (2012). Defining the role of baclofen for the treatment of alcohol dependence: a systematic review of the evidence. *CNS Drugs* 26 (1), pp.69-78.
- Nakamura, N. *et al.* (2014). Endosomes are specialized platforms for bacterial sensing and NOD2 signalling. *Nature* 509 (7499), pp.240-244.
- Nakanishi, T. *et al.* (2000). Cancer cell-targeted drug delivery utilizing oligopeptide transport activity. *Int J Cancer* 88 (2), pp.274-280.
- Nakano, S. *et al.* (1999). Nucleic acid duplex stability: influence of base composition on cation effects. *Nucleic Acids Res* 27 (14), pp.2957-2965.
- Newey, H. and Smyth, D. H. (1959). The intestinal absorption of some dipeptides. *J Physiol* 145 (1), pp.48-56.
- Newstead, S. (2011). Towards a structural understanding of drug and peptide transport within the proton-dependent oligopeptide transporter (POT) family. *Biochem Soc Trans* 39 (5), pp.1353-1358.
- Newstead, S. (2014). Molecular insights into proton coupled peptide transport in the PTR family of oligopeptide transporters. *Biochim Biophys Acta*.
- Newstead, S. *et al.* (2011). Crystal structure of a prokaryotic homologue of the mammalian oligopeptide-proton symporters, PepT1 and PepT2. *EMBO J* 30 (2), pp.417-426.
- Nielsen, C. U. *et al.* (2003). Epidermal growth factor and insulin short-term increase hPepT1-mediated glycylsarcosine uptake in Caco-2 cells. *Acta Physiol Scand* 178 (2), pp.139-148.

- Nielsen, C. U. *et al.* (2001). Epidermal growth factor inhibits glycylsarcosine transport and hPepT1 expression in a human intestinal cell line. *Am J Physiol Gastrointest Liver Physiol* 281 (1), pp.G191-199.
- Ocheltree, S. M. *et al.* (2003). Preliminary investigation into the expression of proton-coupled oligopeptide transporters in neural retina and retinal pigment epithelium (RPE): lack of functional activity in RPE plasma membranes. *Pharm Res* 20 (9), pp.1364-1372.
- Ogihara, H. *et al.* (1996). Immuno-localization of H⁺/peptide cotransporter in rat digestive tract. *Biochem Biophys Res Commun* 220 (3), pp.848-852.
- Ogihara, H. *et al.* (1999). Peptide transporter in the rat small intestine: ultrastructural localization and the effect of starvation and administration of amino acids. *Histochem J* 31 (3), pp.169-174.
- Omkvist, D. H., Brodin, B. and Nielsen, C. U. (2010). Ibuprofen is a non-competitive inhibitor of the peptide transporter hPEPT1 (SLC15A1): possible interactions between hPEPT1 substrates and ibuprofen. *Br J Pharmacol* 161 (8), pp.1793-1805.
- Pan, X. *et al.* (2002). Diurnal rhythm of H⁺-peptide cotransporter in rat small intestine. *Am J Physiol Gastrointest Liver Physiol* 283 (1), pp.G57-64.
- Pan, X. *et al.* (2003). Altered diurnal rhythm of intestinal peptide transporter by fasting and its effects on the pharmacokinetics of ceftibuten. *J Pharmacol Exp Ther* 307 (2), pp.626-632.
- Panitsas, K. E., Boyd, C. A. and Meredith, D. (2006). Evidence that the rabbit proton-peptide co-transporter PepT1 is a multimer when expressed in *Xenopus laevis* oocytes. *Pflugers Arch* 452 (1), pp.53-63.
- Pao, S. S., Paulsen, I. T. and Saier, M. H., Jr. (1998). Major facilitator superfamily. *Microbiol Mol Biol Rev* 62 (1), pp.1-34.
- Papot, S. *et al.* (2002). Design of selectively activated anticancer prodrugs: elimination and cyclization strategies. *Curr Med Chem Anticancer Agents* 2 (2), pp.155-185.
- Parker, J. L., Mindell, J. A. and Newstead, S. (2014). Thermodynamic evidence for a dual transport mechanism in a POT peptide transporter. *Elife* 3.
- Parrish, J. E. and Kipnis, D. M. (1964). Effect of Na on Sugar and Amino Acid Transport in Striated Muscle. *J Clin Invest* 43, pp.1994-2002.
- Paulsen, I. T. and Skurray, R. A. (1994). The POT family of transport proteins. *Trends Biochem Sci* 19 (10), p.404.
- Pedretti, A. *et al.* (2008). Modeling of the intestinal peptide transporter hPepT1 and analysis of its transport capacities by docking and pharmacophore mapping. *ChemMedChem* 3 (12), pp.1913-1921.
- Petroff, O. A. *et al.* (1996). The effect of gabapentin on brain gamma-aminobutyric acid in patients with epilepsy. *Ann Neurol* 39 (1), pp.95-99.
- Pieri, M. *et al.* (2010). The apical (hPepT1) and basolateral peptide transport systems of Caco-2 cells are regulated by AMP-activated protein kinase. *Am J Physiol Gastrointest Liver Physiol* 299 (1), pp.G136-143.
- Pieri, M. *et al.* (2009). The transmembrane tyrosines Y56, Y91 and Y167 play important roles in determining the affinity and transport rate of the rabbit proton-coupled peptide transporter PepT1. *Int J Biochem Cell Biol* 41 (11), pp.2204-2213.
- Pieri, M. *et al.* (2008). Site-directed mutagenesis of Arginine282 suggests how protons and peptides are co-transported by rabbit PepT1. *Int J Biochem Cell Biol* 40 (4), pp.721-730.
- Qiu, A. *et al.* (2006). Identification of an intestinal folate transporter and the molecular basis for hereditary folate malabsorption. *Cell* 127 (5), pp.917-928.
- Rautio, J. *et al.* (2008). Prodrugs: design and clinical applications. *Nat Rev Drug Discov* 7 (3), pp.255-270.
- Reddy, V. S. *et al.* (2012). The major facilitator superfamily (MFS) revisited. *FEBS J* 279 (11), pp.2022-2035.
- Riklis, E. and Quastel, J. H. (1958). Effects of cations on sugar absorption by isolated surviving guinea pig intestine. *Can J Biochem Physiol* 36 (3), pp.347-362.

- Romano, A. *et al.* (2010). Functional expression of SLC15 peptide transporters in rat thyroid follicular cells. *Mol Cell Endocrinol* 315 (1-2), pp.174-181.
- Rubio-Aliaga, I., Boll, M. and Daniel, H. (2000). Cloning and characterization of the gene encoding the mouse peptide transporter PEPT2. *Biochem Biophys Res Commun* 276 (2), pp.734-741.
- Sagne, C. *et al.* (2001). Identification and characterization of a lysosomal transporter for small neutral amino acids. *Proc Natl Acad Sci U S A* 98 (13), pp.7206-7211.
- Saier, M. H., Jr. *et al.* (1999). The major facilitator superfamily. *J Mol Microbiol Biotechnol* 1 (2), pp.257-279.
- Saito, H. *et al.* (1995). Cloning and characterization of a rat H⁺/peptide cotransporter mediating absorption of beta-lactam antibiotics in the intestine and kidney. *J Pharmacol Exp Ther* 275 (3), pp.1631-1637.
- Saito, H. *et al.* (1996). Molecular cloning and tissue distribution of rat peptide transporter PEPT2. *Biochim Biophys Acta* 1280 (2), pp.173-177.
- Saito, H. *et al.* (2008). Regulatory mechanism governing the diurnal rhythm of intestinal H⁺/peptide cotransporter 1 (PEPT1). *Am J Physiol Gastrointest Liver Physiol* 295 (2), pp.G395-402.
- Sakata, K. *et al.* (2001). Cloning of a lymphatic peptide/histidine transporter. *Biochem J* 356 (Pt 1), pp.53-60.
- Saleh, M. and Elson, C. O. (2011). Experimental inflammatory bowel disease: insights into the host-microbiota dialog. *Immunity* 34 (3), pp.293-302.
- Savi, P. *et al.* (2000). Identification and biological activity of the active metabolite of clopidogrel. *Thromb Haemost* 84 (5), pp.891-896.
- Sen, R. and Baltimore, D. (1986). Multiple nuclear factors interact with the immunoglobulin enhancer sequences. *Cell* 46 (5), pp.705-716.
- Shen, H. *et al.* (1999). Localization of PEPT1 and PEPT2 proton-coupled oligopeptide transporter mRNA and protein in rat kidney. *Am J Physiol* 276 (5 Pt 2), pp.F658-665.
- Shimakura, J. *et al.* (2005). Characterization of the human peptide transporter PEPT1 promoter: Sp1 functions as a basal transcriptional regulator of human PEPT1. *Am J Physiol Gastrointest Liver Physiol* 289 (3), pp.G471-477.
- Shimakura, J. *et al.* (2006). The transcription factor Cdx2 regulates the intestine-specific expression of human peptide transporter 1 through functional interaction with Sp1. *Biochem Pharmacol* 71 (11), pp.1581-1588.
- Shiraga, T. *et al.* (1999). Cellular and molecular mechanisms of dietary regulation on rat intestinal H⁺/Peptide transporter PepT1. *Gastroenterology* 116 (2), pp.354-362.
- Shu, C. *et al.* (2002). Role of PEPT2 in peptide/mimetic trafficking at the blood-cerebrospinal fluid barrier: studies in rat choroid plexus epithelial cells in primary culture. *J Pharmacol Exp Ther* 301 (3), pp.820-829.
- Sievers, F. *et al.* (2011). Fast, scalable generation of high-quality protein multiple sequence alignments using Clustal Omega. *Mol Syst Biol* 7, p.539.
- Singer, S. J. and Nicolson, G. L. (1972). The fluid mosaic model of the structure of cell membranes. *Science* 175 (4023), pp.720-731.
- Sitar, D. S. (1996). Clinical pharmacokinetics of bambuterol. *Clin Pharmacokinet* 31 (4), pp.246-256.
- Solcan, N. *et al.* (2012). Alternating access mechanism in the POT family of oligopeptide transporters. *EMBO J*.
- Sondergaard, H. B., Nielsen, C. U. and Brodin, B. (2012). Identification and Characterization of a Novel Nontranslated Sequence Variant of the Human Intestinal Di-/Tripeptide Transporter, hPEPT1. *Int J Pept* 2012, p.743472.
- Steel, A. *et al.* (1997). Stoichiometry and pH dependence of the rabbit proton-dependent oligopeptide transporter PepT1. *J Physiol* 498 (Pt 3), pp.563-569.
- Steiner, H. Y., Naider, F. and Becker, J. M. (1995). The PTR family: a new group of peptide transporters. *Mol Microbiol* 16 (5), pp.825-834.

- Stella, V. J. and Himmelstein, K. J. (1980). Prodrugs and site-specific drug delivery. *J Med Chem* 23 (12), pp.1275-1282.
- Stella, V. J. and Nti-Addae, K. W. (2007). Prodrug strategies to overcome poor water solubility. *Adv Drug Deliv Rev* 59 (7), pp.677-694.
- Stothard, P. (2000). The sequence manipulation suite: JavaScript programs for analyzing and formatting protein and DNA sequences. *Biotechniques* 28 (6), pp.1102, 1104.
- Takahashi, Y. *et al.* (2000). Identification of cAMP analogue inducible genes in RAW264 macrophages. *Biochim Biophys Acta* 1492 (2-3), pp.385-394.
- Takeda, J. *et al.* (2013). Theaflavins, dimeric catechins, inhibit peptide transport across Caco-2 cell monolayers via down-regulation of AMP-activated protein kinase-mediated peptide transporter PEPT1. *Food Chem* 138 (4), pp.2140-2145.
- Tashima, T. (2015). Intriguing possibilities and beneficial aspects of transporter-conscious drug design. *Bioorg Med Chem* 23 (15), pp.4119-4131.
- Temple, C. S. *et al.* (1995). Substrate-charge dependence of stoichiometry shows membrane potential is the driving force for proton-peptide cotransport in rat renal cortex. *Pflugers Arch* 430 (5), pp.825-829.
- Temple, C. S. *et al.* (1998). Peptide mimics as substrates for the intestinal peptide transporter. *J Biol Chem* 273 (1), pp.20-22.
- Terada, T. *et al.* (2000). N-terminal halves of rat H⁺/peptide transporters are responsible for their substrate recognition. *Pharm Res* 17 (1), pp.15-20.
- Terada, T. *et al.* (1999). Functional characteristics of basolateral peptide transporter in the human intestinal cell line Caco-2. *Am J Physiol* 276 (6 Pt 1), pp.G1435-1441.
- Testa, B. (2004). Prodrug research: futile or fertile? *Biochem Pharmacol* 68 (11), pp.2097-2106.
- Teuscher, N. S. *et al.* (2004). Carnosine uptake in rat choroid plexus primary cell cultures and choroid plexus whole tissue from PEPT2 null mice. *J Neurochem* 89 (2), pp.375-382.
- Thamotharan, M. *et al.* (1999). Hormonal regulation of oligopeptide transporter pept-1 in a human intestinal cell line. *Am J Physiol* 276 (4 Pt 1), pp.C821-826.
- Theis, S. *et al.* (2002). Synthesis and characterization of high affinity inhibitors of the H⁺/peptide transporter PEPT2. *J Biol Chem* 277 (9), pp.7287-7292.
- Thwaites, D. T. *et al.* (1995). D-cycloserine transport in human intestinal epithelial (Caco-2) cells: mediation by a H⁽⁺⁾-coupled amino acid transporter. *Br J Pharmacol* 115 (5), pp.761-766.
- Thwaites, D. T. *et al.* (1993). H⁽⁺⁾-coupled dipeptide (glycylsarcosine) transport across apical and basal borders of human intestinal Caco-2 cell monolayers display distinctive characteristics. *Biochim Biophys Acta* 1151 (2), pp.237-245.
- Uchiyama, T. *et al.* (2003). Biophysical evidence for His57 as a proton-binding site in the mammalian intestinal transporter hPepT1. *Pharm Res* 20 (12), pp.1911-1916.
- Vig, B. S. *et al.* (2006). Human PEPT1 pharmacophore distinguishes between dipeptide transport and binding. *J Med Chem* 49 (12), pp.3636-3644.
- Vincze, T., Posfai, J. and Roberts, R. J. (2003). NEBcutter: A program to cleave DNA with restriction enzymes. *Nucleic Acids Res* 31 (13), pp.3688-3691.
- Walker, D. *et al.* (1998). Substrate upregulation of the human small intestinal peptide transporter, hPepT1. *J Physiol* 507 (Pt 3), pp.697-706.
- Wenzel, U. *et al.* (1996). Transport characteristics of differently charged cephalosporin antibiotics in oocytes expressing the cloned intestinal peptide transporter PepT1 and in human intestinal Caco-2 cells. *J Pharmacol Exp Ther* 277 (2), pp.831-839.
- Wenzel, U., Thwaites, D. T. and Daniel, H. (1995). Stereoselective uptake of beta-lactam antibiotics by the intestinal peptide transporter. *Br J Pharmacol* 116 (7), pp.3021-3027.
- Wire, M. B., Shelton, M. J. and Studenberg, S. (2006). Fosamprenavir : clinical pharmacokinetics and drug interactions of the amprenavir prodrug. *Clin Pharmacokinet* 45 (2), pp.137-168.

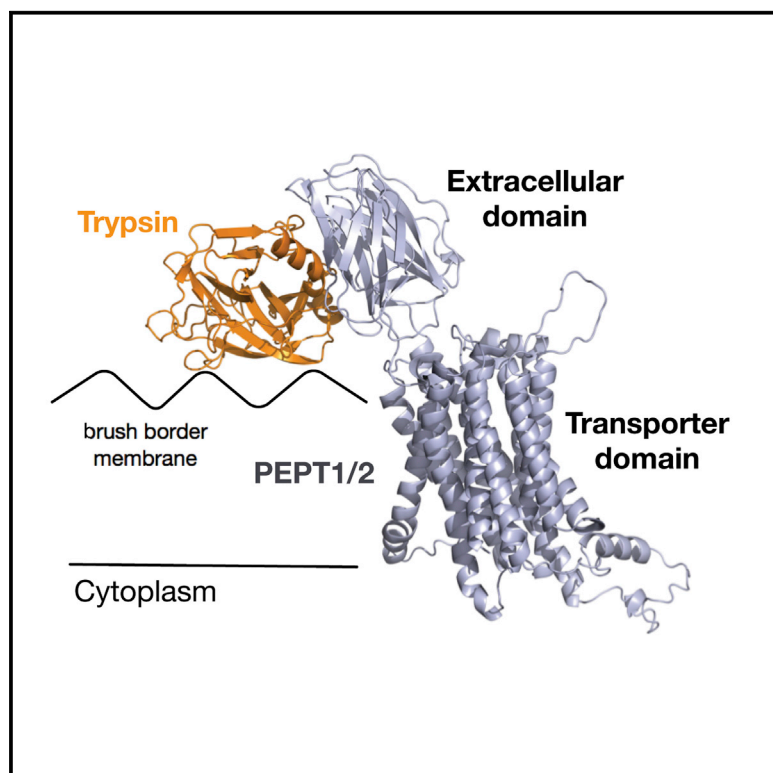
- Wreden, C. C. *et al.* (2003). The H⁺-coupled electrogenic lysosomal amino acid transporter LYAAT1 localizes to the axon and plasma membrane of hippocampal neurons. *J Neurosci* 23 (4), pp.1265-1275.
- Yamashita, T. *et al.* (1997). Cloning and functional expression of a brain peptide/histidine transporter. *J Biol Chem* 272 (15), pp.10205-10211.
- Yan, Z. *et al.* (2011). Bifunctional peptidomimetic prodrugs of didanosine for improved intestinal permeability and enhanced acidic stability: synthesis, transepithelial transport, chemical stability and pharmacokinetics. *Mol Pharm* 8 (2), pp.319-329.
- Yen, P. M. and Chin, W. W. (1994). New advances in understanding the molecular mechanisms of thyroid hormone action. *Trends Endocrinol Metab* 5 (2), pp.65-72.
- Yeung, A. K. *et al.* (1998). Molecular identification of a role for tyrosine 167 in the function of the human intestinal proton- coupled dipeptide transporter (hPepT1). *Biochem Biophys Res Commun* 250 (1), pp.103-107.
- Yoshitomi, K. and Fromter, E. (1984). Cell pH of rat renal proximal tubule in vivo and the conductive nature of peritubular HCO₃⁻ (OH⁻) exit. *Pflügers Arch* 402 (3), pp.300-305.
- Young, M. E., Radda, G. K. and Leighton, B. (1996). Activation of glycogen phosphorylase and glycogenolysis in rat skeletal muscle by AICAR—an activator of AMP-activated protein kinase. *FEBS Lett* 382 (1-2), pp.43-47.
- Zhang, E. Y. *et al.* (2004). Genetic polymorphisms in human proton-dependent dipeptide transporter PEPT1: implications for the functional role of Pro586. *J Pharmacol Exp Ther* 310 (2), pp.437-445.
- Zhu, T. *et al.* (2000). Differential recognition of ACE inhibitors in *Xenopus laevis* oocytes expressing rat PEPT1 and PEPT2. *Pharm Res* 17 (5), pp.526-532.

9 Appendix I: Publication (in press)

Structure

Crystal Structures of the Extracellular Domain from PepT1 and PepT2 Provide Novel Insights into Mammalian Peptide Transport

Graphical Abstract



Authors

John H. Beale, Joanne L. Parker, Firdaus Samsudin, ..., David Meredith, Philip W. Fowler, Simon Newstead

Correspondence

simon.newstead@bioch.ox.ac.uk

In Brief

The crystal structure of PepT1 and PepT2 reported by Beale et al. reveals two immunoglobulin-like domains connected in tandem inserted within the canonical major facilitator superfamily fold. Biophysical analyses reveal a specific interaction with trypsin, suggesting a role in clustering proteolytic activity to the site of peptide uptake across the membrane.

Highlights

- Crystal structure of the extracellular domains of PepT1 and PepT2
- Modular architecture for a mammalian MFS transporter
- Extracellular domains contain immunoglobulin-like fold and interact with trypsin

Accession Numbers

5A9D

5A9H

5A9I



Crystal Structures of the Extracellular Domain from PepT1 and PepT2 Provide Novel Insights into Mammalian Peptide Transport

John H. Beale,^{1,10} Joanne L. Parker,^{1,10} Firdaus Samsudin,^{1,10} Anne L. Barrett,^{1,2} Anish Senan,³ Louise E. Bird,^{4,5} David Scott,^{6,7,8} Raymond J. Owens,^{4,5} Mark S.P. Sansom,^{1,9} Stephen J. Tucker,^{2,9} David Meredith,⁴ Philip W. Fowler,¹ and Simon Newstead^{1,9,*}

¹Department of Biochemistry, University of Oxford, Oxford OX1 3QU, UK

²Clarendon Laboratory, Department of Physics, University of Oxford, Oxford OX1 3PU, UK

³Department of Biological Sciences, Oxford Brookes University, Oxford OX3 0BP, UK

⁴Department of Biological and Medical Sciences, Faculty of Health and Life Sciences, Oxford Brookes University, Oxford OX3 0BP, UK

⁵OPPF-UK, Research Complex at Harwell, Harwell Oxford, Didcot, Oxfordshire OX11 0FA, UK

⁶Research Complex at Harwell, Harwell Science and Innovation Campus, Didcot, Oxfordshire OX11 0FA, UK

⁷ISIS Spallation Neutron and Muon Source, Rutherford Appleton Laboratory, Oxfordshire OX11 0FA, UK

⁸School of Biosciences, School of Biosciences, Sutton Bonington Campus, Leicestershire LE12 5RD, UK

⁹OXION Initiative in Ion Channels and Membrane Transport, University of Oxford OX1 3PU, UK

¹⁰Co-first author

*Correspondence: simon.newstead@bioch.ox.ac.uk

<http://dx.doi.org/10.1016/j.str.2015.07.016>

This is an open access article under the CC BY license (<http://creativecommons.org/licenses/by/4.0/>).

SUMMARY

Mammals obtain nitrogen via the uptake of di- and tri-peptides in the gastrointestinal tract through the action of PepT1 and PepT2, which are members of the POT family of proton-coupled oligopeptide transporters. PepT1 and PepT2 also play an important role in drug transport in the human body. Recent crystal structures of bacterial homologs revealed a conserved peptide-binding site and mechanism of transport. However, a key structural difference exists between bacterial and mammalian homologs with only the latter containing a large extracellular domain, the function of which is currently unknown. Here, we present the crystal structure of the extracellular domain from both PepT1 and PepT2 that reveal two immunoglobulin-like folds connected in tandem, providing structural insight into mammalian peptide transport. Functional and biophysical studies demonstrate that these domains interact with the intestinal protease trypsin, suggesting a role in clustering proteolytic activity to the site of peptide transport in eukaryotic cells.

INTRODUCTION

In mammals, the plasma membrane transporters PepT1 (SLC15A1) and PepT2 (SLC15A2) mediate the uptake and retention of dietary peptides (Adibi, 1997a; Matthews, 1991). PepT1 and PepT2 are proton-coupled symporters, recognizing di- and tri-peptides on the outside of the cell and utilizing the energy stored in the inwardly directed proton electrochemical gradient

($\Delta\mu\text{H}^+$) to drive their uptake into the cell (Daniel and Rubio-Aliaga, 2003; Fei et al., 1994). PepT1 and PepT2 also recognize and transport a number of important drug families, including β -lactam antibiotics and anti-cancer agents (reviewed in Brandsch, 2013), and are important targets in the ongoing attempts of the pharmaceutical industry to improve the pharmacokinetic properties of drug molecules (Brandsch, 2013; Smith et al., 2013).

PepT1 and PepT2 are members of the more widely distributed proton-dependent oligopeptide transporter, or POT, family (TC 2.A.17), which are evolutionarily well conserved from bacteria to man (Daniel et al., 2006). Structurally the POT family belongs to the major facilitator superfamily (MFS), with each member containing 12 transmembrane (TM)-spanning α helices arranged into two TM bundles of six that fold to resemble a V-shaped protein that resides within the inner membrane of bacteria and plasma membrane of eukaryotes (Figure 1) (Covitz et al., 1998; Fei et al., 1994; Yan, 2013). The MFS fold can be further subdivided; with each six-helix bundle being constructed from the inversion of two three-helix repeats (Radestock and Forrest, 2011). We recently proposed a structural framework for understanding the transport mechanism within the POT family based on the ability of the triple-helix repeats to work synergistically to alternate the central binding site to either side of the membrane (Fowler et al., 2015). Recent bioinformatics analyses, including sequence-based structure alignments supported by experimental structure validation, further strengthen the importance of the triple-helix repeats. These analyses show that functionally equivalent positions within the different MFS transporters crystallized to date superimpose in three dimensions. This observation has led to the suggestion that evolution within the MFS may have arisen through intragenic duplication and shuffling of these repeats (Madej et al., 2013; Madej and Kaback, 2013).

Crystal structures of bacterial POT family members have revealed a central peptide-binding site that is highly conserved with the mammalian homologs (Doki et al., 2013; Guettou

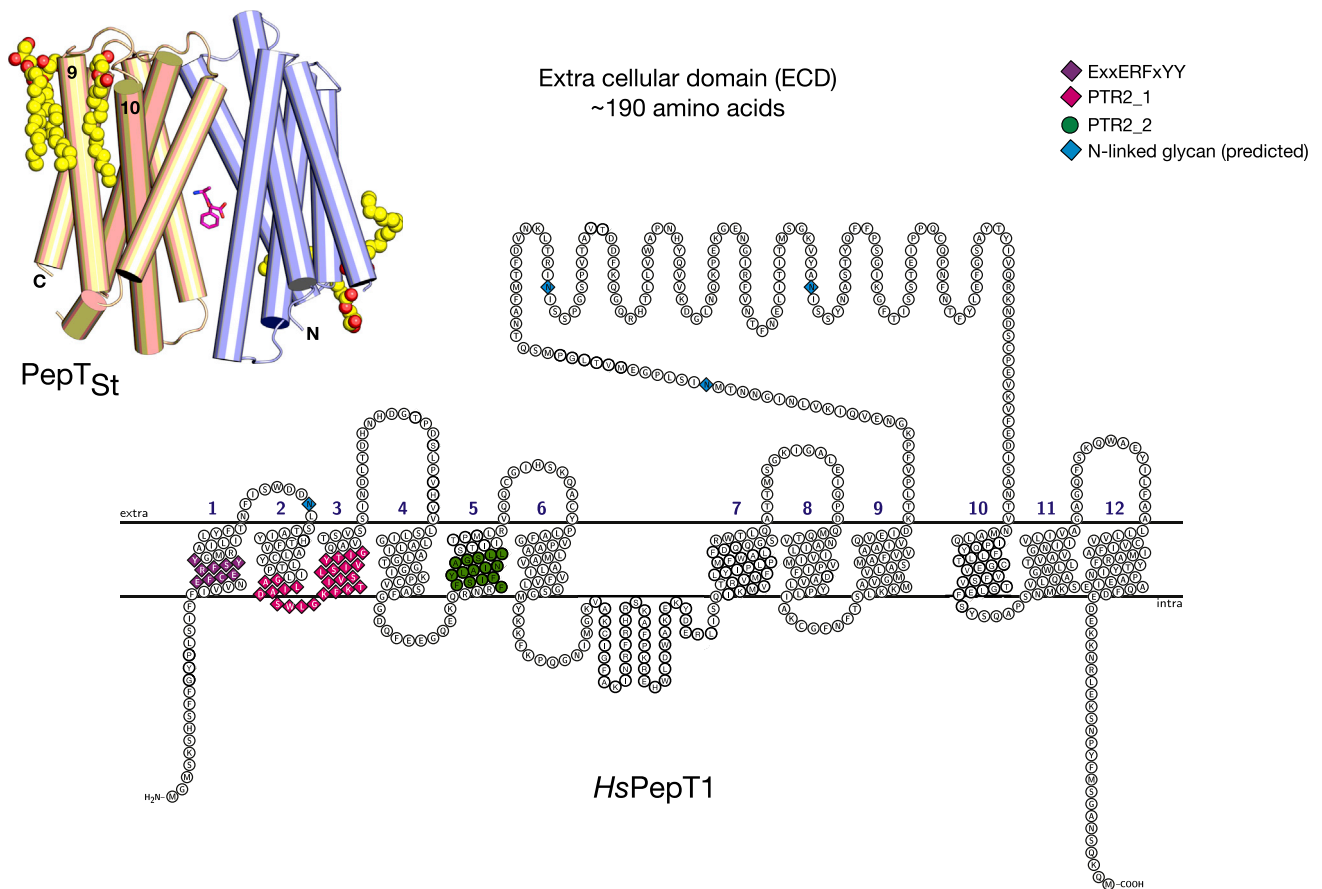


Figure 1. Topology of Mammalian Peptide Transporters

Topology diagram of the human plasma membrane peptide transporter PepT1. Conserved PTR2/POT family signature motifs are indicated along with predicted N-linked glycosylation sites, three of which are in the extracellular domain. Inset: Crystal structure of the bacterial homolog PepT_{St} (PDB: 4D2C). The N- (light blue) and C-terminal (wheat) domains are shown as cylinders, with the bound peptide indicating the location of the central peptide-binding site conserved between mammalian and bacterial proteins.

et al., 2014; Solcan et al., 2012). Both in vivo and in vitro assays have demonstrated that while a wide range of peptide substrates are transported by this family, there is conserved substrate specificity, with both bacterial and the mammalian proteins transporting hydrophobic peptides with approximate micromolar affinity and basic peptides with approximate millimolar affinity (Newstead, 2015). Between PepT1 and PepT2 there also exists a difference in overall substrate affinity, with PepT1 having a lower affinity for peptides and PepT2 a higher affinity (Smith et al., 2013). Recent crystal structures of peptide-bound complexes with a bacterial homolog of PepT1 have also suggested that peptides containing extended side chains, such as arginine and lysine, might adopt a less optimal position within the central peptide-binding site that could explain their lower affinity through less favorable interactions (Lyons et al., 2014).

Although the overall sequence identity between the mammalian and bacterial transporters is well conserved within their respective TM domains, epitope tagging analysis, supported by recent structure-based sequence alignments, reveal that in the mammalian PepT1 and PepT2 proteins there exists a significant portion of the protein that is positioned on the outside of the cell (Covitz et al., 1998; Newstead, 2015) (Figure 1). Intriguingly,

these domains are completely absent not only in the bacterial members of the POT family but also in the plant and fungal homologs (Parker and Newstead, 2014; Sun et al., 2014) (Figure S1). The functional role of this extracellular domain (ECD) is unknown; however, its presence would suggest the requirement for additional functionality to assist peptide uptake in mammals. Many eukaryotic channels and transporters have evolved to incorporate additional structural domains that extend, constrain, or regulate their function (Barabote et al., 2006). For example, eukaryotic CLC proteins contain intracellular CBS (cystathionine β -synthase) domains that regulate activity in response to nucleotides (Markovic and Dutzler, 2007; Meyer et al., 2007; Zifarelli and Pusch, 2009), whereas the voltage-sensing domains of potassium channels regulate channel opening following membrane depolarization (Pongs and Schwarz, 2010). To date, however, no equivalent domains have been described in detail for any member of the MFS, which forms the largest and most diverse family of secondary active transporters in biology (Reddy et al., 2012).

Here, we reveal that a previously annotated extracellular “loop” in early topology models of the human PepT1 and PepT2 transporters in fact consists of two immunoglobulin-like domains connected in tandem. In vitro binding assays

Table 1. Data Collection and Refinement Statistics for *MmPepT1*^{ECD} and *RnPepT2*^{ECD}

	<i>MmPepT1</i> ^{ECD}	<i>MmPepT1</i> ^{ECD} -Hg ^a	<i>RnPepT2</i> ^{ECD} -Se ^a	<i>RnPepT2</i> ^{ECD}
Space group	P2 ₁ 2 ₁ 2 ₁	P2 ₁ 2 ₁ 2 ₁	P3 ₂ 21	P4 ₁ 2 ₁ 2 ₁
Cell dimensions				
<i>a</i> , <i>b</i> , <i>c</i> (Å)	53.48, 70.33, 111.22	53.55, 70.37, 111.16	95.75, 95.75, 165.93	43.1, 43.1, 220.1
α , β , γ (°)	90, 90, 90	90, 90, 90	90, 90, 120	90, 90, 90
Wavelength (Å)	0.968	1.006	0.979	0.976
Resolution (Å)	43–2.10 (2.19–2.10)	70–2.85 (3.05–2.85)	58–2.81 (2.96–2.81)	43–2.06 (2.12–2.06)
<i>R</i> _{merge}	5.0 (79.8)	17.2 (75.6)	15.4 (109)	6.6 (67.1)
Mn/ <i>I</i>	16.4 (2.7)	15.1 (4.1)	12.7 (2.3)	11.5 (2.3)
CC _{1/2} ^b	99.9 (48.0)	99.7 (91.0)	99.9 (69.7)	99.8 (63.9)
Completeness (%)	99.5 (99.0)	99.4 (99.7)	99.9 (99.9)	99.3 (99.5)
Redundancy	4.8 (4.8)	14.0 (14.5)	9.9 (10)	4.1 (4.3)
<i>R</i> _{cullis} (%)		69.2	45.1	
Phasing power ^c		1.492	2.468	
Resolution (Å)	43.6–2.10		58.6–2.81	40.1–2.06
No. of reflections	24, 975		22, 048	13, 635
<i>R</i> _{work} / <i>R</i> _{free}	19.7/23.8		19.7/24.5	19.9/24.0
Ramachandran favored	96.6		92.5	96.3
Ramachandran outliers	0.53		0.17	0
Rmsd				
Bond lengths (Å)	0.010		0.010	0.010
Bond angles (°)	1.18		1.31	1.25

^aFor details on derivatization, see [Experimental Procedures](#).

^bMn(*I*) half-set correlation as reported by Aimless.

^cPhasing power = $\text{rms}(|F_H|/((F_H + F_P) - (F_{PH})))$.

demonstrate that the ECDs interact with the intestinal protease trypsin, potentially answering an interesting observation made in the late 1960s of a specific and tight interaction of trypsin with human intestinal mucosa ([Goldberg et al., 1968, 1969a, 1969b](#)). More surprising was the observation that these domains can be removed with no appreciable loss of transport function. These results provide the first structural and biochemical insights into the mammalian SLC15 family, and demonstrate modularity within the MFS that could have important implications for interpreting the function of these proteins in eukaryotic cells.

RESULTS

Crystal Structures of the Extracellular Domain of PepT1 and PepT2

Using the crystal structures from the bacterial POT family proteins PepT_{So} ([Newstead et al., 2011](#)) and PepT_{St} ([Solcan et al., 2012](#)) that share 31% and 21% identity, respectively, with their mammalian homologs, we identified the probable location of the ECD in the PepT1 transporters ([Figure S1](#)). We subsequently identified the ECD from *Mus musculus*, consisting of residues 391–580, as being stable and amenable to structural and biophysical analysis ([Figure S2](#)). This domain was crystallized and its structure determined using the single anomalous dispersion (SAD) method of phasing using mercury-derivatized protein. The structure was refined to a resolution of 2.1 Å with final *R*_{work} and *R*_{free} of 19.7% and 23.8%, respectively ([Table 1](#)). Following extensive screening, crystals from *Rattus norvegicus* PepT2,

residues 410–601, were also obtained ([Figure S2](#)). The phases were calculated from seleno-L-methionine incorporated protein using the SAD method in space group P3₂21 ([Table 1](#)). A higher-resolution structure in space group P4₁2₁2 was obtained using the P3₂21 crystals as seeds with a single monomer in the asymmetric unit. The final structure refined to a resolution of 2.06 Å with final *R*_{work} and *R*_{free} of 19.9% and 24.0%, respectively.

The crystallographic asymmetric unit of the PepT1^{ECD} crystal contained two monomers that formed a head-to-tail dimer, related by a two-fold non-crystallographic symmetry axis ([Figure 2A](#)), whereas the PepT2^{ECD} construct was crystallized in a monomeric state ([Figure 2B](#)). The overall structure of both ECDs consists of two compact β -sandwich immunoglobulin-like folds each comprising two four-stranded β sheets. The β sandwiches are composed of strands in the order 4-1-7-8 and 3-2-5-6, with a short connecting loop between the end of strand β -8 on lobe one and β -9 on lobe two. Despite having only 22% sequence identity the two structures adopt the same overall structure, superimposing with a root-mean-square deviation (rmsd) of 1.83 Å. Analytical ultracentrifugation on the purified ECDs show that both PepT1^{ECD} and PepT2^{ECD} are monomers in solution ([Figure 2C](#)). This led us to suspect that the head-to-tail dimer observed in the asymmetric unit was the result of crystallization and that the physiological state of the ECD in PepT1 is monomeric, as shown for the PepT2^{ECD}. The bilobal architecture of the ECDs suggested that the two immunoglobulin-like domains have the potential to be highly dynamic, which could represent an important structural and functional difference between PepT1 and pepT2.

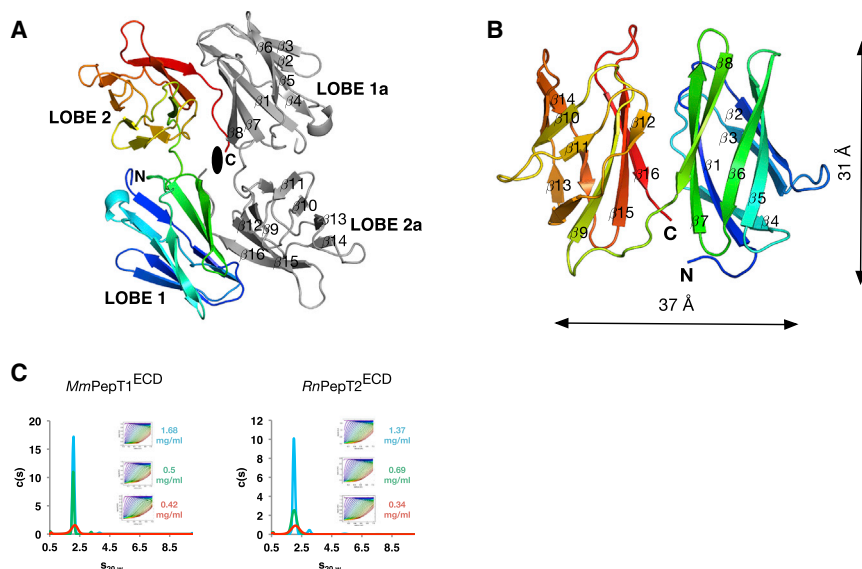


Figure 2. Crystal Structure of the Extracellular Domain from PepT1 and PepT2

(A) The asymmetric unit of *MmPepT1*^{ECD} containing two monomers related by a two-fold non-crystallographic symmetry axis (black oval). One monomer is rainbow colored from the N terminus to the C terminus; the second is shown in gray with the secondary structure labeled from β1 to β16.

(B) Structure of the *RnPepT2*^{ECD} colored from the N (blue) to the C terminus (red) and with the secondary structure components labeled as for (A).

(C) The $s^0_{20,w}$ values of *MmPepT1*^{ECD} and *RnPepT2*^{ECD} from the AUC analysis are 2.16 and 2.22, respectively, consistent with both proteins migrating as a 20-kDa monomer in solution. Inset: the Lamm equation fit profiles for *MmPepT1*^{ECD} and *RnPepT2*^{ECD}.

Salt Bridge Interactions Stabilize the Interface between the Immunoglobulin-like Domains in PepT1

The crystal structures revealed that in the *PepT1*^{ECD} there exist two conserved salt bridge interactions stabilizing the interface between lobe 1 and lobe 2, mediated by Asp574-Lys398 and Asp476-Arg490, whereas in *PepT2*^{ECD} only one equivalent salt bridge interaction is present, between Asp505 and Arg538 (Figures 3A and 3B). To investigate the nature of these interactions, we inserted a 3C protease site into the linker connecting lobe 1 and lobe 2 in *PepT1*^{ECD} (Figure 3C). Following cleavage by the protease 3C of the purified protein, we observed that the two lobes of *PepT1*^{ECD} remain associated down a size-exclusion chromatography column. Repeating this experiment with the Asp574Ala variant, however, resulted in the two lobes migrating independently, thus confirming the importance of the salt bridge in holding the two immunoglobulin-like domains together in the compact arrangement shown in Figure 3A.

The same experiment, however, could not be conducted with *PepT2*^{ECD} as the lobes proved too unstable after cleavage with 3C protease. Therefore, to understand the behavior of *PepT2*^{ECD} in solution we used small-angle X-ray scattering (SAXS), a method that allows the overall shape of a macromolecule to be modeled at low resolution. Guinier analysis of the scattering data in PRIMUS (Petoukhov et al., 2007) shows that *PepT2*^{ECD} has a larger radius of gyration (R_g) compared with *PepT1*^{ECD}, 23.1 versus 18.4 Å (Table 2), which suggests an increase in particle size. A shift to larger scattering distances can also be seen in the $P(r)$ distribution and dimensionless V_c Kratky plot (Rambo and Tainer, 2011) (Figures S3A and S3B), indicating a more elongated structure for *PepT2*^{ECD}. Consistent with this analysis, 3D envelopes of the ECD generated using DAMMIF (Franke and Svergun, 2009) show that *PepT1*^{ECD} forms a compact shape ~48 Å in length whereas *PepT2*^{ECD} is more elongated, approximately 61 Å in length (Figures 3D and S3C). The larger envelope of *PepT2*^{ECD} indicates that the two immunoglobulin-like domains are structurally more dynamic than the *PepT1*^{ECD}, which is consistent with the loss of the second salt bridge and also the location of Asp505 on the unstructured loop connecting lobes 1 and 2.

PepT1 and PepT2 Contain a Functionally Independent Extracellular Domain

To date there have been no studies on the role of the ECDs in either of the mammalian peptide transporters. This is largely due to the ambiguity in identifying where this domain was located with respect to the TM helices. The crystal structure of the ECDs from both *PepT1* and *PepT2* now allow for structure-based homology models of the full-length human transporters to be built (Figure 4A). Molecular dynamics of the models in a palmitoylcholine phosphatidylglycerol membrane bilayer suggest that the domains are likely to adopt a vertical orientation sitting to one side of the transporter (Figure S4).

PepT1 and *PepT2* are the first MFS transporters to date that have been shown to contain a folded structural domain inserted within the “core” MFS fold (Yan, 2013). This raises the important question of whether the ECDs play any role in transport or determine functional differences between *PepT1* and *PepT2*. To investigate this question, we used the homology models to generate a number of different combinations of chimeric and mutant human *PepT1* and *PepT2* transporters that had their ECD domains removed (*PepT1*^{ΔECD}, *PepT2*^{ΔECD}) or swapped (*PepT1*^{ECD2}, *PepT2*^{ECD1}). The resulting constructs were expressed in *Xenopus* oocytes and their relative levels of expression examined (Figure S5). We observed that *PepT1* was very sensitive to modification at or within the ECD, with only the wild-type (WT) showing stable levels of expression. In contrast, we observed high levels of expression for all of the *PepT2* constructs, allowing us to investigate the role of this ECD. Peptide transporters are electrogenic carriers able to concentrate peptides inside the cell using the energy stored in the $\Delta\mu\text{H}^+$ (Fei et al., 1994). We therefore examined their transport properties using two-electrode voltage-clamp (TEVC) recordings in the *Xenopus laevis* oocytes. This technique measures the inward movement of H^+ as a function of external peptide concentration. K_M values for transport of the non-hydrolyzable peptide glycyl-sarcosine (Gly-Sar) were determined for both WT *PepT1* and *PepT2*. The calculated K_M values confirm the previously noted difference in peptide transport of 0.78 ± 0.09 mM and

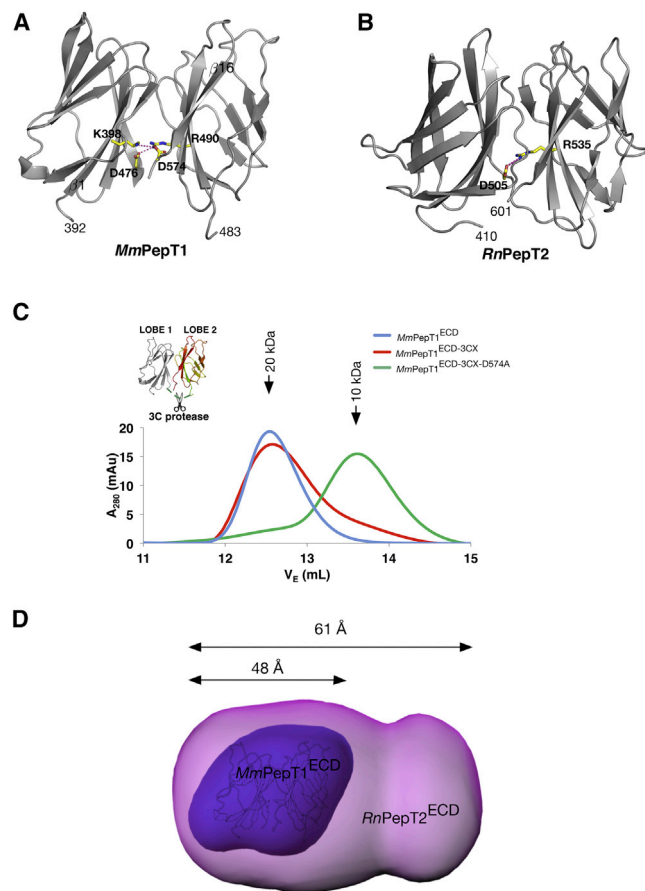


Figure 3. Salt Bridges Stabilize the Interface between the Two Immunoglobulin-like Domains in PepT1^{ECD} and PepT2^{ECD}

(A) Structure of PepT1^{ECD} illustrating the two salt bridges, K398 and D574 and R490 and D476, that form an interaction between the lobes.

(B) Comparative view in RnPepT2^{ECD}, where a single salt bridge is observed between Asp505 and Arg518.

(C) Size-exclusion chromatography traces from the MmPepT1^{ECD}-3CX experiment. The cleaved MmPepT1^{ECD}-3CX constructs elute at the same volume as wild-type, showing that the lobes still interact in solution even after the two lobes are separated. The cleaved MmPepT1^{ECD}-3CX-D574A construct, however, elutes in a larger volume consistent with disruption of the interaction.

(D) DAMMIN envelopes of MmPepT1^{ECD} (dark purple) and RnPepT2^{ECD} (light purple) calculated from the SAXS data, which show lengths of 48 and 61 Å, respectively, and illustrate the more dynamic behavior of PepT2^{ECD}. For scale, a black and white outline of A is overlaid on the MmPepT1^{ECD} envelope.

0.32 ± 0.02 mM for PepT1 and PepT2, respectively (Figure 4B). However, swapping the ECD region from PepT1 to PepT2 (PepT2^{ECD1}) or even deleting it entirely from PepT2 (PepT2^{ΔECD}) resulted in no detectable change in the K_M for uptake of the Gly-Sar peptide, which remained ~ 0.3 mM. Additionally, removal of the salt bridge that stabilizes the interface between lobes 1 and 2 of PepT1 (PepT1^{D573A}) made no observable difference to the K_M of Gly-Sar transport (Figure 4C). We also tested whether these constructs interacted differently with the antibiotic cefaclor, a known substrate of PepT1 and PepT2 (Bretschneider et al., 1999; Luckner and Brandsch, 2005). We found that the K_i of drug uptake in *cis*-inhibition experiments was

also unchanged for all the PepT2 constructs, with a K_i of ~ 0.22 mM, compared with ~ 0.9 mM for WT PepT1 (Figure 4D). This similarity was also shown with a different non-hydrolyzable peptide, lysyl-lysine. These results indicate that the ECD is a structurally independent unit that has no obvious role in substrate specificity or intrinsic peptide transport function, in PepT2 at least. The immunoglobulin-like structure of the ECDs, however, strongly suggested a possible role in binding an external component that might be present in the intestinal lumen. Therefore, to further investigate the function of the ECDs we undertook a series of binding studies to investigate this possibility.

The Extracellular Domain Interacts with the Intestinal Protease Trypsin

Given the expression of both PepT1 and, to a lesser extent, PepT2 in the intestinal brush border membrane, we thought it possible that the interaction partners may be intestinal hormones, including cholecystokinin (CCK8) and thyroid hormone, which has been reported to decrease the surface expression of PepT1 in Caco-2 cells (Ashida et al., 2002). Another possibility was an interaction with the intestinal proteases that create the di- and tri-peptides that are subsequently recognized by PepT1 and PepT2 for transport into the cell. We therefore screened a panel of potential interaction candidates using surface plasmon resonance (SPR). From this panel of potential ligands we observed binding only for the intestinal protease trypsin with both mouse PepT1^{ECD} (K_D 80 ± 0.8 μ M) and rat PepT2^{ECD} (K_D 165 ± 0.5 μ M) (Figures 5A and 5B). However, we observed no significant interaction between PepT1^{ECD} and chymotrypsin or pepsin. It is possible that one function of the ECDs could be to interact with and accumulate peptides in the vicinity of the transporter, although this would be unlikely given the TEVC data. However, to test this we used microscale thermophoresis (MST), which can measure the interaction with small ligands with transporters in solution (Parker and Newstead, 2014). We did not observe an interaction with the peptide Gly-Sar, but this technique did confirm our previous SPR data showing a specific interaction with trypsin (Figure 5A). The K_D calculated using this technique, however, was tighter than that observed using SPR, being 8 ± 0.7 μ M for PepT1^{ECD} and 6 ± 0.5 μ M for PepT2^{ECD}. We interpret this discrepancy with the SPR values as being due to the freedom of interaction of a measurement in solution versus immobilization on a chip surface. To examine the nature of the interaction between trypsin and the ECDs, we repeated the MST binding assay with an increased salt concentration of 0.5 M. This resulted in abolition of the interaction, suggesting that the interaction between trypsin and the ECD is mediated through an electrostatic interface.

Trypsin Recognition Is Localized to a Conserved Di-aspartate Motif on the Extracellular Domain

To identify possible binding sites on the PepT1^{ECD} and PepT2^{ECD} molecules, we mapped the sequence conservation for six different mammalian homologs (Figure S1) onto the crystal structures. We identified two highly conserved charged residues, Asp550 and Glu573 in PepT1^{ECD} and Asp576 and Glu599 in PepT2^{ECD}, located on one face of the ECD structure (Figures 5D and 5E). Both of these residues are found in two conserved sequence motifs at the start of strand β 15 and at the end of

Table 2. SAXS Data Statistics for *MmPepT1*^{ECD} and *RnPepT2*^{ECD}

	R_g (Å)	$I(0)/\text{Conc}$ (mg ml ⁻¹)	V_p (nm ³)	D_{max} (Å)	V_c (Å ²)	Mass (kDa)
<i>MmPepT1</i> ^{ECD}	18.4 ± 1.7	8.6 ± 0.0	33.4	64.3	197	17.1
<i>RnPepT2</i> ^{ECD}	23.0 ± 2.8	14.9 ± 0.0	45.4	73.1	238	20.1

The R_g , $I(0)/\text{Conc}$, V_p , and D_{max} were calculated in PRIMUS. The V_c and particle mass were calculated in ScÅtter, and show that *RnPepT2*^{ECD} has a larger radius of gyration (R_g) in solution, indicating a more flexible arrangement for the two lobe domains.

strand $\beta 16$ in lobe 2 of the mammalian proteins (Figure S6). Removal of these charges abolished the interaction with trypsin (Figures 5D and 5E, insets), further supporting the hypothesis that the function of the ECD is to recruit trypsin to the site of the peptide transport on the plasma membrane. The other face of the ECD, however, does not contain any conserved charged residues, suggesting that this face is unlikely to be important in an electrostatic interaction. Indeed, mutation of several surface residues in mouse *PepT1*^{ECD} resulted in no substantial impact on the K_D of trypsin binding compared with WT protein (Figure S7). The involvement of only two conserved residues in the trypsin interaction may also explain the fast binding kinetics observed in the SPR sensorgrams (Figures 5A and 5B, insets), which suggest that the interaction with trypsin is highly dynamic and likely transient, rather than forming a long-lived complex in the intestinal lumen.

DISCUSSION

The Modular Architecture of *PepT1* and *PepT2*

Mammalian peptide transport is a physiologically important route to both assimilate dietary nitrogen in the form of small di- and tri-peptides from ingested protein and retain peptides in the body by selective reabsorption in the kidneys (Adibi, 1997b; Matthews, 1975; Matthews, 1991). Although originally identified in 1994, the 3D structures of *PepT1* and *PepT2* have remained elusive, and to date no crystal structures are available. However, recent crystal structures of several closely related bacterial homologs provide suitable templates to model the TM domain of the mammalian proteins (Newstead, 2015; Terada and Inui, 2012). Nevertheless, the identity of the ECD, originally identified from hydrophathy analysis and epitope insertion studies (Covitz et al., 1998), has remained elusive. Our functional and structural analysis shows that the ECD is a fully independent module that has been incorporated by the mammalian members of the POT family to function in protein-protein interactions on the outside of the cell. Additional structural domains are found in many families of membrane transporters (Barabote et al., 2006). However, the locations of the ECDs within the *PepT1* and *PepT2* structures are particularly intriguing, in that they are inserted *within* the canonical 12-TM helix MFS fold. This is highly unusual; most additional domains in transporters are appended to either the N- or C-terminal end of the polypeptide chain (Markovic and Dutzler, 2007; Meyer et al., 2007; Warmuth et al., 2009). To our knowledge, this study reports the first structure of an additional domain inserted within the core architecture of a transporter. Interestingly the insertion site within *PepT1* and *PepT2* is the connection between TM9 and TM10, which represents the junction between the two triple-helix repeats that make up the C-terminal bundle within the MFS fold (Radestock

and Forrest, 2011). We recently suggested that these repeats operate in a scissor-like motion that control access to the central peptide-binding site during transport (Fowler et al., 2015). The insertion of the two immunoglobulin-like domains of the ECD, with minimal impact on the ability of *PepT1* and *PepT2* to function as proton-coupled peptide symporters, would appear to support our hypothesis that the two repeats operate in a coordinated but structurally independent manner.

However unusual it may be to observe the ECD inserted within the canonical MFS fold, our finding that both the *PepT1*^{ECD} and *PepT2*^{ECD} interact with trypsin presents a logical role for these domains in mammalian peptide import. It is interesting to note that as far back as 1968 both trypsin and chymotrypsin were observed to interact with and bind to the mucosa of human small intestine (Goldberg et al., 1968, 1969a, 1969b). The assay conditions used here to investigate the binding between the ECD and trypsin closely resemble the pH and ionic strength found in the small intestine (~150 mM NaCl and pH ~6.5) (Fallingborg, 1999; Fordtran et al., 1968), suggesting that the K_D values reported are likely to be in the physiological range. Furthermore, the K_D values reported in this study (μM range) are also consistent with the estimated concentration of trypsin in the small intestine, which was reported to be ~7 μM (Goldberg et al., 1969a). Taken together, these observations support the presence of a physiological interaction between the ECD of *PepT1* and *PepT2* and trypsin in the human body. Our data show that a conserved di-acidic motif on both *PepT1*^{ECD} and *PepT2*^{ECD} presents the most likely interaction site with trypsin. However, the fast binding kinetics show that the interaction is highly dynamic and likely to be transient in nature. We have combined all of the information presented to generate a working hypothesis for how trypsin might interact with *PepT1* and *PepT2* at the plasma membrane (Figure 6). Our data place trypsin on the opposite side of the ECD to the peptide translocation pathway (Newstead, 2015). In this configuration the binding of trypsin would not obstruct subsequent peptide transport, as the protease would be on the opposite side of the transporter from the peptide-binding site.

Why would *PepT1* and *PepT2* have evolved to localize trypsin rather than other proteases, such as chymotrypsin? *PepT1* and *PepT2* play an important physiological role in absorbing small peptides arising from digestion of dietary proteins in the small intestine, as well as in reabsorbing filtered peptides generated from luminal peptidases in the kidney (Adibi, 1997a, 1997b). There is clearly an advantage in tethering a protease to the site of peptide uptake on the plasma membrane, in that the peptides will be locally concentrated at the site needed for their recognition and transport. The localization of trypsin, which recognizes and cleaves the peptide chain at arginine and lysine residues, would therefore increase the concentration of

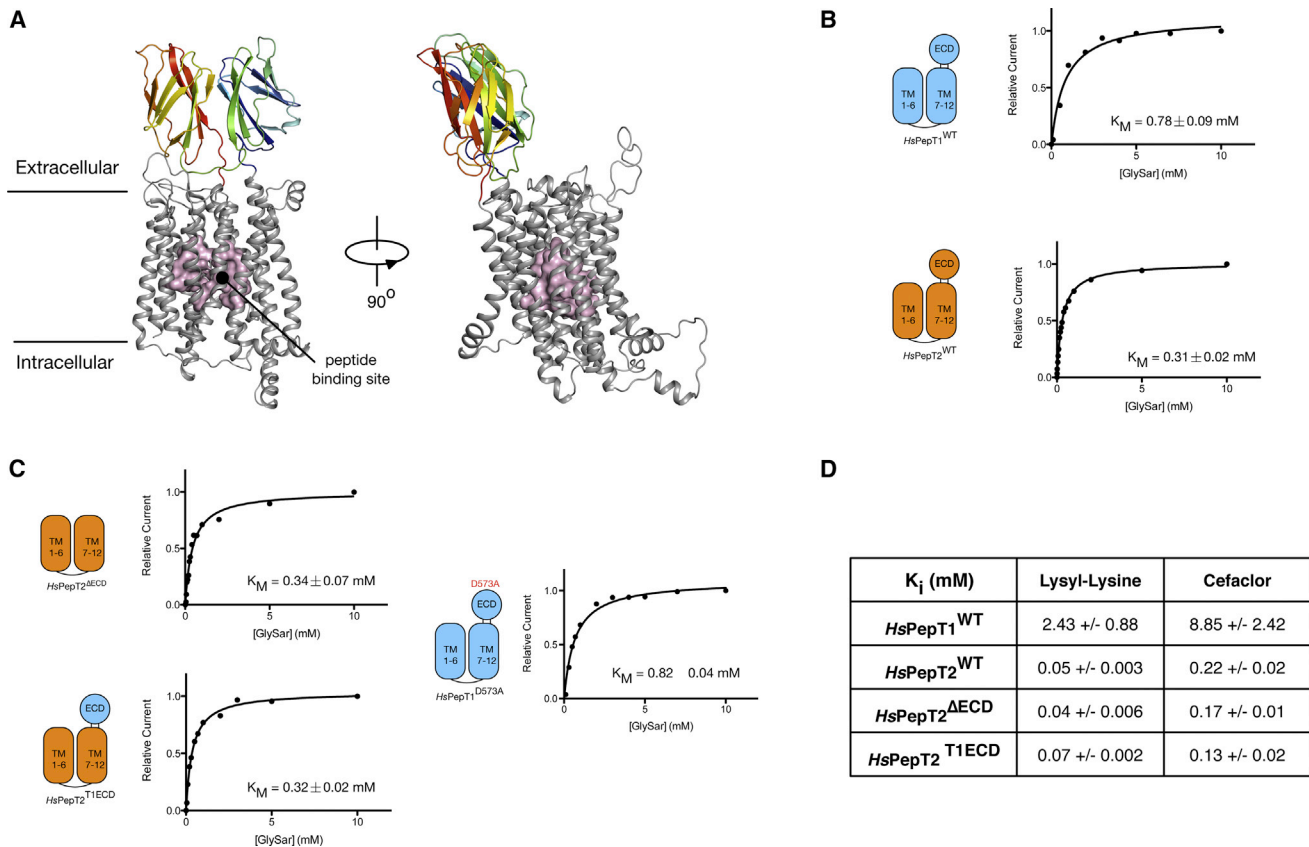


Figure 4. PepT1 and PepT2 are Modular Proteins with Functionally Distinct Domains

(A) Homology model of the human PepT1 transporter generated using the crystal structure of *Mm*PepT1^{ECD} (colored blue to red as in Figure 1B) and the recently determined bacterial homolog PepT_{So} representing the transmembrane portion of the transporter (shown in gray). The peptide-binding site is highlighted (magenta).

(B) Kinetic analysis of Gly-Sar uptake in human PepT1 and PepT2 using the TEVC method.

(C) Kinetic analysis of Gly-Sar uptake in the PepT2^{ΔECD}, PepT2^{T1ECD}, and PepT1^{D573A} constructs.

(D) K_i values for the different constructs for lysyl-lysine and cefaclor are shown, indicating no effect of removing the ECD on peptide or drug uptake in PepT2.

peptides containing these side chains on the outside of the cell directly above the peptide-binding site, and would be expected to improve the efficiency of their uptake through the transporter domain. Indeed, clinical studies of peptide transport in the human body have indicated that the transport of arginine-containing peptides is less efficient (Steinhardt and Adibi, 1986), consistent with our findings from the bacterial homolog of PepT_{So} (Solcan et al., 2012), suggesting that the localization of trypsin is an adaption to increase the concentration of peptides containing arginine and lysine, and therefore improve the transport of these peptides into the cell. We hasten to acknowledge, however, that our data do not unambiguously demonstrate a physiological requirement for trypsin in peptide transport and that our hypothesis will require further in vivo study for it to be supported or refuted.

To our knowledge, this study represents the first structural insight into MFS transporters that exist as multi-domain proteins. Interestingly, a similarly sized ECD is also observed in the SLC22 family of MFS transporters, again inserted between TM9 and TM10 (Kalliokoski and Niemi, 2009), suggesting that other eukaryotic MFS transporters have adopted similar mecha-

nisms to extend their functionality in the cell. The present study and homology models of the human PepT1 and PepT2 transporters therefore not only establish a framework for understanding mammalian peptide uptake, but also show how members of the MFS have evolved to incorporate additional structural domains that expand, augment, or constrain their function in eukaryotic cells.

EXPERIMENTAL PROCEDURES

Cloning, Expression, and Purification of the Extracellular Domains from PepT1 and PepT2

PepT1^{ECD} from *M. musculus* (residues 391–580, UniProtKB: Q9JIP7) was cloned into an N-terminal maltose-binding protein (MBP) fusion expression vector, pOPINM (Berrow et al., 2007). PepT2^{ECD} from *R. norvegicus* (residues 410–601, UniProtKB: Q63424) was cloned into a different MBP fusion expression vector, pLou3, a derivative of pMAL-c5 vector with a tobacco etch virus protease site, to remove the MBP and an N-terminal histidine tag. Recombinant protein was produced in *Escherichia coli* strain BL21-DE3. Isopropyl β-D-1-thiogalactopyranoside was used to induce expression of the recombinant genes; cells were harvested following overnight induction at 25°C. WT and mutant proteins were purified to homogeneity using standard protocols for Ni-immobilized metal affinity chromatography- and amylose-based

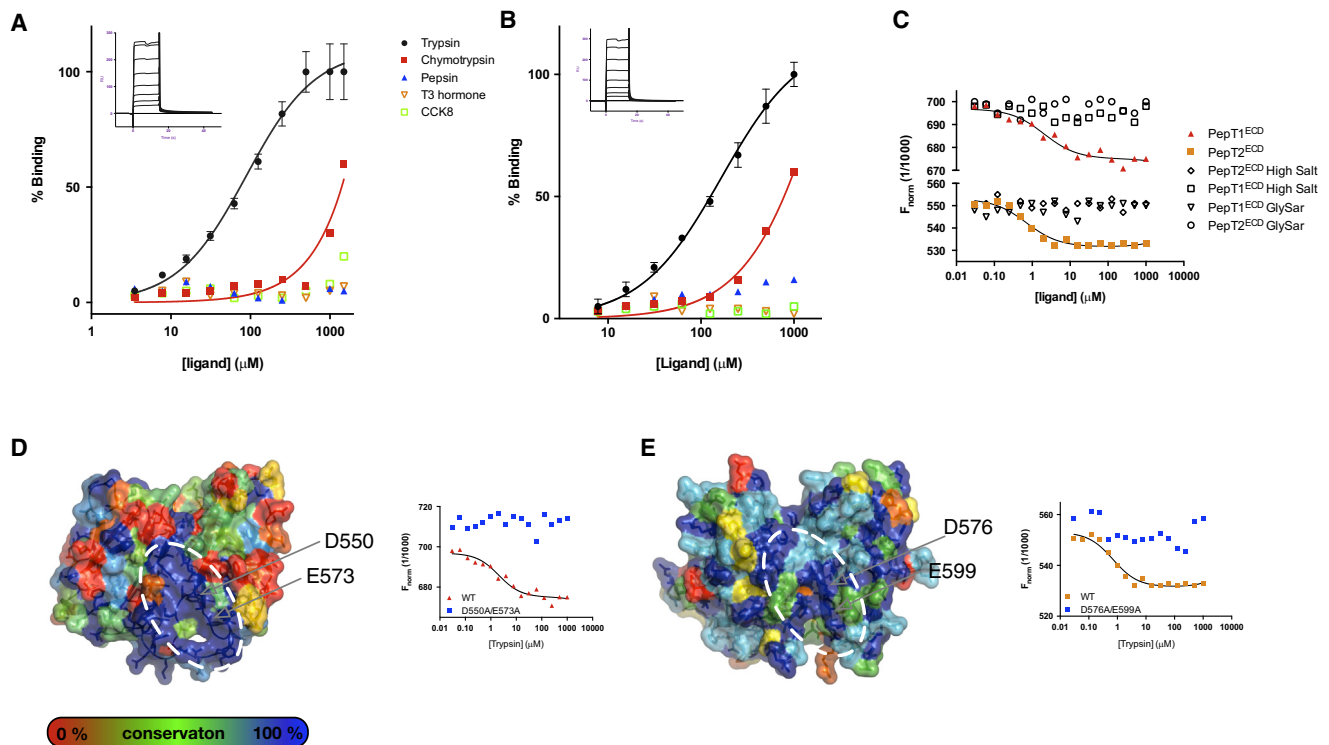


Figure 5. Trypsin Interacts with a Di-acidic Motif on the Extracellular Domain of PepT1 and PepT2

(A) SPR analysis of the *MmPepT1*^{ECD} interaction with trypsin. Inset: SPR sensorgram used to determine the binding constant. RU, response units. Error bars show the SEM (n = 3).

(B) The binding experiment in (A) was repeated with the *RnPepT2*^{ECD} protein.

(C) MST binding analysis reveals no interaction with the Gly-Sar peptide and abolition of trypsin interaction in the presence of high salt.

(D and E) Surface representation of (D) *MmPepT1*^{ECD} and (E) *RnPepT2*^{ECD} with the sequence conservation from cow, dog, chicken, human, mouse, and rat species mapped from blue to red. A highly conserved patch (indicated by the white dashed ellipse) was identified. Insets: MST binding analysis reveals an important role for D550 and E573 in *MmPepT1*^{ECD}, and D576 and E599 in *RnPepT2*^{ECD}, in mediating the electrostatic interaction with trypsin.

purification of the fusion proteins. Seleno-L-methionine-incorporated *PepT2*^{ECD} was produced using an auto-inducing medium, PASM-5052 (Studier, 2005).

Crystallization and Structure Determination

PepT1^{ECD} was crystallized in 20% polyethylene glycol (PEG) 6000, 0.1 M 2-(N-morpholino)ethanesulfonic acid (MES) (pH 6.0), 0.2 M ammonium chloride, at 10 mg ml⁻¹ and 4°C using sitting drop-vapor diffusion plates. All crystals were cryo-protected in mother liquor with 25% glycerol and cryo-cooled in liquid nitrogen for data collection. Diffraction data were collected on beamlines I24, I03, and I04 at Diamond Light Source, Harwell, UK. Initial data processing was carried out using the Xia2 pipeline (Winter et al., 2013) to XDS (Kabsch, 2010). Initial phases for *PepT1*^{ECD} were calculated using SAD with a single mercury-derivatized crystal. The space group was determined to be P2₁2₁2₁. Three mercury sites were initially located using SHELXC/D (Sheldrick, 2010), with their positions further refined and initial phases calculated using SHARP with solvent flattening in SOLOMON (Abrahams and Leslie, 1996). The complete primary structure was assigned in Coot and refined using BUSTER (Blanc et al., 2004) to a final resolution of 2.10 Å and $R_{\text{work}}/R_{\text{free}}$ of 19.7/23.8 (Table 1).

RnPepT2^{ECD} was crystallized in 0.2 M (NH₄)₃ citrate (pH 5.8) and 21% PEG 3350, 10 mg ml⁻¹ at 20°C. Initial phases were calculated using Se-SAD data using autoSOL from the PHENIX crystallography suite (Adams et al., 2010). A starting model was built using PHENIX Auto-Build showing three molecules in the asymmetric unit in space group P3₂21. The complete structure of the three molecules was built in Coot based on this initial map. Refinement of the structure was carried out in BUSTER to a final resolution of 2.81 Å with

an $R_{\text{work}}/R_{\text{free}}$ of 19.7/24.5. To improve the resolution of the *PepT2*^{ECD} structure, we re-screened the original sparse matrix crystal screens using a seed stock generated from the P3₂21 crystals. Crystals grew in 0.2 M CsCl₂ and 15% PEG 3350. A dataset was collected on beamline I03 at Diamond Light Source and processed using XDS to a resolution of 2.06 Å in a new space group, P4₁2₁2. The phases for this new structure were calculated by molecular replacement of the monomeric *PepT2*^{ECD} structure in Phaser (McCoy et al., 2007). The model was refined in BUSTER to a final $R_{\text{work}}/R_{\text{free}}$ of 19.9/24.0.

Homology Models of Human PepT1 and PepT2

Homology models of the human *PepT1* (UniProt: P46059) and *PepT2* (UniProt: Q16348) transporters were built consisting of the crystal structure of a bacterial peptide transporter, *PepT*_{So} (Newstead et al., 2011) (PDB: 2XUT) as the template for the transmembrane region, and the crystal structures of the ECD regions inserted within the extracellular loop connecting TMH9 and TMH10. The two extra helices, HA and HB (residues 226–285), which are only present in a subset of the prokaryotic POT family transporters, were removed prior to the sequence alignment. Initial alignment was generated using Probcons (Do et al., 2005), and this was manually refined in Jalview (Waterhouse et al., 2009) to correctly align the functionally important residues identified previously through functional studies on the eukaryotic and mammalian homologs.

Expression and Functional Characterization of Human PepT1 and PepT2 in *Xenopus* Oocytes

Open reading frames for the human *PepT1* and *PepT2* proteins were cloned into the pBF *Xenopus* oocyte expression vector, which adds the 5' and 3'

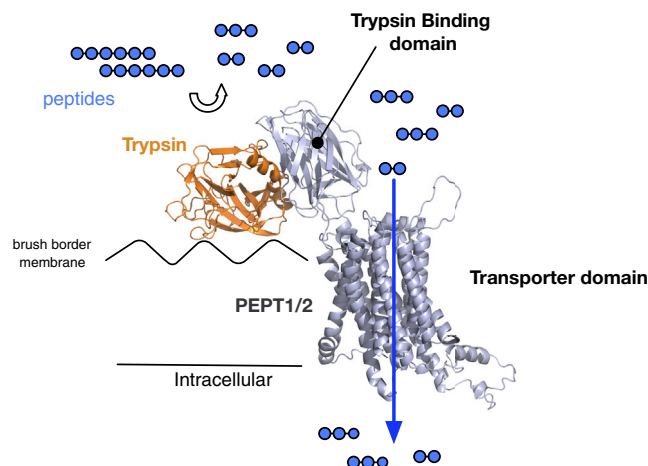


Figure 6. A Model for the Interaction between Trypsin and the Mammalian Peptide Transporters

During protein digestion in the small intestine, trypsin transiently docks onto the conserved di-acidic motif on the trypsin-binding domain, localizing the protease to the main site of peptide import on the brush border membrane. Localization would create an increase in the local concentration of arginine- and lysine-containing peptides (shown here as blue circles), which would be expected to increase the efficiency of their uptake into the cell.

UTRs of the *Xenopus* β -globin gene. ECD deletions and chimeras were generated using extension overlap PCR. A C-terminal FLAG tag epitope was engineered at the C terminus of these genes to aid detection and quantitation of expression by western blot. mRNA for injection was prepared by in vitro transcription using the AmpliCap SP6 High Yield Message Maker kit (Cellscript). *Xenopus* oocytes were injected with 50 ng of mRNA and incubated at 17°C for 3–4 days before recording. For TEVC recordings, microelectrodes were filled with 3 M KCl and had tip resistances of ~ 5 M Ω . Oocytes were voltage-clamped at -50 mV, and a voltage step protocol consisting of 300-ms long pulses from -160 to $+60$ mV in 10-mV increments was used to test oocyte stability and record currents. ND96 solution was used as the bath solution (95.4 mM NaCl, 2 mM KCl, 1.8 mM CaCl₂, 5 mM HEPES [pH 7.5] with NaOH). Test solutions consisted Gly-Sar at desired concentrations in ND96 solution. Transport-associated currents were estimated by subtracting currents recorded on ND96 solution only from those in the presence of substrate for each experiment. The currents at each Gly-Sar concentration were normalized to the maximal current (taken as current observed with 10 mM Gly-Sar) for each oocyte and the current at -120 mV at each Gly-Sar concentration used in non-linear regression analysis. Data were analyzed using Clampfit 10.4.0.36 (Axon Instruments) and non-linear regression analysis was performed on data from single oocytes using GraphPad Prism (version 6.04 for Mac, GraphPad Software). Acquired data were fitted to the Michaelis-Menten equation $I = (I_{\max}[\text{Gly-Sar}]) / (K_M + [\text{Gly-Sar}])$, where current was used in the place of velocity to calculate an apparent K_M for data from each oocyte. Average K_M was then taken as the mean of the K_M values from individual oocytes expressing the specific construct and displayed as mean \pm SEM. Background currents were measured in uninjected oocytes 4 days after incubation. Inhibition experiments with the β -lactam antibiotic cefaclor and the dipeptide lysyl-lysine determined *cis*-inhibition of [³H]-D-Phe-L-Gln uptake by increasing concentrations of cefaclor or lysyl-lysine, using the method of Pieri et al. (2009). 10 ng of mRNA was injected into each oocyte.

Small-Angle X-Ray Scattering

SAXS data were collected at the P12 beamline (PETRA III, Hamburg) at a wavelength of 1.24 Å. Scattered images were collected on a PILATUS 2M detector (Dectris) at 297 K. Twenty images were taken while the sample was continually passed through a quartz capillary. Samples and buffers were prepared using the same protocol used for the area under the curve (AUC) analysis. A concentration series was collected for each sample from 5 to 0.15 mg ml⁻¹. Raw

images were individually examined using PRIMUS (Konarev et al., 2003), and images that showed radiation damage were excluded from the final averaged curves. No concentration-dependent scattering was observed in for PepT1^{ECD}. Merged curves were created for PepT2^{ECD}, as an increase in scattering was observed as a function of concentration in the low scattering angles. To interpret the scattering data, 20 3D models of each ECD were created using DAMMIF (Franke and Svergun, 2009), which were then aligned, clustered, and averaged using DAMAVER (Volkov and Svergun, 2003). DAMMIN (Svergun, 1999) was then used to compare the averaged model against the raw data to ensure a good fit as evaluated using reduced χ^2 values. Envelopes of the models were generated using Sculptor (Birmanns et al., 2011).

Surface Plasmon Resonance

SPR experiments were carried out using a BIAcore T200 instrument (GE Healthcare). Experiments were performed at 20°C in 25 mM MES (pH 6.5), 100 mM NaCl, 10 mM CaCl₂, 0.005% Tween 20, 2 mg ml⁻¹ dextran, and 1 mg ml⁻¹ salmon sperm DNA (Sigma-Aldrich). Either PepT1^{ECD} or PepT2^{ECD} were immobilized on a CM5 chip (GE Healthcare) by amine coupling (GE Healthcare kit) to a total of 1,000 response units. A concentration series of ligand (1000, 500, 250, 125, 62.5, 31.2, 15.6, and 7.81 μ M) was injected over the ECD-coated chip for 45 s at 90 μ l min⁻¹, followed by a 30-s dissociation time. The chip surface was then regenerated with 2 M NaCl for 30 s. Specific binding of trypsin was obtained by subtracting the response from a blank surface from that of the ECD-coated surface. The kinetic sensorgrams were fitted to a global 1:1 interaction model, allowing determination of the dissociation constant, K_D , using BIAevaluation software 1.0 (GE Healthcare).

Microscale Thermophoresis

MST was carried out using a Monolith NT.115 instrument (NanoTemper). Experiments were performed at 22°C in 25 mM MES (pH 6.5) and 100 mM NaCl. Both PepT1^{ECD} and PepT2^{ECD} were mutated to change a surface-exposed serine to a cysteine (PepT1^{ECD}-S437C and PepT2^{ECD}-S427C) and labeled with the blue maleimide labeling kit MO-L006 (NanoTemper). A range of concentrations of the required ligand (range 0.03–1,000 μ M) was incubated with 1.5 μ M of purified labeled protein. The sample was loaded into the NanoTemper glass capillaries and microthermophoresis was carried out using 100% LED power and 80% MST. K_D s were calculated using the mass action equation via the NanoTemper software from duplicate reads of triplicate experiments.

ACCESSION NUMBERS

The atomic coordinates have been deposited in the PDB under accession codes PDB: 5A9D (*Mm*PepT1^{ECD}) and PDB: 5A9H and 5A9I (*Rn*PepT2^{ECD}).

SUPPLEMENTAL INFORMATION

Supplemental Information includes seven figures and can be found with this article online at <http://dx.doi.org/10.1016/j.str.2015.07.016>.

AUTHOR CONTRIBUTIONS

S.N. conceived the study. J.H.B., J.L.P., L.E.B., R.J.O., and S.N. cloned and purified the protein. J.H.B. and S.N. crystallized the protein and collected the X-ray diffraction data, solved the structures, and built and refined the models. A.L.B. and S.J.T. designed, performed, and analyzed the TEVC experiments. A.S. and D.M. designed, performed, and analyzed the radioactive uptake assays. J.H.B. and D.S. designed, performed, and analyzed the AUC experiments. J.H.B. and J.L.P. designed, performed, and analyzed the biochemical and binding assays. F.S., M.S.P.S., and P.W.F. built the full-length PepT1 and PepT2 homology models and designed, performed, and analyzed the molecular dynamics experiments. J.L.P. and S.N. wrote the paper.

ACKNOWLEDGMENTS

This research was funded primarily through the Medical Research Council (MRC) G0900399 and Wellcome Trust 102890/Z/13/Z to S.N. J.H.B. was

funded by an MRC studentship. A.S. was funded through a Professor Nigel Groome Studentship from Oxford Brookes University. We also thank the beamline staff at the Diamond Light Source Ltd. UK (I02, I03, I04) and the support team at the Research Complex at Harwell, UK.

Received: May 11, 2015

Revised: July 22, 2015

Accepted: July 28, 2015

Published: August 27, 2015

REFERENCES

- Abrahams, J.P., and Leslie, A.G.W. (1996). Methods used in the structure determination of bovine mitochondrial F1 ATPase. *Acta Crystallogr. D Biol. Crystallogr.* 52, 30–42.
- Adams, P.D., Afonine, P.V., Bunkóczi, G., Chen, V.B., Davis, I.W., Echols, N., Headd, J.J., Hung, L.-W., Kapral, G.J., Grosse-Kunstleve, R.W., et al. (2010). PHENIX: a comprehensive Python-based system for macromolecular structure solution. *Acta Crystallogr. D Biol. Crystallogr.* 66, 213–221.
- Adibi, S.A. (1997a). The oligopeptide transporter (Pept-1) in human intestine: biology and function. *Gastroenterology* 113, 332–340.
- Adibi, S.A. (1997b). Renal assimilation of oligopeptides: physiological mechanisms and metabolic importance. *Am. J. Physiol.* 272, E723–E736.
- Ashida, K., Katsura, T., Motohashi, H., Saito, H., and Inui, K. (2002). Thyroid hormone regulates the activity and expression of the peptide transporter PEPT1 in Caco-2 cells. *Am. J. Physiol. Gastrointest. Liver Physiol.* 282, G617–G623.
- Barabote, R.D., Tamang, D.G., Abeywardena, S.N., Fallah, N.S., Fu, J.Y., Lio, J.K., Mirhosseini, P., Pezeshk, R., Podell, S., Salampessy, M.L., et al. (2006). Extra domains in secondary transport carriers and channel proteins. *Biochim. Biophys. Acta* 1758, 1557–1579.
- Berrow, N.S., Alderton, D., Sainsbury, S., Nettleship, J., Assenberg, R., Rahman, N., Stuart, D.I., and Owens, R.J. (2007). A versatile ligation-independent cloning method suitable for high-throughput expression screening applications. *Nucleic Acids Res.* 35, e45.
- Birmanns, S., Rusu, M., and Wriggers, W. (2011). Using Sculptor and Situs for simultaneous assembly of atomic components into low-resolution shapes. *J. Struct. Biol.* 173, 428–435.
- Blanc, E., Roversi, P., Vornrhein, C., Flensburg, C., Lea, S.M., and Bricogne, G. (2004). Refinement of severely incomplete structures with maximum likelihood in BUSTER-TNT. *Acta Crystallogr. D Biol. Crystallogr.* 60, 2210–2221.
- Brandsch, M. (2013). Drug transport via the intestinal peptide transporter PepT1. *Curr. Opin. Pharmacol.* 13, 881–887.
- Bretschneider, B., Brandsch, M., and Neubert, R. (1999). Intestinal transport of beta-lactam antibiotics: analysis of the affinity at the H⁺/peptide symporter (PEPT1), the uptake into Caco-2 cell monolayers and the transepithelial flux. *Pharm. Res.* 16, 55–61.
- Covitz, K.M., Amidon, G.L., and Sadée, W. (1998). Membrane topology of the human dipeptide transporter, hPEPT1, determined by epitope insertions. *Biochemistry* 37, 15214–15221.
- Daniel, H., and Rubio-Aliaga, I. (2003). An update on renal peptide transporters. *Am. J. Physiol. Ren. Physiol.* 284, F885–F892.
- Daniel, H., Spanier, B., Kottra, G., and Weitz, D. (2006). From bacteria to man: archaic proton-dependent peptide transporters at work. *Physiology (Bethesda)* 21, 93–102.
- Doki, S., Kato, H.E., Solcan, N., Iwaki, M., Koyama, M., Hattori, M., Iwase, N., Tsukazaki, T., Sugita, Y., Kandori, H., et al. (2013). Structural basis for dynamic mechanism of proton-coupled symport by the peptide transporter POT. *Proc. Natl. Acad. Sci. USA* 110, 11343–11348.
- Do, C.B., Mahabhashyam, M.S., Brudno, M., and Batzoglu, S. (2005). ProbCons: probabilistic consistency-based multiple sequence alignment. *Genome Res.* 15, 330–340.
- Fallingborg, J. (1999). Intraluminal pH of the human gastrointestinal tract. *Dan. Med. Bull.* 46, 183–196.
- Fei, Y.J., Kanai, Y., Nussberger, S., Ganapathy, V., Leibach, F.H., Romero, M.F., Singh, S.K., Boron, W.F., and Hediger, M.A. (1994). Expression cloning of a mammalian proton-coupled oligopeptide transporter. *Nature* 368, 563–566.
- Fordtran, J.S., Rector, F.C., Jr., and Carter, N.W. (1968). The mechanisms of sodium absorption in the human small intestine. *J. Clin. Invest.* 47, 884–900.
- Fowler, P.W., Orwick-Rydmark, M., Radestock, S., Solcan, N., Dijkman, P.M., Lyons, J.A., Kwok, J., Caffrey, M., Watts, A., Forrest, L.R., et al. (2015). Gating topology of the proton-coupled oligopeptide symporters. *Structure* 23, 290–301.
- Franke, D., and Svergun, D.I. (2009). DAMMIF, a program for rapid ab-initio shape determination in small-angle scattering. *J. Appl. Cryst.* 42, 342–346.
- Goldberg, D.M., Campbell, R., and Roy, A.D. (1968). Binding of trypsin and chymotrypsin by human intestinal mucosa. *Biochim. Biophys. Acta* 167, 613–615.
- Goldberg, D.M., Campbell, R., and Roy, A.D. (1969a). Fate of trypsin and chymotrypsin in the human small intestine. *Gut* 10, 477–483.
- Goldberg, D.M., Campbell, R., and Roy, A.D. (1969b). Studies on the binding of trypsin and chymotrypsin by human intestinal mucosa. *Scand. J. Gastroenterol.* 4, 217–226.
- Guettou, F., Quistgaard, E.M., Raba, M., Moberg, P., Low, C., and Nordlund, P. (2014). Selectivity mechanism of a bacterial homolog of the human drug-peptide transporters PepT1 and PepT2. *Nat. Struct. Mol. Biol.* 21, 728–731.
- Kabsch, W. (2010). XDS. *Acta Crystallogr. D Biol. Crystallogr.* 66, 125–132.
- Kalliokoski, A., and Niemi, M. (2009). Impact of OATP transporters on pharmacokinetics. *Br. J. Pharmacol.* 158, 693–705.
- Konarev, P.V., Volkov, V.V., Sokolova, A.V., Koch, M.H.J., and Svergun, D.I. (2003). PRIMUS: a Windows PC-based system for small-angle scattering data analysis. *J. Appl. Cryst.* 36, 1277–1282.
- Luckner, P., and Brandsch, M. (2005). Interaction of 31 beta-lactam antibiotics with the H⁺/peptide symporter PEPT2: analysis of affinity constants and comparison with PEPT1. *Eur. J. Pharm. Biopharm.* 59, 17–24.
- Lyons, J.A., Parker, J.L., Solcan, N., Brintha, A., Li, D., Shah, S.T., Caffrey, M., and Newstead, S. (2014). Structural basis for polyspecificity in the POT family of proton-coupled oligopeptide transporters. *EMBO Rep.* 15, 886–893.
- Madej, M.G., and Kaback, H.R. (2013). Evolutionary mix-and-match with MFS transporters II. *Proc. Natl. Acad. Sci. USA* 110, E4831–E4838.
- Madej, M.G., Dang, S., Yan, N., and Kaback, H.R. (2013). Evolutionary mix-and-match with MFS transporters. *Proc. Natl. Acad. Sci. USA* 110, 5870–5874.
- Markovic, S., and Dutzler, R. (2007). The structure of the cytoplasmic domain of the chloride channel ClC-Ka reveals a conserved interaction interface. *Structure* 15, 715–725.
- Matthews, D.M. (1975). Intestinal absorption of peptides. *Physiol. Rev.* 55, 537–608.
- Matthews, D.M. (1991). Protein absorption: development and present state of the subject (Wiley-Liss).
- McCoy, A.J., Grosse-Kunstleve, R.W., Adams, P.D., Winn, M.D., Storoni, L.C., and Read, R.J. (2007). Phaser crystallographic software. *J. Appl. Crystallogr.* 40, 658–674.
- Meyer, S., Savaresi, S., Forster, I.C., and Dutzler, R. (2007). Nucleotide recognition by the cytoplasmic domain of the human chloride transporter ClC-5. *Nat. Struct. Mol. Biol.* 14, 60–67.
- Newstead, S. (2015). Molecular insights into proton coupled peptide transport in the PTR family of oligopeptide transporters. *Biochim. Biophys. Acta* 1850, 488–499.
- Newstead, S., Drew, D., Cameron, A.D., Postis, V.L.G., Xia, X., Fowler, P.W., Ingram, J.C., Carpenter, E.P., Sansom, M.S.P., McPherson, M.J., et al. (2011). Crystal structure of a prokaryotic homologue of the mammalian oligopeptide-proton symporters, PepT1 and PepT2. *EMBO J.* 30, 417–426.

- Parker, J.L., and Newstead, S. (2014). Molecular basis of nitrate uptake by the plant nitrate transporter NRT1.1. *Nature* 507, 68–72.
- Petoukhov, M.V., Konarev, P.V., Kikhney, A.G., and Svergun, D.I. (2007). ATSAS 2.1—towards automated and web-supported small-angle scattering data analysis. *J. Appl. Crystallogr.* 40, 223–228.
- Pieri, M., Gan, C., Bailey, P., and Meredith, D. (2009). The transmembrane tyrosines Y56, Y91 and Y167 play important roles in determining the affinity and transport rate of the rabbit proton-coupled peptide transporter PepT1. *Int. J. Biochem. Cell Biol.* 41, 2204–2213.
- Pongs, O., and Schwarz, J.R. (2010). Ancillary subunits associated with voltage-dependent K⁺ channels. *Physiol. Rev.* 90, 755–796.
- Radestock, S., and Forrest, L.R. (2011). The alternating-access mechanism of MFS transporters arises from inverted-topology repeats. *J. Mol. Biol.* 407, 698–715.
- Rambo, R.P., and Tainer, J.A. (2011). Characterizing flexible and intrinsically unstructured biological macromolecules by SAS using the Porod-Debye law. *Biopolymers* 95, 559–571.
- Reddy, V.S., Shlykov, M.A., Castillo, R., Sun, E.I., and Saier, M.H. (2012). The major facilitator superfamily (MFS) revisited. *FEBS J.* 279, 2022–2035.
- Sheldrick, G.M. (2010). Experimental phasing with SHELXC/D/E: combining chain tracing with density modification. *Acta Crystallogr. D Biol. Crystallogr.* 66, 479–485.
- Smith, D.E., Clemencon, B., and Hediger, M.A. (2013). Proton-coupled oligopeptide transporter family SLC15: physiological, pharmacological and pathological implications. *Mol. Aspects Med.* 34, 323–336.
- Solcan, N., Kwok, J., Fowler, P.W., Cameron, A.D., Drew, D., Iwata, S., and Newstead, S. (2012). Alternating access mechanism in the POT family of oligopeptide transporters. *EMBO J.* 31, 3411–3421.
- Steinhardt, H.J., and Adibi, S.A. (1986). Kinetics and characteristics of absorption from an equimolar mixture of 12 glycyl-dipeptides in human jejunum. *Gastroenterology* 90, 577–582.
- Studier, F.W. (2005). Protein production by auto-induction in high density shaking cultures. *Protein Expr. Purif.* 41, 207–234.
- Sun, J., Bankston, J.R., Payandeh, J., Hinds, T.R., Zagotta, W.N., and Zheng, N. (2014). Crystal structure of the plant dual-affinity nitrate transporter NRT1.1. *Nature* 507, 73–77.
- Svergun, D.I. (1999). Restoring low resolution structure of biological macromolecules from solution scattering using simulated annealing. *Biophys. J.* 76, 2879–2886.
- Terada, T., and Inui, K.-I. (2012). Chapter 8. Recent advances in structural biology of peptide transporters. In *Current Topics in Membranes, Vol. 70*, M.O. Bevensee, ed. (Elsevier), pp. 257–274.
- Volkov, V.V., and Svergun, D.I. (2003). Uniqueness of ab initio shape determination in small-angle scattering. *J. Appl. Cryst.* 36, 860–864.
- Warmuth, S., Zimmermann, I., and Dutzler, R. (2009). X-ray structure of the C-terminal domain of a prokaryotic cation-chloride cotransporter. *Structure* 17, 538–546.
- Waterhouse, A.M., Procter, J.B., Martin, D.M., Clamp, M., and Barton, G.J. (2009). Jalview Version 2—a multiple sequence alignment editor and analysis workbench. *Bioinformatics* 25, 1189–1191.
- Winter, G., Lobley, C.M.C., and Prince, S.M. (2013). Decision making in xia2. *Acta Crystallogr. D Biol. Crystallogr.* 69, 1260–1273.
- Yan, N. (2013). Structural advances for the major facilitator superfamily (MFS) transporters. *Trends Biochemical Sciences* 38, 151–159.
- Zifarelli, G., and Pusch, M. (2009). Intracellular regulation of human CIC-5 by adenine nucleotides. *EMBO Rep.* 10, 1111–1116.

10 Appendix II

10.1 Alignment of hPepT1 and hPepT2 ECD between TMD9 and TMD10

hPepT1_ECD	NEVQIKVLNIGNNTMNISLPG-----EMVTLGPMSTQNAFMTFDVKNLKR-INISSPGS	53
hPepT2_ECD	QEVFLQVLNLADDEVKVTVVGNNENSLLESIKSFQKTPHYSKLHLKTKSQDFHFLKYH	60
	: ** : : * * * : : : : : : : * : : : . : : * : : . : : : : : : : : : :	
hPepT1_ECD	PVTAVTDDFKQGQRHTLLVWAPN---HYQVVKDGLNQKPEKGENGIRFVNTFNELITITM	110
hPepT2_ECD	NLSLYTEHSVQEKNWYSLVIREDGNSISSMMVKDTESTRTTNGMTTVRFVNTLHKDVNISL	120
	: : * : . * : . * * : : : : . . : : . : * . : * * * * : : : : * : :	
hPepT1_ECD	SGKVIYANISS-YNASTYQFFPSGIKGFTISSTEIPPCQPNFNTFYLEFGSAYTYIVQRK	169
hPepT2_ECD	STDTSNLVGEDYGVSAYRTVQRGEYPAVHCRTEDK---NFSNLNLGLLDFGAAYLFVITNN	177
	* . . * : . . * : . : * : : : . * . . * * : : * * : * * * : : : : . :	
hPepT1_ECD	NDSCPEVKVFEDISA	184
hPepT2_ECD	TNQLGLQAWKIEDIPA	192
	: . . : : : : * * * . *	

10.2 Alignment of hPepT1, hPepT2 and ratPHT1 sequences

(Note: ECD coloured in red)

hPepT1	-----MG-MSKSHS---FFG-----YPLSIFFFIVVNE	23
hPepT2	-----MNPFFQKNESKETLFSFVSIEEVPPRPPSPPKKPSPTICGSNYPLSIAFIVVNE	53
ratPHT1	MEGERAPLLGSRRAAAAAGVFAG-----RRAACGAVLLAE	35
	: : : .*. : : *	
hPepT1	FCERFSYYGMRAILILYFT-NFISWDDNLSTAIYHTFVALCYLTPILGALIADSWLGKFK	82
hPepT2	FCERFSYYGMKAVLILYFL-YFLHWNEDTSTSIYHAFSSLCYFTPILGAAIADSWLGKFK	112
ratPHT1	LLERAAFYGVGTANLVLFNGAPFNWEQAQASQALLLFMGLTYLGSFPGWLADARLGRAR	95
	: ** :*** * *:*: : * : : * . * * : . : * . :*** ** : :	
hPepT1	TIVLSLIVYTIGQAVTSVSSIN-----DLTDHNDGTPDSLPHVH	122
hPepT2	TIIYLSLVYVLGHVIKSLGALP-----ILGGQ-----VVHT	143
ratPHT1	AILLSLALYLLGMLAFFLLAAPRSRSLCGDPHPELVRNCSAPFPNGTAVCPDAAARRCA	155
	:* : : * : * : : : : : : : : .	
hPepT1	VLSLIGLALIALGTGGIKPCVSAFGGDQFEEGQEKQRNRRFSIFYLAINAGSLLSTIITP	182
hPepT2	VLSLIGLSLIALGTGGIKPCVAAFAGDQFEEKHAEERTRYFSVFYLSINAGSLISTFITP	203
ratPHT1	PATFAGLVVLVGLGVATVKANITPFGADQVKDRGPEATRFRFFNWFYWSINLGAILSLGGIA	215
	: : ** *:.***. :*. :.:.***.***.: : *:. * * :** *:.:*	
hPepT1	MLRVQQCGIHSKQACYPLAFGVPAALMAVALIVFVLGSGMYKKFKPQGNIMGKVAKCIGF	242
hPepT2	MLRGDVQCFG--EDCYALAFGVPGLLMVIALVVFAMGSKIYNKPPPEGNIVAQVFKCIWF	261
ratPHT1	YIQQNVSFILT-----GYLIPTVCVAIAFLVFLCGQSVFITKPPDGSFTDMFRILTY	267
	: : : : : : * :.*** * . : . * : * . . : : : :	
hPepT1	AIKNRFRHRSKA-----FPKREHWLDWAKEKYD---ERLISQIKMVTRVMFLYIPL	290
hPepT2	AISNRFKNRSGD-----IPKRQHWLDWAAEKYP---KQLIMDVKALTRVLFLYIPL	309
ratPHT1	SCCSQRRGQRRSGEGLGVFQQSSKHSLEFDSCKMSHGGPFIEDKVEDVKALVKIVPVFLAL	327
	: . : : : . . . : * . . : : : : * : : : : : . *	
hPepT1	PMFWALFDQQGSRWTLQATTMSG-----KIGALEIQPDQMOTVNAILIVIMVPIFDAVL	344
hPepT2	PMFWALLDQQGSRWTLQAIRMN-----NLGFFVLQPDQMQLNPLLVLIPIPLDFVI	363
ratPHT1	IPYWTVYFQMOTTYVLQSLHLKIPEISSITTTHTHTLPAAWLTMFDAVLILLIPLKDKLV	387
	:* : : * : : .** : : . : : : : . : : . : . : * : : *	
hPepT1	YPLIAKCGFNFTSLKKMAVGMVLASMAFVVAIVQVEIDKTLPVFPKGNEVQIKVLNIGN	404
hPepT2	YRLVSKCGINFSSLRKMAVGMILACLAFAVAAVEIKINEMAPAQPGQEVFLQVLNLAD	423
ratPHT1	DPVLRRHGLLPSSLKRIAVGMFFVTCSAFAAGILESKR-----LDLVKE	431
	: : : * : :***: :****. : . : . * . : : : : : : :	
hPepT1	NTMNISLPG-----EMVTLGPMSTNAFMTFDVNKLTR-INISSPGSPVTAVTDDFKQG	457
hPepT2	DEVKVTVVGNENNSLLIESIKSFQKTPHYSKLHLTKSQDFHFLKYHNLSLYTEHSVQE	483
ratPHT1	KTINQTIGG-----	440
	. : : : * :	
hPepT1	QRHTLLVWAPN----HYQVVKDGLNQKPEKGENGIRFVNTFNELITITMSGKVYANISS-	512
hPepT2	KNWYSLVIREDGNSISSMMVKD-TESRTTNGMTTVRFVNTLHKDVNISLSTDTSLNVGED	542
ratPHT1	-----	
hPepT1	YNASTYQFFPSGIKGTISSTEIPPCQCPNFNTFYLEFGSAYTYIVQRKNDSCPEVKVFE	572
hPepT2	YGVSAYRTVQRGEYPAVHCRTEDK---NFSNLNGLLDFGAAYLFVITNNTNQGLQAWKIE	599
ratPHT1	-----V	441
hPepT1	DISANTVNMAQIPQYFLLTCGEVVFVSVTGLEFSYSQAPSNMKSVLQAGWLLTVAVGNII	632
hPepT2	DIPANKMSIAWQLPQYALVTAGEVMFVSVTGLEFSYSQAPSGMKSVLQAAWLLTIAGVNI	659
ratPHT1	VYHAADLPiWWQIPQYVLIGISEIFASIAGLEFAYSAPKMSQSAIMGLFFFFSGIGSFV	501
	* : : * : *** * : . * : . : * : * : * : * : * : * : * : * : *	
hPepT1	---VLIVAGAGQFS--KQWAEYILFAALLLVVCVIFAIMARFYTYINPAEIEAQFDEDEK	687
hPepT2	---VLVVA---QFSGLVQWAEFILFSCLLLVIKLIIFSIMGYYYVPVKTEDMRGPADK---	710
ratPHT1	GSGLLALVSLKAIGWMSSHTDFGNINSCHLHYYFFLLAAIQGATLLLFIVSVKYDR---	558
	: * : . : . : : : : : * : : : : : : : *	

hPepT1	KNRLEKSNPYFMSGANSQKQM	708
hPepT2	--HIPHIQGNMIKLETKKTKL	729
ratPHT1	--QRARTDGGTASTRT-----	572
	: : : . .	

10.3 Alignment of hPepT1 and hPepT2 conserved residues mutated in chapter 6

(Note: Mutated Residues are highlighted in grey)

```

hPepT2      MNPFQKNESKETLFSPVSIIEVPPRPPSPPKKPSPTICGSNPLSIAFIVVNEFCERFSY
hPepT1      -----MGMSKSHSFFGPLSIFFIVVNEFCERFSY
              * : . *****

hPepT2      YGMKAVLILYFLYFLHWNEDTSTSIYHAFSSLCYFTPILGAAIADSWLGKFKTIYLSLV
hPepT1      YGMRAILILYFTNFISWDDNLSTAIYHTFVALCYLTPILGALIADSWLGKFKTIVLSLSIV
              ***:**** * : *::: **:***: * :***:***** *****: **: *

hPepT2      YVLGHVIKSLGALPILG-----GQVVHTVLSLIGLSLIALGTGGIKPCVAAFGGDQ
hPepT1      YTIGQAVTSVSSINDLTDHNHDGTPDSLPHVHVLISLIGLALIALGTGGIKPCVSAFGGDQ
              *.:*:*:*:*:*: * . *.,*****:*****:*****

hPepT2      FEEKHAEERTRYFSVFYLSINAGSLISTFITPMLRGDVQC--FGEDCYALAFGVPGLLMV
hPepT1      FEEGQEKQRNRFFSIFYLAINAGSLLSTIITPMLRVQQCGIHSKQACYPLAFGVPAALMA
              *** : :*.*:*:*:*:*****:*.***** : : * * *****. **.

hPepT2      IALVVFAMGSKIYNKPPPEGNIVAQVFKCIWFAISNRFKNRSGDIPKRQHWLDWAAEKYP
hPepT1      VALIVFVLGSGMYKKFKPQGNIMKVKACIGFAIKNRFRHRSKAFPKREHWLDWAKEKYD
              :*:*.*:*. * : * * :*:*:*: * * * * * :*:*. * :*:*.***** **

hPepT2      KQLIMDVKALTEVLFYIPLPMFVALLDQQGSRWTLQAI RMNRNLGFFVLQPDQMQLVNP
hPepT1      ERLISQIKMVTVMFLYIPLPMFVALFDQQGSRWTLQATTMSGKIGALEIQPDQMOTVNA
              :*: * : * :*:*:*****:***** * . :*: : :*****: *

hPepT2      LLVLIFIFLDFVIYRLVSKCGINFSSLRKMAVGMIACLAFAVAAAVEIKINEMAPAQP
hPepT1      ILIVIMVPIFDAVLYPLIAKCGFNFTSLKKMAVGMVLASMAFVVAIVQVEIDKTLPVFP
              :*:*:*:*. * * * :*:*:*:*:*:*****:*. * * * :*:*: * . *

hPepT2      GPQEVFLQVLNLADDEVKVTVVGNNNSLLIESIKSFQKTP--HYSKLHLK-----TK
hPepT1      KGNEVQIKVLNIGNNTMNISLPGEMVTLGPMSTQNAFMTFDVKNLTRINISSPGSPVTAV
              :* * :*:*:*: : : : * : . . : * . : : : : :

hPepT2      SQDFHFHLKYHNLSLYTEHSVQEKWNYSVLVIREDGNSISSMMVKDTESTRTTNGMTTVRFV
hPepT1      TDDFKQG-QRHTLLVWA-----PNHYQV-----VKDGLNQKPEKGENGIRFV
              :*: * : * * : * * : : . : : : * . : * *

hPepT2      NTLHKDVNISLSTDTSLNVEDYGVSAIRTVQRGEY-----PAVHCRTEDKNFSLNL
hPepT1      NTFNELITITMSGKVYANIS-SYNASTYQFFPSGIKGFTISSTEIPPQCQP-----NFNT
              **.: : :*: * . * :. * .*: * . * : * : * :

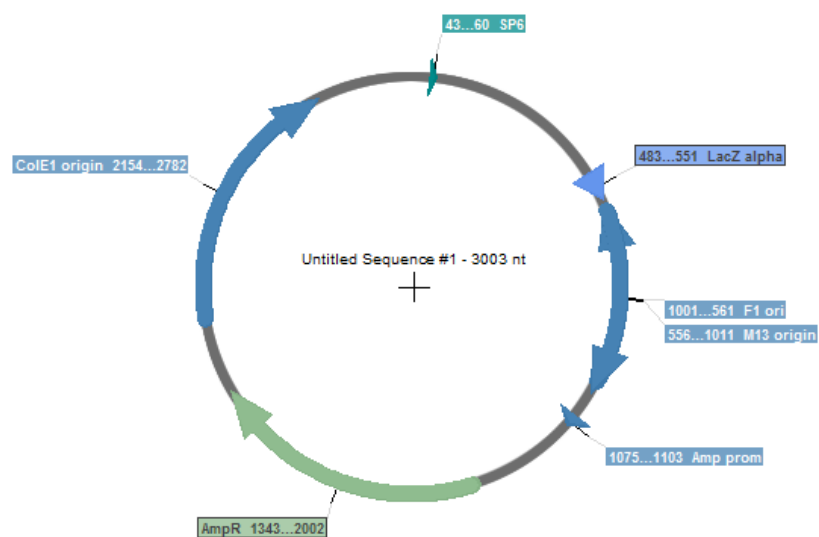
hPepT2      GLLDFGAAYLFVITNNTNQGLQAWKIEDIPANKMSIAWQLPQYALVTAGVFMFSVTGLEF
hPepT1      FYLEFGSAYTYIVQRKNDSCPEVKVFEDISANTVNMAIQIPQYFLLTCGVVFSVTGLEF
              *:***: * : : . : . : . : * * : * * : * * : * * : * * : * * : * *

hPepT2      SYSQAPSGMKSVLQAAWLLTIAVGNIIVLVVAQFSG-LVQWAEFILFSCLLLVICLIFSI
hPepT1      SYSQAPSNMKSVLQAGWLLTVAVGNIIVLVAGAGQFSKQWAEYILFAALLLVVCVIFAI
              ***** *****:*****: * . *****:***:***:***:***: *

hPepT2      MGYYYVPVKTEDMRGPADKHIPHIQGNMIKLETKKTKL-----
hPepT1      MARFYTYINPAEIEAQFDEDEKKN-----RLEKSNPYFMSGANSQKQM
              * . : * . : : : . * : : : * : : :

```

10.4 PBF vector diagram



List of Bioinformatics websites

Websites	Function	Reference (if any)
http://web.expasy.org/translate/	Translation of DNA to protein sequence	(Gasteiger <i>et al.</i> , 2003)
http://www.ebi.ac.uk/Tools/msa/clustalo/	Multiple protein/DNA sequence alignment tool	(Sievers <i>et al.</i> , 2011)
http://graphpad.com/quickcalcs/Grubbs1.cfm	Outlier test	
http://www.neb.com/tools/index.aspx?req=nebcutter	Program used to detect restrictions sites in DNA	(Vincze <i>et al.</i> , 2003)
http://www.basic.northwestern.edu/biotools/oligocalc.html	Online tool to determine T _m of DNA	(Nakano <i>et al.</i> , 1999)
http://www.bioinformatics.org/sms/rev_comp.html	Online tool to obtain reverse complement of DNA sequences	(Stothard, 2000)

11 Appendix III: Presentations

Oral presentations

- Anish Senan, David Meredith (2013). Structural and functional characterisation of SLC15 peptide transporters. School of Life Sciences Postgraduate Symposium, Oxford Brookes University, Oxford, UK

Poster Presentations

- Anish Senan, David Meredith (2014). A step closer to understanding the functional role of the large extracellular loop in the SLC15 class of peptide transporters. . School of Life Sciences Postgraduate Symposium, Oxford Brookes University, Oxford, UK
- Anish Senan, David Meredith (2014). PepT1 and PepT2: Novel insights into the function of the large extracellular domain. Late breaking abstracts, IUPS, London, UK.

12 Appendix IV: Permissions for copyright figures

**JOHN WILEY AND SONS LICENSE
TERMS AND CONDITIONS**

Aug 05, 2015

This Agreement between Anish Senan ("You") and John Wiley and Sons ("John Wiley and Sons") consists of your license details and the terms and conditions provided by John Wiley and Sons and Copyright Clearance Center.

License Number	3682461051172
License date	Aug 05, 2015
Licensed Content Publisher	John Wiley and Sons
Licensed Content Publication	Journal of Physiology
Licensed Content Title	Stoichiometry and pH dependence of the rabbit proton-dependent oligopeptide transporter PepT1.
Licensed Content Author	A Steel,S Nussberger,M F Romero,W F Boron,C A Boyd,M A Hediger
Licensed Content Date	Feb 1, 1997
Pages	7
Type of use	Dissertation/Thesis
Requestor type	University/Academic
Format	Electronic
Portion	Figure/table
Number of figures/tables	1
Original Wiley figure/table number(s)	Figure 3
Will you be translating?	No
Title of your thesis / dissertation	Structure function studies of SLC15 peptide transporters
Expected completion date	Aug 2015
Expected size (number of pages)	240
Requestor Location	Anish Senan S208A Sinclair building Oxford Brookes University Gipsy lane Oxford, United Kingdom OX3 0BP Attn: Anish Senan
Billing Type	Invoice
Billing Address	Anish Senan S208A Sinclair building Oxford Brookes University Gipsy lane Oxford, United Kingdom OX3 0BP Attn: Anish Senan

**JOHN WILEY AND SONS LICENSE
TERMS AND CONDITIONS**

Aug 05, 2015

This Agreement between Anish Senan ("You") and John Wiley and Sons ("John Wiley and Sons") consists of your license details and the terms and conditions provided by John Wiley and Sons and Copyright Clearance Center.

License Number	3682470158479
License date	Aug 05, 2015
Licensed Content Publisher	John Wiley and Sons
Licensed Content Publication	Journal of Physiology
Licensed Content Title	Computational modelling of H ⁺ -coupled peptide transport via human PEPT1
Licensed Content Author	Megumi Irie,Tomohiro Terada,Toshiya Katsura,Satoshi Matsuoka,Ken-ichi Inui
Licensed Content Date	Jun 13, 2005
Pages	11
Type of use	Dissertation/Thesis
Requestor type	University/Academic
Format	Electronic
Portion	Figure/table
Number of figures/tables	1
Original Wiley figure/table number(s)	Figure 2
Will you be translating?	No
Title of your thesis / dissertation	Structure function studies of SLC15 peptide transporters
Expected completion date	Aug 2015
Expected size (number of pages)	240
Requestor Location	Anish Senan S208A Sinclair building Oxford Brookes University Gipsy lane Oxford, United Kingdom OX3 0BP Attn: Anish Senan
Billing Type	Invoice
Billing Address	Anish Senan S208A Sinclair building Oxford Brookes University Gipsy lane Oxford, United Kingdom OX3 0BP

**JOHN WILEY AND SONS LICENSE
TERMS AND CONDITIONS**

Aug 05, 2015

This Agreement between Anish Senan ("You") and John Wiley and Sons ("John Wiley and Sons") consists of your license details and the terms and conditions provided by John Wiley and Sons and Copyright Clearance Center.

License Number	3682490896002
License date	Aug 05, 2015
Licensed Content Publisher	John Wiley and Sons
Licensed Content Publication	The EMBO Journal
Licensed Content Title	Crystal structure of a prokaryotic homologue of the mammalian oligopeptide-proton symporters, PepT1 and PepT2
Licensed Content Author	Simon Newstead,David Drew,Alexander D Cameron,Vincent L G Postis,Xiaobing Xia,Philip W Fowler,Jean C Ingram,Elisabeth P Carpenter,Mark S P Sansom,Michael J McPherson,Stephen A Baldwin,So Iwata
Licensed Content Date	Dec 3, 2010
Pages	10
Type of use	Dissertation/Thesis
Requestor type	University/Academic
Format	Electronic
Portion	Figure/table
Number of figures/tables	2
Original Wiley figure/table number(s)	Figure 1A and 1B
Will you be translating?	No
Title of your thesis / dissertation	Structure function studies of SLC15 peptide transporters
Expected completion date	Aug 2015
Expected size (number of pages)	240
Requestor Location	Anish Senan S208A Sinclair building Oxford Brookes University Gipsy lane Oxford, United Kingdom OX3 0BP Attn: Anish Senan
Billing Type	Invoice
Billing Address	Anish Senan S208A Sinclair building Oxford Brookes University

WILEY

Title: Alternating access mechanism in the POT family of oligopeptide transporters**Author:** Nicolae Solcan, Jane Kwok, Philip W Fowler, Alexander D Cameron, David Drew, So Iwata, Simon Newstead**Publication:** The EMBO Journal**Publisher:** John Wiley and Sons**Date:** Jun 1, 2012

Copyright © 2012 European Molecular Biology Organization

Logged in as:

Anish Senan

Account #:
3000947114

LOGOUT

Open Access Article

This article is available under the terms of the Creative Commons Attribution Non-Commercial License CC BY-NC (which may be updated from time to time) and permits non-commercial use, distribution and reproduction in any medium, provided the original work is properly cited.

For an understanding of what is meant by the terms of the Creative Commons License, please refer to [Wiley's Open Access Terms and Conditions](#).

Permission is not required for non-commercial reuse. For commercial reuse, please hit the "back" button and select the most appropriate commercial requestor type before completing your order.

BACK

CLOSE WINDOW

**JOHN WILEY AND SONS LICENSE
TERMS AND CONDITIONS**

Aug 05, 2015

This Agreement between Anish Senan ("You") and John Wiley and Sons ("John Wiley and Sons") consists of your license details and the terms and conditions provided by John Wiley and Sons and Copyright Clearance Center.

License Number	3682491302567
License date	Aug 05, 2015
Licensed Content Publisher	John Wiley and Sons
Licensed Content Publication	Angewandte Chemie International Edition
Licensed Content Title	How to Make Drugs Orally Active: A Substrate Template for Peptide Transporter PepT1
Licensed Content Author	Patrick D. Bailey,C. A. Richard Boyd,J. Ramsey Bronk,Ian D. Collier,David Meredith,Keith M. Morgan,Catherine S. Temple
Licensed Content Date	Feb 1, 2000
Pages	4
Type of use	Dissertation/Thesis
Requestor type	University/Academic
Format	Electronic
Portion	Figure/table
Number of figures/tables	1
Original Wiley figure/table number(s)	Figure 1a
Will you be translating?	No
Title of your thesis / dissertation	Structure function studies of SLC15 peptide transporters
Expected completion date	Aug 2015
Expected size (number of pages)	240
Requestor Location	Anish Senan S208A Sinclair building Oxford Brookes University Gipsy lane Oxford, United Kingdom OX3 0BP Attn: Anish Senan
Billing Type	Invoice
Billing Address	Anish Senan S208A Sinclair building Oxford Brookes University Gipsy lane Oxford, United Kingdom OX3 0BP